



HAL
open science

Functionalization of Multi-Walled Carbon Nanotubes with Polymers

Meltem Tunckol

► **To cite this version:**

Meltem Tunckol. Functionalization of Multi-Walled Carbon Nanotubes with Polymers. Materials. Institut National Polytechnique de Toulouse - INPT, 2012. English. NNT : 2012INPT0066 . tel-04244943

HAL Id: tel-04244943

<https://theses.hal.science/tel-04244943v1>

Submitted on 16 Oct 2023

HAL is a multi-disciplinary open access archive for the deposit and dissemination of scientific research documents, whether they are published or not. The documents may come from teaching and research institutions in France or abroad, or from public or private research centers.

L'archive ouverte pluridisciplinaire **HAL**, est destinée au dépôt et à la diffusion de documents scientifiques de niveau recherche, publiés ou non, émanant des établissements d'enseignement et de recherche français ou étrangers, des laboratoires publics ou privés.



Université
de Toulouse

THÈSE

En vue de l'obtention du
DOCTORAT DE L'UNIVERSITÉ DE TOULOUSE

Délivré par :
Institut National Polytechnique de Toulouse (INP Toulouse)

Discipline ou spécialité :
Chimie Organométallique et de Coordination

Présentée et soutenue par :
Meltem TUNCKOL

le : mercredi 18 juillet 2012

Titre :
Fonctionnalisation de Nanotubes de Carbone Multi-Parois par des Polymères
Functionalization of Multi-Walled Carbon Nanotubes with Polymers

Ecole doctorale :
Sciences de la Matière (SDM)

Unité de recherche :
Laboratoire de Chimie de Coordination (LCC), Equipe Catalyse et Chimie Fine

Directeur(s) de Thèse :
Prof. Philippe SERP, Professeur à l'INP - ENSIACET, Toulouse
Dr. Jérôme DURAND, Maître de conférences à l'INP - ENSIACET, Toulouse

Rapporteurs :
Dr. Jean-Marie RAQUEZ, Professeur à l'Université de Mons
Prof. Manuel Fernando PEREIRA, Professeur à l'Universidade de Porto

Membre(s) du jury :
Borja COTO, Directeur de recherche au Centro Tecnológico Tekniker
Prof. Constantin VAHLAS, Directeur de recherche du CNRS à l'INP - ENSIACET, Toulouse
Prof. Jose-Ramon SARASUA, Professeur à l'Universidad del País Vasco, Bilbao

Acknowledgments

The research work presented in this thesis was carried out in the Catalysis and Fine Chemicals group of « Laboratoire de Chimie de Coordination », UPR CNRS 8241, at ENSIACET (Ecole Nationale Supérieure des Ingénieurs en Arts Chimiques Et Technologiques), INPT (Institut National Polytechnique de Toulouse) from March 2009 to July 2012.

My most sincere thanks to Professor Philippe Serp, for giving me the opportunity to carry out this PhD study under his supervision and for his guidance and continuous support during the course of this work. I appreciate his advices, suggestions and giving me the option to pursue my own ideas.

I wish to express my gratitude to my co-supervisor, Dr Jérôme Durand, for his support, encouragement and good advices throughout the thesis.

I would like to thank my PhD jury members, Professor Manuel Fernando Pereira, Professor Jean-Marie Raquez, Professor Constantin Vahlas, Professor Jose Ramon Sarasua and Borja Coto, for their valuable time and suggestions.

Special thanks to Professor Jose Ramon Sarasua for offering me a unique opportunity to work for 3 months in the Biopolymers and Thermoplastics Materials Laboratory at the University of the Basque Country in Bilbao. The author would like to thank the entire team in Bilbao for their warm hospitality.

I also wish to express my gratitude to François Malbosc for giving me the opportunity to work in Solvionic. I am equally thankful to Sébastien Fantini from Solvionic for his guidance and help on the ionic liquid synthesis

I would like to thank all the participants of the POCO project for their interesting discussions during the many meetings.

The experimental part of this work could not have been accomplished without the assistance of many people, whose contributions I gratefully acknowledge. Especially thanks to Vincent Colliere for the SEM and TEM measurements and also for the friendly discussions we had during the long microscopy sessions. I equally thank Jean-François Meunier for the TGA and DSC measurements and for dealing with my countless emails. Christine Rey Rouch is acknowledged for the particle size measurements. I appreciate a lot her kindness and

availability for help. I am indebted to Nicolas Mauran from LAAS-CNRS for the electrical measurements. I thank Corinne Routaboul for the Raman analyses and Régis Laurent for the SEC measurements. I thank Ester Zuza for her help on the preparation of polyetherimide films, and Aitor Espartero for the DMA measurements. I also thank Andrea Terenzi and Laura Peponi from ECNP, Italy, for their contribution in this thesis work.

Next, I would like to thank my colleagues and all present and former members of the Catalysis and Fine Chemicals group, who I enjoyed to work with during my stay in Toulouse. I am especially thankful to Dr Revathi Bacsa for the fruitful discussions, suggestions and practical help related to the work and for the pleasant time we had during these years; and to Dr Bruno Machado for his practical help, valuable friendship and encouragement. Special thanks, also, to Xueqiang Qi, one of my newest office mates, for all his help and being such a nice person; and to Ganna Gogolieva for the fun time we had. Dr Duc Hanh Nguyen, Dr Florence Gayet, Dr Delphine Crozet, Dr Mustapha Oubenali, Dr Romain Adcock, Dr Julien Beausoleil, Liping Zhang, Kévin Fourmy, Xiaojiang Li, Trang Nguyen, Jamal El Karroumi, Pierre Lonchambon, Abdelouahd Oukhrib, Annas Benyounes are thanked for their friendship and support during the period of my research work. Thanks to Professor Martine Urrutigoity for her moral support and to Dr Odile Dechy-Cabaret for her helpful comments during my thesis defense rehearsal.

Many thanks also to the whole LCC and ENSIACET staff. The author would like to thank all those people who cooperated in one way or the other way to complete the research work in time.

I would be remiss if I did not acknowledge my undergraduate professors at the Chemistry Department of Istanbul Technical University, for contributing to my success.

Finally, a warm thank for my family for ever trusting me and supporting my choices, and to my beloved friends for their support and motivation through especially difficult moments.

This work was carried out in the framework of the European research project POCO, 7th Framework Programme, under grant agreement n° CP-IP 213939-1. I gratefully acknowledge the financial support of the European Commission for the project.

Meltem Tunçkol

Résumé

Cette thèse traite de la modification de surface des nanotubes de carbone avec des polymères. Le chapitre I présente l'état de l'art des matériaux hybrides associant des liquides ioniques avec des nanotubes de carbone (NTC) ou du graphenes. Le chapitre II commence par un aperçu général de l'adsorption non-covalente de polymères sur la surface de NTC, suivi d'une description détaillée de l'étude réalisée sur la fonctionnalisation non covalente des nanotubes de carbone avec divers liquides ioniques polymérisable (LIP) à base d'imidazolium. Dans ce cadre, nous avons comparé deux méthodes expérimentales: la polymérisation *in situ* et le mélange en solution. Une des applications les plus importantes des NTC se situe dans le domaine des nanocomposites polymères/NTC. Le chapitre III décrit la formation de composites polyetherimide/NTC à partir des NTC-LIP obtenue dans la chapitre II. La préparation des composites en utilisant la méthode dite « solvant casting » est détaillée. Les NTC bruts, oxydés à l'acide nitrique et fonctionnalisés par le LIP ont été comparés. Des mesures mécaniques, thermiques et électriques de ces composées ont été aussi réalisées. Le dernier chapitre, divisé en deux sections, traite de la fonctionnalisation covalente des nanotubes de carbone avec une variété de polymères en utilisant deux approches différentes: "*grafting from*" et "*grafting to*". En utilisant la première approche, nous avons réalisé la croissance de chaînes de polyamide (PA) à partir de la surface de nanotubes de carbone fonctionnalisés avec le caprolactame par polymérisation anionique par ouverture de cycle. Les propriétés de traction des composites à base de PA ainsi préparées ont été étudiées. La polymérisation radicalaire de monomères vinyliques à base de LI de type imidazolium greffés à la surface de NTC est également présentée dans cette partie. Dans la deuxième partie du chapitre IV, nous présentons plusieurs stratégies de fonctionnalisation, y compris l'addition radicalaire et le greffage sur les défauts de NTC, pour la préparation des NTC fonctionnalisés de manière covalente avec des polymères compatibles avec des matrices époxy.

Mots clés : nanotubes de carbones multi-parois, liquide ioniques, nanocomposite de polymère, polyétherimide, polyamide, époxy.

Abstract

This thesis deals with the surface modification of multi-walled carbon nanotubes with polymers with the aim to achieve a high level of dispersion in polymer matrices. **Chapter I** gives a comprehensive review of the state of the art of hybrids of ionic liquids with carbon nanomaterials, particularly, nanotubes and more recently, graphene. **Chapter II** starts with a general overview of the non-covalent adsorption of polymers onto the CNT surfaces followed by a detailed description of the study carried out on the non-covalent functionalization of CNTs with various imidazolium based polymerized ionic liquids (PIL). For this purpose, we further compare the two experimental methods: *in situ* polymerization and solution mixing. One of the most important applications of CNT is in polymer/CNT composites. **Chapter III** describes the formation of polyetherimide/CNT composites starting from PIL-CNT hybrids obtained in Chapter II. The preparation and characterization of composites using solvent casting methods have been detailed. Pristine, acid oxidized and PIL functionalized CNTs have been compared. Mechanical, thermal and electrical property measurements on these composites have also been described. The last chapter – **Chapter IV**, divided into two sections, discusses the covalent functionalization of CNTs with a variety of polymers using two main approaches: “grafting from” and “grafting to”. Using the first approach we have grown polyamide (PA) chains from the surface of caprolactam grafted CNTs by anionic ring opening polymerization. The tensile properties of the PA based composites prepared therefrom containing pristine, amine- and PA-functionalized CNTs have been investigated. The radical polymerization of vinyl imidazolium based IL monomers attached to the activated CNT surface is also given in this section. In the second part of Chapter IV, we have reported several “grafting to” functionalization strategies including radical addition and “defect site” grafting used for the preparation of CNTs covalently attached with polymers intended to blend well with epoxy matrices.

Key words: multi-walled carbon nanotubes, ionic liquid, polymerized ionic liquid, polymer nanocomposite, polyetherimide, polyamide, epoxy.

Table of contents

List of acronyms	1
General introduction	5
Chapter I: Literature review of carbon nanomaterial–ionic liquid hybrids	
I.1 Introduction	11
I.2 CNT–IL hybrids	13
<i>I.2.1 Preparation and characterization</i>	<i>13</i>
<i>I.2.1.1 CNT–IL hybrid formation by « soft » physical methods</i>	<i>15</i>
<i>I.2.1.1.1 Bucky gels</i>	<i>16</i>
<i>I.2.1.1.2 CNT–polymerized IL hybrids</i>	<i>19</i>
<i>I.2.1.1.3 CNT–IL hybrid formation in liquid dispersions</i>	<i>23</i>
<i>I.2.1.2 CNT–IL hybrid formation by « hard » chemical methods</i>	<i>26</i>
<i>I.2.2 Applications</i>	<i>30</i>
<i>I.2.2.1 Electrochemical devices</i>	<i>31</i>
<i>I.2.2.1.1 Electrochemical sensors</i>	<i>31</i>
<i>I.2.2.1.1.1 CNT–bucky gel electrodes</i>	<i>33</i>
<i>I.2.2.1.1.2 CNT–IL paste electrodes</i>	<i>34</i>
<i>I.2.2.1.1.3 CNT–IL electrodes by solvent casting</i>	<i>36</i>
<i>I.2.2.1.1.4 Enzyme/protein immobilization</i>	<i>37</i>
<i>I.2.2.1.1.5 Factors impacting the electrode performance</i>	<i>41</i>
<i>I.2.2.1.2 Actuators</i>	<i>43</i>
<i>I.2.2.1.3 Other applications in electrochemistry</i>	<i>46</i>
<i>I.2.2.2 Support for metal nanoparticles</i>	<i>47</i>
<i>I.2.2.3 Antiwear and lubricant additives</i>	<i>53</i>
<i>I.2.2.4 CNT–IL/Polymer composites</i>	<i>55</i>
I.3 Graphene-IL hybrids	59
<i>I.3.1 Preparation and characterization</i>	<i>59</i>

<i>I.3.2 Potential applications of graphene–IL hybrids</i>	65
<i>I.3.2.1 Electrochemical sensors and biosensors</i>	65
<i>I.3.2.2 Graphene–IL/polymer composites</i>	68
<i>I.3.2.3 Other applications</i>	71
I.4 Concluding remarks	75
References	76

Chapter II: Non-covalent functionalization of multi-walled carbon nanotubes with polymerized ionic liquids

II.1 Introduction	101
<i>II.1.1 Adsorption of polymers on the surface of CNTs</i>	101
<i>II.1.1.1 General adsorption phenomenon</i>	101
<i>II.1.1.2 Copolymers</i>	107
<i>II.1.1.3 Dendritic polymers</i>	108
<i>II.1.1.4 Polyelectrolytes</i>	109
<i>II.1.1.5 Polymerized ionic liquids</i>	111
<i>II.1.1.6 Effects of defects and disorders in CNTs on polymer adsorption</i>	113
II.2 Results and discussion	116
<i>II.2.1 Characterization of CNTs</i>	116
<i>II.2.2 Preparation of polymerized ionic liquids</i>	121
<i>II.2.3 Non-covalent functionalization of the CNTs by PIL</i>	127
<i>II.2.3.1 Functionalization by “solution-mixing”</i>	128
<i>II.2.3.2 Functionalization by in situ polymerization</i>	132
<i>II.2.4 Solvent dispersions of CNTs</i>	138
<i>II.2.5 Incorporation of CNTs into gels</i>	143
II.3 Conclusions	146
References	148

Chapter III: Polymerized ionic liquid functionalized carbon nanotube/polyetherimide composites

III.1 Introduction	159
III.2 Results and Discussion	161
<i>III.2.1 Functionalization of CNTs with PIL</i>	<i>161</i>
<i>III.2.2 Incorporation of CNTs into the polymer matrix</i>	<i>168</i>
<i>III.2.3 Mechanical, thermal and electrical properties of the composites</i>	<i>172</i>
III.3 Conclusions	182
References	184
Chapter IV: Polymer grafted carbon nanotubes using covalent functionalization strategy	
IV.1 The covalent “grafting from” approach	189
<i>IV.1.1 Introduction</i>	<i>189</i>
<i>IV.1.2 Results and discussion</i>	<i>190</i>
<i>IV.1.2.1 PA6 functionalized CNTs</i>	<i>190</i>
<i>IV.1.2.1.1 Synthesis</i>	<i>190</i>
<i>IV.1.2.1.2 Polyamide/CNT composites</i>	<i>198</i>
<i>IV.1.2.2 Covalent PIL functionalization of CNTs</i>	<i>201</i>
IV.2. The covalent “grafting to” approach	205
<i>IV.2.1 Introduction</i>	<i>205</i>
<i>IV.2.2 Results and discussion</i>	<i>213</i>
<i>IV.2.2.1 Functionalization of CNTs by radical addition</i>	<i>213</i>
<i>IV.2.2.1.1 Polymer synthesis</i>	<i>213</i>
<i>IV.2.2.1.2 Functionalization of CNTs</i>	<i>217</i>
<i>IV.2.2.2 Functionalization of CNTs by “defect site” chemistry</i>	<i>225</i>
IV.3 Conclusions	231
References	233
General conclusions and perspectives	241

Chapter V: Experimental details

V.1 Materials	247
V.2 Experimental procedures	248
<i>V.2.1 Purification of CNTs</i>	248
<i>V.2.2 Preparation of oxidized CNTs</i>	248
<i>V.2.3 Acid-base titration for the determination of carboxylic acid concentration</i>	248
<i>V.2.4 Preparation of ionic liquid monomers</i>	248
<i>V.2.4.1 Preparation of 1-vinyl-3-ethylimidazolium bromide, [VEIM]Br</i>	248
<i>V.2.4.2 Preparation of 1-vinyl-3-ethylimidazolium bis(trifluoromethanesulfonyl)imide</i>	249
<i>V.2.4.3 Preparation of 1-(2-hydroxyethyl)-3-vinylimidazolium chloride</i>	249
<i>V.2.4.4 Preparation of 1-(2-hydroxyethyl)-3-vinylimidazolium bis(trifluoromethanesulfonyl)imide</i>	249
<i>V.2.5 General procedure for the polymerization of ionic liquid monomers</i>	250
<i>V.2.5.1 Preparation of poly[3-(2-hydroxyethyl)-1-vinylimidazole]bromide</i>	250
<i>V.2.6 Non-covalent functionalization of CNTs with polymerized ionic liquids</i>	250
<i>V.2.6.1 General procedure for solution-mixing</i>	250
<i>V.2.6.2 General procedure for in situ polymerization</i>	251
<i>V.2.6.3 Anion exchange of CNT–poly[VEIM]Br</i>	251
<i>V.2.6.4 General procedure for CNT–polymer gel preparation</i>	251
<i>V.2.6.5 Functionalization of CNTs with poly(3-vinyl-1-ethylimidazolium dodecylbenzene sulfonate)</i>	252
<i>V.2.7 Preparation of polyetherimide/carbon nanotube composite films</i>	252
<i>V.2.8 Polymerization of caprolactam</i>	253
<i>V.2.9 Polymerization of N-vinylformamide</i>	253
<i>V.2.10 Preparation of polyvinylamine hydrochloride</i>	254
<i>V.2.11 Polymerization of 2-hydroxy-3-phenoxypropyl acrylate</i>	254

V.2.12 Covalent functionalization of CNTs	254
V.2.12.1 Functionalization of CNTs with caprolactam	254
V.2.12.2 Polyamide functionalized CNTs	255
V.2.12.3 Functionalization of CNTs with 1,8-diaminooctane	255
V.2.12.4 Functionalization of CNTs with 1-(2-hydroxyethyl)-3-vinylimidazolium chloride, bromide or bis(trifluoromethanesulfonyl)imide	255
V.2.12.5 Preparation of cross-linked CNTs	256
V.2.12.6 In situ polymerization of 1-vinyl-3-ethylimidazolium bis(trifluoromethanesulfonyl)imide in the presence of CNT-[VEHIM]NTf ₂	256
V.2.12.7 In situ polymerization of 1-vinyl-3-ethylimidazolium bromide in the presence of CNT-[VEHIM]Br	257
V.2.12.8 Functionalization of CNTs with polyvinylformamide	257
V.2.12.9 Functionalization of CNTs with polyvinylamine	257
V.2.12.10 Functionalization of CNTs with poly(2-hydroxy-3-phenoxypropyl acrylate)	258
V.2.12.11 Functionalization of CNTs with epoxy	258
V.2.13 Preparation of polyamide/CNT composites	258
V.3 Instruments and measurements	259
V.3.1 Transmission electron microscope	259
V.3.1.1 Microtoming	259
V.3.1.2 Staining	259
V.3.2 Field emission gun scanning electron microscopy	260
V.3.3 Thermogravimetric analysis	260
V.3.4 Differential scanning calorimetry	260
V.3.5 Particle size analysis	260
V.3.6 Elemental analyses	261
V.3.7 XPS analysis	261
V.3.8 Specific surface area and porosity measurements	261
V.3.9 Molecular weight analysis	261

<i>V.3.10 Raman analysis</i>	262
<i>V.3.11 Infrared spectroscopy</i>	262
<i>V.3.12 Nuclear magnetic resonance spectrometer</i>	262
<i>V.3.13 Ultrasonication</i>	262
<i>V.3.14 Compression molding</i>	263
<i>V.3.15 Tensile testing</i>	263
<i>V.3.16 Dynamic mechanical analysis</i>	263
<i>V.3.17 Electrical measurements</i>	263

List of acronymes

AIBN	Azobisisobutyronitrile
AFM	Atomic force microscopy
AROP	Anionic ring opening polymerization
ATR	Attenuated total reflectance
BCP	Block copolymer
BET	Brauner-Emmet-Teller
CNT	Carbon nanotube
CP	Caprolactam
CVD	Chemical vapor deposition
DCC	<i>N,N'</i> -Dicyclohexylcarbodiimide
DCM	Dichloromethane
DMA	Dynamic mechanical analysis
DMF	Dimethylformamide
DMSO	Dimethyl sulfoxide
DSSC	Dye-sensitized solar cell
DWCNT	Double-walled carbon nanotubes
EAP	Electroactive polymer
EDLC	Electric double layer capacitor
FTIR	Fourier transform infrared spectroscopy
GCE	Glassy carbon electrode
GS	Graphene sheets
GO	Graphene oxide
IL	Ionic liquid

MD	Molecular dynamics
MWCNT	Multi-walled carbon nanotube
NMP	N-methyl-2-pyrrolidone
NMR	Nuclear magnetic resonance
PA	Polyamide
PA6	Polyamide-6
PA66	Polyamide-6,6
PANI	Polyaniline
PEDOT	Poly(3,4-ethylenedioxythiophene)
PEG	Polyethyleneglycol
PEI	Polyetherimide
PHPPA	Poly(2-hydroxy-3-phenoxypropyl acrylate)
PIL	Polymerized ionic liquid
PMMA	Poly(methyl methacrylate)
PmPV	Poly(m-phenylenevinylene-co-2,5-dioctoxy-p-phenylenevinylene)
PNVF	Poly(N-vinylformamide)
PS	Polystyrene
PSS	Polystyrene sulfonate
PVA	Poly(vinylamine)
PVdF	Polyvinylidene difluoride
rGO	Reduced graphene oxide
SDBS	Sodium dodecylbenzene sulfonate
SEC	Size-exclusion chromatography
SEM	Scanning electron microscope

STM	Scanning tunneling microscopy
SWCNT	Single-walled carbon nanotube
TEM	Transmission electron microscopy
TGA	Thermogravimetric analysis
THF	Tetrahydrofuran
UV-Vis	Ultraviolet-visible
XPS	X-Ray photoelectron spectroscopy

Ionic liquids

[BMIM]	1-butyl-3-methylimidazolium
[BMPy]	1-butyl-1-methylpyridinium
[BMPyr]	1-butyl-1-methylpyrrolidinium
[BPy]	1-butylpyridinium
[EMIM]	1-ethyl-3-methylimidazolium
[OMIM]	1-octyl-3-methylimidazolium
[OPyr]	n-octyl pyridinium
[VBIM]	1-vinyl-3-butylimidazolium
[VEIM]	1-vinyl-3-ethylimidazolium
[VHEIM]	1-hydroxyethyl-3-vinylimidazolium
[VHIM]	1-vinyl-3H-imidazolium

General introduction

Polymer nanocomposite materials can be made using different type of nanofillers and polymer matrices. Among the different nanofillers, carbon nanotubes (CNT) have been extensively studied because of their exceptional mechanical and electrical properties. Due to these extraordinary properties, great enthusiasm exists among researchers around the world as they explore the immense potential of CNT/polymer nanocomposites. The level of activity is illustrated by the number of journal articles published within the last fifteen years (Figure 1). This increase of interest about CNTs has been followed by a reduction in the production prices. This has been possible mainly due to the development of production processes by CNT manufacturing companies like ARKEMA or BAYER. Price reduction run in parallel with an increase of the CNTs demand, and it is foreseen that this tendency will be accelerated in a near future.

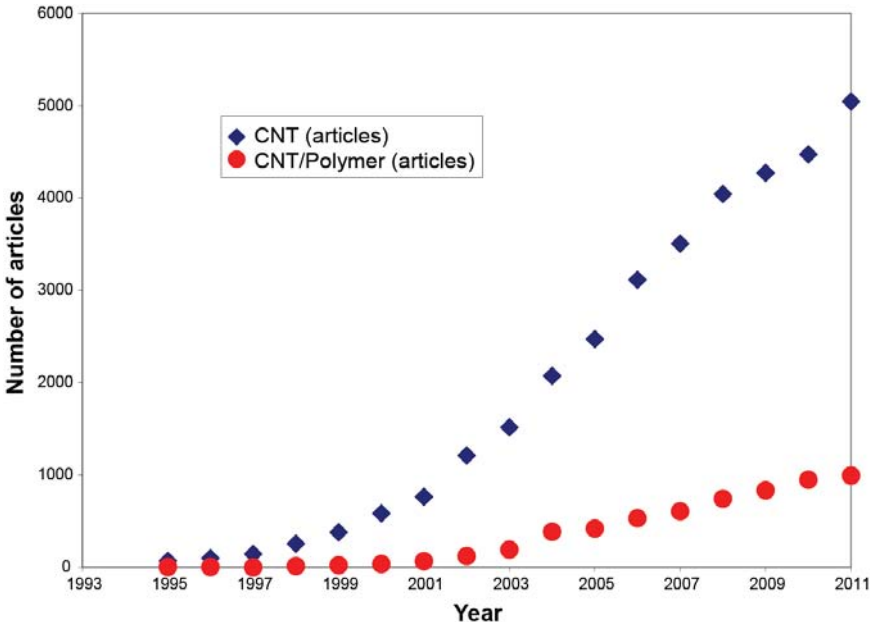


Figure 1. Number of journal articles published on carbon nanotubes and CNT/polymer composites as a function of year.

The utilization of CNTs as reinforcement to design novel composites is a quite old idea. However, nowadays their practical and extensive use in commercial materials is still missing. The scientific literature addresses various aspects of nanotube production, functionalization and applications, as well as the fabrication and characterization of polymer nanocomposites with various types of carbon nanotubes and dispersion methods. One of the missing points is a lack of knowledge based approach to achieve the nanostructuring level required to optimize the CNT/polymer nanocomposite performances and an in deep investigation into the polymer/nanotube interphase.

The present work has been realized in the frame of a European large scale collaborative project named POCO (Carbon Nanotube Confinement Strategies to Develop Novel Polymer Matrix Composites). The main objective of POCO is to get innovative polymer nanocomposites filled with CNTs in order to obtain materials with tailor made and superior properties. Therefore, maximum research efforts within POCO have been addressed to the achievement of nanocomposites in which the CNTs are confined, ordered, structured or aligned into the polymer matrix in order to obtain new knowledge into the CNT/polymer interphase. The final goal of this project is to reach the predicted and expected excellent properties of CNT/polymer nanocomposites in terms of mechanical, electrical, surface and tribological behaviors. By reaching this ambitious goal, POCO could pave the way towards CNT/polymer nanocomposite products for the aerospace, automotive, building and biomedical industries. The work plan of this project that associates 17 partners is shown in Figure 2.

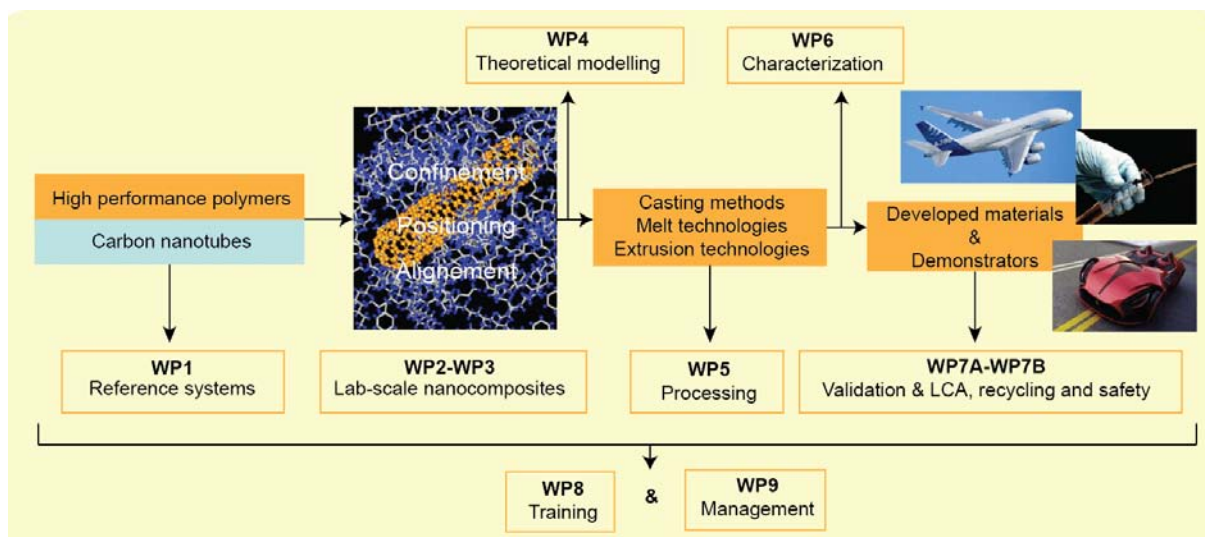


Figure 2. Work plan of POCO project.

The role of our team in this project was to study the selective functionalization of carbon nanotubes (WP2). Indeed, the non-polar nature of CNT surface induces serious problems concerning their dispersion in polymer matrices. Thus, CNT surfaces have to be modified in order to avoid agglomeration and to be suitably integrated in the matrices. Different approaches have followed: (i) physisorption/chemisorption of polymerized ionic liquids (PIL), (ii) grafting of polymers onto oxidized nanotubes, and (iii) growing of polymer chains similar or compatible with the polymer matrices of composites onto functionalized CNT surfaces using initiators, *via* ‘grafting from’ or ‘grafting to’ techniques.

The present manuscript is composed of five chapters. Chapter I gives a comprehensive literature review of carbon nanomaterials (CNT and graphene) – ionic liquid (including PIL) hybrid materials. Chapter II describes the results obtained for the non-covalent functionalization of CNT with PIL. Chapter III details the preparation of CNT/polyetherimide composites as well as their mechanical, thermal and electrical properties. Chapter IV presents the results on the covalent functionalization of CNT with various polymers, which should be

compatible with the epoxy matrix. Finally, Chapter V provides the experimental details of this work.

Chapter I:
**Literature review of carbon nanomaterial–ionic
liquid hybrids**

Chapter I: Literature review of carbon nanomaterial–ionic liquid hybrids

I.1 Introduction

Carbon nanotubes (CNTs) are a unique form of carbon presenting outstanding mechanical, thermal and electronic properties. Their first high resolution TEM observations date from the beginning of the 90s [1,2]. They can be considered as a rolled-up sheet of graphene. Besides having a single cylindrical wall (single-walled CNTs, SWCNTs), nanotubes can be composed of multiple concentric cylinders (multi-walled CNTs, MWCNTs). Over the last two decades, a great number of research activities have been devoted to their potential application for energy storage and conversion devices, sensors, probes, conductive and high-strength composites, to cite some of them [3]. However, to date, the widespread application of CNTs has been limited by difficulty in processing due to their tendency to agglomerate. In order to fully exploit their properties, it is important that CNTs are well dispersed in the matrix or solution. Therefore, the development of new and efficient methods to disperse CNTs is of fundamental importance to improve the properties of the resulting materials. In this respect, ionic liquids emerge as an alternative material for obtaining well-dispersed carbon nanomaterials. The term ionic liquids (ILs) refers to liquids composed entirely of ions, which are fluid around or below 100 °C. Over the past few years, ionic liquids gained considerable attention as “green media” for chemical reactions, owing to their unique characteristics, as low toxicity, high boiling point, high ionic conductivity and good solvation properties, which dramatically change the outcome of various reactions. Their properties can also be adjusted to meet the requirements of a particular process. For this reason, they have been at the same time referred to as “designer solvents”. Other than being used as solvent for organic synthesis, they have a wide range of applications as tailored lubricants, high-performance liquid electrolytes

in devices or composite materials, with nanoparticles and polymers [4]. They can also find application in electrochemical analysis to prepare novel modified electrodes and electrochemical biosensors [5]. The combination of ILs and carbon nanotubes was firstly reported in 2003, when Fukushima et al [6] found that CNTs could form gelatinous materials, also called bucky gels, upon being ground with room temperature ILs (RTILs). Since then, CNT–IL hybrids have attracted great attention and their application in different fields from electrochemistry to polymer composites has been extensively studied (Figure I.1).

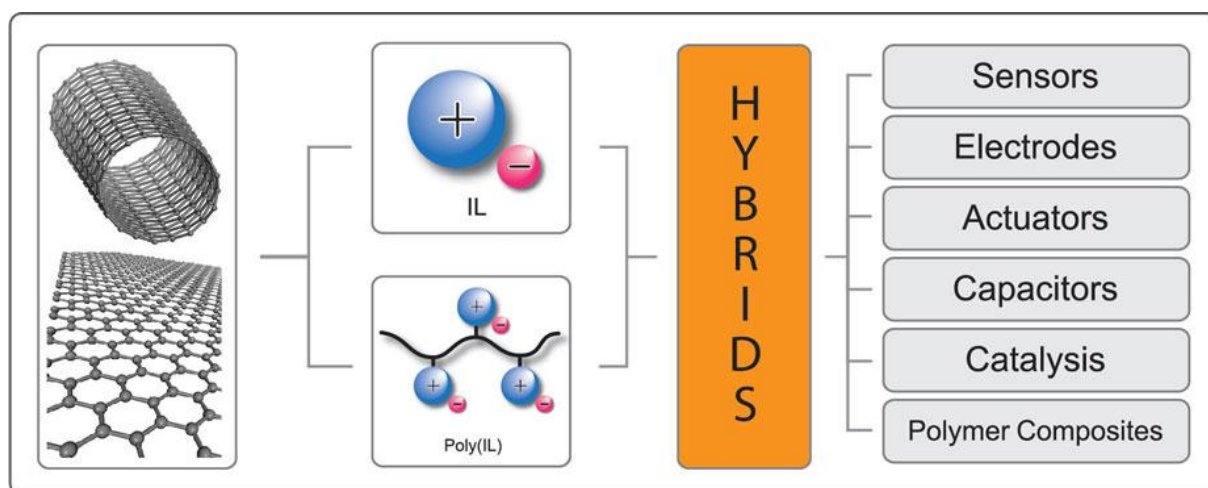


Figure I.1. Emerging applications of carbon nanomaterial–ionic liquid hybrids

CNT–IL based hybrids offer the possibility to improve the device performances and to develop novel multifunctional materials by combining the individual properties of both components, such as the high electric conductivity and tensile strength of CNTs with the high ionic conductivity and solvation ability of ILs. Furthermore, by simple anion exchange reactions, the solubility of the nanomaterials modified by ILs can be easily tuned. The synergistic effect of CNTs and ILs promotes several catalytic reactions and direct electrochemistry of proteins/enzymes [7,8]. Despite continuous efforts, the methods to process CNTs have not yet met commercial expectations, and now its cousin graphene is on

the rise. Within the family of carbon nanomaterials, graphene is another emerging class of material that has been intensively studied (Figure I.1) since its direct observation and characterization reported in 2004 [9]. As it is an unrolled form of carbon nanotube, both its properties and the problems in its processing are similar. Thus, almost every functionalization and dispersion approach applicable to CNT can also be applied to graphene. The number of scientific papers published each year on carbon nanomaterial–IL hybrids has been steadily increasing. Most works on carbon nanomaterial–IL hybrids refer to CNTs. The present chapter will focus on CNT–IL hybrids, including their preparation, characterization and potential applications. In the last part, we will review graphene–IL hybrids with brief comparisons to CNT–based ones.

I.2 CNT–IL hybrids

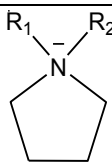
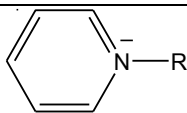
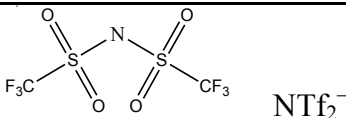
I.2.1 Preparation and characterization

Some years ago, Fukushima et al. [6] found that RTILs are capable of dispersing CNTs. Since this discovery, a lot of research has been focused on the preparation of CNT–IL hybrids by various methods. In these hybrids, except a few cases [10,11] where ILs have been confined in CNTs, ILs are coated on the outer surface of CNTs *via* covalent or non-covalent methods. There, ILs can have three major roles. While they can be used in small quantities to disperse CNTs in a matrix or solution, they can, as well, act as a binder between CNTs and another component. IL can also be the main component of the hybrid in which CNTs can disperse readily without any additional dispersing agent. Whatever the main role of the IL in the resulting materials, all of them are fabricated taking advantage of the synergistic effect of CNTs and ILs and, for the non-covalent method, the attractive CNT–IL interactions. There

are not many systematic studies concerning the non-covalent interactions between CNTs and ILs, and there is a debate over the nature of these interactions. Most of the researchers publishing in this domain have assumed that IL interacts with CNT through cation- π and/or π - π interactions. In their investigations, Subramaniam and coworkers [12] observed a slight up shift of 3–4 cm^{-1} for both D and G bands in the Raman spectra of MWCNTs physically modified by an IL, which they attributed to the cation- π interaction between the imidazolium cation and the π -electrons of nanotubes and/or to the perturbation of π - π stacking of the graphene layers of the nanotubes. In another investigation [13], FTIR studies showed an evidence of this type of interaction. On the other hand, Wang et al. [14] carried out a systematic study on the mixtures of ILs and SWCNTs using Raman and IR spectroscopies, together with molecular modeling, which revealed that the interactions are weak van der Waals with no obvious influence on the electronic structure of SWCNTs. As we will see, many contradicting results exist in the literature concerning the Raman and IR analyses of CNT-IL hybrids. In this section different preparation methods and characterizations that have been reported in the literature for CNT-IL hybrids have been summarized. Table I.1 shows the most common cations and anions used for the preparation of CNT-IL hybrids. It is worth mentioning that ILs are not limited to N-containing cations, and that a huge number of combinations is possible.

Table I.1. The most common cations and anions used for CNT-IL hybrid preparation.

Cations	R_1	R_2
	H,	C_2H_5 , CH_3
	C_4H_9 ,	C_8H_{17}

Imidazolium	C_2H_3	C_2H_5
	C_4H_9	CH_3
Pyrrolidinium		
	R	
	C_2H_5, C_4H_9	
Pyridinium		
Anions		
		
Cl^- , Br^- , BF_4^- , PF_6^-		

1.2.1.1 CNT-IL hybrid formation by “soft” physical methods

Non-covalent functionalization methods offer an easy way to modify the surface of CNTs without altering their chemical structure. This is particularly important for applications where high electrical conductivity is demanded. Thanks to the specific interactions between ILs and CNTs, non-covalent functionalization can be easily carried out. In this context, we will discuss different types of CNT-IL hybrids prepared with non-covalent interactions including bucky gel, CNT-polymerized IL hybrids and CNT-IL hybrids formed in liquid dispersions.

1.2.1.1.1 Bucky gels

In 2003, Fukushima et al [6] discovered the formation of gelatinous soft materials called “bucky gels” composed of SWCNTs and imidazolium ion-based ILs. The discovery of bucky gel has attracted much attention in the carbon nanotube community as it enables to prepare soft materials with well dispersed CNTs, combining the unique properties of ILs and CNTs. While the traditional dispersants require appropriate solvents, ILs disperse CNTs forming soft materials, which can be used for a wide variety of applications, mainly in the field of electrochemistry. Bucky gels can be easily prepared by grinding (or strongly sonicating) a mixture of CNTs and IL (Figure I.2). In the original report, an imidazolium-based IL was mixed with 0.5–1 wt.% (critical gel concentration) of SWCNTs. However, the formation of bucky gel is not only limited to SWCNTs and imidazolium-based ILs. Similar gelation can take place with a variety of CNTs [15–17] and ILs, e.g., pyridinium- and pyrrolidinium-based ILs [18,19]. Furthermore, the amount of CNTs can be increased up to 20% by grinding [20] and up to 33 wt.% by a two-step process using a ball-mill method [21]. The formation of the gel has been reported to be originating from the possible specific interactions between the cation of the IL and the π -electrons of nanotube surface. The molecular ordering of non-volatile ILs and the networking of CNTs by weak physical bonds give rise to the formation of the gel. Gel formation highly increases the dispersion of CNTs. The dispersions formed by the addition of the bucky gel in an appropriate solvent are much more stable than those formed by mixing CNTs and IL [22].

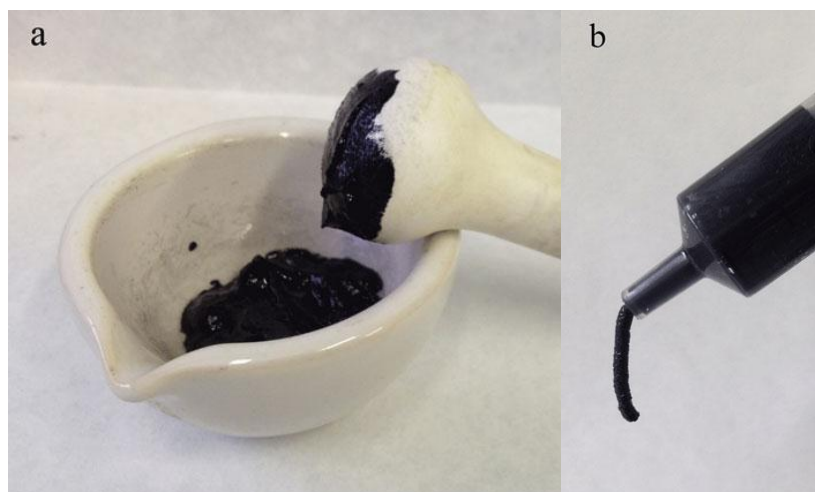


Figure I.2. Picture of a bucky gel (a) prepared by grinding a suspension of MWCNTs in the ionic liquid [BMIM]NTf₂ and (b) extruded from a syringe.

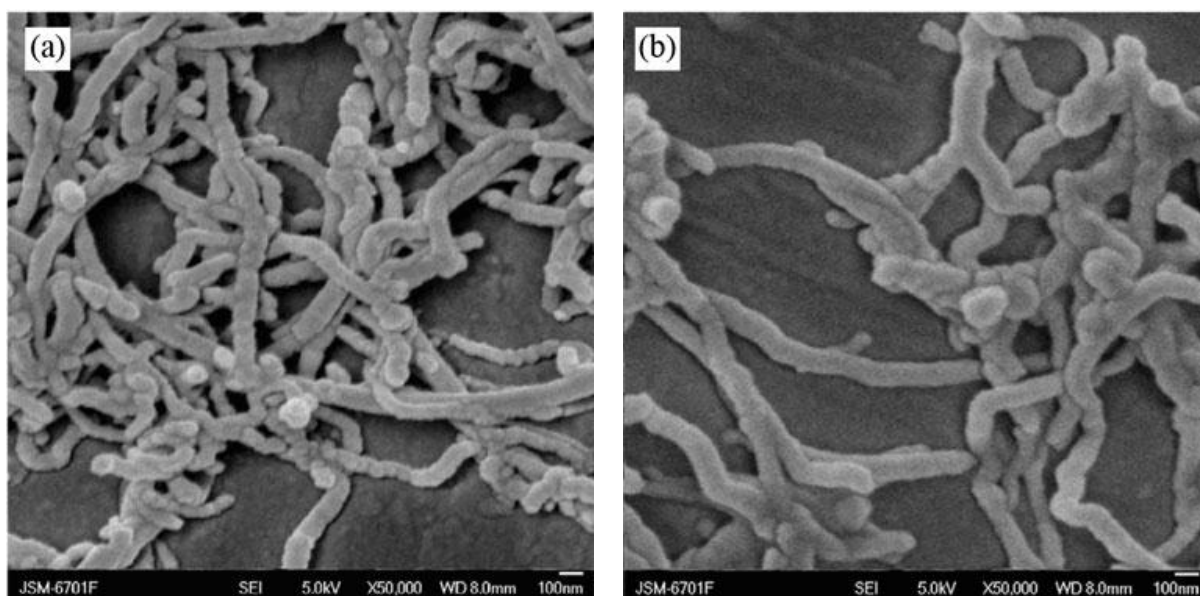


Figure I.3. SEM images of (a) MWCNTs and (b) MWCNT-IL gel (1:4) dispersed in ethanol by sonication. (Scale bar = 100 nm) [23]

The formation of CNT-IL hybrid can be analyzed by different techniques such as SEM, TEM, Raman, XPS, UV-Vis and FTIR. The SEM images in Figure I.3 show the morphologies of pristine MWCNTs and MWCNT-IL gel. The image of the latter reveals that the diameter of the CNTs has increased and IL covers uniformly the surface of the CNTs,

which are less tangled than the unmodified ones. Raman spectroscopy is a powerful tool for the structural characterization of CNTs. Figure I.3 shows examples of Raman spectra of SWCNTs, SWCNT–IL hybrid and neat IL. The adsorption of IL significantly changes the spectrum of CNTs. While in the spectrum of purified CNTs, the disorder-induced D-band at 1340 cm^{-1} is negligible; its intensity increases significantly in the case of modified CNTs. This is attributed to overlapping Raman features coming from the added layers on CNTs. There are contradicting results on the Raman shift in the literature. For example, Du et al. [24] observed two shifts on the Raman spectrum of a bucky gel (Figure I.4). The peak at around 1095 cm^{-1} coming from the IL upshifted to 1120 cm^{-1} in the gel. Another upshift of 22 cm^{-1} has been observed in the tangential G-band of SWCNTs at 1565 cm^{-1} . Zhao et al [25] reported a slight upshift of around 2 cm^{-1} in the G-band of MWCNTs. The authors pointed it as a confirmation of the charge transfer from IL to CNTs due to the cation– π or π – π interactions. On the other hand, several groups [6,26,27] did not observe any peak shifts on the spectra of the SWCNT–IL gel, which was explained by the absence of any structural modification.

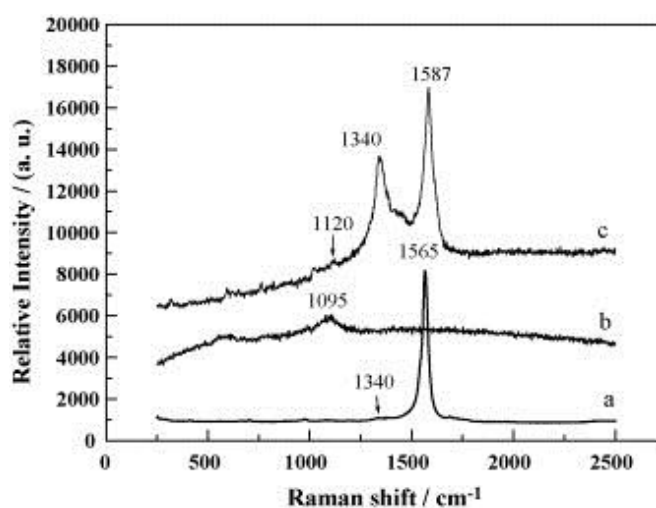


Figure I.4. Raman spectra of purified SWCNTs (a), [BMIM]BF₄ (b), and SWCNT–[BMIM]BF₄ gel (c) collected using a 514.5 nm excitation energy [24].

As far as XPS analysis is concerned, a typical bucky gel based on SWCNTs and an imidazolium IL exhibits a peak at 399.5 eV corresponding to the N 1s binding energy of the imidazolium ion [24]. Further peak analysis using a nonlinear regression reveals that the main peak includes two different types of N 1s contributions at 399.4 and 401.0 eV. The presence of different types of nitrogen atoms in the gel indicates that the imidazolium ion has been modified due to the interactions with the CNT. Additionally, a shift of the absorption band of IL in the UV–Vis spectra of the gel can suggest some kind of non-covalent interactions between IL and CNTs [23,27]. Xiao et al [22] observed that the carbonyl and hydroxyl peaks of MWCNT–COOH shifted on the IR spectra of CNT–IL gel. The interactions between IL and CNT can induce a change in the thermal properties of the components. The onset point of decomposition of IL in the gel shifts to a higher temperature [15] and the DSC profiles significantly differs from those of neat IL [6]. It is worth mentioning that similar phenomenon has also been observed for IL supported on silica, except that, in that case, IL decomposes at a lower temperature than neat IL [28]. The authors suggested that the strength of IL–support interaction can be estimated through an evaluation of the thermal stability of the IL component by TGA. In fact, according to XRD patterns, in both cases IL losses its polycrystalline structure; however, while silica changes its structure to amorphous, CNT incorporation triggers the long-range molecular ordering of IL, which can be associated with the increased thermal stability.

1.2.1.1.2 CNT–polymerized IL hybrids

Recently, much attention has been paid to polymerized ionic liquids or polymeric ionic liquids (PILs), which are prepared from polymerizable IL monomers [29]. They combine some of the unique properties of ILs with the improved mechanical stability and dimensional control. They find potential applications in various fields such as ionic conductive materials, sorbents, porous materials, dispersants, polymeric electrolytes and electroactive polymers.

PILs are commonly obtained from the IL monomers bearing a vinyl or acryloyl group as polymerizable group on the cation moiety through thermally initiated free radical polymerization. Non-covalent wrapping of CNTs in ILs does not lead to very stable dispersions of CNTs in water or organic solvents [25]. On the other hand, covalent functionalization usually requires several reaction steps and the electronic structure of CNTs can be disrupted. Yet polymerized ionic liquids could wrap CNTs to form stable dispersions and strong hybrids. CNT–PIL hybrids have been developed in parallel with CNT–IL hybrids [6].

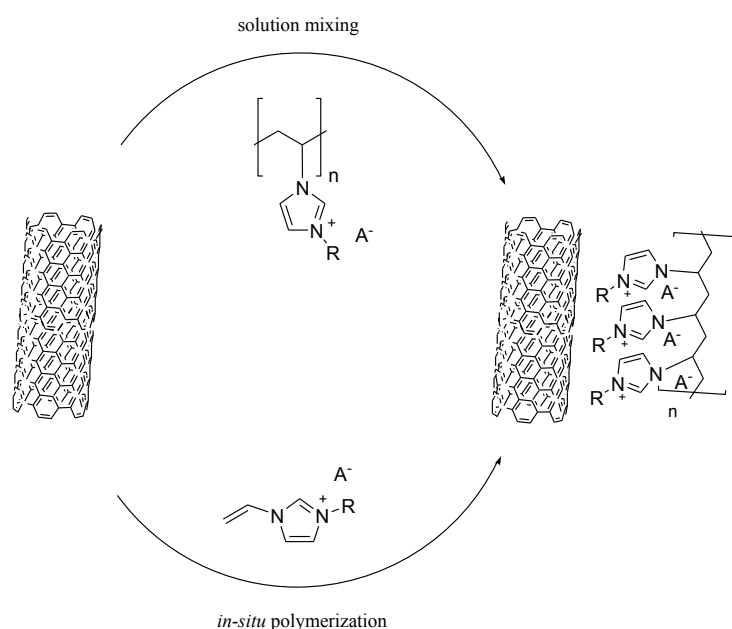


Figure I.5. Schematic representation of two routes for non-covalent functionalization of CNTs.

Generally two methods are used to functionalize CNTs by PILs: *in situ* and solution-mixing (Figure I.5). The first method involves free-radical polymerization of the IL monomer in the presence of CNTs. In the second one, CNTs and previously synthesized PILs are mixed in an appropriate solvent. By simple anion exchanges, the properties of the resulting hybrids can be

modified. Generally the two methods can be successfully used to functionalize CNTs with similar quantity of imidazolium-based PIL. Bucky gels can be in situ polymerized using polymerizable IL monomers [30,31]. Interestingly, CNT–PILs can also be precipitated as bucky gel if the CNT loading does not exceed 2 wt.% during polymerization [15]. With hydrophilic PILs, acid oxidized CNTs can be used to increase the dispersibility [15]; however, the acid oxidation process causes some structural damage to the CNTs [30]. As for CNT–IL, the PIL coating on the CNT surface can be characterized using various common characterization methods including TEM, SEM, TGA, IR, XPS and Raman spectroscopy.

The amount of the PIL layer on the surface of CNTs can be calculated from the sharp weight loss in the range of 500–700 K in the TGA curves. FTIR spectrum of PIL modified CNTs shows the additional peaks coming from the PIL layer. As for CNT–IL, contradicting results have been obtained from the Raman analysis of CNT–PIL hybrids in different studies. Fukushima's group [30] has found no change in the Raman spectra of the SWCNT–PIL hybrid prepared by in situ method compared to that of the unmodified SWCNTs. On the other hand, other groups reported a down shift of 3 cm^{-1} of the G band of SWCNT–PIL prepared by in situ method [15] and an up shift of 8 cm^{-1} for the sample prepared by solution mixing method [32]. Furthermore, the D/G ratio significantly decreased [15,32] or slightly increased [33] in different examples. While the reason for the decrease is not clear, the D/G increase of the MWCNTs was reported to be due to the slight structural damage caused by the PIL modification process. Marcilla et al [34] developed a reversible method based on PILs, which allows the transfer of CNTs between aqueous and organic phases (Figure I.6).

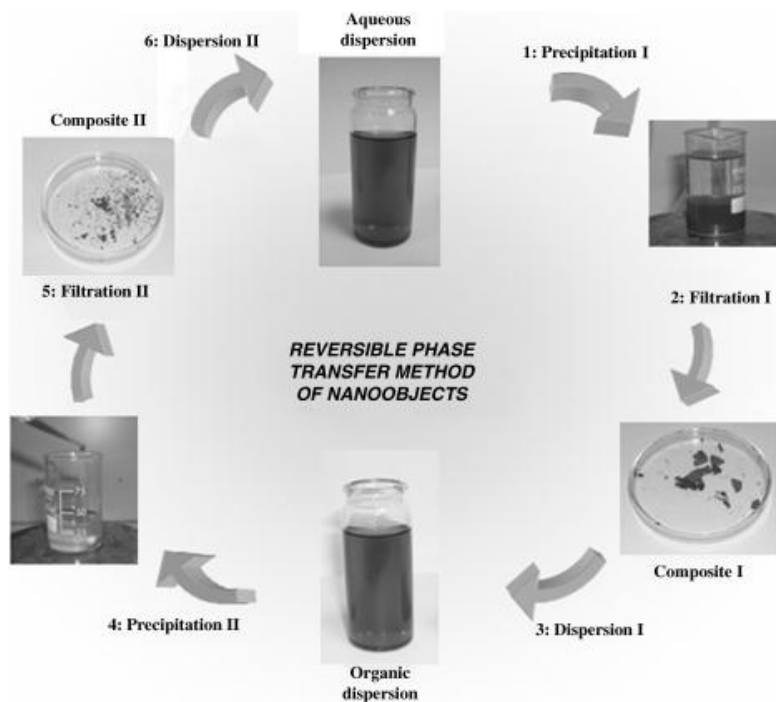


Figure I.6. Procedure for the reversible transfer method of nano-objects between aqueous and organic phases [34].

The CNT–PIL hybrid recovered from one phase can be dispersed in another one through simple anion exchange reaction of the PIL. During the precipitation of the anion-exchanged polymer, the PIL stabilized CNTs are trapped in the polymeric matrix resulting in the formation of a homogeneous CNT–PIL hybrid. This reversible process can be repeated many times without causing any loss in the properties of the CNTs. The resulting dispersions remain stable for several weeks.

The formation of the PIL film on the surface of CNTs enables to anchor different types of materials for the construction of functional hybrids or composites. For example CNT–PIL hybrids can be used as an effective template for anchoring conducting polymers such as poly(3,4-ethylenedioxy thiophene) (PEDOT) [32]. IL acts as a linker between CNTs and PEDOT by only non-covalent interactions. Due to their high stability, PIL coated CNTs can

be efficiently used to modify electrodes for direct electrochemistry and biosensing applications [31], or to deposit uniformly metal nanoparticles on CNTs for supported catalysis applications [33,35].

1.2.1.1.3 CNT–IL hybrid formation in liquid dispersions

As already pointed out, the major obstacle in processing CNTs is their poor dispersion in organic and aqueous solvents. Up to now, different approaches have been used to disperse them in solvents, including polymer and DNA wrapping, side-wall functionalization, adsorption of aromatic molecules and addition of surfactants [14]. However, none of them is fully suitable for large-scale applications. Recent studies have shown that ILs can be used to stabilize efficiently CNTs in various solvents. Although generally all types of ILs can disperse well CNTs, as mentioned above, PIL is particularly effective in preparing long-term stable organic dispersions. As far as aqueous dispersions are concerned, long-chain ILs, which behave as surfactant, can be a good alternative. Stable aqueous dispersions of CNTs are especially needed in the field of biotechnology and water-soluble polymer hybrids. Traditional ionic surfactants, such as sodium dodecyl sulfate (SDS), are not thermally stable for melt-blend processing [13]. Several types of long- and short-chain ILs have been investigated to disperse CNTs in aqueous solvents. As traditional surfactants, IL-based surfactants adsorb on the CNT surface *via* their hydrophobic long alkyl chain orienting their hydrophilic cationic imidazolium groups toward the aqueous phase. The positive charges created on the CNTs prevent them to aggregate. Surfactant-like long-chain ILs such as 1-alkyl-3-methylimidazolium bromides [36], butyl- α,β -bis(dodecylimidazolium bromide) [37], carbazole tailed ILs (1-n-(*N*-carbazole)alkyl]-3-methylimidazolium bromide) [38] and imidazolium ion-based ILs with hexadecyl alkyl chain [39,40] have been found to be quite effective in dispersing CNTs in water. Additionally, the functional groups (e.g., thiol) of the alkyl chain-ends of the surfactants can enable the direct self-assembly of the CNTs from

aqueous dispersion on solid surfaces such as gold (Figure I.7). To measure the efficiency of a dispersing agent and to quantify the amount of individual CNTs in a solution, UV–Vis–NIR spectroscopy can be used. While CNTs in bundles are not active in the UV–Vis–NIR region, individual CNTs exhibit a characteristic absorption band at around 260 nm [37]. Another method used to evaluate the dispersion stability is ζ -potential measurement. A measured potential of a suspension less than -15 mV and more than $+15$ mV indicates the stability of the suspension [39]. Raman spectroscopy is used to reveal the type of dispersed CNTs and any structural damage caused during processing.

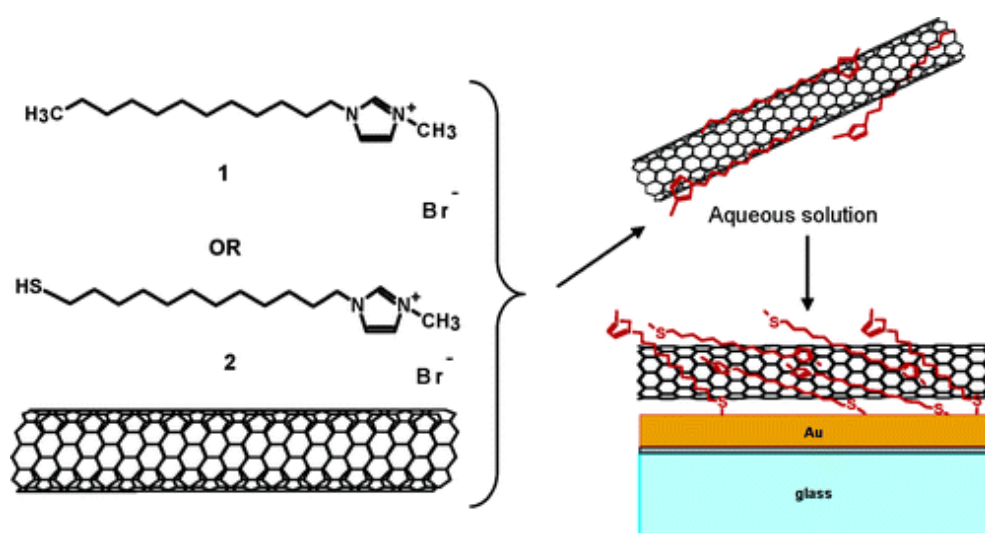


Figure I.7. Schematic illustration of noncovalent functionalization, thiolation, and self-assembly of SWCNTs with 1-alkyl-3-methylimidazolium bromides [36].

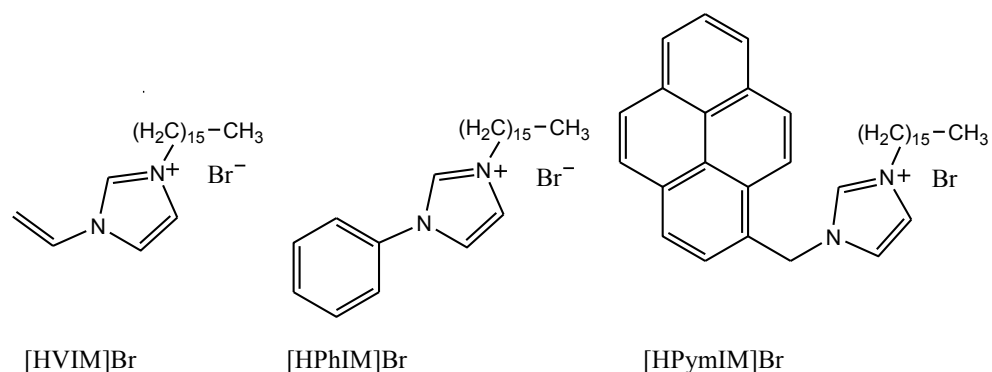


Figure I.8. Investigated ionic liquid surfactants with a hexadecyl alkyl chain [39].

The dispersing ability of the surfactants generally increases with the increasing length of the alkyl chain [37,38]. This effect is reflected by an increased absorbance on the UV–NIR-spectrum. The effect of different groups at the 3-position of the imidazole ring with a hexadecyl alkyl chain (Figure I.8) on the CNT dispersing ability has been investigated [39]. Through a systematic study, it has been found that hydrophobic groups (e.g., phenyl group) increase the affinity of the surfactant toward CNTs, but a too hydrophobic group decreases the water solubility of the surfactant, thus favoring the self-assembly. Hence, a good balance between the hydrophilic and hydrophobic domains is needed to get a good CNT surfactant. Results of this study demonstrate that 1-hexadecyl-3-phenylimidazolium bromide ([HPhIM]Br) is the most efficient one among the investigated surfactants. Liu et al [37] showed that IL-based Gemini (dimeric) surfactants, which consist of two imidazole ring head groups and two hydrophobic chains separated with a spacer, are more effective in dispersing CNTs than the IL-based monomeric surfactants. The long alkyl chain ILs form aqueous dispersions of CNTs, which remain stable for months. However, it is challenging to disperse CNTs using very small amounts of dispersing agent by physical methods. Zhou et al [41] investigated the dispersion of CNTs using very small amounts of short-chain ILs in water and found that ILs bearing both an amino group and imidazolium or pyridinium core are very effective in dispersing CNTs in water. A very small quantity of IL, as little as 1.4 wt.% of the CNT–IL hybrid, is sufficient to achieve this. The interactions of these ILs with CNTs have been found to be stronger than those of other ILs investigated. CNT–IL hybrid can also be used as an emulsifier. Gao et al [42] prepared oil-in-water emulsions stabilized solely by the adsorption of CNT–IL hybrid at the oil-water interface. Moreover, the size of the droplets can be controlled by the amount of CNT and IL added into the mixture.

I.2.1.2 CNT–IL hybrid formation by “hard” chemical methods

The functionalization of CNTs by ILs *via* covalent method is another approach to produce CNT–IL hybrids. This approach offers some advantages over the non-covalent one in terms of flexibility on the IL choice, and control over the functionalization degree. Furthermore, as the CNT and IL are linked chemically, the CNT–IL hybrid is expected to be more stable. As far as drawbacks are concerned, this methodology requires several functionalization steps and causes the disruption of the extended π -networks of the CNTs, impairing their desired mechanical and electrical properties, which is particularly true for SWCNTs [13]. The covalent modification of CNTs by ILs can be carried out in two ways: IL can be either directly grafted to the CNT surface or generated on the CNT after the imidazole component is grafted. For the first method, CNTs are firstly purified and oxidized using a strong acid to introduce carboxyl groups, which enable to graft amine or hydroxyl terminated ILs to the CNT surface. The surface carboxylic acid groups can be activated using either thionyl chloride (SOCl_2) [43,44], or *N,N'*-dicyclohexylcarbodiimide (DCC) in DMF [45,46]. In the second method [44,47,48], the imidazole derivative is reacted with the activated surface of the CNT through its functional group as in the example given in Figure I.9 (a). Subsequent reaction with an alkyl halide gives the corresponding IL-functionalized CNTs. The anion exchange can be easily carried out on the IL-grafted CNTs to tune their solubility and other properties such as conductivity and wettability.

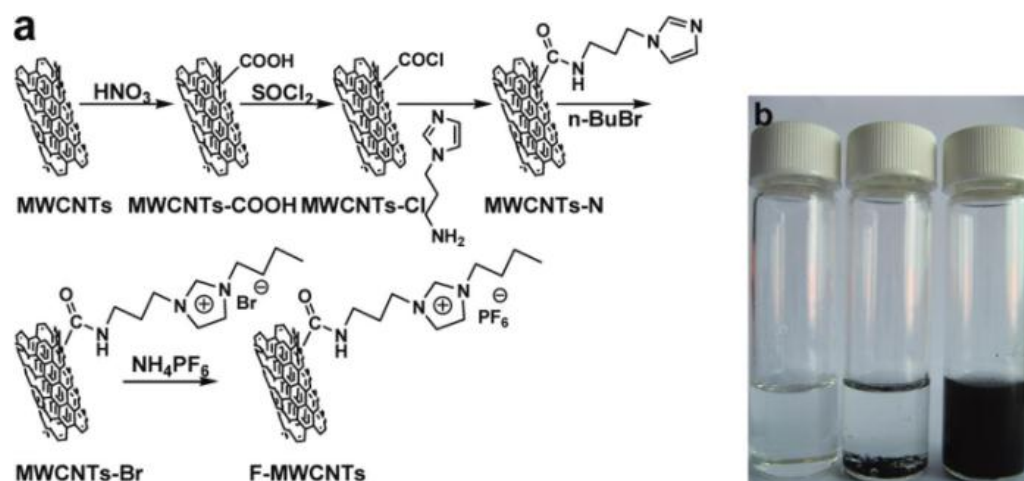


Figure I.9. (a) Schematic procedures for synthesizing functionalized MWCNTs and (b) photos of pure $[\text{BMIM}]\text{PF}_6$, $[\text{BMIM}]\text{PF}_6$ suspensions of pristine MWCNTs, and functionalized MWCNTs (from left to right). The samples were equilibrated for 2 weeks after preparation [44].

Characterization of chemically modified CNTs is quite problematic. Techniques commonly used in organic chemistry such as NMR, FTIR or UV-Vis do not always give reliable results. Different methods should be used in combination and the results should be carefully interpreted in order to verify the nature of the modification. The most commonly used characterization techniques for these hybrids include Raman spectroscopy, FTIR, TGA and XPS. Although FTIR spectra of CNTs are not generally easily interpreted, the strong carbonyl peak of functionalized CNTs is useful to determine any covalent grafting. A shift of this peak indicates the successful grafting of IL to the CNT. While the C=O vibration of the carboxylic acid group exhibits a peak at around 1710 cm^{-1} , functionalization shifts this peak to around 1650 cm^{-1} and 1725 cm^{-1} for amide and ester groups, respectively. Additionally, anion transformations can be observed through the characteristic bands of each anion. For example, Figure I.10 shows the typical FTIR spectra of MWCNTs and functionalized MWCNTs. The

carbonyl vibration peak of the carboxylic acid at 1717 cm^{-1} shifts to 1641 cm^{-1} after amine terminated IL is grafted to the CNT. The relative intensities of these two bands can indicate the grafting degree. The band at 830 cm^{-1} corresponds to the P–F stretching vibration of the PF_6 anion of the IL.

In the Raman spectra (Figure I.11) of pristine SWCNT, acid-treated SWCNT (SWCNT–COOH) and IL-grafted SWCNT, we can observe a gradual increase of the D band. In the Raman spectra of acid-treated CNTs, an increase of the disorder induced D-band compared to the pristine CNTs can be an indication of successful grafting of –COOH groups because grafting generates sp^3 hybridized carbon atoms on the carbon framework. However, in the case of CNT–IL, it is difficult to assess covalent functionalization based on Raman features, since IL molecules attach to the surface –COOH groups and this process does not further alter the structure of the CNTs. Furthermore, increase of the D/G band ratios and shifts of Raman bands have also been reported for CNT non-covalently modified by ILs [15,25,32,33,49].

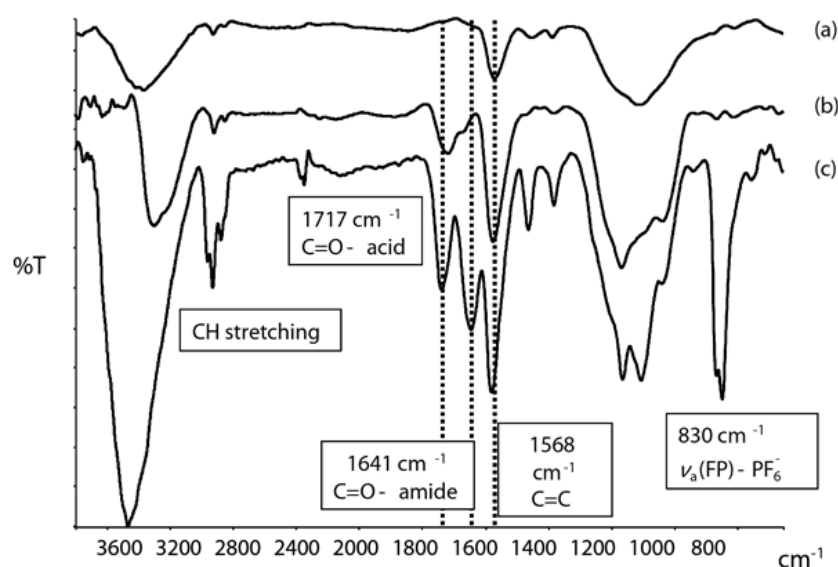


Figure I.10. FTIR spectra of MWCNTs (a), oxidized-MWCNTs (b) and MWCNT–IL– PF_6

[48].

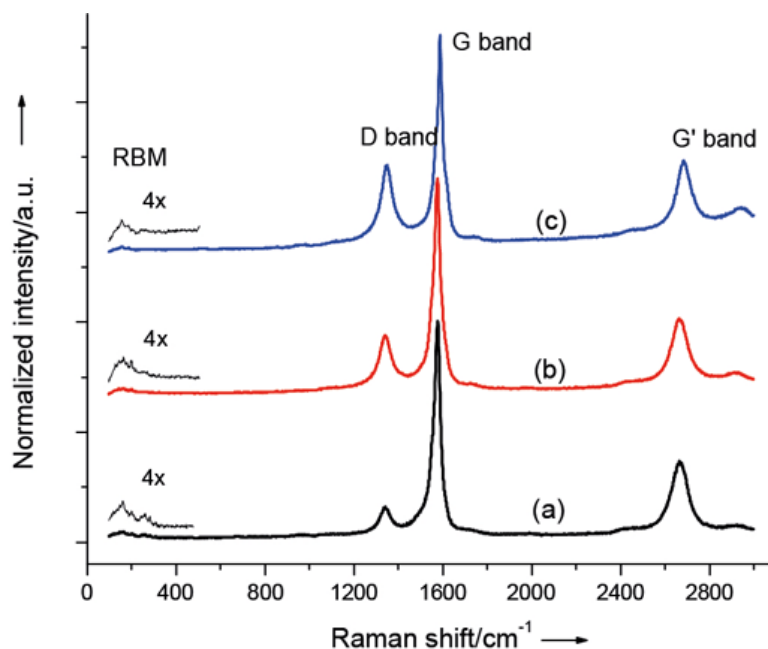


Figure I.11. Raman spectra of SWCNTs (a), SWCNT-COOH (b), and SWCNT-IL-Br (c) [46].

X-ray photoelectron spectroscopy is another technique that can be used to analyze the grafting of IL to CNTs and the type of anions present in the CNT-IL. In different studies [42–45,47], the strong N 1s signal at around 401 eV or 402 eV has been attributed to the grafted imidazolium moiety. ζ potential measurements can also be used to verify covalent grafting. While the ζ potential of CNT-COOH has been found to be between -60 and -42 mV, it goes up to $+23$ mV after CNTs are functionalized with $\text{NH}_2\text{-IL}$ [45,50].

The amount of the grafted IL moiety can be determined from TGA. Under air atmosphere, the onset decomposition temperature of pristine CNTs occurs between 773 K and 873 K depending on the sample and the heating rate. For the functionalized ones usually two major weight losses are observed. The first weight loss that is below 623 K and the second one after 773 K correspond to the decomposition of IL and CNT fragments, respectively. The thermal

stability of the modified CNTs depends on the type of the IL counteranion. For example, according to the TGA curves in Figure I.12, the stability of the MWCNTs bearing BF_4^- or PF_6^- anions increased, whereas the functionalized MWCNTs bearing Br^- or NTf_2^- anions decomposed at a significantly lower temperature. However, the nature of this anion effect on the thermostability of CNTs has not yet been rationalized.

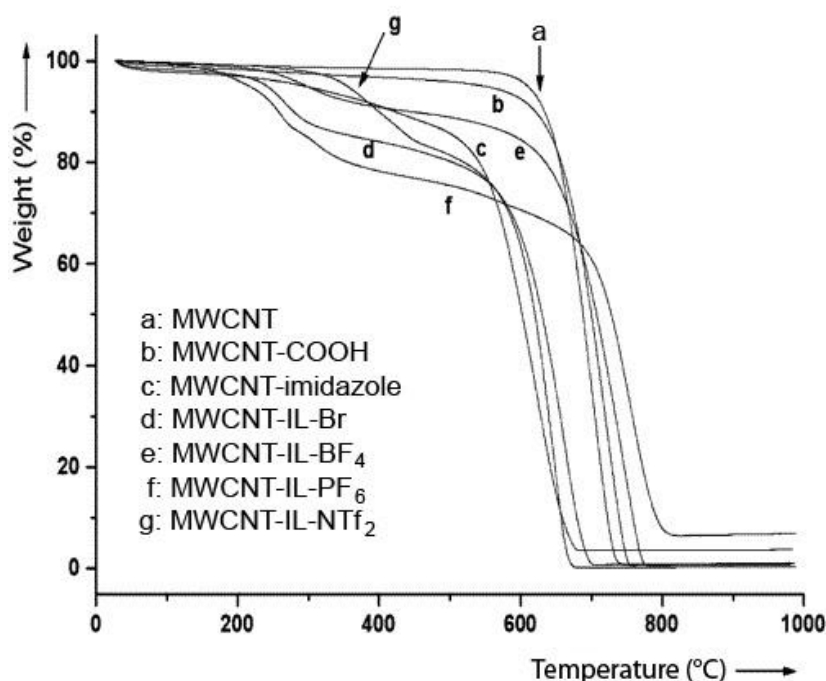


Figure I.12. TGA curves of MWCNTs before and after various functionalization and anion-exchange steps (heating rate, 20 K min^{-1} ; air flow, 20 mL min^{-1}) [47].

1.2.2 Applications

CNT-IL hybrids have been extensively studied in the field of electrochemistry, catalysis and composite materials. Potential applications include sensors, actuators, super capacitors, dye-sensitized solar cells, elastic conductors, supports for metal nanoparticles, additives for lubricants and polymer nanocomposites. ILs can function as dispersant and/or binder for CNTs, as well as, as major component in the final hybrid or composite.

1.2.2.1 Electrochemical devices

Due to the unique electrical properties of ILs and CNTs, their combination is particularly useful for the fabrication of electrochemical devices. The studies in this field mainly concentrate on the sensing and biosensing area.

1.2.2.1.1 Electrochemical sensors

CNTs possess remarkable electrocatalytic properties and they have been evaluated in electroanalytical chemistry for constructing CNT-based sensors [51]. However, the applications of CNTs in sensing and biosensing field have been greatly hindered because of their poor dispersibility in many solvents [52]. Besides, especially due to their good electrochemical stability, conductivity and wide electrochemical windows, ILs have become very promising materials for modifying electrodes [5]. CNT-IL based electrodes can display better performances compared to electrodes based on either IL or CNTs, owing to their synergistic effect. Fukushima et al [6] found that the bucky gel based polymer at a CNT loading of 3.8 wt.% had an electrical conductivity of 0.56 S cm^{-1} at room temperature, and therefore CNT-IL hybrid could be used to improve the performance of electrodes. Following this finding and the developments in IL or CNT based electrodes, Zhao et al [16] firstly combined these two materials in 2004 to build a novel electrode and investigated its electrochemical properties. The authors prepared a gel by grinding MWCNTs and 1-butyl-3-methylimidazolium hexafluorophosphate ([BMIM]PF₆) with an enzyme and coated a thin layer of the prepared mixture on the electrode surface. They found that the modified gold and glassy carbon electrodes could efficiently catalyze the reduction of O₂ and H₂O₂ in aqueous solution.

It was rapidly seen that CNT-IL electrodes could have great application potential in electroanalysis. Compared to other type of modified electrodes, CNT-IL modified ones show

the advantages of easy preparation and replacement, rapid response, low-cost, long-term stability, and low detection limit. They display high sensitivity and selectivity for the detection of various electroactive compounds. This is partly because ILs interact with CNTs and form finer bundles, thus more active sites of CNTs are exposed [52,53]. Besides, due to their good biocompatibility, the CNT–IL based electrodes constitute a suitable matrix to immobilize biomolecules like enzymes and proteins. The modified electrodes allow efficient electron transfer between electrodes and the immobilized molecules, which can catalyze various reactions. Recently, CNT–IL modified electrodes have been widely used in investigating the direct electrochemistry of proteins/enzymes and for probing chemical or biological species. These studies establish a foundation for fabricating novel biosensors and bioreactors. The superiority of CNT–IL electrodes comes from the synergistic effect of CNTs and ILs [7,8]. So far, they have been used for the electrochemical detection of various biological molecules such as rutin [23], DNA [53,54], dopamine [55–57], serotonin [55], guanine and adenine [58] and estradiol [52], as well as, ascorbic acid [57,59], alcohols [60,61], hydroquinone [62], glucose [63], H₂O₂ [64], folic acid [7], dextromethorphan [8], quinine sulfate [65], methylparathion [66], nitric oxide [67], chloramphenicol [68], uric acid [69], nitro aromatic compounds [70,71], xanthin [72,73], Sudan dyes [74], lead ions [75] and Ce(III) ions [76]. After enzyme/protein immobilization, they have also been used efficiently in the biosensing of H₂O₂ [16,24,26,31,77–81], O₂ [16,24,31,82], glucose [27,64,83–90], nitrite [22], paraoxan [91], D-amino acids [92], trichloroacetic acid [93,94], NaNO₂ [93], NADH [95,96] and alcohols [96]. One drawback of IL-based electrodes is that they display very high background currents, which can limit their uses for trace analysis. The increased capacitive currents are basically due to the greater accumulation of ions at the water interface of the liquid salts compared to non-conductive binders, such as mineral oil [97]. This is exacerbated further when CNTs are combined with ILs, because the capacitive charging

current of the modified electrode is highly increased due to the increased effective surface area of the electrode by using CNTs [98]. To overcome this problem, some alternative methods have been developed by different groups, which will be mentioned below. In the preparation of CNT–IL modified electrodes, the most frequently used ILs are 1-octyl-3-methylimidazolium hexafluorophosphate ([OMIM]PF₆), [BMIM]PF₆ and 1-butyl-3-methylimidazolium tetrafluoroborate ([BMIM]BF₄). There are also a few examples where a polymerized ionic liquid is used. For example, Jia et al [99] formed a novel PIL by chemically attaching the IL on a polymer and mixed it with MWCNTs in solution. The prepared PIL combined the advantages of IL and the polymer. Xiao et al [31] wrapped SWCNTs with a polymerized IL, 1-vinyl-3-ethyl imidazolium bromide ([VEIM]Br) and casted them on the glassy carbon electrode (GCE). They obtained superior electrocatalytic activities than those obtained with a simple IL–CNT modified electrode. There are various methods to modify the surface of a gold, glassy carbon or graphite electrode using CNTs and ILs. It can be modified either by applying a direct mixture of CNTs and ILs (e.g., bucky gel or paste) or by casting a solution of CNT/IL or CNT/IL/polymer on the electrode. CNT–IL electrodes can also be prepared by layer-by-layer deposition [77,78,100], which consists of depositing each modifier one after another, e.g., first IL and then CNTs on the electrode surface. An enzyme or protein and/or polymer layer can be included and the order of deposition can be reversed.

1.2.2.1.1.1 CNT–IL bucky gel electrodes

One way of fabricating CNT–IL electrodes is to prepare bucky gels and then to smear them onto a gold or glassy carbon electrode. Despite its ease of preparation, this method has still some drawbacks. One drawback of gel modified electrodes is that most of the time the gel is mechanically coated on the electrode surface and does not stick well. In addition, the control of the thickness of the modified gel layer is difficult and affects the electrochemical properties of the electrode. Finally, they suffer from very high background currents as it is the case of

most of the CNT–IL electrodes, which can limit their usages in trace analysis. Xiao et al [22] observed that by grinding ILs with CNTs, the electrochemical response was improved compared to a CNT–IL electrode that was prepared without grinding. There exist some other types of CNT gel electrode examples than the common glassy or graphite carbon electrodes. For example, Zhang et al [84] built a RTIL-supported three-dimensional network SWCNT electrode. At this novel electrode, CNTs can be functionalized electrochemically by enzymes or other types of molecules and used for sensor/biosensor applications. For preventing the leaking of gel electrodes, Li et al [67] developed a nafion-coated microelectrode of which cavity they filled with a SWCNT–IL bucky gel.

1.2.2.1.1.2 CNT–IL paste electrodes

CNT–IL paste electrodes [7,8,54,59,64,76,98] differ from gel electrodes in their composition; a higher proportion of CNT results in a relatively solid material compared to the gel. Figure 13 shows the SEM micrographs of the surface of different carbon paste electrodes. The carbon materials at the surface of the carbon paste electrode and CNT/carbon paste electrode are isolated and there is no conducting binding material between them (Figure I.13 (a) and (b)). On the other hand, the surface of the IL-based electrodes (Figure I.13 (c) and (d)) is uniform and IL fills in the voids between carbon particles/nanotubes. As a result, the conductivity of IL-based electrodes is highly increased.

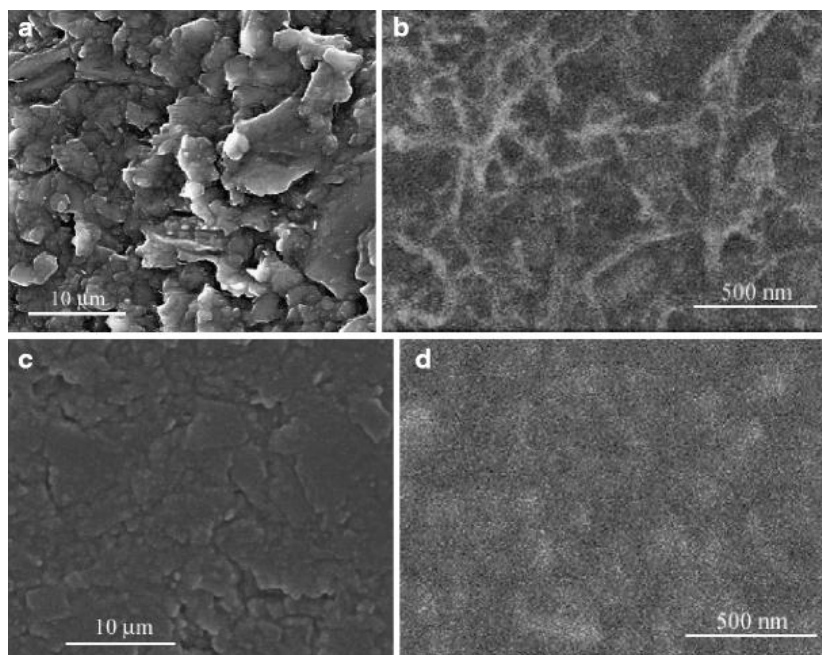


Figure I.13. SEMs of the surface of carbon paste electrode (a), CNT/carbon paste electrode (b), IL/carbon paste electrode (c), and CNT-IL carbon paste electrode (d) [8].

Zhang et al. [54] obtained a far better reproducibility with a paste electrode of CNT-[BMIM]PF₆ than the CNT-[BMIM]PF₆ gel electrode reported previously [57]. The detection limit for DNA sensing was much lower than the CNT paste electrodes prepared with different binders such as mineral oil and chitosan. Another interesting CNT-IL paste electrode was fabricated using an unusual IL [64]. The particularity of n-octyl-pyridinium hexafluorophosphate, [nOPyr]PF₆, is that it gives very low background currents. This IL is solid at RT and does not form bucky gel with CNTs; however because of its sticky nature, it forms a stable material upon grinding with CNTs. Kachoosangi et al [64] compared the as-prepared CNT-IL paste electrode with other types of electrodes and they found that the combination of CNTs with the [nOPyr]PF₆ gave the best electrode performance for the detection of various species. From the SEM images of the electrode surfaces, it is clearly observed that the surfaces of MWCNT-[nOPyr]PF₆ and graphite-[nOPyr]PF₆ are more uniform and homogeneous (Figure I.14 (a) and (d)), the former being the best. Although the

superiority of this unique IL has not been fully understood, it is thought to be related to its solid physical state and/or its less hydrophilic chemical structure than liquid [BMIM]PF₆.

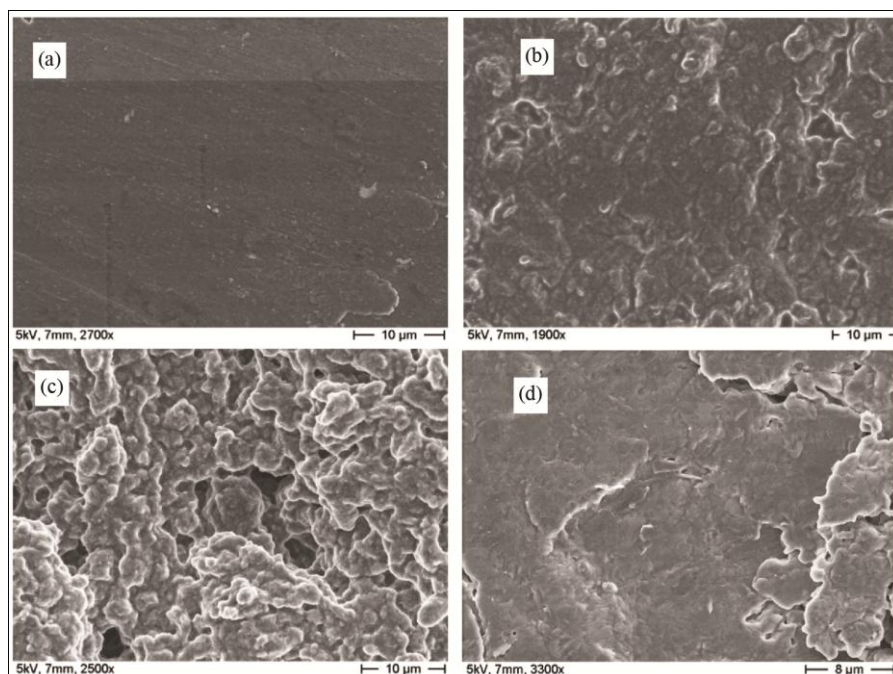


Figure I.14. SEM images of the surfaces of the MWCNT/[nOPyr]PF₆ (A), MWCNT/[BMIM]PF₆ (B), MWCNT/Mineral oil (C), and Graphite/[nOPyr]PF₆ (D) electrodes. Accelerating voltage, 5 kV; carbon/binder composition ratio, 10:90 wt % [64].

For decreasing the very high background currents in CNT–IL paste electrodes, Kachoosangi et al [98] used steady state voltammetry at a rotating disk electrode. The enhanced mass transport to the electrode under the hydrodynamic conditions created increases the Faradaic redox current, which obscures the capacitive charging current of the CNT–IL paste electrode.

1.2.2.1.1.3 CNT–IL electrodes by solvent casting

IL, CNTs and any other components can be casted from a solvent onto the electrode. For this, the electrode modifiers are deposited onto the electrode in either single or several steps (layer-

by-layer) [31,77,78,81,87,100] as illustrated in Figure I.15. The thickness of the modified layer can be controlled more easily with this preparation method than for gel or paste electrodes [77].

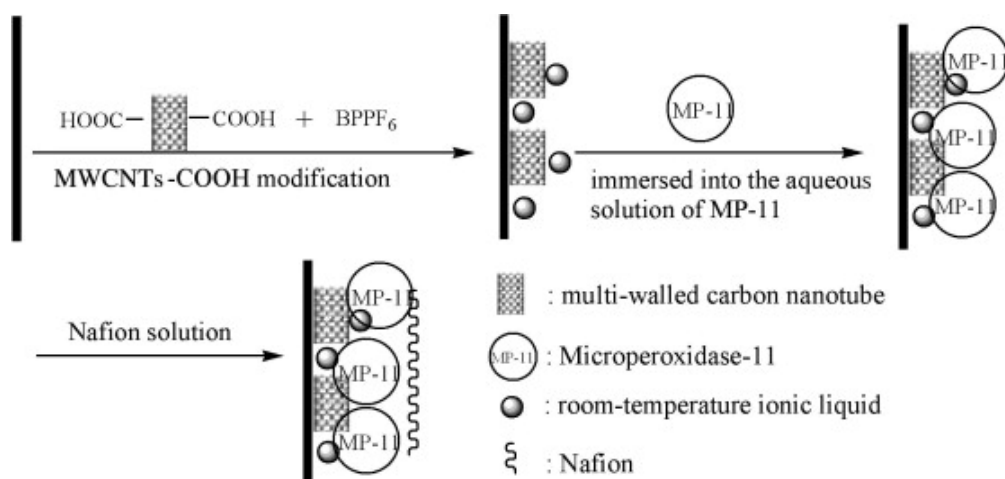


Figure I.15. Preparation approach of (MP-11)-Nafion-MWCNTs-RTIL/GCE [78].

CNTs and ILs can be integrated into polymeric matrices to fabricate an electrode with high stability. Due to their biocompatibility and excellent film forming ability, chitosan, nafion and hyaluronic acid have been widely used as matrix in biosensors and biocatalysis. CNTs, ILs and these polymers can form a uniform suspension with the aid of grinding and ultrasonication [22,71,79,80,86,93,95]. When the suspension is cast on a glassy carbon electrode and dried, a hybrid film coated electrode is obtained. By this way, the CNT-IL is entrapped in the polymer, which forms a stable film on the electrode.

1.2.2.1.1.4 Enzyme/protein immobilization

The combination of CNTs and ILs provides an electrically conductive, biocompatible and porous microenvironment suitable for the immobilization of enzymes and proteins. CNTs and ILs synergistically promote the direct electron transfer between the immobilized species and the electrode [7,8]. Recently, CNT-IL electrodes have been efficiently used to immobilize

biological macromolecules. In most of the cases, significant improvements in terms of sensitivity, detection limit, stability and repeatability have been obtained. Table I.2 shows the detection limits of CNT–IL electrodes for biosensing applications in the literature.

Table I.2. Detection limits of CNT–IL electrodes for biosensing applications.

Electrode	Immobilized molecule	Target species	Detection limit	Ref.
(MWCNT–NH ₂)-[BMIM]BF ₄ /GCE	Catalase	H ₂ O ₂	3.7 nM	[77]
MWCNTs-[EMIM]BF ₄ /GCE	Hemoglobin	Nitrite	0.81 μM	[100]
MWCNTs-[BMIM]Br-Chitosan/GCE	Hemoglobin	Trichloroacetic acid	0.4 mM	[93]
MWCNTs-[BMIM]Br-Chitosan/GCE	Hemoglobin	NaNO ₂	0.1 mM	[93]
MWCNTs-[BMIM]BF ₄ -Nafion/GCE	Hemoglobin	H ₂ O ₂	0.8 μM	[79]
MWCNTs-[BPy]PF ₆ /GCE	Microperoxidase-11	H ₂ O ₂	3.8 nM	[78]
MWCNTs-[BMIM](BF ₄ /PF ₆ /Tf ₂ N)gel/AuE	Organophosphorus hydrolase	Paraoxan	≤ 2 μM	[91]
MWCNTs-[BMPyr]NTf ₂ /GCE	Chlorpromazine	NADH	80 nM	[96]
MWCNTs-[BMPyr]NTf ₂ /GCE	Alcohol dehydrogenase	Ethanol	5 μM	[96]
SWCNTs-[BMIM]BF ₄ /GCE	D-Pro DH	D-amino acids	2 μM	[92]
MWCNTs-[EMIM]BF ₄ -Chitosan/GCE	Cytochrome <i>c</i>	H ₂ O ₂	0.8 μM	[80]
MWCNTs-[BMIM]BF ₄ -GNP/GCE	Cytochrome <i>c</i>	H ₂ O ₂	3 μM	[81]
MWCNTs-[BMIM]BF ₄ -HA/GCE	Glucose oxidase	Glucose	0.03 mM	[86]

SWCNTs-NH ₂ [EMIM]Br-GNP/GCE	Glucose oxidase	Glucose	0.8 μM	[88]
SWCNTs-[BMIM]PF ₆ -gel/GCE	Hematin*	Trichloroacetic acid	0.38 μM	[94]

MP-11 : microperoxidase; HRP : peroxidase from horsedish; heme-containing proteins/enzymes : myoglobin, cytochrome *c*, and horseradish peroxidase. [BPy]PF₆ : *N*-butylpyridinium hexafluorophosphate; [BMPyr]NTf₂ : *N*-butyl-*N*-methylpyrrolidinium bis (trifluoromethylsulfonyl) imide; D-Pro DH : D-proline dehydrogenase; GNP : gold nanoparticles; GCE : glassy carbon electrode; GE : graphite electrode; AuE : gold electrode; HA : hyaluronic acid. *Mimic of hemeprotein.

The electrode surface area and the amount of the immobilized enzyme are not the real reasons for the increased performance as they have been found to be very similar for the CNT–IL based and other type of electrodes. The increase in the electrode sensitivity of enzyme immobilized CNT–IL is found to be related to the higher reactivity of the enzyme-substrate than those of the other electrodes [92]. The IL units attached (chemically or physically) to the surface of CNTs provide an extra ionic affinity between CNTs and the immobilized enzyme, which facilitates the electron transfer [89]. Figure I.16 illustrates the process of electron transfer from the underlying electrode surface through the carbon nanotube to the immobilized glucose oxidase (GOD) enzyme.

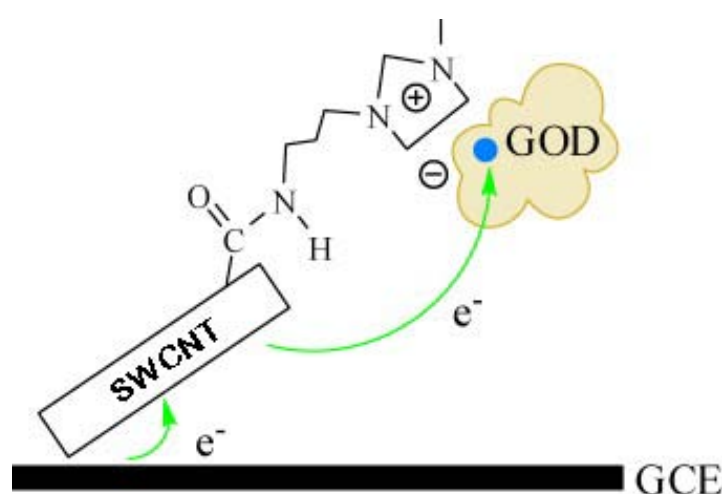


Figure I.16. SWCNT–IL–GOD bionano hybrid-modified glassy carbon electrode [89].

Du et al. [24] investigated the structure of proteins immobilized on SWCNT– [BMIM]BF₄ and SWCNT–[BMIM]PF₆ electrodes. UV–Vis and circular dichroic spectroscopies revealed that proteins do not undergo any structural change and can still retain their bioelectrocatalytic activity in the hybrids. In numerous other studies, it is stated that enzymes/proteins immobilized on the surface of CNT–IL electrodes present enhanced activity. The electrochemical response of the electrodes was found to be increased with the addition of IL to the CNT/electrodes [7,22,33,53,59,60,77–80,85,86,91,92,100]. For example, Figure I.17 shows the cyclic voltammograms (CV) of different modified electrodes. Catalase (Ct) enzyme immobilized on the NH₂–MWCNT–IL/GC electrode surface shows a pair of well-defined and nearly symmetric redox anodic and cathodic peaks while the peaks of Ct–MWCNTs/GC electrode are very weak.

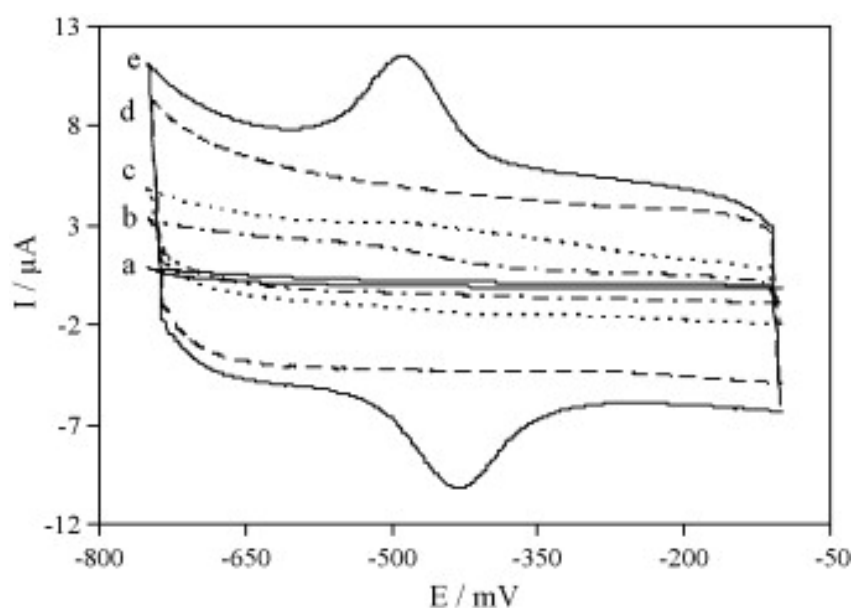


Figure I.17. Cyclic voltammograms of different modified electrodes: (a) Ct/GC, (b) MWCNTs/GC, (c) Ct–MWCNTs/GC, (d) MWCNT–IL/GC and (e) Ct–MWCNT–IL/GC. The results were obtained in 0.1 M phosphate buffer solution, pH 7.0, at the scan rate of 0.1 V s⁻¹

[77].

However, there are a few contradicting results on the electrocatalytic activity of CNT–IL materials in the literature. For example, Wu et al [87] reported that although enzymes in SWCNT–IL material are stable and retain their native structure, the presence of ILs cause the enzymes to lose their activities. They compared different SWCNT hybrids containing three types of ILs, [BMPy]BF₄, [BMPyr]BF₄ or [BMIM]BF₄, and found that the existence of IL in the SWCNT–IL modified electrode decreased the electrocatalytic activity of the enzyme following the sequence [BMPy]⁺ > [BMPyr]⁺ > [BMIM]⁺. The lower decrease obtained with [BMPy]⁺ was attributed to the charge transfer from the SWCNT to IL, which increases the conductance of SWCNTs. Nevertheless, the voltammetric responses at the CNT–IL electrodes were higher than those at the bare GC. The contradicting results may be due to the different preparation methods used. However, it is known that if the ion concentration is too high, the enzyme could lose its activity due to the high ionic strength [101].

1.2.2.1.1.5 Factors impacting the electrode performance

Several factors can affect the electrochemical performance of CNT–IL hybrid based electrodes. In addition to different electrode preparation methods and electrode types, CNT:IL ratio, the amount of CNT–IL hybrid, the thickness of CNT–IL hybrid for gel and paste electrodes, the type of IL and the operation temperature can have an impact on the electrode performance. The optimization of CNT/IL ratio is particularly important for the electrochemical response of the electrode [7,23,27,53,54,78]. IL adsorption on the surface of CNT is crucial for enzyme immobilization [77]. IL is needed to efficiently adsorb enzymes on CNTs and furthermore to separate CNTs from each other. However, IL slows down the electron transfer to some extent resulting in broadened voltammetric peaks. Very high viscosity and specific interactions of ILs with CNTs can cause the passivation of the electrochemically active sites of CNTs and decrease the sensitivity of the electrode [27]. Furthermore, due to the large capacitance of ILs, the CNT–IL electrodes have high

backgrounds [7]. Additionally, in the case of paste electrodes, too much CNT addition can cause the electrode to be easily damaged. Therefore, the right CNT:IL ratio should be found for best electrode performance. It was reported that the current response was the highest when the mixing ratio of MWCNTs to IL was 1:4 for a CNT gel electrode [62]. For a CNT paste electrode, while the optimized CNT to IL ratio was 15:85 in a case [98], it was 7:3 in another [54]. Wan et al used a CNT:IL ratio of 1:7 for the best performance of a layer-by-layer modified electrode [78]. Besides, the thickness of the gel layer on the electrode should be optimized to obtain high responses, stability and lower background current [23,63].

The type of IL also affects the electrochemical response of CNT–IL electrodes. For biocatalysis not all ILs are suitable; enzymes are usually active in hydrophobic ILs containing BF_4^- , PF_6^- , or NTf_2^- anions; whereas hydrophilic ILs containing Cl^- , NO_3^- , CF_3CO_2^- , CF_3SO_3^- , CH_3CO_2^- inhibit enzymes [102]. A possible explanation is that the lower hydrogen-bond basicity of the enzyme-compatible anions minimizes interference with the internal hydrogen bonds of enzymes [102]. Also, the hydrophilic ILs could remove the internally bound water from the enzyme [101]. Yet, Wu et al [85] reported to have successfully used 1-ethyl-3-methylimidazolium acetate, $[\text{EMIM}]\text{CH}_3\text{CO}_2$ in a CNT–IL hybrid for the immobilization of glucose oxidase. In order to investigate the effect of anion structure, Lee and Hong [91] prepared CNT–IL gel electrodes using three types of ILs as binders. The sensitivity of the hybrids for the detection of an organophosphorous compound followed the order: $[\text{BMIM}]\text{PF}_6 > [\text{BMIM}]\text{NTf}_2 > [\text{BMIM}]\text{BF}_4$. Very viscous ILs can also have a negative effect on the sensitivity of the electrode [26]. When hydrophobic CNT–IL are used for electrode modification, the use of graphite electrodes instead of the common glassy carbon electrodes results in a more stable structure as the layer of graphite is also hydrophobic [82]. Most of the electrode measurements have been conducted at room temperature; however, the operation temperature can also affect the electrochemical response of IL based electrodes as

the electrolytic conductivity of ionic liquids increases with temperature [103]. Musameh et al [97] found that the signals can be enhanced and stabilized by operating ionic liquid-carbon paste electrodes at elevated temperatures. Chen et al [59] firstly designed an electrically heated IL [OPy]PF₆/MWCNT electrode. The detection limit for ascorbic acid significantly decreased when the operating temperature was increased to 328 K.

1.2.2.1.2 Actuators

In recent years, there has been a growing interest in the area of artificial muscle for biomimetics and robotics applications. For these, a high performing actuator should be lightweight, low power, silent and fast-moving, working in air and exhibiting large-displacement. For this purpose low voltage electroactive polymer (EAP) actuators have been extensively studied and developed. While the first EAP actuators required electrolyte, the first “dry” ones, developed later on, contained IL but their lifetime and responsivity were limited. Fukushima et al [20] developed the first “dry” actuator based on CNT–IL hybrid soon after the discovery of bucky gel. Later on, bucky gel actuators have been further investigated by several groups [17,104-108].

The actuator based on CNTs and IL is simply fabricated using the layer-by-layer casting method. It is composed of a polymer supported IL electrolyte layer (1:1, IL:polyvinylidene difluoride (PVdF)) sandwiched between two polymer supported bucky gel electrode layers (20:48:32, CNT:IL:PVdF in a typical electrode) (Figure I.18). Thus, IL has two roles in the actuator. While being an internal electrolyte between the electrodes, it is a conducting binding material for CNTs at the electrode. As all the layers consist of IL material, they are perfectly fused together, as seen by SEM (Figure I.19). The advantages of the bucky gel actuator are that it is easily fabricated, does not need any external electrolyte and operates quickly in air for a long time at low applied voltages. Although CNT content is much lower in the bucky gel

actuator than that in the SWCNT-sheet based actuator dipped in IL, the displacement of the actuator is comparable, which is due to the good dispersion of CNTs in the gel. If the CNT content can be further increased, the generated strain and stress of the actuator will be even higher [21]. The problem is that the maximum CNT content in the electrode layer is generally limited to 13 wt.% using the simple agate mortar process. Preparing the bucky gel electrode in two steps using ball-mill method allow to increase the CNT content up to 22 wt.% [21].

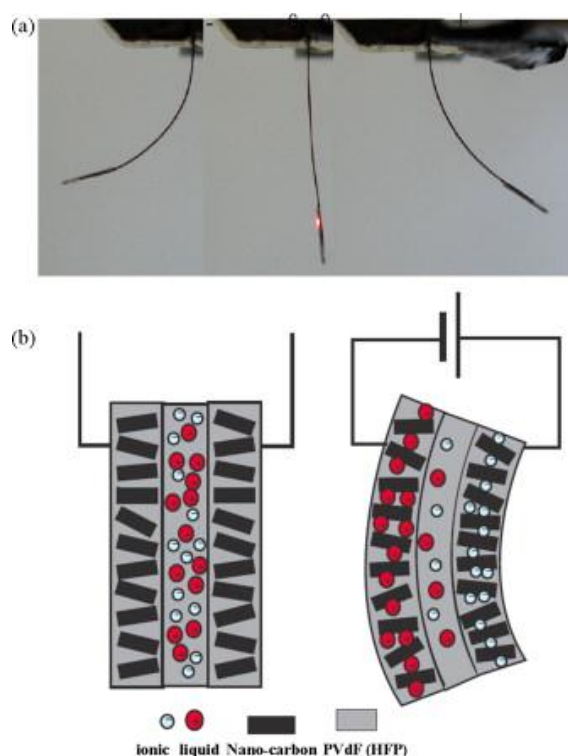


Figure I.18. (a) Performances of a bucky-gel actuator in response to alternating square-wave voltages, (b) schematic drawing of the response modeling of the bucky-gel actuator based on the ion transfer mechanism [21].

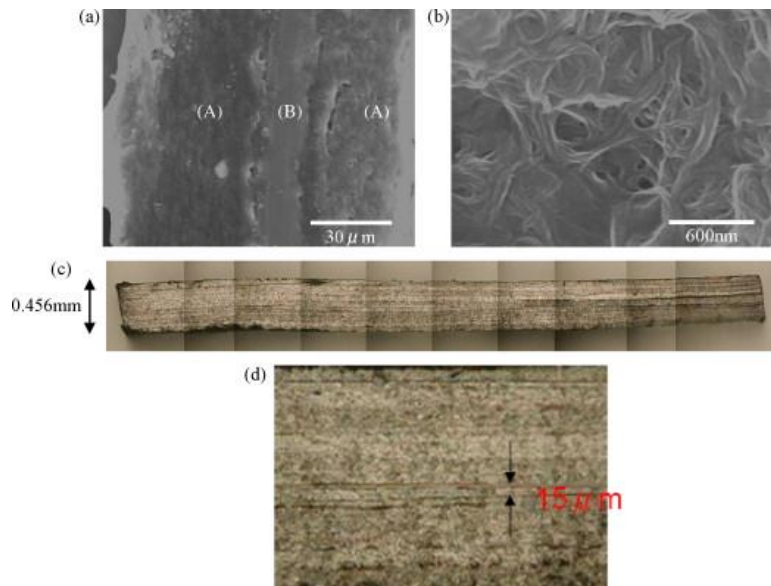


Figure I.19. SEM and optical-micrograph (OM) of a bucky-gel actuator; (a) SEM of a cross-section of a bucky-gel actuator strip of 95 μm in thickness. (A) Bucky-gel electrode layers and (B) an ionic gel electrolyte layer. (b) SEM of a surface of a bucky-gel electrode. (c) OM of cross-section of a bucky-gel actuator of 0.465 mm in thickness. (d) Large view of (c) [21].

The first prototype of the bucky gel actuator has shown to be quite promising for applications in the field of artificial muscle. In this respect, a lot of efforts have been devoted to the research and development of these innovative actuators. The performance of the bucky gel actuator can be further improved by hot-pressing the layers [21], changing the type of internal IL, using additives for the electrode [109,110] or electrolyte layers [111], cross-linking CNTs [107,112] as well as using super-growth SWCNTs [17] or amide modified CNTs [113]. As the bending motion is supposed to be created by the transfer of ions in addition to the changes in C—C bond length induced by “charge injection”, the effect of IL type has been investigated [104,106,114]. While at low frequencies, the bending motion of bucky gel actuators depends on the ion size of IL, at high frequencies it depends on viscosity [106]. The conductivity and capacitance of the bucky gel actuators can be increased by using additives in

the electrode and electrolyte [105]. In a study, addition of a polyaniline, which is a conductive polymer, to the electrode layer enhanced the performance of the actuator by increasing both capacitance and conductivity of the electrode [109]. In another study, it has been found that the addition of Li salts into the electrolyte highly improves the response time and generated strain of the bucky gel actuator by increasing the conductivity and capacitance, respectively [111]. A fully biocompatible actuator based on chitosan biopolymer, CNTs and IL [115] has been developed for implantable biomedical devices. All these advances have provided considerable improvements in the development of CNT–IL actuator, which should take its place in the field of artificial muscles in the near future. Nevertheless, there is still a long way to go in this hot research topic of nanomaterials.

1.2.2.1.3 Other applications in electrochemistry

The potential applications of CNT–IL in electrochemistry are not limited to electrochemical sensors and actuators. They have also been investigated for the construction of other type of electrochemical devices such as elastic conductors, energy-storage devices and energy convertors. Electric double-layer capacitors (EDLCs), also known as supercapacitors, are electrochemical energy storage devices that are capable of being charged and discharged at higher rates than most batteries. The development of new materials with large usable external surface area for improved energy and power densities represent an ongoing challenge. Katakabe et al [116] showed that in terms of high capacitance and low electrode resistance, the performance of SWCNT based EDLCs can be highly improved by the use of bucky gel as the electrode material. Although the capacitance was lower compared to that of the activated carbon based EDLCs, the capacitance per unit surface area was higher. Besides, its ease of preparation represents an advantage. High flexibility and lightness are attractive properties for components in energy storage devices, such as supercapacitors and batteries. Pushparaj et al [117] recently developed a nanocomposite paper based on MWCNTs, IL and cellulose, which

can be rolled up, twisted or bent. The produced material has comparable discharge capacity to other flexible energy-storage devices reported. The potential of CNT–IL hybrids in energy conversion devices has been demonstrated by different studies. A light-driven thermoelectric convertor based on a SWCNT–IL gel hybrid generated sufficient electrical energy to power a LED [118]. Dye-sensitized solar cells (DSSCs) using MWCNT–IL/PEDOT/PSS as counter electrode have been reported to display high photovoltaic performance (overall light conversion efficiency, $\eta = 4.8\%$) close to that of DSCs using expensive Pt counter electrodes ($\eta = 4.9\%$) [25]. The performance decreased significantly using the same electrode without IL ($\eta = 4.1\%$). Kawano et al [119] prepared a solid-state DSC, which eliminates the problems of leakage, using a polymerized ionic liquid as solid electrolyte and SWCNT–IL gel as counter electrode. The novel DSSC demonstrated good performance ($\eta = 3.7\%$) and stability. Alternatively, Lee et al [120] obtained a light conversion efficiency of 3.49% by using an iodine-free all-solid-state electrolyte based on a binary IL mixture incorporated with SWCNTs (10 wt.%).

1.2.2.2 Support for metal nanoparticles

Metal nanoparticles supported on CNTs have been studied for heterogeneous catalysis applications, electrochemical determinations and sensor applications, and given encouraging results for further developments [51]. The nanoparticles on CNTs are active and easy to separate for recycling [121]. However, agglomeration of nanoparticles can occur over time, resulting in a loss of catalytic activity [35]. Therefore, dispersing nanoparticles stably and uniformly on CNTs without losing their catalytic activity has been the center of attention for good catalyst performances. In this regard, CNT–IL hybrid emerges as a novel support to deposit evenly metal nanoparticles with long-term stability using very mild conditions. In these hybrids, ILs act both as a dispersant for CNTs and as a binder between nanoparticles

and CNTs. So far, this method has been successfully applied to immobilize Pd [121-124], Pt [33,35,45,61,73,125-127], Ru [126], PtRu [33,128], Rh [126], Ir [126], Au [50,68,127] and iron fluoride [129] metal nanoparticles on CNTs; and the prepared hybrids displayed enhanced stability and (electro)catalytic activity compared to CNT supports without ILs. The CNT–IL support can be prepared through covalent or non-covalent functionalization. Non-covalent functionalization can be preferred over the covalent one to preserve the original electronic structure of CNTs, whereas covalent functionalization enables to attach IL onto CNTs in a manner that they do not leak from the surface. The HRTEM micrograph in Figure I.20 shows a CNT coated with an IL phase. The IL phase is successfully immobilized on the surface of the CNT covalently functionalized with imidazolium-based ionic moieties [28]. Alternatively, polymerized ionic liquids can be used to increase the stability of the film layer on CNTs [33,35,122]. CNT–IL hybrid does not only stabilize pre-formed nanoparticles but also serves as a support for the synthesis of nanoparticles. The most common method used for this is to deposit the nanoparticle precursor on the surface of the IL-modified CNTs. In the formation process of the nanoparticles, the cation of ILs plays an important role by interacting with the negatively charged metal precursor [45]. Furthermore, low interfacial tensions of ILs increase the nucleation rate, leading to smaller nanoparticles of which size [126] and amount [45] can be controlled by the amount of IL immobilized on the CNT surface. Increasing the amount of IL results in smaller nanoparticles, however increasing it further than a certain amount does not have any influence on the shape or size of the particles. Table I.3 shows the average sizes of the metal nanoparticles formed on CNT–IL supports.

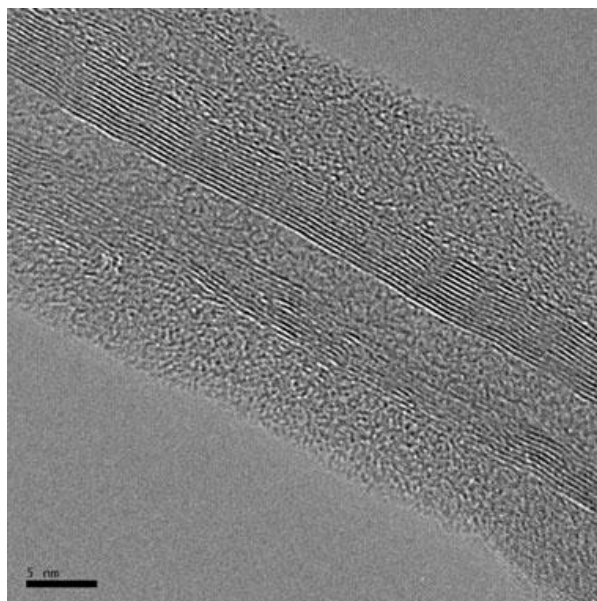


Figure I.20. HRTEM micrograph of IL-grafted CNT with supported ionic liquid phase.

Table I.3. Average sizes of metal nanoparticles formed on CNT–IL supports.

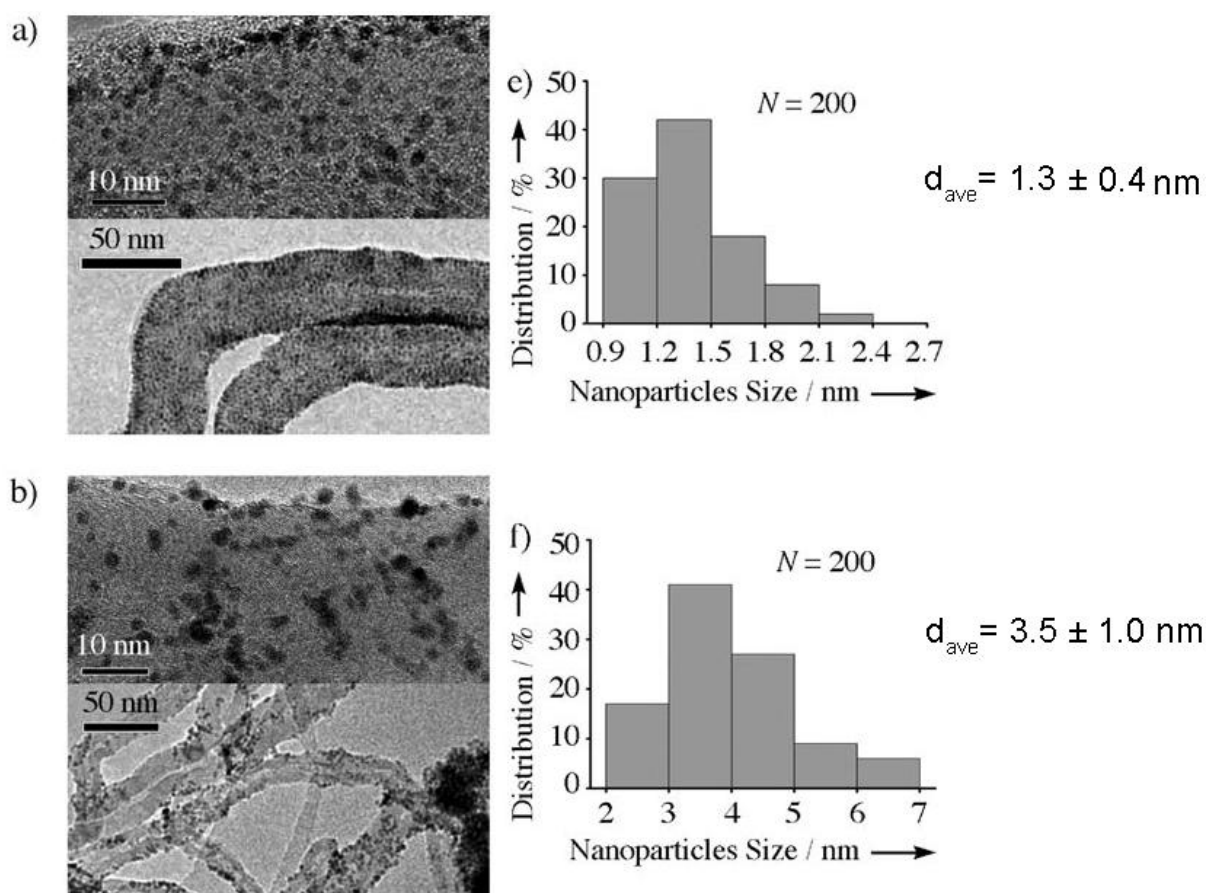
Hybrid	Precursor	Particle	Particle Size (nm)	Ref.
MWCNTs-[BMIM]BF ₄	RuCl ₃	Ru	3.11 ± 0.49	[126]
(MWCNTs-[BMIM]PF ₆) _{gel}	H ₂ PtCl ₆	Pt	100	[61]
MWCNTs-[OMIM]PF ₆	H ₂ PtCl ₆ ·6H ₂ O	Pt	~ 5	[73]
MWCNTs-[BMIM]BF ₄	PtCl ₂	Pt	2-3	[125]
MWCNTs-NH ₂ -IL ^a	K ₂ PtCl ₄	Pt	~ 3	[45]
MWCNTs-[BMIM]BF ₄	K ₂ PtCl ₆	Pt	2.21 ± 0.21	[126]
MWCNTs-[BMIM]PF ₆	K ₂ PtCl ₆	Pt	1.99 ± 0.26	[126]
MWCNTs-[HMIM]PF ₆	K ₂ PtCl ₆	Pt	2.36 ± 0.24	[126]

MWCNTs-[BPy]BF ₄	K ₂ PtCl ₆	Pt	2.78 ± 0.30	[126]
MWCNTs-poly[VEIM]BF ₄	H ₂ PtCl ₆	Pt	1.9 ± 0.5	[33]
MWCNTs-poly[VEIM]BF ₄	H ₂ PtCl ₆ /RuCl ₃	PtRu	1.3 ± 0.4	[33]
MWCNTs-[BMIM]BF ₄	K ₂ PtCl ₆ /RuCl ₃	PtRu	2.10 ± 0.42	[126]
MWCNTs-[BMIM]BF ₄	H ₂ PtCl ₆ .6H ₂ O/RuCl ₃	PtRu	3.4	[128]
MWCNTs-[BMIM]BF ₄	RhCl ₃	Rh	3.51 ± 0.42	[126]
MWCNTs-[BMIM]BF ₄	IrCl ₃	Ir	1.80 ± 0.27	[126]
MWCNTs-NH ₂ -poly[VBIM]Cl/Br/PF ₆	Na ₂ PdCl ₄	Pd	4-5	[122]
MWCNTs-NH ₂ IL ^b	Na ₂ PdCl ₄	Pd	10 ± 0.5	[121]
SWCNTs-,DWCNTs-[BMIM]BF ₄	HAuCl ₄ .3H ₂ O	Au	1.68	[10]
SWCNTs-[BMIM]BF ₄	Fe(NO ₃) ₃ .9H ₂ O	FeF _{2.5} .0.5H ₂ O	~ 10	[129]

^a1-(3-aminopropyl)-3-methylimidazolium bromide, ^b1-(3-aminopropyl)-3-butylimidazolium bromide, [VBIM] : 1-vinyl-3-butylimidazolium.

Wu et al. [33] investigated the efficiency of CNT–IL hybrid as support for the growth of Pt and PtRu nanoparticles by comparing it to CNTs without IL. The results show that the particles synthesized on the CNT–IL support are smaller and distributed more uniformly (Figure I.21). The authors suggested that while CNT–IL presents high concentration of available growing sites for the particles, the randomly distributed defects on unmodified CNTs cause particles to aggregate. Yu et al [61] developed an electrochemical method for in situ formation and deposition of Pt nanoparticles onto MWCNTs in bucky gel. They could deposit the Pt nanoparticles more effectively onto the CNTs since both the precursor and CNTs are well dispersed in the gel matrix and in good interaction with the IL. While with the

conventional electrochemical methods, the nanoparticles are deposited on the outer surface of the CNT layer, with this method, they are homogeneously deposited on almost every CNT within the layer. Li et al [129] used a BF_4^- anion based IL, which acted as in situ dispersant and binder for CNT wiring of electrodes, to provide fluoride anions during the formation of iron fluoride nanoparticles. The outwardly oriented anions of the IL physically coated on the CNTs reacted readily with the surrounding iron(III) precursor under mild conditions.



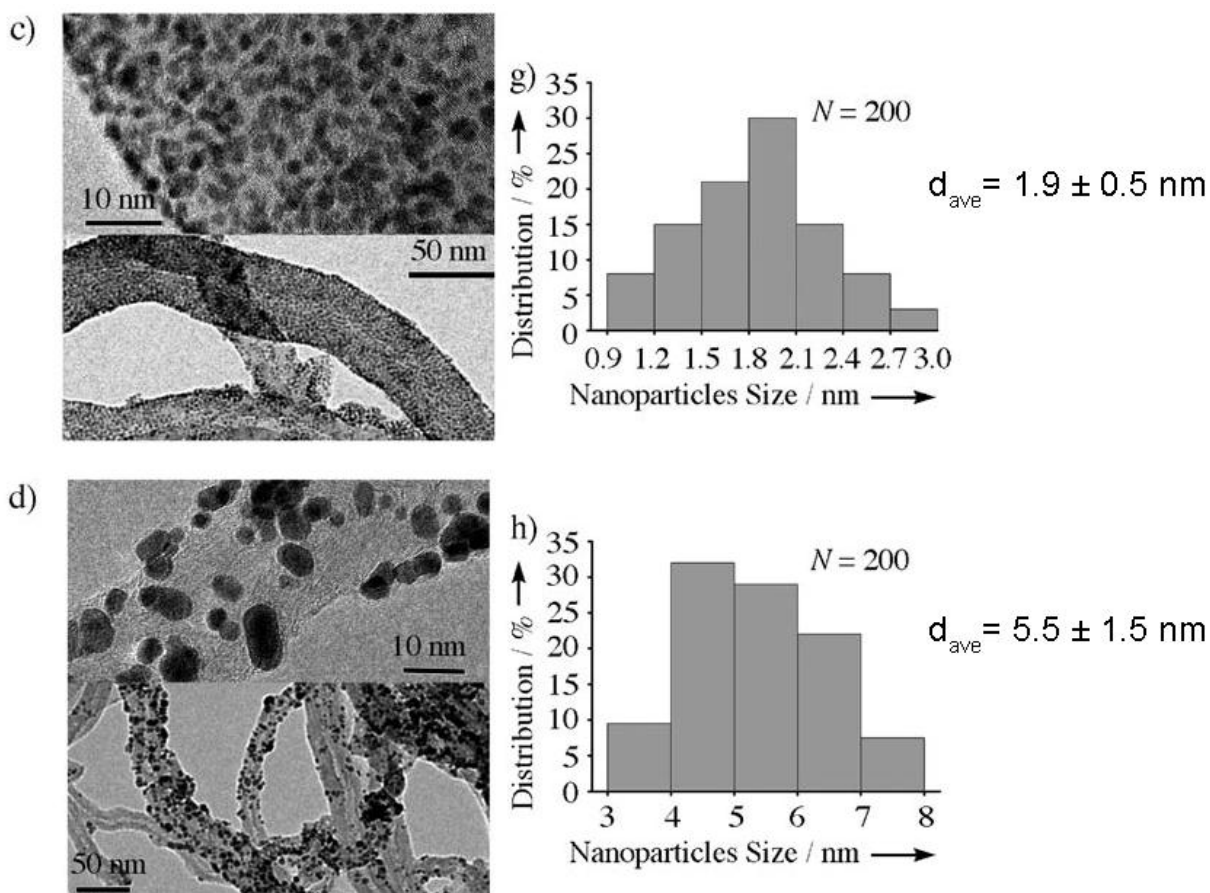


Figure I.21. TEM images (left) and size distributions (right) of nanoparticles of nanohybrids. (a and e) PtRu/CNT-PIL; (b and f) PtRu/CNTs; (c and g) Pt/CNT-PIL; (d and h) Pt/CNTs [33].

Alternatively, Baba et al [10] demonstrated that by using IL-introduced plasma technique, Au nanoparticles with small diameters can grow densely on the inner surface of open-ended SWCNTs and double-walled CNTs. Encapsulating nanoparticles into the CNTs is suggested to increase their catalytic performance [10]. The type of IL can influence the formation and catalytic activity of the nanoparticles [121,122,126]. Chu et al [126] concluded that the anion has little effect on the formation of nanoparticles but it is rather the IL cations that play a key role. From the data for metallic particles presented in Table I.3, it seems that PIL-functionalized CNT supports lead to the formation of smaller particles. This could be

attributed to both the enhanced stability of the hybrid support and increased number of nucleation sites immobilized on CNT. Chun et al [121] investigated the anion effects on the electrocatalytic activity of Pd nanoparticles supported on imidazolium-based PIL functionalized CNTs toward oxygen reduction reaction. Their results suggest that the nature of the anion has a significant effect on the kinetics of the reaction, which is due to the interactions of the anion species with the electrolyte.

1.2.2.3 Antiwear and lubricant additives

Up to now, little research has been conducted on the tribological properties of CNT–IL hybrids. They have started to be investigated only recently for potential applications as lubricant and antiwear additive. Although CNTs are considered as a good solid lubricant with an ultra-low friction coefficient, they do not always improve wear and friction properties of the matrix polymer [130]. As IL is known to exhibit good tribological performance, CNTs can be modified by ILs to improve the tribological properties of polymer composites. Most of the work on this topic to date has been carried out by Bermudez et al. They investigated the influence of addition of CNTs modified by ILs on the wear, abrasive wear and friction behaviours of polymers [130,131]. They added SWCNTs modified by [OMIM]BF₄ into different types of thermoplastics. The results have shown that the addition of modified CNTs does not have the same influence on all types of polymers (Table I.4). This can be attributed to the differences in the distribution of CNT–ILs in different polymer matrices [131]. The authors obtained the best performance concerning the tribological properties with polystyrene (PS).

Table I.4. Dry friction coefficients of polymers and polymer composites [131].

Material	Friction coefficient (standard deviation)
PS	1.06 (0.035)
PS + 1%CNT	0.89 (0.089)
PS + 1% <i>m</i> CNT	0.86 (0.042)
PMMA	0.10 (0.013)
PMMA + 1%CNT	0.88 (0.071)
PMMA + 1% <i>m</i> CNT	1.04 (0.013)
PC	1.19 (0.036)
PC + 1%CNT	1.17 (0.082)
PC + 1% <i>m</i> CNT	1.15 (0.015)

PS : polystyrene ; PMMA : polymethylmethacrylate ; PC : polycarbonate; *m*CNT : IL-modified SWCNT.

Neat ILs have proven to have potential applications as lubricant or lubricant additives for various materials due to their good tribological performance even under harsh conditions [130]. Anti-wear properties of ionic liquids can be further improved by using additives and CNTs can be used as additive. However, here as well, the dispersibility of CNTs is a key factor to improve the tribological properties of pure IL, as poorly dispersed CNTs may cause abrasive wear [44]. Several groups [44,132] added MWCNTs chemically modified by a hydroxyl/amine terminated IL into IL lubricants (i.e., [BMIM]PF₆ and 1-methyl-3-hexylimidazolium hexafluorophosphate) and obtained improved lubricant performances for steel–steel contact at CNT–IL concentrations as low as 0.1 wt.%. The authors attributed the higher performances to the unique shape of CNTs, which disperse uniformly in the lubricant upon modification with IL. CNTs can also be used as additive for IL lubricants without being subjected to chemical modification. As an external lubricant for polycarbonate-stainless steel

contact, the mixture of CNTs and 1-octyl-3-methylimidazolium chloride, [OMIM]Cl, decreased the friction coefficient up to 70 % with respect to the neat IL [49]. Ultrasonication increases the efficiency of lubrication. Ultrasonicated samples showed significantly better performance compared to solely mechanically ground ones.

1.2.2.4 CNT-IL/Polymer composites

CNTs are ideal candidates for reinforcing and electrically conducting fillers in high strength, light-weight, multifunctional polymer composites. However, there are several challenges for developing high performance CNT/polymer composites, including homogeneous dispersion of CNTs in the polymer matrix and achieving strong interfacial bonding between the CNTs and the matrix. To overcome the problems associated with agglomeration and compatibility between CNTs and the matrix, CNTs have been modified using covalent or non-covalent approaches. Non-covalent approaches, which are usually preferred to preserve the original CNT structure, include addition of surfactants and aromatic molecules. However, these compounds are usually toxic and their presence can impair the properties of the composite, thus post-treatment process is usually required to remove these additives [137]. Furthermore, their processing temperatures are limited. ILs can provide an easy way to prepare CNT/polymer composites by means of cation- π / π - π or van der Waals interactions. Due to their high-thermal stability, they easily endure the high temperatures used during the melt-blending process of the polymers [13]. Since most polymers are melt-blend processed or cured at temperatures higher than 473 K, thermal stability is an important aspect that should be taken into account in the choice of the appropriate dispersant. Moreover, the combination of their properties can be used to fabricate multi-functional polymer composites. Based on the requirements an optimal IL amount should be chosen in the composites. While CNTs disperse better by increasing the IL amount, excess IL can act as plasticizer and affect the mechanical properties of the resulting composite [12]. Bellayer et al [13] prepared a polystyrene (PS)

composite by melt mixing at 468 K with 1,2-dimethyl-3-hexadecylimidazolium tetrafluoroborate, ([DMHDIM]BF₄, modified MWCNTs. From the TEM images of PS composites at a CNT loading of 0.5 wt.% (Figure I.22), it is observed that after IL modification, the dispersion of the CNTs has significantly improved when compared to before modification.

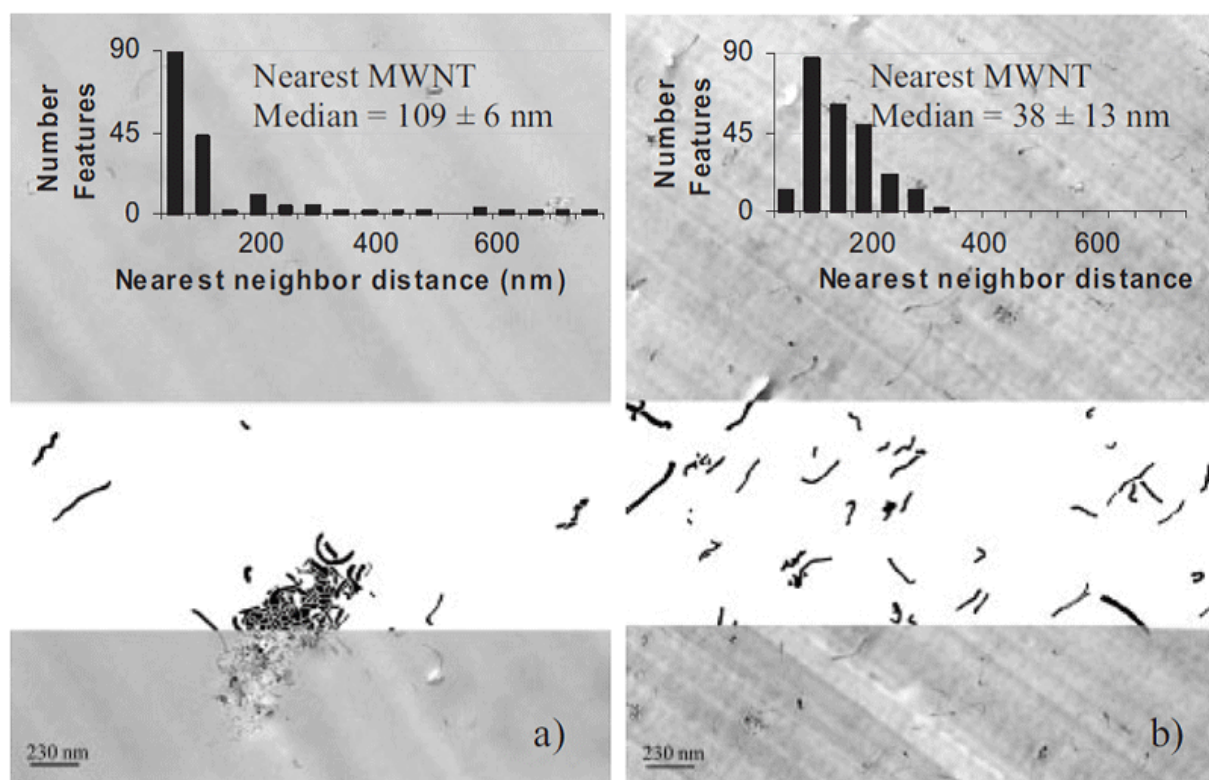


Figure I.22. TEM images of PS/MWCNT (without [DMHDIM]BF₄) (a) and PS/MWCNT–[DMHDIM]BF₄ (1:1) (b) [13].

ILs have been particularly used to produce high-performance elastomer composites with homogeneously dispersed CNTs [133–135]. Sekitani et al [133] dispersed super-growth SWCNTs uniformly in a fluorinated polymer matrix with the aid of an IL ([BMIM]NTf₂). They first prepared a bucky gel by grinding the CNTs with the IL and then incorporated it in the polymer matrix by stirring and sonication. In this way, they could increase the CNT content up to 20% in the composite and fabricate an elastic conductor without impairing the

mechanical properties of the matrix. In another study, an IL with an ethylene end group acts as a coupling agent between the CNTs and the matrix by reacting with the active sites of a diene rubber during the curing process [135]. The coupling ILs showed the best improvement in the conductivity and elastic properties of the rubber composites among others. With the incorporation of 3 wt.% CNTs, the conductivity increased by seven orders of magnitude. The TEM images in Figure I.23 show the interesting morphology of the composite. At low magnification (Figure I.23 (a) and (b)) a relatively well dispersed CNT network is observed. The dark phases that are observed consist of a three-dimensional interconnected glob like structures called “cellular structures” (Figure I.23 (c) and (d)), which further indicates the strong binding between the CNTs and the matrix.

In another study, Subramaniam et al [12] developed a polychloroprene based conducting elastic material by the incorporation of non-covalently modified MWCNTs using IL ([BMIM]NTf₂). A loading of 3 wt.% CNT resulted in an increase of nine orders of magnitude in the initial electroconductivity of the insulator polymer. When a conducting polymer is used as matrix, the enhancement of the electrical properties is more pronounced in the CNT/polymer composites [136]. For example, when PIL functionalized SWCNTs were added into a conducting polymer, i.e., poly(3,4-ethylenedioxythiophene) (PEDOT), at a loading of only 0.4 %, the increase in the electroconductivity was over 20-fold [136].

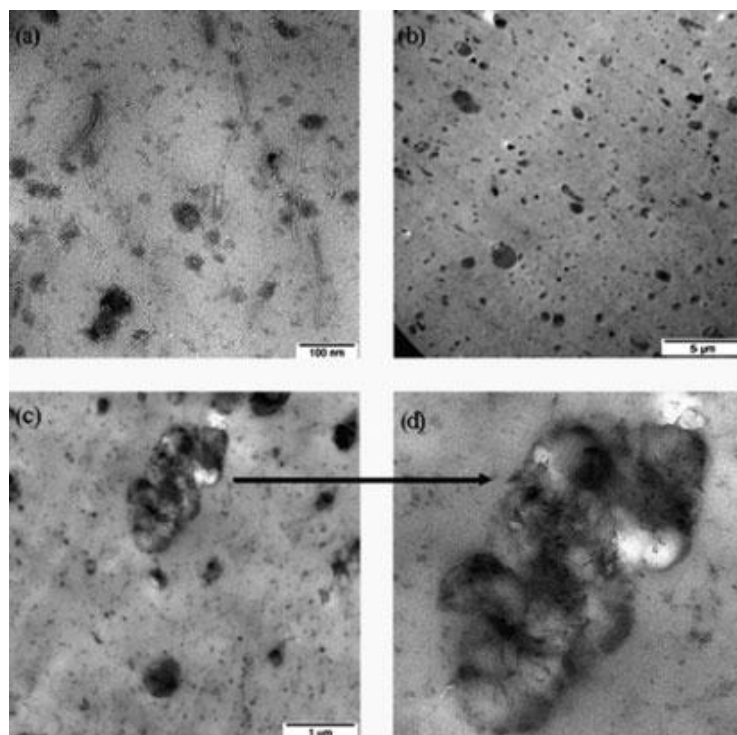


Figure I.23. TEM image of cross-linked rubber matrix loaded with 3 wt.% CNTs in the presence of 1-allyl-3-methylimidazolium chloride (a) exhibiting the evenly distributed CNTs with interconnecting network, (b) overall dispersion of the CNTs, (c) the clusters of ‘cellular structure’ formed by CNTs and (d) a magnified image of the cellulation structure [135].

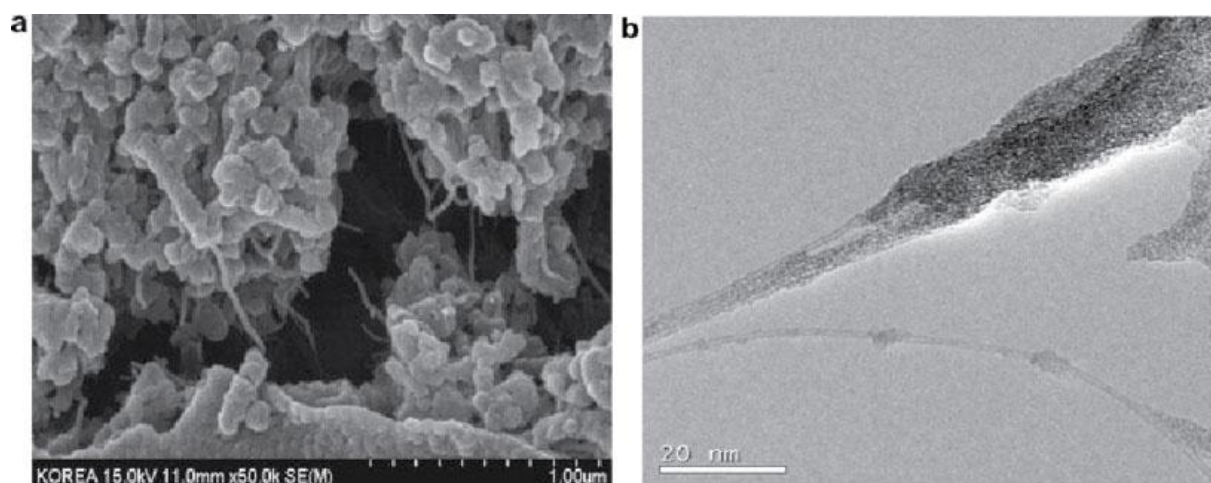


Figure I.24. (a) SEM image on the crack-section of SWCNT–PIL:PEDOT hybrid film. (b) TEM images of SWCNT–PIL:PEDOT hybrids [136].

Figure I.24 (a) shows the crack section of the composite film. The homogeneous dispersion of CNTs in the crack section and the bundles bridging the crack faces are observed. The TEM image confirms that the PEDOT layer is adsorbed onto the SWCNT surface (Figure I.24 (b)). A different approach to fabricate CNT/polymer composite with the aid of IL is to modify the polymer with the IL before CNT addition. For example polyurethane was chemically modified with IL units to form a new kind of poly(ionic liquid) [137]. The added CNTs dispersed well in the matrix by interacting with the IL moieties of the polymer and resulted in a composite with enhanced mechanical and thermal properties.

Recently, imidazolium-based ionic liquids have been found to be good solvents for cellulose [138]. These ILs have also been used to prepare electrically conducting CNT reinforced cellulose fibers [138,139]. In these studies, before incorporation into the cellulose matrix, CNTs have been non-covalently modified by IL. This modification increased their dispersibility in cellulose. For example, a CNT reinforced cellulose fiber has been prepared by dry-jet-wet-spinning method at different loadings of 1-allyl-3-methylimidazolium chloride modified MWCNTs [138]. The increase in the tensile strength of the resulted fiber was highest (40 %) at a CNT loading of 4%. Higher CNT loadings resulted in aggregation of CNTs. In another study [139], the maximum increase in the tensile strength of the spun cellulose fiber was 30% at a CNT loading of 7%, using MWCNTs non-covalently modified with 1-ethyl-3-methylimidazolium acetate.

I.3. Graphene-IL hybrids

I.3.1 Preparation and characterization

Graphene, a one-atom-thick planar sheet of sp^2 hybridized carbon, has emerged as a promising new nanomaterial for a variety of potential applications including electronic and

optoelectronic devices, chemical sensors, nanocomposites and energy storage [140]. Like CNTs, graphene exhibits many outstanding properties such as large specific surface area, high electrical and thermal conductivity, excellent chemical stability and mechanical stiffness. Graphite, which is cheap and readily available, consists of stacked graphene sheets (GSs). Therefore, one of the most convenient methods for the mass production of graphene sheets is the exfoliation of graphite in the liquid phase [141]. Recently, many attempts to produce graphene sheets in large quantities *via* chemical reduction of exfoliated graphite oxide (GO) have been reported [142]. During the oxidation process of graphite, the unique electronic properties of graphene dramatically degrade. The electrical conductivity of the graphene oxide sheets can be partially restored by the reduction step; however, this results in their irreversible agglomeration. Therefore, different strategies to disperse graphene sheets before or during reduction step have been used, including pH-controlled reduction, stabilization by various polymeric or surfactant dispersants and covalent/non-covalent functionalization [143]. Ionic liquid, which has been proved to be effective for CNT functionalization, can also be used for covalent and non-covalent functionalization of graphene.

The exfoliation of layered graphene oxide in aqueous and organic solvents has been shown to be highly improved by the ring-opening reaction of the epoxy groups present in the GO structure with the amine end groups of an IL [143]. Both the repulsion between the resultant cation-charged GO sheets and the high solubility of the grafted IL contribute to the formation of long-term stable graphene dispersions in a wide range of aqueous and organic solvents. The average interlayer spacing between the exfoliated graphenes in water increased from around 0.96 nm for the well exfoliated GO sheets to 1.49 nm due to the presence of IL.

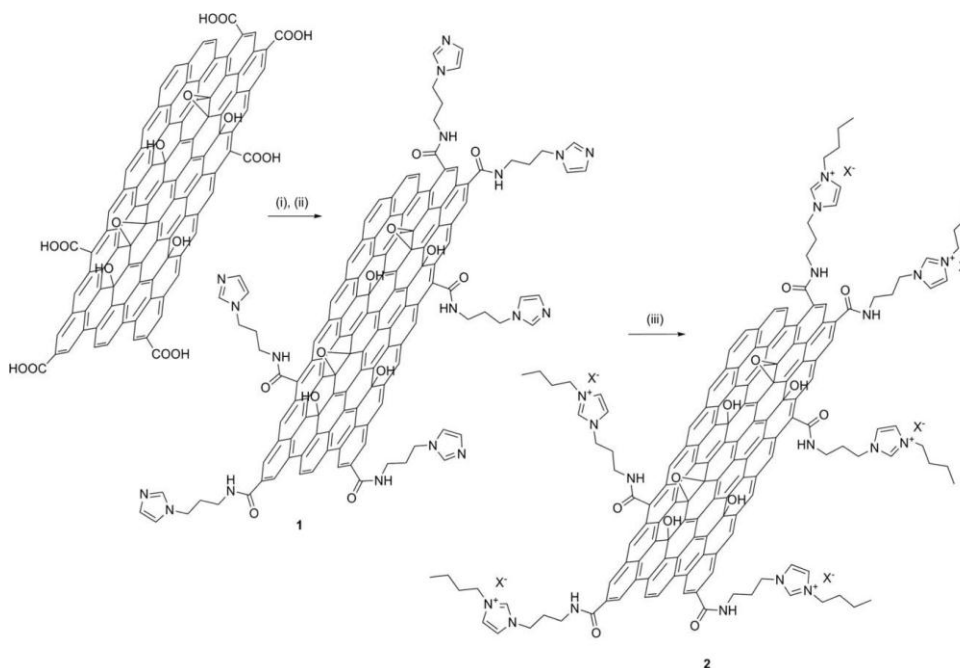


Figure I.25. Preparation of imidazolium-modified graphene-oxide hybrid materials. (i) Oxalyl chloride (COCl_2), $80\text{ }^\circ\text{C}$, 18 h, (ii) 1-(3-aminopropyl)imidazole, $100\text{ }^\circ\text{C}$, 18 h, (iii) 1-bromobutane, $90\text{ }^\circ\text{C}$, 18 h [145].

By using the same approaches used for the covalent functionalization of CNTs, IL units can be grafted to the carboxylic acid groups of GO (Figure I.25) [143,144]. The resultant IL-grafted GOs can be dispersed in various organic solvents. By subsequent anion-exchange reaction, an extra functionality can be introduced to graphene. For example Karousis et al [145] used a photoactive anionic porphyrin as counter anion of the IL-grafted graphene sheets for potential application in optoelectronic devices.

IL can adsorb on the graphene surface through the non-covalent interactions of anion and/or cation with graphene. Recent studies [146,147] show that for hydrophobic IL, both the anion and cation – the imidazolium ring slightly tilted to the surface plane with the alkyl chain extended parallel to the surface plane – are orientated at the graphene surface. For hydrophilic

IL, there is no immediate interaction between the anion and graphene surface. The results also show that there is some charge transfer between the ions and graphene. Thanks to these interactions, it is possible to exfoliate graphite into graphene sheets and to prepare processable graphene dispersions using IL. Wang et al [148] obtained few-layer graphene sheets, mostly with less than five layers, by direct exfoliation of pristine graphite in [BMIM]NTf₂ and [BMPy]NTf₂ with the aid of sonication for one hour. The resulting colloidal suspension had a concentration of 0.95 mg mL⁻¹ of exfoliated graphene. Nuvoli et al [149] showed that by optimizing the initial graphite concentration and increasing the sonication time up to 24 h, it is possible to obtain a few-layer graphene concentration as high as 5.33 mg mL⁻¹. The high exfoliation of graphite in IL is attributed to the surface tension of ILs close to that of graphite, which favors the exfoliation process, and to the ionicity of ILs, which stabilizes the exfoliated graphene sheets. Zhang et al [150] successfully prepared stable dispersions of reduced graphene oxide (rGO) sheets in hydrophilic imidazolium- and pyridinium-based ionic liquids at relatively high concentrations, up to 7.0 mg mL⁻¹, without the addition of a stabilizer or surfactant. The resulting graphene-IL dispersions can be dispersed in various organic solvents. Alike CNTs, graphene sheets can also form a gel hybrid by grinding or sonicating a mixture of graphene and IL, suggesting a similar molecular ordering of IL through cation- π and/or π - π interactions [150–153]. The SEM images in Figure I.26 (c) and (d) show the surface morphology of the graphene-IL gel.

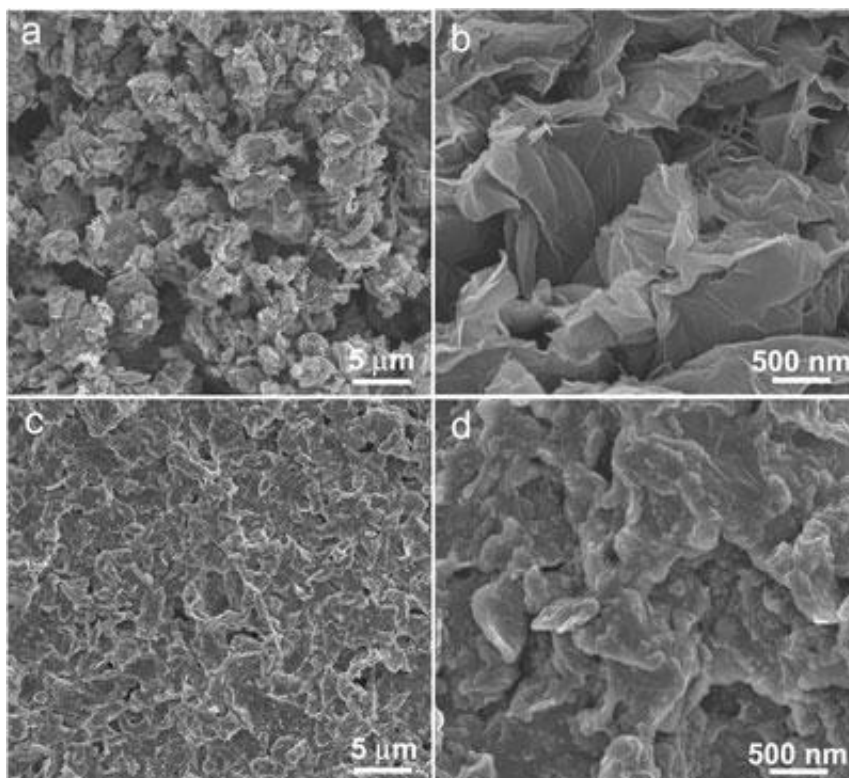


Figure I.26. SEM images of 3-D graphene material with low (a) and high (b) magnification; and of 3-D graphene/IL gel nanohybrid with low (c) and high (d) magnification [151].

Polymeric ionic liquids have also been used to obtain long-term stable dispersions of graphene sheets in IL, aqueous or organic media [142,154–156]. The addition of a hydrophilic PIL followed by the reduction step of suspended GO sheets in water results in a highly stable aqueous dispersion of graphene sheets, which can be extracted into a hydrophobic IL phase [142], or readily transferred to an organic phase by an in situ anion exchange step [154]. It should be noted that polymeric form of IL highly increases the stability of graphene sheets during the reduction process. Furthermore, the reducing capability of imidazolium-based PIL leads to a more effective reduction of graphene oxide as confirmed by XPS [156]. Figure I.27 (a) and (b) shows the TEM images of the PIL modified and unmodified GO sheets after chemical reduction. It is observed that in the absence of PIL, reduced GO sheets form thick multilayers by stacking, while PIL modification results predominantly in thin graphene layers composed of single- or few-layer graphene sheets. AFM analysis gives the average thickness

of graphene layers. The average thicknesses of a graphene sheet and a GO sheet are 0.34 and ~ 1 nm, respectively. The reported average thickness values for various PIL–graphene sheets prepared in different studies are between 1.6 nm and 3.0 nm [142,154–156]. The difference in thickness between a monolayer of GO and graphene-PIL sheet is likely due to the adsorbed PIL. Preparation of GO sheets and their in situ or subsequent functionalization can be time-consuming and polluting if hazardous chemicals are used.

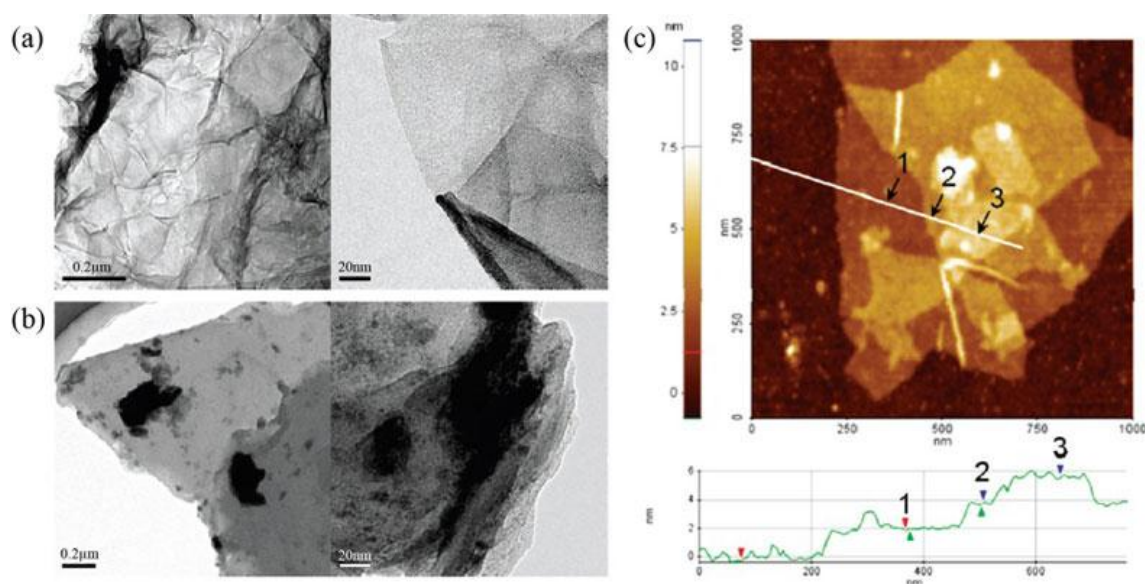


Figure I.27. TEM images of the chemically converted graphene sheets (a) in the presence of and (b) in the absence of PIL; (c) tapping mode AFM image of the PIL–rGO processed from organic suspension. Height profiles across the PIL–rGO sheets indicating a thickness of ~ 1.9 nm [154].

Alternatively, by using an electrochemical process, graphene sheets can be directly obtained from graphite with the aid of IL under mild conditions. As illustrated in Figure I.28, pristine graphite rods are electrochemically exfoliated in IL and water at room temperature [141,157]. The resultant IL functionalized graphene sheets have an average thickness of 1.1 nm as determined by AFM. Taking into account the thickness of the IL layer, it has been shown that with this method it is possible to obtain individual graphene nanosheets in one step. Further

studies [158] on the mechanism of this exfoliation revealed that the graphite exfoliation occurs by a complex interplay of water oxidation at the anode and intercalation of IL anions. It has been shown that by altering the water content and the counter anion of IL, it is possible to produce different types of carbon nanomaterials, including graphene sheets, graphene nanoribbons and carbon nanoparticles. XPS analysis revealed that this method also generates oxygen containing groups on the graphene. The chemical functionalization of the graphene sheets by ILs occurs only when a concentrated IL with less than 10% water content is used as electrolyte. The as-functionalized graphene sheets have a higher conductivity (by an order of magnitude) than the rGO ones.

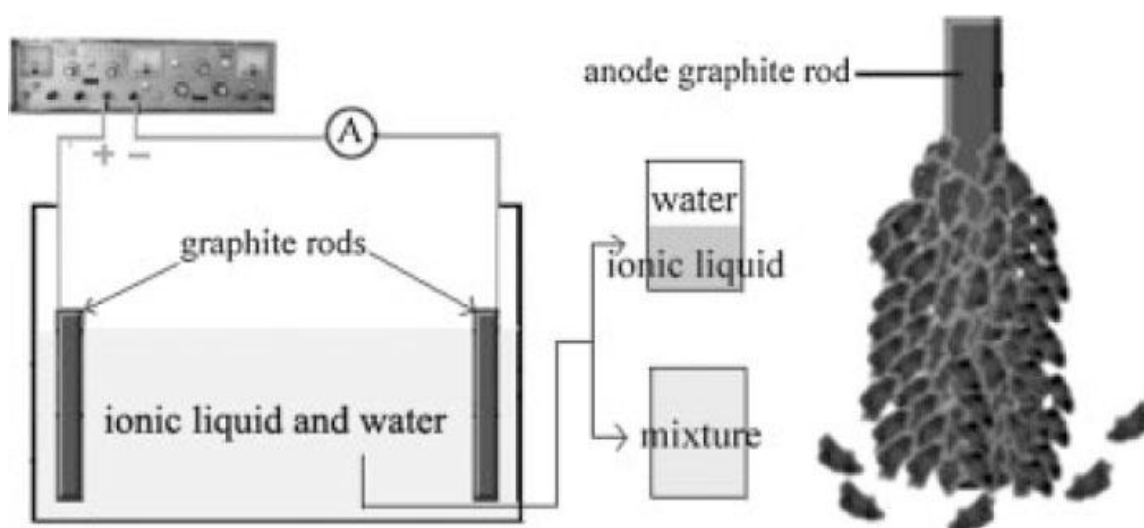


Figure I.28. Experimental set-up diagram for electrochemical exfoliation of graphite (left), and the exfoliation of the graphite anode (right) [141].

1.3.2 Potential applications of graphene-IL hybrids

1.3.2.1 Electrochemical sensors and biosensors

Graphene has emerged as a new material which competes with CNTs for fabricating electrochemical sensing and biosensing devices, owing to its large specific surface area, good

biocompatibility and ability to promote electron transfer between electroactive species and electrodes [159]. As in the case of CNTs, the studies on potential applications of graphene–IL hybrids are concentrated in the field of electrochemistry, particularly in the area of sensing. As expected, modification with IL improves the stability and dispersion of graphene sheets as well as the electron transfer between the target species and graphene. Moreover, the combination of graphene sheets and IL *via* physical or chemical interactions can provide a favorable micro-environment for the immobilization of enzymes/proteins, and IL can enhance their catalytic activity. To date, graphene–IL modified electrodes have been successfully applied to detect organic and inorganic molecules such as glucose [160–162], hydroquinone [163], catechol [163], guanine and adenine [165], ascorbic acid [165], dopamine [165], ethanol [166], trinitrotoluene (TNT) [152,167], azithromycin [168], 2-chlorophenol [169], hydrogen peroxide [170–173], nitric oxide [151] and nitrate [174]. Graphene–IL based biosensor has also been used to detect DNA damage [175]. In these studies, graphene has been used as thermally or chemically rGO. In a study [166], it was reported that after reduction of the oxygen containing groups of the IL functionalized GO, the graphene promoted the electron transfer of NADH oxidation much better. Alternatively, 3-D graphene sheets, which are obtained by heating graphite oxide under vacuum at 423 K, have also been used [151,152]. Table I.5 summarizes the graphene–IL electrochemical sensors for which detection limits have been reported.

Table I.5. Detection limits of GS–IL modified electrodes

Electrode	Immobilized enzyme	Target species	Detection limit	Ref.
GS–[BMIM]PF ₆ /AuE	Glucose oxidase	Glucose	0.376 mM	[161]
GS–poly[VBIM]Br/GCE	Glucose oxidase	Glucose	0.267 mM	[162]

GS-[BMIM]BF ₄ -AuNPs/GCE	Glucose oxidase	Glucose	0.13 mM	[176]
GS-NH ₂ -IL-Chitosan/GCE	Alcohol dehydrogenase	Ethanol	5 μM	[166]
(GS-PDDA)-[BMIM]BF ₄ - PDDA/GCE	Hemoglobin	Nitrate	0.04 μM	[174]
(GS-TiO ₂)-[BMIM]PF ₆ - Chitosan/GCE	Hemoglobin	H ₂ O ₂	0.3 μM	[170]
GS-[BMIM]PF ₆ /CCE	Hemoglobin	H ₂ O ₂	0.3 μM	[172]
GS-[BMIM]PF ₆ -CTAB/GCE	Myoglobin	H ₂ O ₂	1.29 μM	[173]
GS-PFIL-Prussian blue/AuE	-	H ₂ O ₂	1 μM	[171]
GS-[BMIM]PF ₆ /GCE	-	Azithromycin	0.19 μM	[168]
(GS-PDDA)-[BMIM]BF ₄ -Pd- Nafion/GCE	-	2-Chlorophenol	1.5 μM	[169]
GS-[BMIM]PF ₆ /GCE	-	Hydroquinone	10 nM	[163]
GS-[BMIM]PF ₆ /GCE	-	Catechol	20 nM	[163]
((3D-GS)-[BMIM]PF ₆) _{gel} - Nafion/CPE	-	Nitric oxide	16 nM	[151]
GS-NH ₂ -IL/CPE	-	Guanine	65 nM	[164]
GS-NH ₂ -IL/CPE	-	Adenine	32 nM	[164]
GS-NH ₂ -IL/GCE	-	Trinitrotoluene	4 nM	[167]
((3D-GS)-[BMIM]PF ₆) _{gel} /CPE	-	Trinitrotoluene	0.5 nM	[152]

PFIL : Polyethylenimine-functionalized IL; PDDA : poly(diallyldimethylammonium chloride); CPE : Carbon paste electrode; CCE : Carbon ceramic electrode; CTAB : Cetyltrimethylammonium bromide; NH₂-IL : 1-(3-aminopropyl)-3-methylimidazolium bromide.

It has been reported that graphene usually exhibits better electroanalytical or electrochemical performance than CNTs [159]. As for CNT- and graphene-IL based sensors, the published results cannot be compared to each other because those electrodes were prepared by different methods. There are just a few comparative studies in the literature. In two studies [152,167] where MWCNT- and graphene-IL based paste and glassy carbon electrodes were investigated for TNT detection, it was demonstrated that graphene based ones displayed higher charge transfer rate and better conductivity as compared to CNT-IL based ones. Furthermore, they exhibited higher sensitivity and lower detection limit for TNT sensing. Ng et al. [151] found that glassy carbon electrode modified with graphene-IL gel hybrid exhibited a higher response for NO detection compared to the one modified with MWCNT-IL gel hybrid. The authors attributed it to the larger electrochemically active surface area of graphene-IL gel hybrid. A recent study [177] showed that graphene-IL hybrid can also be used for highly selective gas sensing. Graphene-IL films were prepared by reduction of GO sheets in the presence of IL. The authors constructed a gas sensor using layer-by-layer assembly of these films with a polymer on an appropriate solid support. The graphene layers are separated by the intercalation of IL and the spacing between the layers can be controlled by the length of the alkyl chain of the imidazolium salt. Depending on the IL type and the spacing between the layers, the amount of the adsorbed gas can be controlled. Gas sensor based on GO without an IL component gives no adsorption.

1.3.2.2 Graphene-IL/polymer composites

The polymer nanocomposite field is currently dominated by CNT as filler. Graphene has also great potential as nanofiller in polymer composites. It has been demonstrated that at low nanofiller content, graphene nanosheets are more efficient than CNTs in transferring their mechanical properties to the composite because of their higher specific surface area, two-dimensional geometry and improved adhesion at the nanofiller-polymer interface [178].

While the inner surface of CNTs is inaccessible to polymer molecules, the entire volume of graphene is exposed to its surrounding. Due to its geometry, graphene nanosheet is also more effective in conductivity enhancement than CNTs [179]. As with CNTs, the major challenge in the processing of bulk-quantity graphene sheets is the prevention of aggregation. The dispersions of IL functionalized graphene sheets allow graphene sheets to be intimately mixed with many organic polymers, facilitating synthesis of graphene-polymer composites. Liu et al [141] prepared a graphene/polystyrene composite by blending IL functionalized graphene sheets and polymer in an organic solvent. The compatible groups present in the polymer and IL resulted in strong polymer-graphene interface, which was observed by UV-Vis spectroscopy. The authors reported that the resultant composite has an electrical conductivity 3–15 times better than that of PS composites filled with SWCNTs. Zhou et al [155] used a “grafting from” approach to prepare graphene/polyaniline (PANI) composite nanosheets with high electrical conductivity. The $S_2O_8^{2-}$ counter anion of the PIL adsorbed on the graphene sheets by non-covalent interactions initiates the oxidative polymerization of aniline on the surface of the graphene sheets. The authors observed that during polymerization, PANI replaces the adsorbed PIL on the surface of graphene sheets by its stronger π - π interactions with the graphene. In the absence of PIL, the same polymerization reaction results in a mixture of aggregated graphene and PANI. Similarly to the study performed with CNTs [136], Tung et al [156] anchored PEDOT, a conjugated electroactive polymer, on polymerized ionic liquid modified graphene. The 22-fold increase in the electrical conductivity of the resultant composite at a loading of 0.3 wt.% is comparable to the 20-fold increase obtained with the similar composite based on SWCNTs at the same loading. Saxena et al [157] incorporated graphene sheets electrochemically functionalized with a fluoroalkylphosphate based imidazolium IL into PEDOT, a conjugated electroactive polymer, and investigated the electrochemistry and electrochromism of the resultant nanocomposite films. During the

oxidative electropolymerization process, the rate of polymerization was much higher in the electrolyte consisting of IL-functionalized graphene sheets than in the one consisting of the rGO sheets, owing to the favorable nucleation effect of IL counter anion. The deposited IL-graphene/PEDOT films displayed higher electrochemical activity, larger optical modulation, higher electronic conductivity, improved electrochromic coloration efficiency and faster color-switching response compared to rGO/PEDOT films.

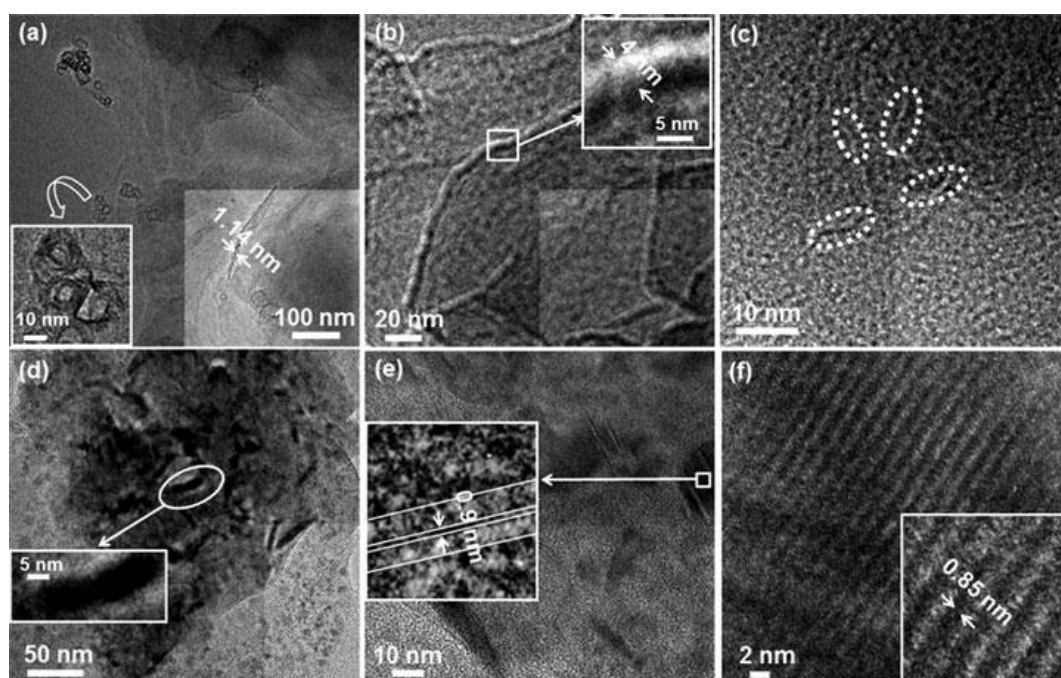


Figure I.29. HRTEM images of (a) neat IL functionalized graphene (ILFG), (b) neat RGO, (c) the PEDOT-RGO nanocomposite, (d) PEDOT-ILFG, (e) coexisting crystalline and amorphous phases in PEDOT-ILFG and (f) a relatively defect free crystalline of ILFG in PEDOT-ILFG [157].

The HRTEM image of neat ionic liquid functionalized graphene (ILFG) in Figure I.29 (a) shows the crumpled silk-like monolayers and few layers of graphene, which are seen as darker regions. The thickness of the monolayer is 1.1 nm as shown in the right inset. There are also some aggregated flakes, which are shown in the left inset. The lattice fringes of 0.85

nm corresponding to the IL functionalized graphene stacks in the polymer are higher than the lattice constant of 0.34 nm probably due to the entrapped IL cations (Figure I.29 (f)). Reddy et al [153] used a bucky gel based on reduced GO layers and an imide anion-based imidazolium IL to improve the redox, electronic and optical properties of another conductive polymer, poly(3,4-ethylenedioxyppyrole). In another study [180], a solid polymer electrolyte membrane with high mechanical strength and ionic conductivity was fabricated by incorporating PIL modified graphene sheets into a protic IL/sulfonated polyimide matrix. Concerning the ionic conductivity, loading of functionalized graphene at only 0.5 wt.% enables to reduce the protic IL content of the membrane by 20%. However, further graphene loading reduces the conductivity of the material. At high operating temperatures (373–423 K), the value of the storage modulus of the resultant hybrid increases up to 25 times compared to the neat membrane.

1.3.2.3 Other applications

Other potential applications of graphene-IL hybrids have also been explored in diverse areas, such as support for metal nanoparticles, electrode in super capacitors, quasi-solid state electrolyte for dye-sensitized solar cells and additive in IL lubricants. IL coated graphene sheets provide large surface area with abundant nucleation sites for growing nanoparticles. For example, Marquardt et al [181] formed and deposited small Ru and Rh nanoparticles with narrow size distributions ($\text{Ru} = 2.2 \pm 0.4 \text{ nm}$ and $\text{Rh} = 2.8 \pm 0.5 \text{ nm}$) on the surface of thermally reduced graphene sheets, which were well separated into individual flakes in the IL. Yang et al [176] obtained uniformly distributed, small gold nanoparticles using graphene sheets non-covalently functionalized with IL as support. As shown in the TEM micrograph in Figure 29c, nanoparticles of $7.2 \pm 0.17 \text{ nm}$ are uniformly distributed on the surface of the graphene coated with IL. According to the AFM images in Figure I.30b and d, the average thicknesses of the graphene-IL layer and the gold nanoparticles are $1.5 \pm 0.22 \text{ nm}$ and $7.1 \pm$

0.23 nm, respectively. The authors constructed a high performing glucose sensor using this hybrid material. Li et al [165] prepared graphene sheets functionalized with a polymer bearing IL units, which they used as support to grow and stabilize Pt nanoparticles of an average size of 2.1 nm. The resultant hybrid can be efficiently used for the simultaneous determination of ascorbic acid and dopamine. This is achieved partly by the electrostatic attraction of the cationic IL polymer to negatively charged ascorbic acid and rejection to positively charged dopamine.

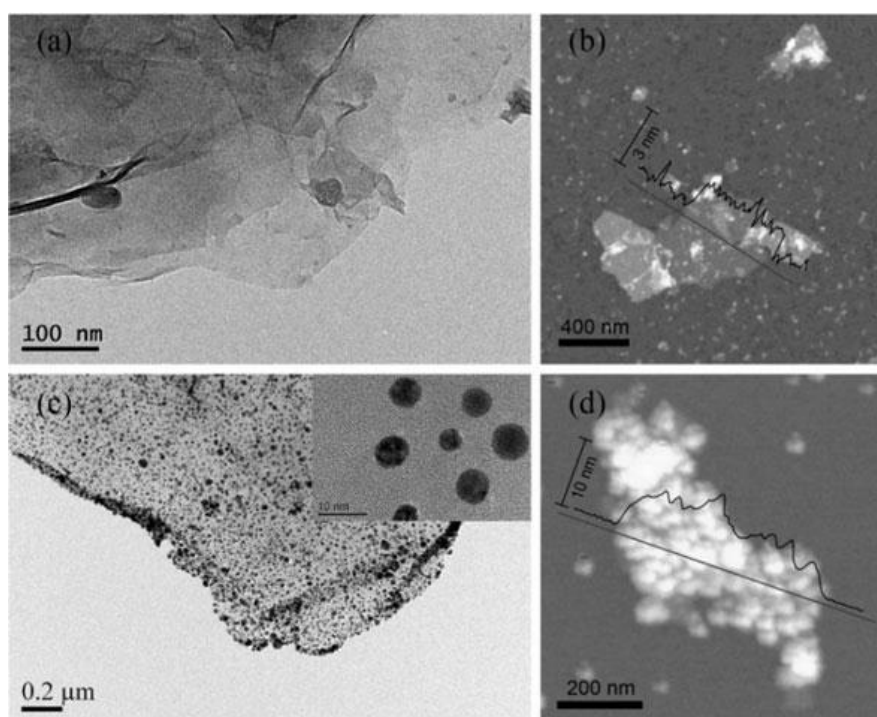


Figure I.30. (A and C) TEM micrographs of rGO-IL and AuNP/rGO-IL hybrids. (B and D) AFM images of rGO-IL and AuNP/rGO-IL hybrids. Inset is line profile across the rGO-IL and AuNP/rGO-IL hybrids showing the roughened surface profile, respectively [176].

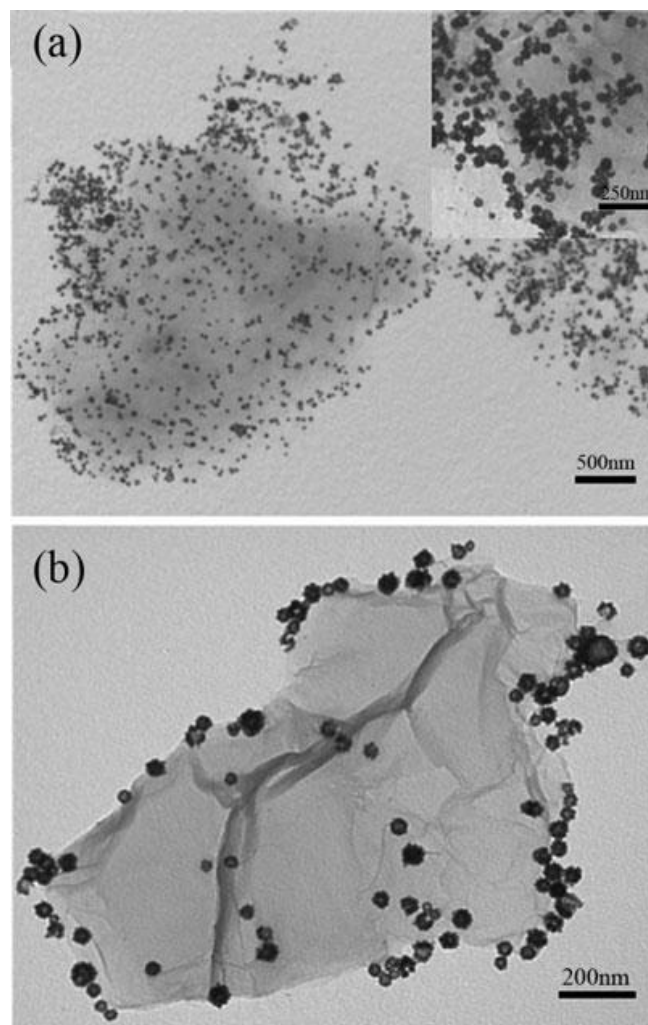


Figure I.31. TEM micrographs of (A) IL-GO-AuPd NPs and (B) polyethenimine functionalized GO-AuPd nanohybrids [182].

Chai et al [182] assembled hollow flower-like AuPd alloy nanoparticles on the surface of IL-functionalized graphene by blending. The well-distributed IL moieties grafted on the epoxy groups of the GO act as a binder between the nanoparticles and the graphene surface. As seen in the TEM micrograph in Figure I.31a, the nanoparticles are uniformly adsorbed on the surface of the positively charged graphene-IL sheets, whereas only few particles are attached to the edges and folds of the polyethenimine functionalized graphene (Figure I.31b). This is because the polymer attaches rather to the highly active $-\text{COOH}$ end groups, which are found mostly on the edges of graphene. The as-prepared graphene-IL-AuPd nanoparticle hybrid

exhibited higher electrocatalytic activity than AuPd nanoparticles toward the oxidation of formic acid. Zhu et al [183] assembled IL-grafted graphene and platinum nanoparticle films using a layer-by-layer assembly technique. The introduction of IL on the surface of graphene sheets does not only enable to disperse well the graphene sheets in water during processing but also provides a building block for the assembly of the nanohybrid layers. The as-developed nanohybrid material exhibits high electrocatalytic activity toward oxygen reduction. Supercapacitor constructed based on rGO electrode and IL electrolyte has showed excellent performance with a specific capacitance of 132 F/g [184]. In a study [185], PIL modification of rGO enhanced the compatibility of the electrode with the IL electrolyte. Moreover, the PIL between the graphene sheets increased the accessibility of the IL electrolyte by increasing the interlayer spacing. The resultant supercapacitor exhibited a specific capacitance of 187 F/g. Very recently, Zhu et al [186] achieved an estimated practical energy density of ~ 20 Wh/kg, comparable to that of conventional lead-acid batteries, using an activated microwave-expanded GO with an extremely high surface area as electrode and [BMIM]BF₄ as electrolyte.

Ahmad et al [187] used carbon based nanomaterials in ionic liquid as quasi-solid state electrolyte for dye-sensitized solar cells. Addition of between 20 and 40 wt.% graphene in IL, 1-methyl-3-propylimidazolium iodide, [MPIM]I, results in a quasi-solid state product. The light conversion efficiency of the neat electrolyte, [MPIM]I, can be increased from 0.16% to 1.43%, 2.10% and 2.50% by using SWCNTs (7 wt.%), graphene (30 wt.%) and a mixture of graphene (12 wt.%) and SWCNTs (3 wt.%) as the extended electron transfer materials, respectively. The use of graphene sheet as the load-carrying phase in the RTIL-based nanohybrid lubrication films for surfaces like polished silicon and diamond-like carbon can be quite interesting to improve the nanotribological properties of the films. However, dispersion of the graphene sheets in the IL phase is a great challenge. Pu et al [188] showed that by the

addition of reduced graphene sheets, non-covalently functionalized with [BMIM]BF₄ at a 0.2 wt.% loading, the nanolubricating and antiwear properties of [BMIM]PF₆ are highly improved.

I.4. Concluding remarks

Carbon nanotubes, due to their outstanding mechanical, thermal and electronic properties, and ionic liquids, as green media, have been extensively studied during the last two decades. In spite of these massive research investments, up to now, and for different reasons, relatively few industrial applications based on these potentially high value chemicals have emerged. In a relatively short period of time, a large body of work has been devoted, both in the academia and industrial sectors, to the combination of these two chemicals to produce hybrid materials that should allow fully exploiting the properties of each of the components. In particular, several studies have shown that the dispersibility of CNTs in polymeric matrices, or the dispersion of nanoparticles on graphene can be highly improved by IL incorporation. Thus, a rich chemistry based on the covalent or non-covalent grafting of IL or polymerizable IL species on CNT and, more recently, graphene has emerged. However, today, the exact nature of the non-covalent interaction between a graphene surface and ILs is poorly understood, and both experimental and modelling studies are definitively needed for a better understanding of such interaction, which can allow the production of gels. A better understanding of the surface chemistry, as well as a good control of CNT quality (length, diameter, helicity) should allow the definition of high performance materials for different applications such as sensors, actuators, antiwear and lubricants, electrocatalysis or energy converters.

References

- [1] Iijima S. Helical microtubules of graphitic carbon. *Nature* 1991;354:56–8.
- [2] Bethune DS, Klang CH, de Vries MS, Gorman G, Savoy R, Vazquez J, et al. Cobalt-catalysed growth of carbon nanotubes with single-atomic-layer walls. *Nature*. 1993;363(6430):605–7.
- [3] Monthieux M, Serp P, Flahaut E, Razafinimanana M, Laurent C, Peigney A, et al. Introduction to carbon nanotubes. In: Bhushan B, editor. *Handbook of nano-technology*. 3rd ed. New York: Springer; 2010, p. 47–118.
- [4] Torimoto T, Tsuda T, Okazaki K, Kuwabata S. New frontiers in materials science opened by ionic liquids. *Adv Mater* 2010;22(11):1196–221.
- [5] Opallo M, Lesniewski A. A review on electrodes modified with ionic liquids. *J Electroanal Chem* 2011;656(1–2):2–16.
- [6] Fukushima T, Kosaka A, Ishimura Y, Yamamoto T, Takigawa T, Ishii N, et al. Molecular ordering of organic molten salts triggered by single-walled carbon nanotubes. *Science* 2003;300(5628):2072–4.
- [7] Xiao F, Ruan CP, Liu LH, Yan R, Zhao FQ, Zeng BH. Single-walled carbon nanotube-ionic liquid paste electrode for the sensitive voltammetric determination of folic acid. *Sens Actuators B* 2008 ; 134(2):895–901.
- [8] Heli H, Majdi S, Jabbari A, Sattarahmady N, Moosavi-Movahedi A. Electrooxidation of dextromethorphan on a carbon nanotube–carbon microparticle–ionic liquid composite: applied to determination in pharmaceutical forms. *J Solid State Electrochem* 2010;14(8):1515–23.
- [9] Novoselov KS, Geim AK, Morozov SV, Jiang D, Zhang Y, Dubonos SV, Grigorieva IV, Firsov AA. Electric field effect in atomically thin carbon films. *Science* 2004;306(5696):666–9.

- [10] Baba K, Kaneko T, Hatakeyama R, Motomiyac K, Tohjic K. Synthesis of monodispersed nanoparticles functionalized carbon nanotubes in plasma-ionic liquid interfacial fields. *Chem Commun* 2010;46(2):255–7.
- [11] Chen S, Wu G, Sha M, Huang S. Transition of ionic liquid [bmim][PF₆] from liquid to high-melting-point crystal when confined in multiwalled carbon nanotubes. *J Am Chem Soc* 2007;129(9):2416–7.
- [12] Subramaniam K, Das A, Heinrich G. Development of conducting polychloroprene rubber using imidazolium based ionic liquid modified multi-walled carbon nanotubes. *Compos Sci Technol* 2011;71(11):1441–9.
- [13] Bellayer S, Gilman JW, Eidelman N, Bourbigot S, Flambard X, Fox DM, et al. Preparation of homogeneously dispersed multiwalled carbon nanotube/polystyrene nanocomposites via melt extrusion using trialkyl imidazolium compatibilizer. *Adv Funct Mater* 2005;15(6):910–6.
- [14] Wang J, Chu H, Li Y. Why single-walled carbon nanotubes can be dispersed in imidazolium-based ionic liquids. *ACS Nano* 2008;2(12):2540–6.
- [15] Hong SH, Tung TT, Trang LKH, Kim TY, Suh KS. Preparation of single-walled carbon nanotube (SWNT) gel composites using poly(ionic liquids). *Colloid Polym Sci* 2010; 288(9):1013–8
- [16] Zhao F, Wu X, Wang M, Liu Y, Gao L, Dong S. Electrochemical and bioelectrochemistry properties of room-temperature ionic liquids and carbon composite materials. *Anal Chem* 2004;76(17):4960–7.
- [17] Mukai K, Asaka K, Sugino T, Kiyohara K, Takeuchi I, Terasawa N, et al. Highly conductive sheets from millimeter-long single-walled carbon nanotubes and ionic liquids: application to fast-moving, low-voltage electromechanical actuators operable in air. *Adv Mater* 2009;21(16):1582–5.

- [18] Chun K-Y, Oh Y, Rho J, Ahn J-H, Kim Y-J, Choi HR, et al. Highly conductive, printable and stretchable composite films of carbon nanotubes and silver. *Nature Nanotech* 2010;5(12):853–7.
- [19] Nieto de Castro CA, Lourenço M, Ribeiro APC, Langa E, Vieira SIC, Goodrich P, et al. Thermal properties of ionic liquids and ionic liquids of imidazolium and pyrrolidinium liquids. *J Chem Eng Data* 2009;55(2):653–61.
- [20] Fukushima T, Asaka K, Kosaka A, Aida T. Fully plastic actuator through layer-by-layer casting with ionic-liquid-based bucky gel. *Angew Chem Int Ed* 2005;44(16):2410–3.
- [21] Mukai K, Asaka K, Kiyohara K, Sugino T, Takeuchi I, Fukushima T, et al. High performance fully plastic actuator based on ionic-liquid-based bucky gel. *Electrochim Acta* 2008;53(17):5555–62.
- [22] Xiao F, Liu L, Li J, Zeng J, Zeng B. Electrocatalytic oxidation and voltammetric determination of nitrite on hydrophobic ionic liquid-carbon nanotube gel-chitosan composite modified electrodes. *Electroanalysis* 2008;20(18):2047–54.
- [23] Liu X, Li L, Zhao X, Lu X. Electrochemical behavior of rutin on a multi-walled carbon nanotube and ionic liquid composite film modified electrode. *Colloids Surf B* 2010;81(1):344–9.
- [24] Du P, Liu S, Wu P, Cai C. Preparation and characterization of room temperature ionic liquid/single-walled carbon nanotube nanocomposites and their application to the direct electrochemistry of heme-containing proteins/enzymes. *Electrochim Acta* 2007;52(23):6534–47.
- [25] Zhao L, Li Y, Liu Z, Shimizu H. Carbon nanotube-conducting polymer core-shell hybrid using an imidazolium-salt-based ionic liquid as a linker: designed as a potential platinum electrode alternative material for large-scale solution processing. *Chem Mater* 2010;22(21):5949–56.

- [26] Tao W, Pan D, Liu Q, Yao S, Nie Z, Han B. Optical and bioelectrochemical characterization of water-miscible ionic liquids based composites of multiwalled carbon nanotubes. *Electroanalysis* 2006;18(17):1681–8.
- [27] Zhao Y, Liu H, Kou Y, Li M, Zhu Z, Zhuang Q. Structural and characteristic analysis of carbon nanotubes-ionic liquid gel biosensor. *Electrochem Commun* 2007;9(10):2457–62.
- [28] Rodriguez-Perez L, Coppel Y, Favier I, Teuma E, Serp P, Gomez M. Imidazolium-based ionic liquids immobilized on solid supports: effect on the structure and thermostability. *Dalton Trans* 2010;39(32):7565–8.
- [29] Green O, Grubjesic S, Lee S, Firestone MA. The design of polymeric ionic liquids for the preparation of functional materials. *J Macromol Sci Polymer Rev* 2009; 49(4):339–60.
- [30] Fukushima T, Kosaka A, Yamamoto Y, Aimiya T, Notazawa S, Takigawa T. Dramatic effect of dispersed carbon nanotubes on the mechanical and electroconductive properties of polymers derived from ionic liquids. *Small* 2006;2(4):554–60.
- [31] Xiao C, Chu X, Wu B, Pang H, Zhang X, Chen J. Polymerized ionic liquid-wrapped carbon nanotubes: the promising composites for direct electrochemistry and biosensing of redox protein. *Talanta* 2010;80(5):1719–24.
- [32] Kim T, Tung TT, Lee T, Kim J, Suh KS. Poly(ionic liquid)-mediated hybridization of single-walled carbon nanotubes and conducting polymers. *Chem Asian J* 2010;5(2):256–60.
- [33] Wu B, Hu D, Kuang Y, Liu B, Zhang X, J. Chen. Functionalization of carbon nanotubes by an ionic-liquid polymer: dispersion of Pt and PtRu nanoparticles on carbon nanotubes and their electrocatalytic oxidation of methanol. *Angew Chem Int Ed* 2009;48(26):4751–4.
- [34] Marcilla R, Curri ML, Cozzoli PD, Martínez MT, Loinaz I, Grande H, et al. Nano-objects on a round trip from water to organics in a polymeric ionic liquid vehicle. *Small* 2006;2(4):507–12.

- [35] Wu B, Hu D, Yu Y, Kuang Y, Zhang X, Chen J. Stabilization of platinum nanoparticles dispersed on carbon nanotubes by ionic liquid polymer. *Chem Commun* 2010;46(42):7954–6.
- [36] Kocharova N, Ääritalo T, Leiro J, Kankare J, Lukkari J. Aqueous dispersion, surface thiolation, and direct self-assembly of carbon nanotubes on gold. *Langmuir* 2007;23(6):3363–71.
- [37] Liu Y, Yu L, Zhang S, Yuan J, Shi L, Zheng L. Dispersion of multiwalled carbon nanotubes by ionic liquid-type Gemini imidazolium surfactants in aqueous solution. *Colloid Surface A* 2010;359(1-3):66–70.
- [38] Dong B, Su Y, Liu Y, Yuan J, Xu J, Zheng L. Dispersion of carbon nanotubes by carbazole-tailed amphiphilic imidazolium ionic liquids in aqueous solutions. *J Colloid Interface Science* 2011;356(1):190–5.
- [39] Crescenzo AD, Demurtas D, Renzetti A, Siani G, De Maria P, Meneghetti M, et al. Disaggregation of single-walled carbon nanotubes (SWNTs) promoted by the ionic liquid-based surfactant 1-hexadecyl-3-vinyl-imidazolium bromide in aqueous solution. *Soft Matter* 2009;5(1):62–6.
- [40] Crescenzo AD, Aschi M, Canto ED, Giordani S, Demurtas D, Fontana A. Structural modifications of ionic liquid surfactants for improving the water dispersibility of carbon nanotubes: an experimental and theoretical study. *Phys Chem Chem Phys* 2011;13(23):11373–83.
- [41] Zhou X, Wu T, Ding K, Hu B, Hou M, Han B. The dispersion of carbon nanotubes in water with the aid of very small amounts of ionic liquid. *Chem Commun* 2009;14:1897–9.
- [42] Gao L, Yin H, Wang D. Ionic liquids assisted formation of an oil/water emulsion stabilised by a carbon nanotube/ionic liquid composite layer. *Phys Chem Chem Phys* 2010;12(11):2535–40.

- [43] Yu B, Zhou F, Liu G, Liang Y, Huck WTS, Liu W. The electrolyte switchable solubility of multi-walled carbon nanotube/ionic liquid (MWCNT/IL) hybrids. *Chem Commun* 2006;22:2356–8.
- [44] Wang B, Wang X, Lou W, Hao J. Rheological and tribological properties of ionic liquid-based nanofluids containing functionalized multi-walled carbon nanotubes. *J Phys Chem C* 2010;114(19):8749–54.
- [45] Guo S, Dong S, Wang E. Constructing carbon nanotube/Pt nanoparticle hybrids using an imidazolium-salt-based ionic liquid as a linker. *Adv Mater* 2010;22(11):1269–72.
- [46] Zhang Y, Shen Y, Yuan J, Han D, Wang Z, Zhang Q, et al. Design and synthesis of multifunctional materials based on an ionic-liquid backbone. *Angew Chem Int Ed* 2006;45(35):5867–70.
- [47] Park MJ, Lee JK, Lee BS, Lee Y, Choi IS, Lee S. Covalent modification of multiwalled carbon nanotubes with imidazolium-based ionic liquids: effect of anions on solubility. *Chem Mater* 2006;18(6):1546–51.
- [48] Rodríguez-Pérez L, Teuma E, Falqui A, Gómez M, Serp P. Supported ionic liquid phase catalysis on functionalized carbon nanotubes. *Chem Commun* 2008;35:4201–3.
- [49] Carrión F, Sanes J, Bermúdez M-D, Arribas A. New single-walled carbon nanotubes–ionic liquid lubricant. Application to polycarbonate–stainless steel sliding contact. *Tribol Lett* 2011;41(1):199–207.
- [50] Wang Z, Zhang Q, Kuehner D, Xua X, Ivaskab A, Niua L. The synthesis of ionic-liquid-functionalized multiwalled carbon nanotubes decorated with highly dispersed Au nanoparticles and their use in oxygen reduction by electrocatalysis. *Carbon* 2008;46(13):1687–92.
- [51] Ahammad AJS, Lee J-J, Rahman MA. Electrochemical sensors based on carbon nanotubes. *Sensors* 2009;9(4):2289–319.

- [52] Tao H, Wei W, Zeng X, Liu X, Zhang X, Zhang Y. Electrocatalytic oxidation and determination of estradiol using an electrode modified with carbon nanotubes and an ionic liquid. *Microchim Acta* 2009;166(1):53–9.
- [53] Zhang W, Yang T, Zhuang X, Guo Z, Jiao K. An ionic liquid supported CeO₂ nanoshuttles-carbon nanotubes composite as a platform for impedance DNA hybridization sensing. *Biosens Bioelectron* 2009;24(8):2417–22.
- [54] Zhang X, Jiao K, Wang X. Paste electrode based on short single-walled carbon nanotubes and room temperature ionic liquid: preparation, characterization and application in DNA detection. *Electroanalysis* 2008;20(12):1361–6.
- [55] Sun Y, Fei J, Hou J, Zhang Q, Liu Y, Hu B. Simultaneous determination of dopamine and serotonin using a carbon nanotubes-ionic liquid gel modified glassy carbon electrode. *Microchim Acta* 2009;165(3):373–9.
- [56] Zhao Y, Gao Y, Zhan D, Liu H, Zhao Q, Kou Y, et al. Selective detection of dopamine in the presence of ascorbic acid and uric acid by a carbon nanotubes-ionic liquid gel modified electrode. *Talanta* 2005;66(1):51–7.
- [57] Liu Y, Zou X, Dong S. Electrochemical characteristics of facile prepared carbon nanotubes–ionic liquid gel modified microelectrode and application in bioelectrochemistry. *Electrochem Commun* 2006;8(9):1429–34.
- [58] Liu T, Zhu X, Cui L, Ju P, Qu X, Ai S. Simultaneous determination of adenine and guanine utilizing PbO₂-carbon nanotubes-ionic liquid composite film modified glassy carbon electrode. *J Electroanal Chem* 2011;651(2):216–21.
- [59] Chen Y, Chen X, Lin Z, Dai H, Qiu B, Sun J, et al. An electrically heated ionic-liquid/multi-wall carbon nanotube composite electrode and its application to electrochemiluminescent detection of ascorbic acid. *Electrochem Commun* 2009;11(6):1142–5.

- [60] Xiao F, Zhao F, Zeng J, Zeng B. Novel alcohol sensor based on PtRuNi ternary alloy nanoparticles–multi-walled carbon nanotube–ionic liquid composite coated electrode. *Electrochem Commun* 2009;11(7):1550–3.
- [61] Yu P, Qian Q, Lin Y, Mao L. In situ formation of three-dimensional uniform Pt/carbon nanotube nanocomposites from ionic liquid/carbon nanotube gel matrix with enhanced electrocatalytic activity toward methanol oxidation. *J Phys Chem C* 2010;114(8):3575–9.
- [62] Liu X, Ding Z, He Y, Xue Z, Zhao X, Lu X. Electrochemical behavior of hydroquinone at multi-walled carbon nanotubes and ionic liquid composite film modified electrode. *Colloids Surf B Biointerfaces* 2010;79(1):27–32.
- [63] Zhu H, Lu X, Li M, Shao Y, Zhu Z. Nonenzymatic glucose voltammetric sensor based on gold nanoparticles/carbon nanotubes/ionic liquid nanocomposite. *Talanta* 2009;79(5):1446–53.
- [64] Kachoosangi RT, Musameh MM, Abu-Yousef I, Yousef JM, Kanan SM, Xiao L, et al. Carbon nanotube–ionic liquid composite sensors and biosensors. *Anal Chem* 2008;81(1):435–42.
- [65] Zhan XM, Liu LH, Gao ZN. Electrocatalytic oxidation of quinine sulfate at a multiwall carbon nanotubes-ionic liquid modified glassy carbon electrode and its electrochemical determination. *J Solid State Electrochem* 2011;15(6):1185–92.
- [66] Fan S, Xiao F, Liu L, Zhao F, Zeng B. Sensitive voltammetric response of methylparathion on single-walled carbon nanotube paste coated electrodes using ionic liquid as binder. *Sensor Actuat B-Chem* 2008;132(1):34–9.
- [67] Li CM, Zang J, Zhan D, Chen W, Sun CQ, Teo AL, et al. Electrochemical detection of nitric oxide on a SWCNT/RTIL composite gel microelectrode. *Electroanalysis* 2006;18(7):713–8.

- [68] Xiao F, Zhao F, Li J, Yan R, Yu J, Zeng B. Sensitive voltammetric determination of chloramphenicol by using single-wall carbon nanotube–gold nanoparticle–ionic liquid composite film modified glassy carbon electrodes. *Anal Chim Acta* 2007;596(1):79–85.
- [69] Yan Q, Zhao F, Li G, Zeng B. Voltammetric determination of uric acid with a glassy carbon electrode coated by paste of multiwalled carbon nanotubes and ionic liquid. *Electroanalysis* 2006;18(11):1075–80.
- [70] Zhao F, Liu L, Xiao F, Li J, Yan R, Fan S, et al. Sensitive voltammetric response of p-nitroaniline on single-wall carbon nanotube-ionic liquid gel modified glassy carbon electrodes. *Electroanalysis* 2007;19(13):1387–93.
- [71] Chen J, Yang G, Chen M, Li W. Sensitive determination of 4-nitrophenol based on multi-walled carbon nano-tube/ionic liquid/chitosan composite film modified electrode. *Russ J Electrochem* 2009;45(11):1287–91.
- [72] Xiao F, Ruan C, Li J, Liu L, Zhao F, Zeng B. Voltammetric determination of xanthine with a single-walled carbon nanotube-ionic liquid paste modified glassy carbon electrode. *Electroanalysis* 2008;20(4):361–6.
- [73] Liu L, Xiao F, Li J, Wu W, Zhao F, Zeng B. Platinum nanoparticles decorated multiwalled carbon nanotubes – ionic liquid composite film coated glassy carbon electrodes for sensitive determination of theophylline. *Electroanalysis* 2008;20(11):1194–9.
- [74] Chailapakul O, Wonsawat W, Siangproh W, Grudpan K, Zhao Y, Zhu Z. Analysis of sudan I, sudan II, sudan III, and sudan IV in food by HPLC with electrochemical detection: comparison of glassy carbon electrode with carbon nanotube-ionic liquid gel modified electrode. *Food Chem* 2008;109(4):876–82.
- [75] Wan Q, Yu F, Zhu L, Wang X, Yang N. Bucky-gel coated glassy carbon electrodes, for voltammetric detection of femtomolar leveled lead ions. *Talanta* 2010;82(5):1820–5.

- [76] Ganjali MR, Khoshsafar H, Shirzadmehr A, Javanbakht M, Faridbod F. Improvement of carbon paste ion selective electrode response by using room temperature ionic liquids (RTILs) and multi-walled carbon nanotubes (MWCNTs). *Int J Electrochem Sci* 2009;4:435 – 43.
- [77] Rahimi P, Rafiee-Pour H-A, Ghourchian H, Norouzi P, Ganjali MR. Ionic-liquid/NH₂-MWCNTs as a highly sensitive nano-composite for catalase direct electrochemistry. *Biosens Bioelectron* 2010;25(6):1301–6.
- [78] Wan J, Bi J, Du P, Zhang S. Biosensor based on the biocatalysis of microperoxidase-11 in nanocomposite material of multiwalled carbon nanotubes/room temperature ionic liquid for amperometric determination of hydrogen peroxide. *Anal Biochem* 2009;386(2):256–61.
- [79] Zhang Y, Zheng J. Direct electrochemistry and electrocatalysis of hemoglobin based on nafion-room temperature ionic liquids-multiwalled carbon nanotubes composite film. *Chin J Chem* 2011;29(4):685–90.
- [80] Zhang Y, Zheng J. Direct electrochemistry and electrocatalysis of cytochrome C based on chitosan–room temperature ionic liquid-carbon nanotubes composite. *Electrochim Acta* 2008;54(2):749–54.
- [81] Xiang C, Zou Y, Sun L-X, Xu F. Direct electron transfer of cytochrome C and its biosensor based on gold nanoparticles/room temperature ionic liquid/carbon nanotubes composite film. *Electrochem Commun* 2008;10(1):38–41.
- [82] Liu Y, Huang L, Dong S. Electrochemical catalysis and thermal stability characterization of laccase–carbon nanotubes-ionic liquid nanocomposite modified graphite electrode. *Biosens Bioelectron* 2007;23(1):35–41.
- [83] Liu Y, Liu L, Dong S. Electrochemical characteristics of glucose oxidase adsorbed at carbon nanotubes modified electrode with ionic liquid as binder. *Electroanalysis* 2007;19(1):55–9.

- [84] Zhang Y, Shen Y, Li J, Niu L, Dong S, Ivaska A. Electrochemical functionalization of single-walled carbon nanotubes in large quantities at a room-temperature ionic liquid supported three-dimensional network electrode. *Langmuir* 2005;21(11):4797–800.
- [85] Wu X, Zhao F, Varcoe JR, Thumser AE, Avignone-Rossa C, Slade RCT. Direct electron transfer of glucose oxidase immobilized in an ionic liquid reconstituted cellulose–carbon nanotube matrix. *Bioelectrochemistry* 2009;77(1):64–8.
- [86] Shangguan X, Zheng J, Zhang H, Tang H. Direct electrochemistry and electrocatalysis behaviors of glucose oxidase based on hyaluronic acid-carbon nanotubes-ionic liquid composite film. *Chin J Chem* 2010;28(10):1890–6.
- [87] Wu X, Zhao B, Wu P, Zhang H, Cai C. Effects of ionic liquids on enzymatic catalysis of the glucose oxidase toward the oxidation of glucose. *J Phys Chem B* 2009;113(40):13365–73.
- [88] Gao R, Zheng J. Amine-terminated ionic liquid functionalized carbon nanotube-gold nanoparticles for investigating the direct electron transfer of glucose oxidase. *Electrochem Commun* 2009;11(3):608–11.
- [89] Zhang Y, Shen Y, Han D, Wang Z, Song J, Li F, et al. Carbon nanotubes and glucose oxidase bionanocomposite bridged by ionic liquid-like unit: preparation and electrochemical properties. *Biosens Bioelectron* 2007;23(3):438–43.
- [90] Li J, Zhao F, Wang G, Gui Z, Xiao F, Zeng B. Novel composite of multiwalled carbon nanotubes and gold nanoparticles stabilized by chitosan and hydrophilic ionic liquid for direct electron transfer of glucose oxidase. *Electroanalysis* 2009;21(2):150–6.
- [91] Choi BG, Park H, Park TJ, Kim DH, Lee SY, Hong WH. Development of the electrochemical biosensor for organophosphate chemicals using CNT/ionic liquid bucky gel electrode. *Electrochem Commun* 2009;11(3):672–5.

- [92] Tani Y, Itoyama Y, Nishi K, Wada C, Shoda Y, Satomura T, et al. An amperometric D-amino acid biosensor prepared with a thermostable D-proline dehydrogenase and a carbon nanotube-ionic liquid gel. *Anal Sci* 2009;25(7):919–23.
- [93] Zhu Z, Qu L, Li X, Zeng Y, Sun W, Huang X. Direct electrochemistry and electrocatalysis of hemoglobin with carbon nanotube-ionic liquid-chitosan composite materials modified carbon ionic liquid electrode. *Electrochim Acta* 2010;55(20):5959–65.
- [94] Tu W, Lei J, Ju H. Functionalization of carbon nanotubes with water-insoluble porphyrin in ionic liquid: direct electrochemistry and highly sensitive amperometric biosensing for trichloroacetic acid. *Chem Eur J* 2009;15(3):779–84.
- [95] Wang Q, Tang H, Xie Q, Tan L, Zhang Y, Li B, et al. Room-temperature ionic liquids/multi-walled carbon nanotubes/chitosan composite electrode for electrochemical analysis of NADH. *Electrochim Acta* 2007;52(24):6630–7.
- [96] Salimi A, Lasghari S, Noorbakhash A. Carbon nanotubes-ionic liquid and chlorpromazine modified electrode for determination of NADH and fabrication of ethanol biosensor. *Electroanalysis* 2010;22(15):1707–16.
- [97] Musameh MM, Kachoosangib RT, Compton RG. Enhanced stability and sensitivity of ionic liquid–carbon paste electrodes at elevated temperatures. *Analyst* 2008;133(1):133–8.
- [98] Kachoosangi RT, Wildgoose GG, Compton RG. Room temperature ionic liquid carbon nanotube paste electrodes: overcoming large capacitive currents using rotating disk electrodes. *Electroanalysis* 2007;19(14):1483–9.
- [99] Jia F, Shan C, Li F, Niu L. Carbon nanotube/gold nanoparticles/polyethylenimine-functionalized ionic liquid thin film composites for glucose biosensing. *Biosens Bioelectron* 2008;24(4):945–50.

- [100] Wei W, Jin HH, Zhao GC. A reagentless nitrite biosensor based on direct electron transfer of hemoglobin on a room temperature ionic liquid/carbon nanotube-modified electrode. *Microchim Acta* 2009;164(1-2):167–71.
- [101] Zhao H, Olubajo O, Song Z, Sims AL, Person TE, Lawal RA. Effect of kosmotropicity of ionic liquids on the enzyme stability in aqueous solutions. *Bioorg Chem* 2006;34(1):15–25.
- [102] Park S, Kazlauskas RJ. Biocatalysis in ionic liquids – advantages beyond green technology. *Curr Opin Chem Biol* 2003;14(4):432–37.
- [103] Widegren JA, Saurer EM, Marsh KN, Magee JW. Electrolytic conductivity of four imidazolium-based room-temperature ionic liquids and the effect of a water impurity. *J Chem Thermodyn* 2005;37(6):569–75.
- [104] Terasawa N, Takeuchi I, Matsumoto H. Electrochemical properties and actuation mechanisms of actuators using carbon nanotube-ionic liquid gel. *Sensor Actuat B-Chem* 2009;139(2):624–30.
- [105] Randriamahazaka H, Asaka K. Electromechanical analysis by means of complex capacitance of bucky-gel actuators based on single-walled carbon nanotubes and an ionic liquid. *J Phys Chem C* 2010;114(41):17982–8.
- [106] Terasawa N, Takeuchi I, Matsumoto H, Mukai K, Asaka K. High performance polymer actuator based on carbon nanotube-ionic liquid gel: effect of ionic liquid. *Sensor Actuat B-Chem* 2011;156(2):539–45.
- [107] Ceseracciu L, Biso M, Ansaldo A, Futaba DN, Hata K, Barone AC, et al. Mechanics and actuation properties of bucky gel-based electroactive polymers. *Sensor Actuat B-Chem* 2011;156(2):949–53.
- [108] Biso M, Ricci D. Multi-walled carbon nanotubes plastic actuator. *Phys Status Solidi B* 2009;246(11–12):2820–3.

- [109] Sugino T, Kiyohara K, Takeuchi I, Mukai K, Asaka K. Actuator properties of the complexes composed by carbon nanotube and ionic liquid: The effects of additives. *Sensor Actuat B-Chem* 2009;141(1):179–86.
- [110] Sugino T, Kiyohara K, Takeuchi I, Mukai K, Asaka K. Improving the actuating response of carbon nanotube/ionic liquid composites by the addition of conductive nanoparticles. *Carbon* 2011;49(11):3560–70.
- [111] Terasawa N, Takeuchi I, Mukai K, Asaka K. The effects of Li salts on the performance of a polymer actuator based on single-walled carbon nanotube-ionic liquid gel. *Polymer* 2010;51(15):3372–6.
- [112] Biso M, Ansaldo A, Futaba DN, Hata K, Ricci D. Cross-linking super-growth carbon nanotubes to boost the performance of bucky gel actuators. *Carbon* 2011;49(7):2253–7.
- [113] Biso M, Ansaldo A, Futaba DN, Hata K, Ricci D. Benchmarking bucky gel actuators: Chemically modified commercial carbon nanotubes versus super-growth carbon nanotubes. *Phys Status Solidi B* 2010;247(11–12):3055–8.
- [114] Takeuchi I, Asaka K, Kiyohara K, Sugino T, Terasawa N, Mukai K, et al. Electromechanical behavior of fully plastic actuators based on bucky gel containing various internal ionic liquids. *Electrochim Acta* 2009;54(6):1762–8.
- [115] Lu L, Chen W. Biocompatible composite actuator: A supramolecular structure consisting of the biopolymer chitosan, carbon nanotubes, and an ionic liquid. *Adv Mater* 2010;22(33):3745–8.
- [116] Katakabe T, Kaneko T, Watanabe M, Fukushima T, Aida T. Electric double-layer capacitors using "bucky gels" consisting of an ionic liquid and carbon nanotubes. *J Electrochem Soc* 2005;152(10):A1913–6.
- [117] Pushparaj VL, Shaijumon MM, Kumar A, Murugesan S, Ci L, Vajtai R. Flexible energy storage devices based on nanocomposite paper. *PNAS* 2007;104(34):13574–7.

- [118] Miyako E, Nagata H, Funahashi R, Hirano K, Hirotsu T. Light-driven thermoelectric conversion based on a carbon nanotube–ionic liquid gel composite. *ChemSusChem* 2009;2(8):740–2.
- [119] Kawano R, Katakabe T, Shimosawa H, Khaja Nazeeruddin M, Gratzel M, Matsui H, et al. Solid-state dye-sensitized solar cells using polymerized ionic liquid electrolyte with platinum-free counter electrode. *Phys Chem Chem Phys* 2010;12(8):1916–21.
- [120] Lee C-P, Lin L-Y, Chen P-Y, Vittal R, Ho K-C. All-solid-state dye-sensitized solar cells incorporating SWCNTs and crystal growth inhibitor. *J Mater Chem* 2010;20(18):3619–25.
- [121] Chun YS, Shin JY, Song CE, Lee S. Palladium nanoparticles supported onto ionic carbon nanotubes as robust recyclable catalysts in an ionic liquid. *Chem Commun* 2008;8:942–4.
- [122] Shin JY, Kim YS, Lee Y, Shim H, Lee C, Lee S. Impact of anions on electrocatalytic activity in palladium nanoparticles supported on ionic liquid–carbon nanotube hybrids for the oxygen reduction reaction. *Chem Asian J* 2011;6(8):2016–21.
- [123] Lee JK, Kim M. Hydrogenation of aryl ketones using palladium nanoparticles on single-walled carbon nanotubes in an ionic liquid. *Tetrahedron Lett* 2011;52(4):499–501.
- [124] Rodríguez-Pérez L, Pradel C, Serp P, Gómez M, Teuma E. Supported ionic liquid phase containing palladium nanoparticles on functionalized multiwalled carbon nanotubes: catalytic materials for sequential Heck coupling/hydrogenation process. *ChemCatChem* 2011;3(4):749–54.
- [125] Park HS, Choi BG, Yang SH, Shin WH, Kang JK, Jung D. Ionic-liquid-assisted sonochemical synthesis of carbon-nanotube based nanohybrids: control in the structures and interfacial characteristics. *Small* 2009;5(15):1754–60.

- [126] Chu H, Shen Y, Lin L, Qin X, Feng G, Lin Z, et al. Ionic-liquid-assisted preparation of carbon nanotube-supported uniform noble metal nanoparticles and their enhanced catalytic performance. *Adv Funct Mater* 2010;20(21):3747–52.
- [127] Zhang H, Cui H. Synthesis and characterization of functionalized ionic liquid-stabilized metal (gold and platinum) nanoparticles and metal nanoparticle/carbon nanotube hybrids. *Langmuir* 2009;25(5):2604–12.
- [128] Guo D. Novel synthesis of PtRu/multi-walled carbon nanotube catalyst via a microwave-assisted imidazolium ionic liquid method for methanol oxidation. *J Power Sources* 2010;195(21):7234–7.
- [129] Li C, Gu L, Tong J, Maier J. Carbon nanotube wiring of electrodes for high-rate lithium batteries using an imidazolium-based ionic liquid precursor as dispersant and binder: a case study on iron fluoride. *Nanoparticles* 2011;5(4):2930–8.
- [130] Bermúdez, MD, Carrión FJ, Espejo C, Martínez-López E, Sanes J. Abrasive wear under multiscratching of polystyrene + single-walled carbon nanotube nanocomposites. Effect of sliding direction and modification by ionic liquid. *Appl Surf Sci* 2011;257(21):9073–81.
- [131] Carrión FJ, Espejo C, Sanes J, Bermúdez MD. Single-walled carbon nanotubes modified by ionic liquid as antiwear additives of thermoplastics. *Compos Sci Technol* 2010;70(15):2160–7.
- [132] Yu B, Liu Z, Zhou F, Liu W, Liang Y. A novel lubricant additive based on carbon nanotubes for ionic liquids. *Mater Lett* 2008;62(17–18):2967–9.
- [133] Sekitani T, Noguchi Y, Hata K, Fukushima T, Aida T, Someya T. A rubberlike stretchable active matrix using elastic conductors. *Science* 2008;321(5895):1468–72.
- [134] Likožar B. Diffusion of ionic liquids into elastomer/carbon nanotubes composites and tensile mechanical properties of resulting materials. *Scientia Iranica* 2010;17(1):35–42.

- [135] Das A, Stöckelhuber KW, Jurk R, Fritzsche J, Klüppel M, Heinrich G. Coupling activity of ionic liquids between diene elastomers and multi-walled carbon nanotubes. *Carbon* 2009;47(14):3313–21.
- [136] Tung TT, Kim TY, Suh KS. Nanocomposites of single-walled carbon nanotubes and poly(3,4-ethylenedioxythiophene) for transparent and conductive film. *Org Electron* 2011; 12(1):22–8.
- [137] Liu L, Zheng Z, Gu C, Wang X. The poly(urethane-ionic liquid)/multi-walled carbon nanotubes composites. *Compos Sci Technol* 2010;70(12):1697–703.
- [138] Zhang H, Wang Z, Zhang Z, Wu J, Zhang J, He J. Regenerated cellulose/multiwalled-carbon-nanotube composite fibers with enhanced mechanical properties prepared with the ionic liquid 1-allyl-3-methylimidazolium chloride. *Adv Mater* 2007;19(5):698–704.
- [139] Rahatekar SS, Rasheed A, Jain R, Zammarano M, Koziol KK, Windle AH, Gilman JW, Kumar S. Solution spinning of cellulose carbon nanotube composites using room temperature ionic liquids. *Polymer* 2009;50(19):4577–83.
- [140] Singh V, Joung D, Zhai L, Das S, Khondaker SI, Seal S. Graphene based materials: past, present and future. *Prog Mater Sci* 2011;56(8):1178–271.
- [141] Liu N, Luo F, Wu H, Liu Y, Zhang C, Chen J. One-step ionic-liquid-assisted electrochemical synthesis of ionic-liquid-functionalized graphene sheets directly from graphite. *Adv Funct Mater* 2008;18(10):1518–25.
- [142] Zhou X, Wu T, Ding K, Hu B, Hou M, Han B. Dispersion of graphene sheets in ionic liquid [bmim][PF₆] stabilized by an ionic liquid polymer. *Chem Commun* 2010;46(3):386–8.
- [143] Yang H, Shan C, Li F, Han D, Zhang Q, Niu L. Covalent functionalization of polydisperse chemically-converted graphene sheets with amine-terminated ionic liquid. *Chem Commun* 2009;26:3880–2.

- [144] Bhunia P, Hwang E, Min M, Lee J, Seo S, Some S, et al. A non-volatile memory device consisting of graphene oxide covalently functionalized with ionic liquid. *Chem Commun* 2012;48(6):913–5.
- [145] Karousis N, Economopoulos SP, Sarantopoulou E, Tagmatarchis N. Porphyrin counter anion in imidazolium-modified graphene-oxide. *Carbon* 2010;48(3):854–60.
- [146] Baldelli S, Bao J, Wub W, Pei S. Sum frequency generation study on the orientation of room-temperature ionic liquid at the graphene–ionic liquid interface. *Chem Phys Lett* 2011; 516(4–6):171–3.
- [147] Ghatee MH, Moosavi F. Physisorption of hydrophobic and hydrophilic 1-alkyl-3-methylimidazolium ionic liquids on the graphenes. *J Phys Chem C* 2011;115(13):5626–36.
- [148] Wang X, Fulvio PF, Baker GA, Veith GM, Unocic RR, Mahurin SM, Chib M, Dai S. Direct exfoliation of natural graphite into micrometre size few layers graphene sheets using ionic liquids. *Chem Commun* 2010;46(25):4487–9.
- [149] Nuvoli D, Valentini L, Alzari V, Scognamillo S, Bon SB, Piccinini M, et al. High concentration few-layer graphene sheets obtained by liquid phase exfoliation of graphite in ionic liquid. *J Mater Chem* 2011;21(10):3428–31.
- [150] Zhang B, Ning W, Zhang J, Qiao X, Zhang J, He J, et al. Stable dispersions of reduced graphene oxide in ionic liquids. *J Mater Chem* 2010;20(26):5401–3.
- [151] Ng SR, Guo CX, Li CM. Highly sensitive nitric oxide sensing using three-dimensional graphene/ionic liquid nanocomposite. *Electroanalysis* 2011;23(2):442–8.
- [152] Guo CX, Z. Lu ZS, Lei Y, Li CM. Ionic liquid–graphene composite for ultratrace explosive trinitrotoluene detection. *Electrochem Commun* 2010;12(9):1237–40.
- [153] Reddy BN, Deepa M, Joshi AG, Srivastava AK. Poly(3,4-Ethylenedioxyppyrrrole) enwrapped by reduced graphene oxide: how conduction behavior at nanolevel leads to increased electrochemical activity. *J Phys Chem C* 2011;115(37):18354–65.

- [154] Kim T, Lee H, Kim J, Suh KS. Synthesis of phase transferable graphene sheets using ionic liquid polymers. *ACS Nano* 2010;4(3):1612–8.
- [155] Zhou X, Wu T, Hu B, Yang G, Han B. Synthesis of graphene/polyaniline composite nanosheets mediated by polymerized ionic liquid. *Chem Commun* 2010;46(21):3663–5.
- [156] Tung TT, Kim TY, Shim JP, Yang WS, Kim H, Suh KS. Poly(ionic liquid)-stabilized graphene sheets and their hybrid with poly(3,4-ethylenedioxythiophene). *Org Electron* 2011;12(12):2215–24.
- [157] Saxena AP, Deepa M, Joshi AG, Bhandari S, Srivastava K. Poly(3,4-ethylenedioxythiophene)-ionic liquid functionalized graphene/reduced graphene oxide nanostructures: improved conduction and electrochromism. *ACS Appl Mater Interfaces* 2011; 3(4):1115–26.
- [158] Lu J, Yang J, Wang J, Lim A, Wang S, Loh KP. One-pot synthesis of fluorescent carbon nanoribbons, nanoparticles, and graphene by the exfoliation of graphite in ionic liquids. *ACS Nano* 2009;3(8):2367–75.
- [159] Gan T, Hu S. Electrochemical sensors based on graphene materials. *Microchim Acta* 2011;175(1):1–19.
- [160] Shan C, Yang H, Song J, Han D, Ivaska A, Niu L. Direct electrochemistry of glucose oxidase and biosensing for glucose based on graphene. *Anal Chem* 2009;81(6):2378–82.
- [161] Yang MH, Choi BG, Park H, Hong WH, Lee SY, Park TJ. Development of a glucose biosensor using advanced electrode modified by nanohybrid composing chemically modified graphene and ionic liquid. *Electroanalysis* 2010; 22(11):1223–28.
- [162] Zhang Q, Wu S, Zhang L, Lu J, Verproot F, Liu Y, et al. Fabrication of polymeric ionic liquid/graphene nanocomposite for glucose oxidase immobilization and direct electrochemistry. *Biosens Bioelectron* 2011;26(5):2632–7.

- [163] Liu Z, Wang Z, Cao Y, Jing Y, Liu Y. High sensitive simultaneous determination of hydroquinone and catechol based on graphene/BMIMPF₆ nanocomposite modified electrode. *Sens Actuators B* 2011;157(2):540–6.
- [164] Du M, Yang T, Ma S, Zhao C, Jiao K. Ionic liquid-functionalized graphene as modifier for electrochemical and electrocatalytic improvement: comparison of different carbon electrodes. *Anal Chim Acta* 2011;690(2):169–74.
- [165] Li F, Chai J, Yang H, Han D, Niu L. Synthesis of Pt/ionic liquid/graphene nanocomposite and its simultaneous determination of ascorbic acid and dopamine. *Talanta*. 2010;81(3):1063–8.
- [166] Shan C, Yang H, Han D, Zhang Q, Ivaskac A, Niu L. Electrochemical determination of NADH and ethanol based on ionic liquid-functionalized graphene. *Biosens Bioelectron* 2010;25(6):1504–8.
- [167] Guo S, Wen D, Zhai Y, Dong S, Wang E. Ionic liquid–graphene hybrid nanosheets as an enhanced material for electrochemical determination of trinitrotoluene. *Biosens Bioelectron* 2011;26(8):3475–81.
- [168] Peng JY, Hou CT, Liu XX, Li HB, Hu XY. Electrochemical behavior of azithromycin at graphene and ionic liquid composite film modified electrode. *Talanta*. 2011;86(0):227–32.
- [169] Shi J, Zhua J. Sonoelectrochemical fabrication of Pd-graphene nanocomposite and its application in the determination of chlorophenols. *Electrochim Acta* 2011;56(17):6008–13.
- [170] Sun J, Huang K, Zhao S, Fan Y, Wu Z. Direct electrochemistry and electrocatalysis of hemoglobin on chitosan-room temperature ionic liquid-TiO₂-graphene nanocomposite film modified electrode. *Bioelectrochem* 2011;82(2):125–30.
- [171] Mao Y, Bao Y, Wang W, Li Z, Li F, Niu L. Layer-by-layer assembled multilayer of graphene/Prussian blue toward simultaneous electrochemical and SPR detection of H₂O₂. *Talanta* 2011;85(4):2106–12.

- [172] He Y, Zheng J, Li K, Sheng Q, Qiao N. A hydrogen peroxide biosensor based on room temperature ionic liquid functionalized graphene modified carbon ceramic electrode. *Chin J Chem* 2010;28(12):2507–12.
- [173] Liao H, Wu H, Wang J, Liu J, Jiang Y, Sun S, et al. Direct electrochemistry and electrocatalysis of myoglobin immobilized on graphene-CTAB-ionic liquid nanocomposite film. *Electroanalysis* 2010;22(19):2297–302.
- [174] Liu K, Zhang J, Yang G, Wang C, Zhu J. Direct electrochemistry and electrocatalysis of hemoglobin based on poly(diallyldimethylammonium chloride) functionalized graphene sheets/room temperature ionic liquid composite film. *Electrochem Commun* 2010;12(3):402–5.
- [175] Qiu Y, Qu X, Dong J, Ai S, Han R. Electrochemical detection of DNA damage induced by acrylamide and its metabolite at the graphene-ionic liquid-nafion modified pyrolytic graphite electrode. *J Hazard Mater* 2011;190(1–3):480–5.
- [176] Yang MH, Choi BG, Park H, Park TJ, Hong WH, Lee SY. Directed self-assembly of gold nanoparticles on graphene-ionic liquid hybrid for enhancing electrocatalytic activity. *Electroanalysis* 2011; 23(4):850–7.
- [177] Ji Q, Honma I, Paek S, Akada M, Hill JP, Vinu A, et al. Layer-by-layer films of graphene and ionic liquids for highly selective gas sensing. *Angew Chem Int Ed* 2010;49(50):9737–39.
- [178] Rafiee MA, Rafiee J, Wang Z, Song H, Yu Z, Koratkar N. Enhanced mechanical properties of nanocomposites at low graphene content. *ACS Nano* 2009;3(12):3884–90.
- [179] Xie SH, Y. Liu YY, Li JY. Comparison of the effective conductivity between composites reinforced by graphene nanosheets and carbon nanotubes. *Appl Phys Lett* 2008; 92(24):243121–3.

- [180] Ye Y, Tseng C, Shen W, Wang J, Chen K, Cheng M, et al. A new graphene-modified protic ionic liquid-based composite membrane for solid polymer electrolytes. *J Mater Chem* 2011;21(28):10448–53.
- [181] Marquard D, Vollmer C, Thomann R, Steurer P, Mülhaupt R, Redel E, et al. The use of microwave irradiation for the easy synthesis of graphene-supported transition metal nanoparticles in ionic liquids. *Carbon* 2011;49(4):1326–32.
- [182] Chai J, Li F, Hu Y, Zhang Q, Han D, Niu L. Hollow flower-like AuPd alloy nanoparticles: One step synthesis, self-assembly on ionic liquid-functionalized graphene, and electrooxidation of formic acid. *J Mater Chem* 2011;21(44):17922–9.
- [183] Zhu C, Guo S, Zhai Y, Dong S. Layer-by-layer self-assembly for constructing a graphene/platinum nanoparticle three-dimensional hybrid nanostructure using ionic liquid as a linker. *Langmuir* 2010;26(10):7614–18.
- [184] Fu C, Kuang Y, Huang Z, Wang X, Yin Y, Chen J, et al. Supercapacitor based on graphene and ionic liquid electrolyte. *J Solid State Electrochem* 2011;15(11):2581–5.
- [185] Kim TY, Lee HW, Stoller M, Dreyer DR, Bielawski CW, Ruoff RS, et al. High-performance supercapacitors based on poly(ionic liquid)-modified graphene electrodes. *ACS Nano* 2011;5(1):436–42.
- [186] Zhu Y, Murali S, Stoller MD, Ganesh KJ, Cai W, Ferreira PJ, et al. Carbon-based supercapacitors produced by activation of graphene. *Science* 2011;332:1537–41.
- [187] Ahmad I, Khan U, Gun'ko YK. Graphene, carbon nanotube and ionic liquid mixtures: towards new quasi-solid state electrolytes for dye sensitised solar cells. *J Mater Chem* 2011;21(42):16990–6.
- [188] Pu J, Wan S, Zhao W, Mo Y, Zhang X, Wang L, et al. Preparation and tribological study of functionalized graphene–IL nanocomposite ultrathin lubrication films on Si substrates. *J Phys Chem C* 2011;115(27):13275–84.

Chapter II:

Non-covalent functionalization of multi-walled carbon nanotubes with polymerized ionic liquids

Chapter II: Non-covalent functionalization of multi-walled carbon nanotubes with polymerized ionic liquids

II.1 Introduction

Non-covalent treatment is particularly attractive because of the possibility of adsorbing various groups on CNT surface without disturbing the extended π -conjugation of the nanotubes. The main advantage of using polymers instead of small molecular surfactants is that the polymers provide coatings with considerably higher integrity and stability as they have much more sites to interact with the CNT surface. Their extended chains can also provide sufficient steric interactions to repel nanotubes from each other for stabilization. Non-covalent adsorption can be regarded as functionalization if the polymers form an irreversible layer on the surface of CNTs. In order to understand the non-covalent functionalization, it is instructive first to take a brief look at the general adsorption phenomenon of polymers on the surface of CNTs.

II.1.1 Adsorption of polymers on the surface of CNTs

II.1.1.1 General adsorption phenomenon

Polymers adsorb onto the surface of CNTs through physical interactions, disrupting the van der Waals interactions that cause CNTs to aggregate into bundles. The polymer alters its lowest energy configuration (coil configuration in a solvent) in order to coat or wrap around the nanotube in an ordered fashion due to the interaction with the nanotube [1]. The separation of CNT bundles is suggested to occur through a so-called “unzipping” mechanism

(Figure II.1), where penetration of polymer segments into the spaces between CNTs, as they wrap around the CNT surface, leads to the debundling of CNT aggregates [2].

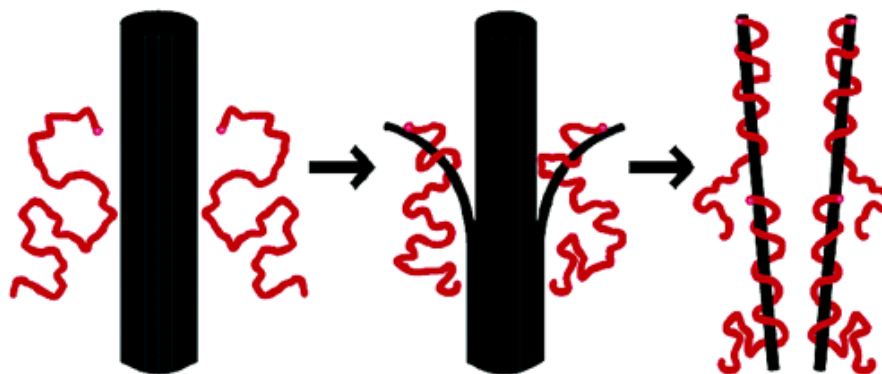


Figure II.1. Illustration of the so-called “unzipping” process of CNT bundles by polymers [3].

Many experimental works have reported adsorption of polymeric chains on the surface of CNTs from either aqueous or organic solvents [4]. However, the driving forces in determining the polymer-adsorption of CNTs have been widely debated. In general, it has been accepted that various noncovalent intermolecular interactions, such as π - π , CH- π , hydrophobic interactions and van der Waals attractive forces play a significant role in promoting the adsorption of chain-like polymers on the surface of CNTs. In addition to these interactions, the CNT radius and polymer stiffness are other important factors that contribute to polymer adsorption process, which will be discussed in this section.

Before the helical polymer-wrapping process was proposed for CNTs [5], conjugated polymers, exhibiting strong π - π interactions had been exploited for the formation of polymer-CNT complexes [6]. Later, Connell et al [5] observed that various linear water-soluble polymers wrap tightly around SWCNTs and proposed that wrapping is a general phenomenon driven largely by thermodynamics to eliminate the hydrophobic interface

between the tubes and their aqueous medium. According to their estimations, the free energy cost of forcing a linear polymer into a wrapping conformation around a nanotube is largely less than the energy gain by the elimination of the hydrophobic interface. The same authors proposed a multi helical wrapping conformation for the semi-flexible and rigid chains, which allows high surface coverage with low backbone strain (Figure II.2).

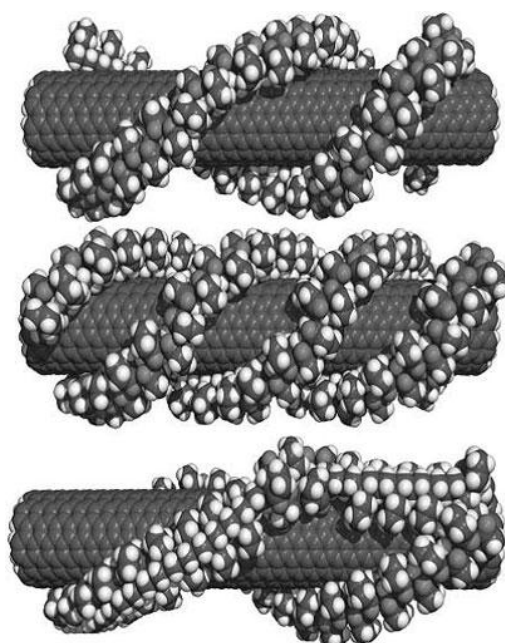


Figure II.2. Possible helical wrapping arrangements [5].

On the other hand, Baskaran et al [7] suggested that adsorption is a universal phenomenon that could occur from nonspecific molecular interactions between carbon-hydrogen groups (CH groups) of the polymers and π -system of the CNT. Although this interaction is very weak (only one-tenth of the hydrogen bond), a long molecule containing many CH linkages would sufficiently interact with CNTs and form molecular complex under appropriate conditions. The authors used different types of common polymers such as poly(methyl methacrylate) (PMMA), polystyrene (PS) and polybutadiene (PBD), which are only CH donor molecules for examining the effect of CH- π interaction with the MWCNTs. Based on experimental results,

the authors also suggested that the polymer wrapping through CH- π interactions is discontinuous and does not cover all the surface of the CNT, leading to aggregation at high concentrations of CNT.

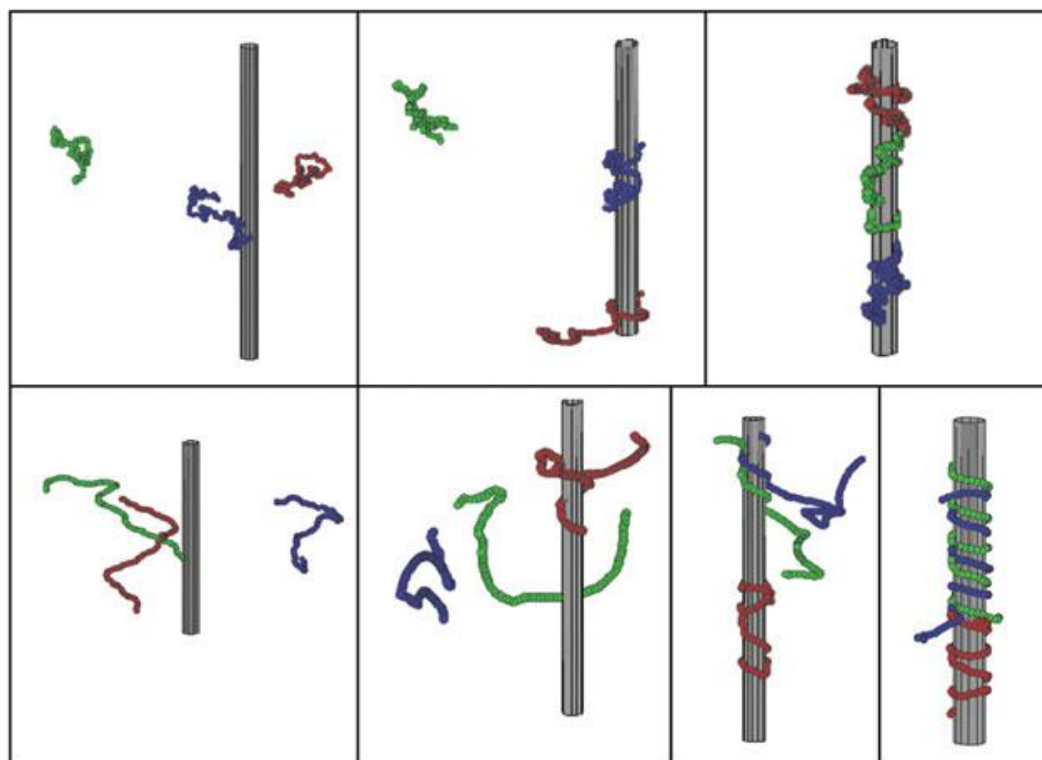


Figure II.3. Simulation snapshots of flexible (top) and rigid (bottom) chains at different simulation times [8].

Later, Gurevitch et al [8, 9] showed by a systematic computational study that weakly attractive van der Waals interactions are sufficient to induce polymer wrapping of nanotube with sufficiently large outer diameter for all degrees of chain flexibility. They found that the adsorption behavior of the chains strongly depend on the cylinder radius and the degree of chain stiffness. The adsorbed conformations range from randomly adsorbed conformations of the flexible chain to perfect helical or multi-helical conformations of the rigid chains (Figure II.3). Adsorption appears to occur in a sequential manner, wrapping the nanotube nearly one

monomer at a time from the point of contact. Once adsorbed, the chains travel on the surface of the cylinder, retaining their helical conformations for the semi-flexible and rigid chains. While flexible chains show negligible overlap at high polymer concentrations leading to a thicker and nonuniform polymer coating, the semi-flexible and rigid chains wrap around the CNT in multiple helices, which results in uniform monolayer coverage of the nanotube surface. The driving force for helical adsorption of semi-flexible and rigid chains is entropic. On the other hand, flexible chains experience significant entropy loss upon adsorption and therefore adsorb in a “cloud” conformation, which balance the entropy loss and the gain from adsorption. Since only non-specific weakly attractive interactions were considered in these works, the authors concluded that helical wrapping of nanotubes is a ‘general phenomenon’ of semi-flexible and stiff polymers. Tallury et al [10, 11] also explored the effect of polymer stiffness on the SWCNT–polymer adhesion in vacuo *via* molecular dynamics (MD) simulations. Their simulations indicated that polymers with flexible backbones tend to adhere to the SWCNT in random conformations but not helically. In contrast, polymers with stiff and semi-flexible backbones tend to wrap around the SWCNT with more distinct conformations although not always helically.

To directly image the wrapping requires scanning tunneling microscopy (STM), which is capable of providing the molecular level resolution necessary to distinguish wrapping from some other chain configuration. For example, a conjugated polymer, poly(3-hexyl-thiophene), has been shown to wrap around MWCNTs into a double helix by STM analysis (Figure II.4).

From the above discussions, it can be derived that coating or wrapping is a general phenomenon occurring between polymers and carbon nanotubes, for which van der Waals attraction constitutes the leading driving force. On the other hand, specific monomer structure such as an aromatic ring or the nature of the atoms plays a very important role in determining the strength of the interaction between nanotubes and polymers. Several experimental and

theoretical studies [1, 12–15] showed that CNT has a good interaction with aromatic polymers. Figure II.5 shows examples of some commonly studied aromatic polymers. To maximize the π - π interaction, aromatic rings align parallel to CNT surfaces, which increases the polymer–CNT adhesion. Yang et al [16] further investigated the effect of aromatic monomer structure and carried out MD simulations of the interactions of a number of polymers with SWCNTs. They found that polymers with backbones containing aromatic rings have stronger interactions with the CNT surface than those with aromatic side groups. Significant differences in adhesion energy also exist between similar polymers with different aromatic backbones [17].

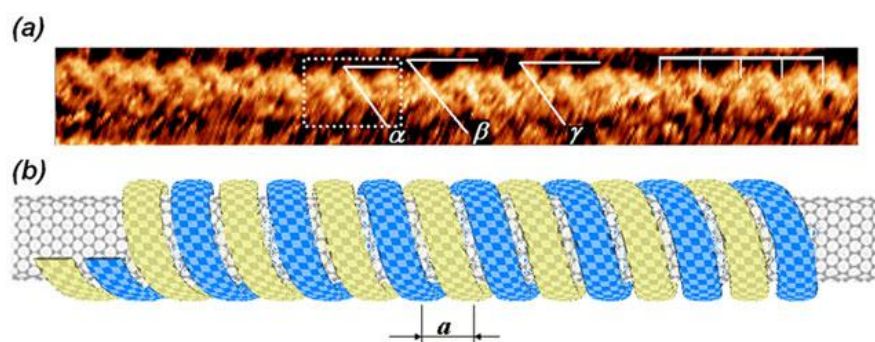


Figure II.4. (a) Unfiltered STM image of a MWCNT covered by poly(3-hexyl-thiophene) self-organized into a coiled structure, (b) Schematic representation of a double helical structure with coils equally spaced at a distance a [18].

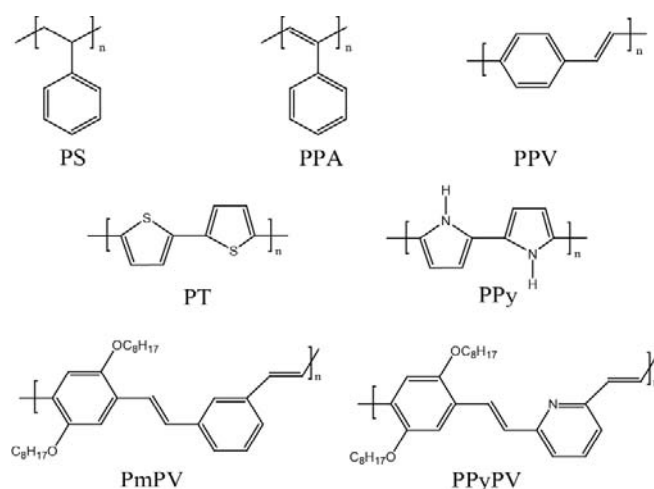


Figure II.5. Examples of investigated aromatic polymers.

Adsorption of polymers onto the CNT surface has been generally explained using neutral linear homopolymers as model, probably due to simplicity. This phenomenon can be further discussed for heteropolymers (copolymers), for other nonlinear polymer architectures, including dendritic polymers, or for ionic polymers, including polyelectrolytes and polymerized ionic liquids.

II.1.1.2 Copolymers

Owing to the strong π - π interactions with CNTs, conjugated or aromatic polymers have attracted considerable attention for the non-covalent surface modification of CNTs. However, this type of polymers has limited solubility, particularly in aqueous solutions, due to the strong inter-chain π - π interactions [19]. Block copolymers (BCPs) offer an advantage over homopolymers as the structure of the polymer blocks can be specifically designed to improve the performance of CNT-polymer composites. BCPs can be designed in such a way that one block of the polymer will form a close interaction with the CNT walls, while the other block(s) with affinity to the solubilizing medium will increase both the dispersion in appropriate solvents and the interfacial binding between the CNTs and the polymer matrix. For this reason, they are also called “amphiphilic copolymers”. Compared to homopolymers, BCPs adsorb on CNTs in more random wrapping conformations. A sufficiently long hydrophobic block will adsorb onto the CNT surface in a helical manner, whereas the polar block extends to the bulk [2]. This configuration not only provides steric repulsion between CNTs but also increases the adhesion between the CNT-polymer interface by allowing for entanglement between the adsorbed polymers and matrix polymers. As a result of this specific configuration, block copolymers are better dispersants for CNTs than the corresponding random copolymers [20]. Figure II.6 shows the blocks with affinity for the medium extending away from the nanotube, forming loops and tails for triblock and diblock copolymers, respectively. With short adsorbing blocks, a non-wrapping mechanism is also possible, which

has been reported to improve the dispersibility [20]. In addition, as amphiphilic block copolymers are known to have tendency to self-assemble, micelle formation on CNT surface has also been reported [21]. So far, a wide range of charged and neutral copolymers have been reported for CNT dispersion [19, 20, 22-27].

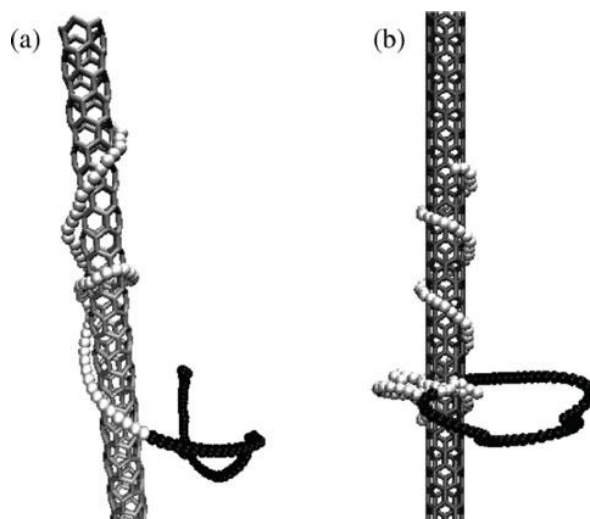


Figure II.6. Simulation snapshots of (a) diblock and (b) triblock copolymer–CNT systems [2].

II.1.1.3 Dendritic polymers

Dendritic polymers, including hyperbranched, multi-armed star and dendrimeric polymers have also been studied for the non-covalent surface modification of CNTs [28-35], but to a lesser extent than linear polymers. Depending on the degree of branching, these polymers either wrap around the CNTs or adsorb on the surface without wrapping due to their three-dimensional globular and sphere like structural architectures. They exhibit higher solubility and lower viscosity in the melt and solution states compared to linear polymers of the same molar mass. If the branches contain certain types of groups such as aromatic, dendritic polymers have been reported to have stronger interactions with the CNT surface compared to their linear analogues, due to the expanded branches [32]. Furthermore, it is suggested that the

branched architectures can discriminate between different CNT diameters in contrast to their linear analogues [35]. The key to their success is that the highly branched polymer with an appropriate degree of branching provides certain pockets that offer better fit for the SWCNTs while linear polymer can wrap around CNT bundles as well as around single tubes. Figure II.7 shows the illustrations of a variety of dendritic polymers adsorbed on the surface of CNTs.

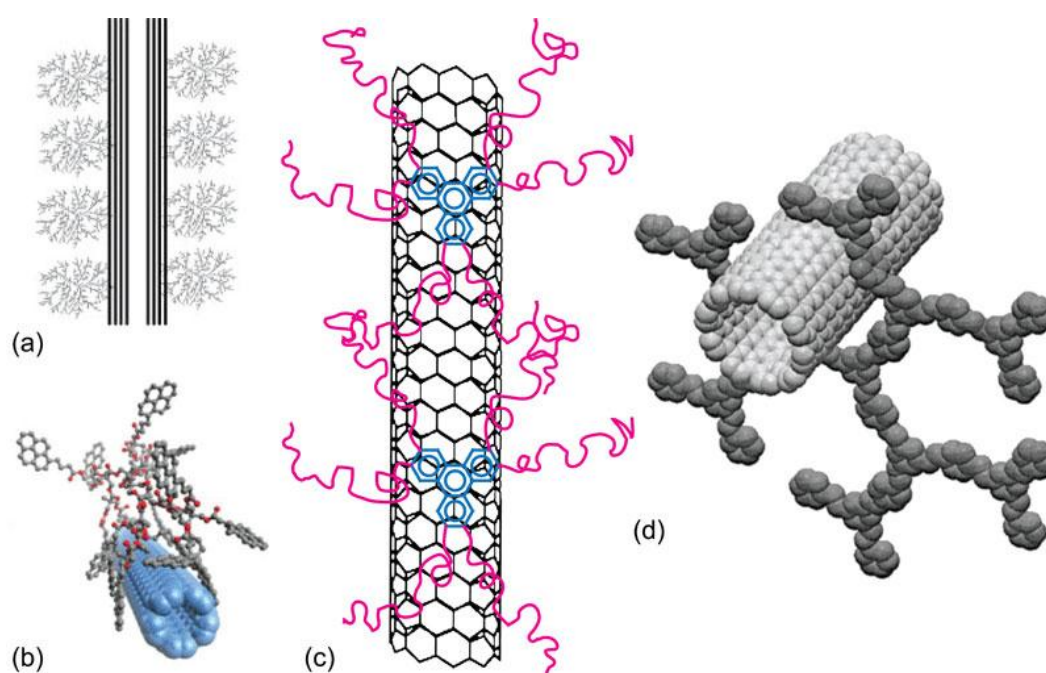


Figure II.7. Adsorption of (a) hyperbranched polymers, (b) dendron polymer and (c) six-armed star polymers onto the surface of CNTs; and (c) a SWCNT accommodated in the pocket of a dendrimer polymer.

II.1.1.4 Polyelectrolytes

Polyelectrolytes partially or completely dissociate into ions in water, making the chains positively or negatively charged. Some common polyelectrolytes used for CNT modification are shown in Figure II.8.

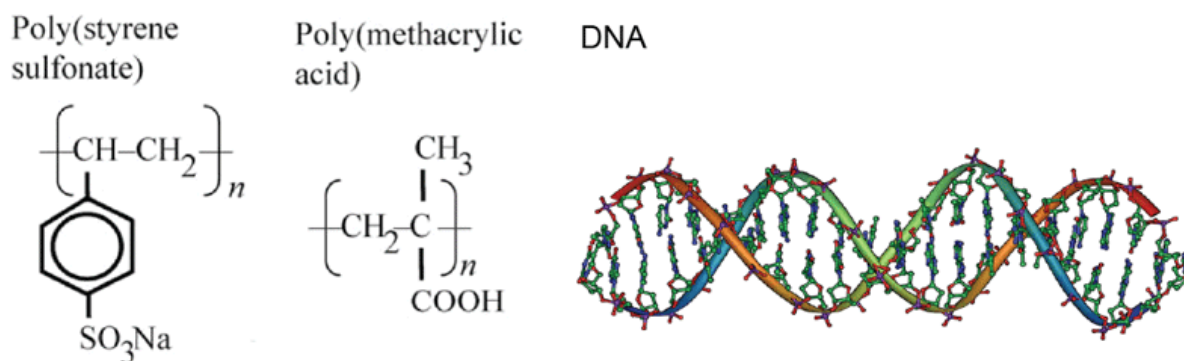


Figure II.8. Examples of polyelectrolytes used for CNT modification.

Although the mechanism and conformation of charged chains adsorbed on CNTs have been little studied compared to neutral polymer chains, they have been generally reported to wrap around CNTs similarly to neutral polymers, mostly in a helical manner [5, 36, 37]. The stabilization of polyelectrolyte coated CNTs can be explained by long-range repulsive interactions between the positively or negatively charged polymer chains, which prevent the possible aggregation of CNTs [38]. Dispersions of CNTs have been obtained with weak or strong polyelectrolytes such as DNA, polysoap, sodium polystyrene sulfonate (PSS), poly(diallyldimethylammonium chloride) and poly(allylamine hydrochloride) (PAH chloride) with varying degrees of success [39-42]. The conformation of the polyelectrolytes highly depends on the ionic strength of the solution. Huang et al [37] observed very little or no coating of PAH or PSS on SWCNTs at low ionic strength, but the thickness of the coated polymer increased steadily using layer-by-layer deposition method by the addition of NaCl into the solution (Figure II.9). The authors suggested that at low ionic strength, the polymer chains are too rigid to bend around the thin nanotube and the deposition cannot occur. On the other hand, they observed that deposition occurs on SWCNTs with larger diameter at all ionic strengths. Indeed, it is known that in the absence of salt, the chains of polyelectrolytes are locally rigid rod-like due to the intrachain electrostatic repulsion, and the polymer chains extend as the polymer concentration decreases [43]. A polyelectrolyte chain in salt solution

behaves as a semi-flexible polymer with salt-concentration-dependent persistence length. At sufficiently high salt concentration, the electrostatic interactions between the monomers are totally screened and the polyelectrolytes behave like neutral polymers in a good solvent. Temperature and pH are other factors that highly influence the deposition of polyelectrolytes on CNTs [44, 45]. It is evident that the adsorption mechanism and conformation are much more complicated for polyelectrolytes than for neutral polymers as they depend on many parameters and they still need to be studied further.

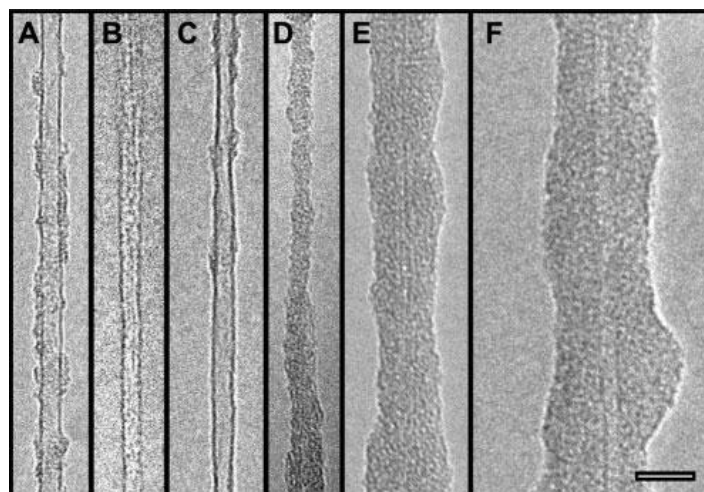


Figure II.9. TEM images of single-walled carbon nanotubes after polymer deposition for ionic strengths of (A) 0.05 M, (B) 0.1 M, (C) 0.2 M, (D) 0.4 M, (E) 0.65 M, and (F) 1.05 M. (scale bar = 10 nm) [37].

II.1.1.5 Polymerized ionic liquids

Polymerized ionic liquids can be classified as a new class of polyelectrolytes on the basis of their chemical structure. On the other hand, PILs are synthesized from liquid salt monomers in opposition to polyelectrolytes which are synthesized from solid salt monomers. Unlike polyelectrolytes, which are mostly water soluble, most PILs are soluble in polar organic solvents due to their hydrophobic counter-ions. As in the case of polyelectrolytes, PILs can be further classified based on the ionic charge they carry in the chain backbone, as polycations,

polyanions or polyzwitterions (Figure II.10). Although polyzwitterions are synthesized from solid salt monomers, they are usually included in the PIL family. Different types of copolymers and macromolecular architectures such as branched, dendritic or ramified structures are also potentially possible [46]. The largest variety of PILs synthesized so far include imidazolium based polycation-type PILs with a variety of counter-anions. Polyanion-type PILs have been synthesized so far to a much smaller extent due to the relatively more difficult task of synthesizing anionic-type monomeric ILs. Polyzwitterions are a relatively unexplored area.

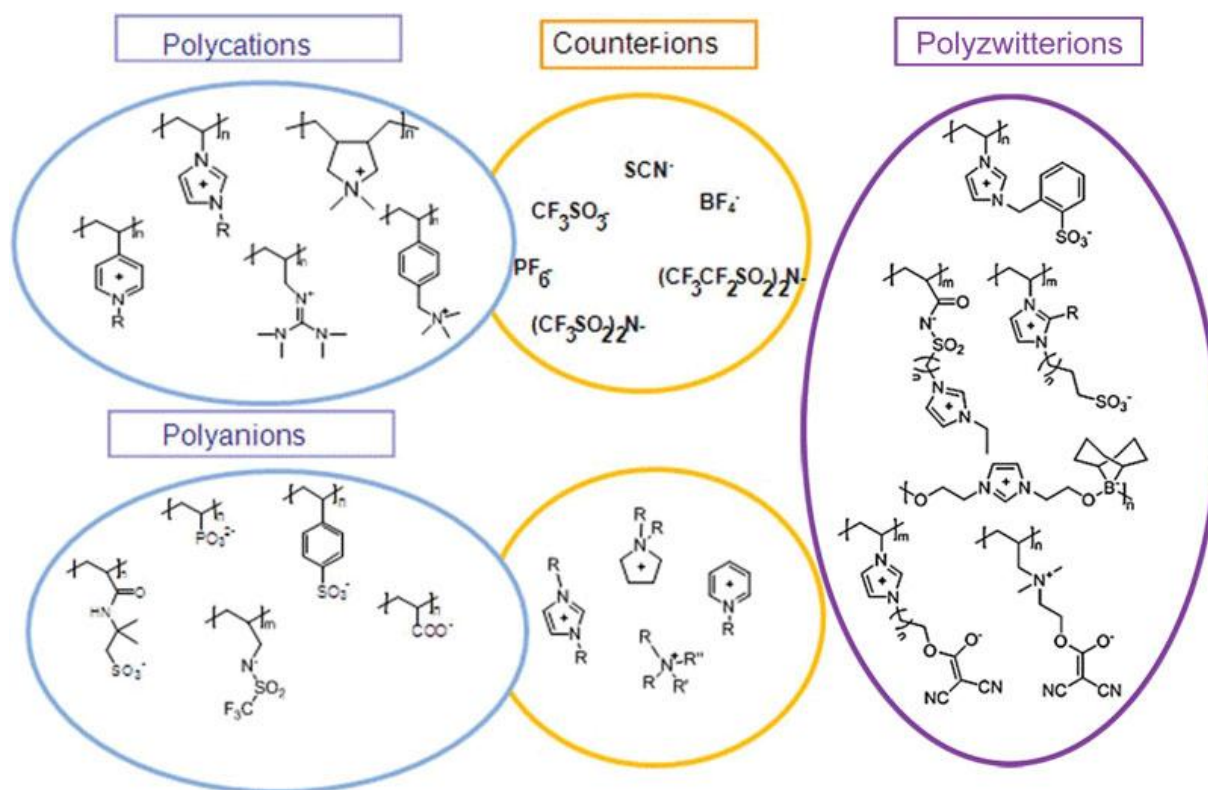


Figure II.10. Representative chemical structures of polymeric ionic liquids.

Little is known about the solution behaviour of PILs. The question is whether they behave similarly in organic solvents to strong polyelectrolytes in aqueous solution. The study of Chen et al [47] revealed solution behaviours such as viscosity scaling relationships similar

compared to other polyelectrolyte solutions. However, further properties should be investigated, such as the ionic association of PIL in various solvents. Some studies revealed some important aspects of the ionic association behavior of ILs in solution [48, 49]. The results suggested that organic solvents enhance the ionic association of ILs, whereas water promotes their dissociation significantly. It is also likely that polymerized ionic liquids are not dissociated in organic solvents inversely to polyelectrolytes in aqueous solutions. Furthermore, there is no systematic study on the mechanism of PIL adsorption onto the CNTs or on the conformation of the adsorbed PIL. Despite the lack of the knowledge in this field, several experimental studies show that PILs adsorb strongly onto the surface of CNTs [50–54].

II.1.1.6 Effects of defects and disorders in CNTs on polymer adsorption

Adsorption of polymers has been explained considering that the nanotubes are defect-free perfect cylinders. However, it is nearly impossible to obtain perfect CNT samples. The question that naturally arises is whether the nature of polymer adsorption is altered by the defects or disorders present on the carbon nanotubes. The most conventional types of defects, like vacancies and interstitials, are introduced during post-synthesis and unlikely to be found in pristine CNTs [55]. Two adjacent pentagon–heptagon pairs, known as Stone-Wales 5–7–7–5 defects, are relatively a common type of defect. Equally likely are various topology-changing combinations of 5–7 pairs (Figure II.11). The concentration of these defects found on CNTs highly depends on the synthesis method. For example, it has been reported that the plasma method introduces about 2.5 times more above mentioned defects when compared to the chemical vapor deposition (CVD) method [55].

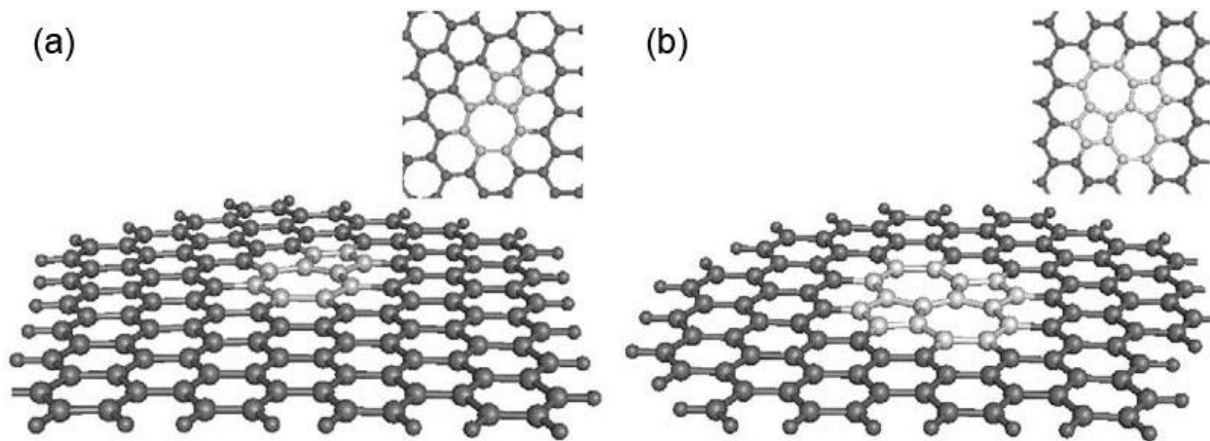


Figure II.11. (a) A single 5-7 defect and (b) a 5-7-7-5 Stone-Wales configuration [55].

Although the 5-7 defects create topological changes, such a pair will create only a small local deformation in the width of the nanotube and may also induce small localized bends in the nanotube body, depending on their orientation in the hexagonal network [56] (Figure II.12). Therefore, the cylindrical structure of the nanotubes is maintained.

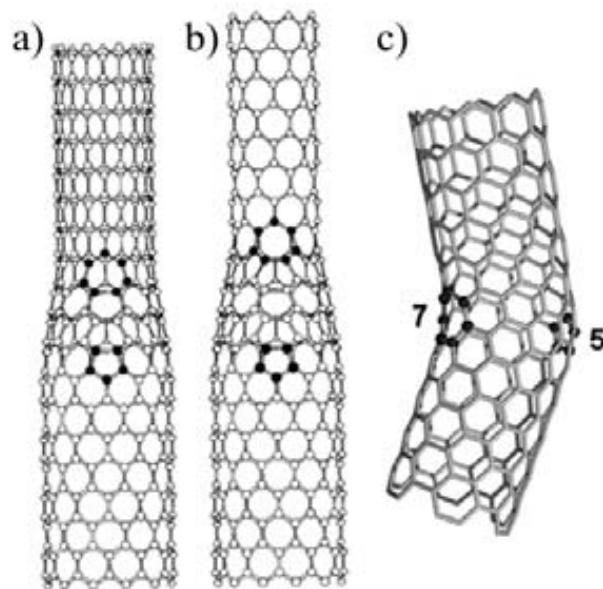


Figure II.12. Atomistic models of a metal-metal (a) and two metal-semiconductor (b,c)

SWCNT heterojunctions [55].

It must be pointed out that the CNT end cap is itself an unavoidable defect or cluster of defects. With a possible exception for very long CNTs, the concentration of two end defects per CNT is overwhelmingly larger than all other categories of intrinsic defects combined for high-quality CNTs [55]. Therefore, the concentration of intrinsic defects should be low enough not to have an influence on the adsorption of polymers. The effect should be more significant for CNTs with a large amount of defects. For example, when a conjugated polymer passes through regions with defects that break the π -conjugation, the polymer–nanotube interaction becomes weaker due to the diminished π - π interactions. Therefore, when CNTs are covered with such molecules, the effective interfacial area corresponding to the π - π interaction will be lower for CNTs with higher defects [57]. A specific case is observed for crystalline polymers, where the intrinsic defects on the nanotube structure can act as nucleation sites for crystal growth [58].

Another category of disorder is due to impure or noncrystalline starting material. Unlike the point defects that are thermodynamically intrinsic to CNTs, amorphous carbons and distorted or incomplete graphitic shells are unnecessary but common products of CNT synthesis. While the incorporated disorders should not affect polymer adsorption onto the CNT surface, the carbonaceous materials found on the surface could have an influence as they prevent the polymer interaction with the tube walls. The extent of this influence is not known as theoretical studies consider mostly seamless perfect tubes but it has been reported that conjugated or/and aromatic polymers show preferential interactions with CNTs over amorphous carbon [59]. This technique has been even effectively used to purify CNTs; the residual amorphous carbon can be removed by filtration, and nanotubes can be recovered through polymer unwrapping that occurs by changing the solvent system [60]. Practically all CNTs contain these carbonaceous contaminants and it is very difficult to remove completely

these impurities without damaging the wall structure with the known purification methods including acid treatment. Nevertheless, experimental studies report the presence of adsorbed polymer layers on the surface of CNTs, which indicates that despite the presence of the above mentioned impurities, polymer wrapping/adsorption can still occur.

For this study, we selected polymerized ionic liquids as ideal polymers for the non-covalent functionalization of pristine MWCNTs mainly for the following reasons:

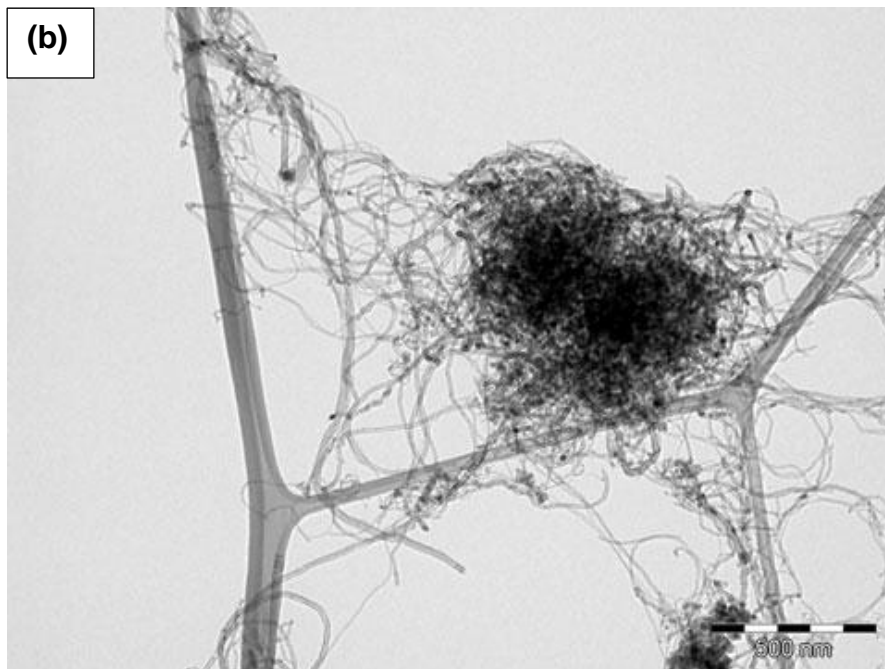
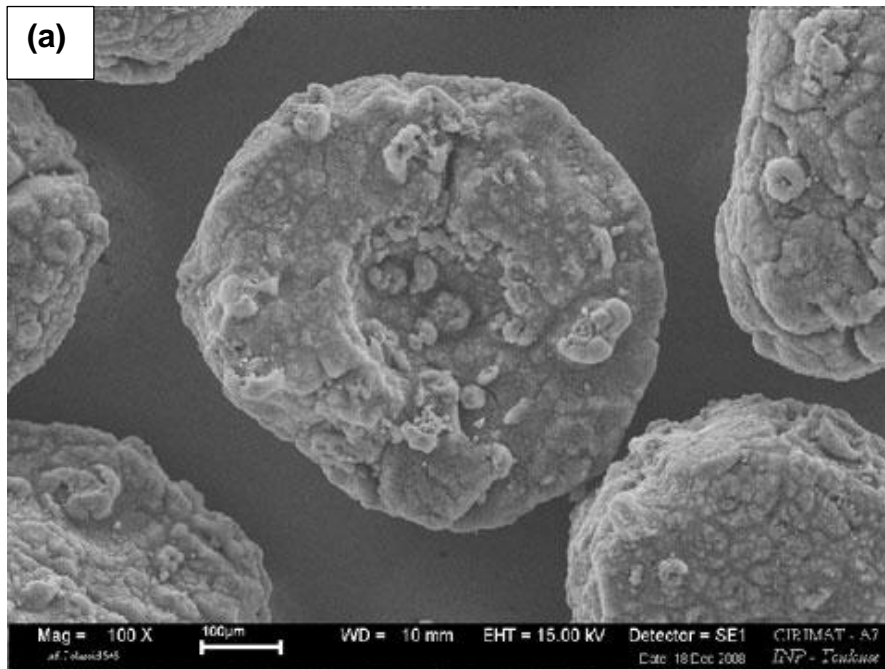
- PILs coat readily on the CNT surface without any additives or pretreatments;
 - with PILs usually high enough irreversible coating occurs due to the strong interactions with the CNT surface;
 - the properties of PILs such as solubility, glass-transition temperature and thermal stability can be easily tuned by selecting appropriate combination of cations and anions;
- and lastly because
- polymerized ionic liquid is a promising new area which needs to be further explored.

Furthermore, in this study, we wanted to evaluate two common synthesis methods: solution-mixing and *in situ* methods for non-covalently functionalizing CNTs with several imidazolium based polymerized ionic liquids including alkyl, hydroxyalkyl substituted or protic PILs.

II.2 Results and discussion

II.2.1 Characterization of CNTs

The Graphistrength[®] C100 MWCNTs with an average wall number ranging from 5 to 15 were synthesized over iron (Fe) catalyst on an aluminium substrate by catalytic chemical vapor deposition. The average outer diameter is between 10–15 nm and the length range is 0.1–10 μm .



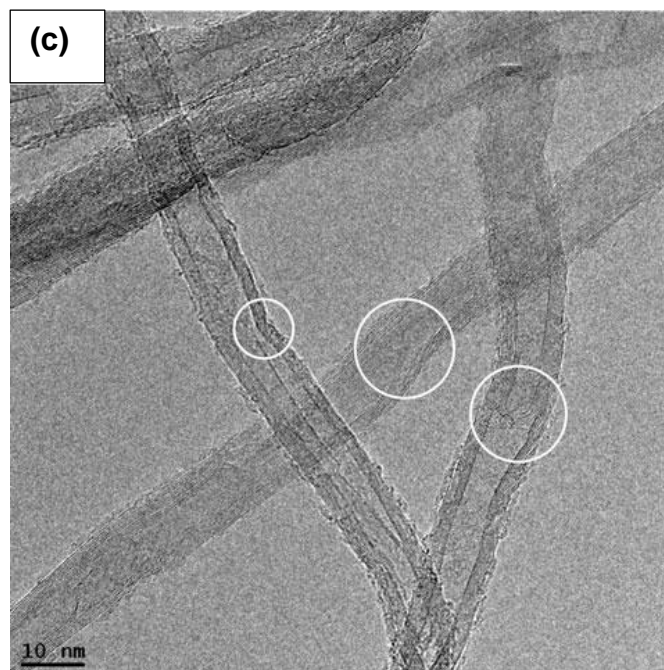


Figure II.13. (a) SEM image (scale bar = 100 μm) and (b,c) TEM images (scale bar = 500 and 10 nm) of pristine MWCNTs used in this study.

The SEM image in Figure II.13 (a) shows the micro-sized CNT agglomerates and the TEM images show that the CNTs used in this study are not perfect cylinders; there is variation in thickness of the tube wall along the perimeter, and the outer diameter ranges at some points with bending (Figure II.13 (b)). Tubes with closed internal caps also exist. Furthermore, the presence of disordered carbon impurities on the surface of CNTs is observable.

In air, disordered carbon species (e.g., amorphous carbons) oxidize below 400 $^{\circ}\text{C}$, whereas CNTs burn at higher temperatures of 400–750 $^{\circ}\text{C}$. As demonstrated in Figure II.14, the pristine MWCNTs used in this study exhibit relatively sharp weight loss profiles, the onset being at around 500 $^{\circ}\text{C}$, which is typical for high quality CNTs. TGA results indicate insignificant amount of disordered carbon on pristine MWCNTs. After purification, the thermal stability increases slightly, probably due to the elimination of the carbonaceous impurities. The labile oxygen-containing groups introduced to the CNT surface by nitric acid

treatment decompose below 500 °C, broadening the weight loss profile. The first weight loss below 100 °C is attributed to the absorbed water in the sample. The weight loss corresponding to the oxygen containing groups has been found to be 9% for the sample used in this study. If we assume that all these groups are carboxylic acid, the weight loss corresponds to about 1.2 carboxylic acid groups for 45 C atoms of the nanotube. However, by an acid-base titration, the concentration of acidic sites has been found to be 0.254 mmol/gr CNT, which corresponds to 1.5 surface carboxylic acid groups for 6000 C atoms. It should be noted that the surface grafting density is much higher as the number of walls is between 5 and 15. This result shows that nitric acid treatment introduces acidic sites including carboxylic acids, lactones and phenols but also carbonyls, anhydrides, ethers and quinones as shown by the temperature programmed desorption experiments in another study [61].

Any remaining mass after complete oxidation in air can be attributed to metal contaminants, such as transition metal catalysts. As Figure II.14 shows, pristine CNTs contains about 10.24 wt.% of residual ash at 800 °C. The acid treatment removes the metal impurities, and the amount of residual ash decreases. Thus, the ash content was found to be 4.36 wt.% upon purification by concentrated H₂SO₄ and 0.97 wt.% upon oxidation by concentrated HNO₃ under reflux for 3 hours.

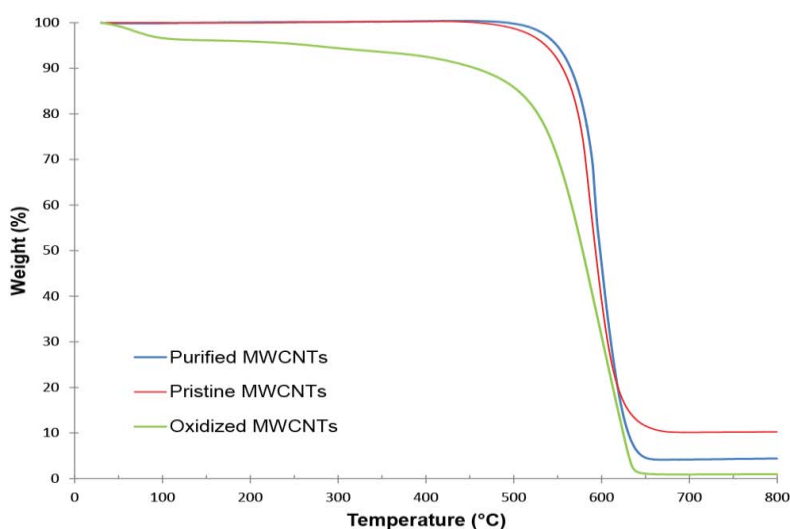


Figure II.14. TGA curves of pristine, purified and oxidized MWCNTs.

The ash content determined by thermal analysis is expected to be higher than the real metal impurity content as the weight of the impurities increases due to the oxidation of Fe and Al during the thermal treatment. As shown in Table II.1, the metal impurities can be more accurately measured by elemental analysis.

Table II.1. The metal impurities determined by elemental analysis.

Impurity	Pristine CNTs	Purified CNTs	Acid-oxidized CNTs
Fe	2.46%	1.59%	0.44%
Al	2.57%	< 500 ppm	< 500 ppm

From these results, it is observed that the Al content in the pristine CNT sample approaches to zero, whereas the Fe cannot be completely removed even after oxidation with nitric acid. This is due to the encapsulated iron catalyst in the CNTs as revealed by the TEM analysis of the nitric acid oxidized CNTs (Figure II.15).

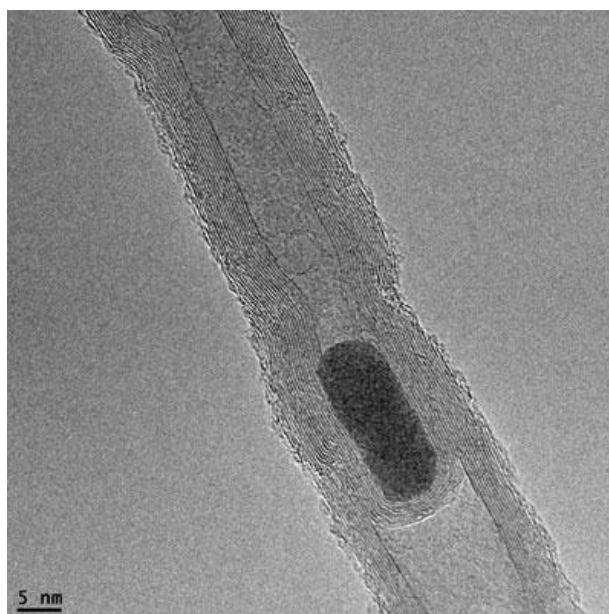


Figure II.15. Iron catalyst encapsulated in the nitric acid oxidized CNT.

The structure of the CNTs was characterized by Brunauer–Emmet–Teller (BET) analysis of nitrogen cryo-adsorption isotherms. The specific surface area, pore size and total pore specific volume of CNTs are listed in Table II.2. It can be seen that the purification process leads to a slight decrease in the specific surface area of the nanotubes. Subsequent treatment with concentrated nitric acid at 120 °C for 3 hours was found to increase the specific surface area of the purified nanotubes by around 35%. This shows that nitric acid treatment removes the amorphous carbon, carbon black and carbon nanoparticles introduced by CVD preparation process, and probes inner cavities of the CNTs, exposing their internal surface area, and thereby increasing the specific surface area. The adsorption isotherms were of Type IV which is typical of a mesoporous material (2–50 nm). The pore sizes of the pristine and purified CNTs have been found to be ≈ 45 nm. The inter-space between tubes in bundles is probably responsible for the pores measured. Nitric acid treatment causes significant alteration of the pore structure. After a 3 h boiling period, the pore size has decreased to 13 nm, which can be attributed to the availability of the internal diameters of the tubes opened by the oxidation process.

Table II.2. Specific surface area, pore size and porosities of CNTs.

Sample	S_{BET} ($\text{m}^2 \text{g}^{-1}$)	Pore size (nm)	V_p ($\text{cm}^3 \text{g}^{-1}$)
Pristine CNTs	218	45	2.439
Purified CNTs	201	43	2.152
Oxidized CNTs	271	13	0.897

S_{BET} = BET surface area; V_p = pore specific volume

II.2.2 Preparation of polymerized ionic liquids

In this study, we prepared a series of polymerized ionic liquids based on 1-vinylimidazolium homopolymers substituted with hydrogen, ethyl, and hydroxyethyl substituents and counter-

anions of bromide (Br^-) and bis[(trifluoromethyl)sulfonyl]imide (NTf_2^-) (Figure II.16). We used the conventional free radical polymerization method using AIBN as a thermal radical initiator. As illustrated in Figure II.17, there are two general synthetic routes to prepare PIL: (i) anion exchange of monomers and subsequent polymerization and (ii) polymerization and subsequent anion exchange reaction. We took the first route to prepare most of our polymers (**poly1–3**). We exclusively carried out an anion-exchange reaction over **poly4** to obtain **poly5**.

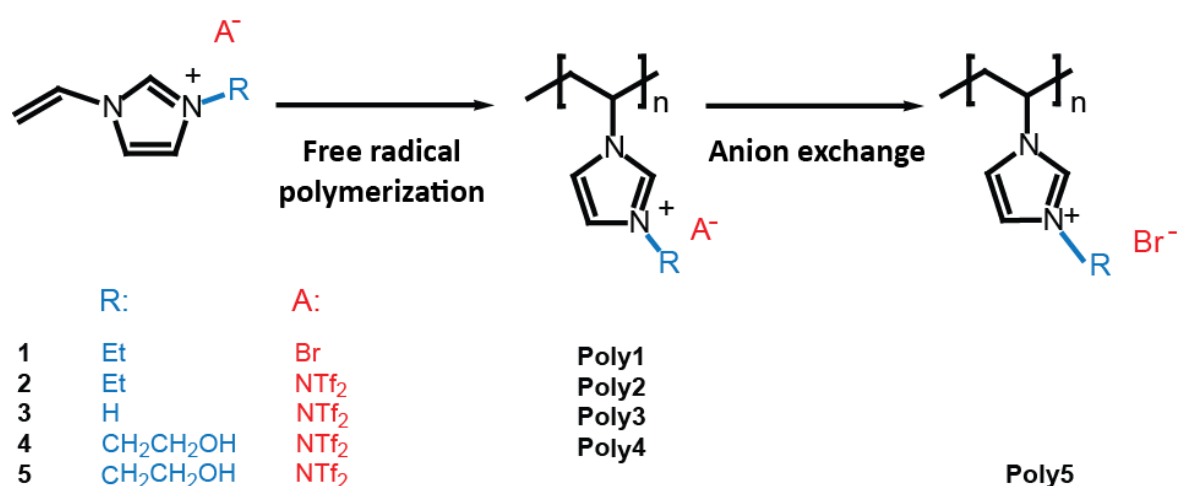


Figure II.16. Preparation of the PILs used in this study.

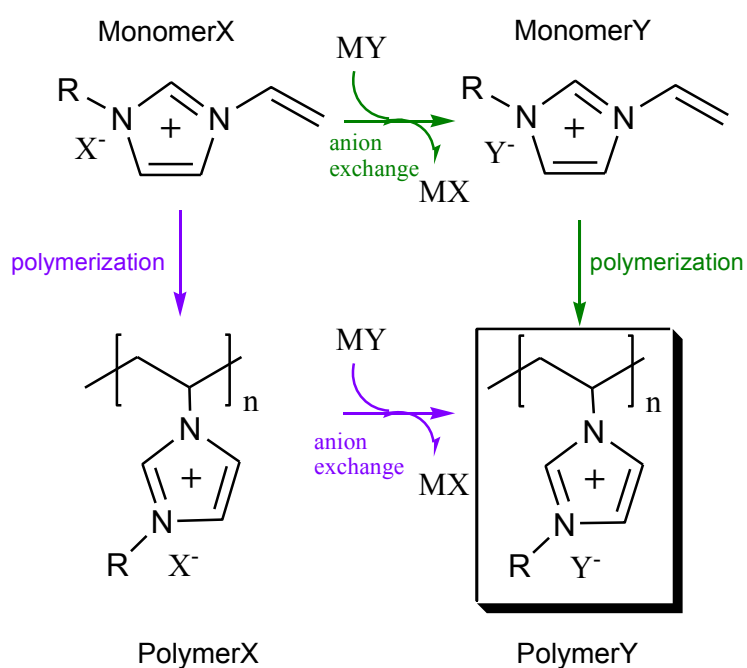


Figure II.17. Illustration of two general synthetic routes for PIL preparation.

All the vinyl functionalized IL monomers were successfully polymerized as verified by IR and NMR spectroscopies. The absence of the monomer in the resulting products was confirmed by IR analysis by checking the disappearance of the peak at around 1660 cm^{-1} , which corresponds to the stretching vibration of C=C double bond (Figure II.18).

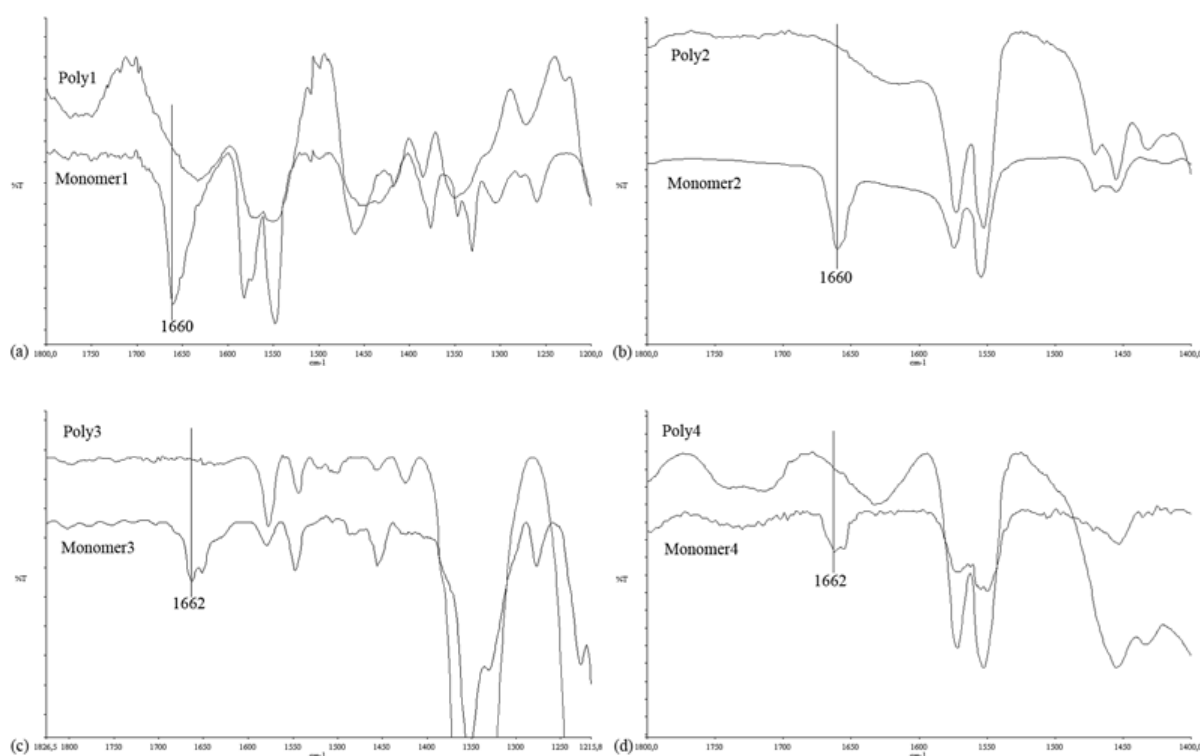


Figure II.18. IR spectra of (a) monomer **1** and **poly1**, (b) monomer **2** and **poly2**, (c) monomer **3** and **poly3** and (d) monomer **4** and **poly4**.

In the solution ^1H NMR spectra of the polymerized products (**poly1-3**), a significant broadening of the signals was observed (Figure II.19). The disappearance of the vinyl signals in the 5–7.5 ppm region is observed with the appearance of new signals in the 2–5 ppm region attributed to the protons of the polymeric backbones.

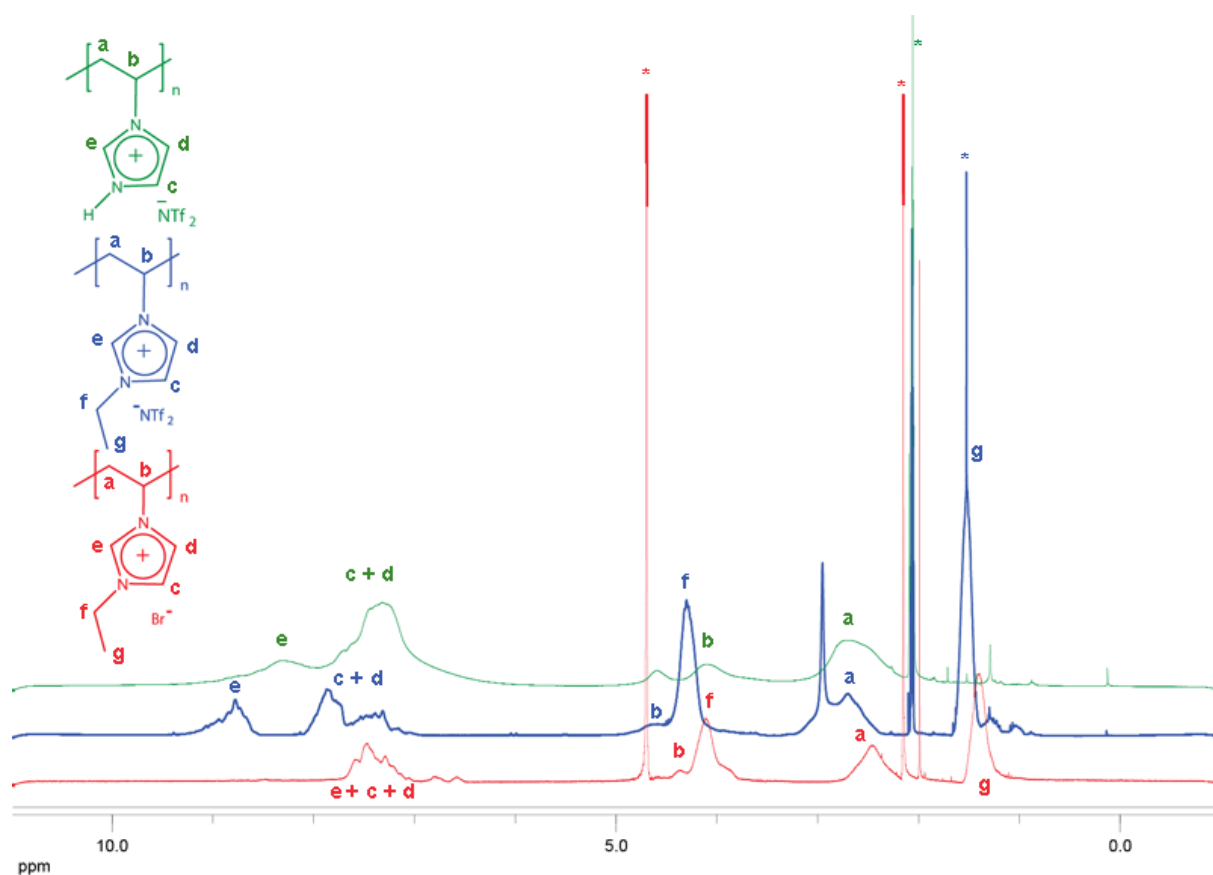


Figure II.19. ^1H NMR spectra of **poly1** in D_2O (red), **poly2** acetone- d_6 (blue) and **poly3** acetone- d_6 (green). The solvent peaks are marked with asterisks.

The polymerization of the hydroxyethyl substituted monomer **4** gave **poly4**, which is able to form a gel with certain polar aprotic solvents such as acetone and acetonitrile, probably due to the network of polymer chains joined by H bonds. The polymer swells up to 34 times its own weight at room temperature to form a free standing stable gel (Figure II.20 (a)). No gel formation, neither solubility is observed in other organic solvents such as, dichloromethane, chloroform, methyl acetate or ethanol. Furthermore, upon switching the NTf_2^- counter-anion of **poly4** to Br^- by anion metathesis, the new polymer, **poly5**, forms a hydrogel with water. It has a high water intake capacity: in only 5 minutes, at room temperature, it absorbs water 70 times its own weight.

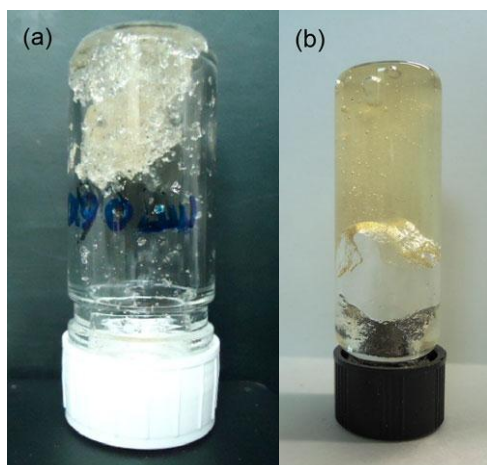


Figure II.20. Photographs of free-standing (a) **poly4**-acetone organogel and (b) **poly5** hydrogel.

The structures of **poly4** and **poly5** were characterized by solid-state NMR because of the impossibility to perform solution NMR due to gelation. Figure II.21 shows the ^1H - ^{13}C cross-polarization (CP) spectra of **poly4** and **poly5**.

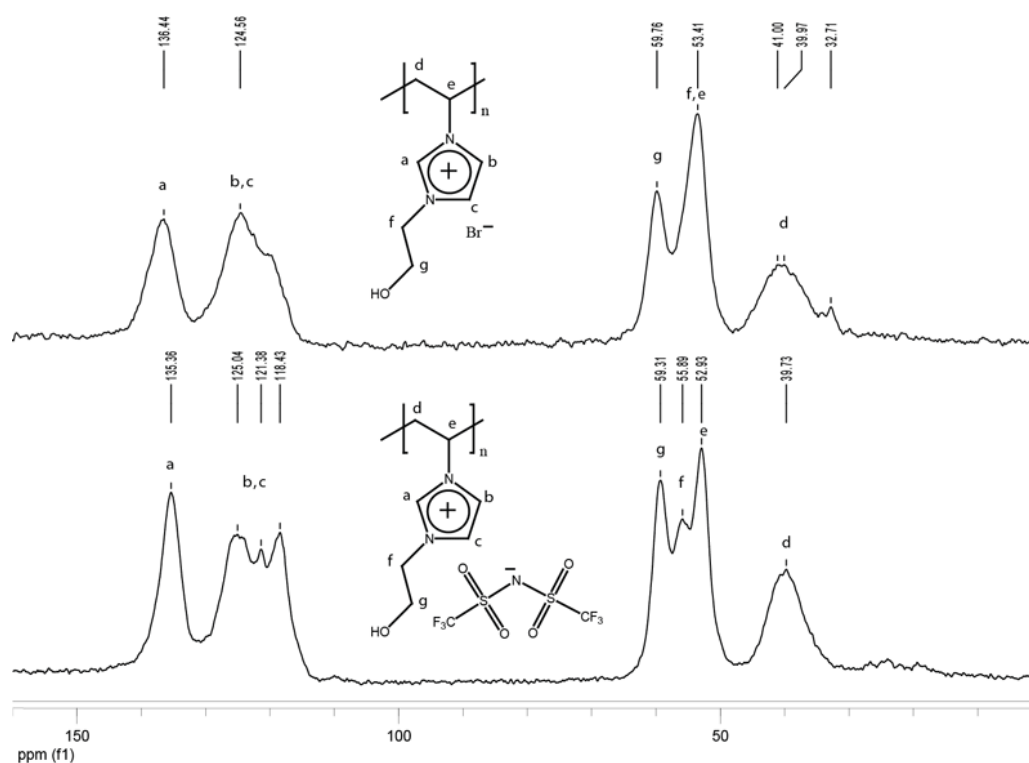


Figure II.21. Solid-state NMR ^1H - ^{13}C CP spectra of (bottom) **poly4** and (top) **poly5**.

The broad peaks are due to the amorphous structure of the polymers. The vinyl carbon signals of the monomers at around 110 ppm were also absent on these spectra. In addition, the ^{19}F spectrum (not shown) of **poly4** showed a peak at 79.96 ppm due to the fluorine atoms of the NTf_2^- counter-anion.

Due to polymer aggregation and column interaction, molecular weight analysis was not possible for the PIL polymers, which is a common difficulty encountered with this type of ionic polymers [62]. In any case, this chapter will not deal with molecular weight as polymer adsorption is rather insensitive to molecular weight in good solvent conditions for the polymer [63].

Thermal properties of the resulted polymers have been studied by TGA ($10\text{ }^\circ\text{C min}^{-1}$ under air) and DSC ($10\text{ }^\circ\text{C min}^{-1}$ under N_2 flow). Table II.3 lists the decomposition temperatures (T_d) and mid-point glass transition temperatures (T_g) of the polymerized ILs determined from the TGA curves at 5 wt.% loss and from the DSC curves respectively. According to the DSC results, all the polymers are amorphous. The analysis results also show that the thermal properties of the PILs highly depend on the type of counter-anion. As a general rule, as the anion size increases regardless of the alkyl substituent length, T_g decreases and the onset of weight loss, T_d , increases [62]. The results are mostly in agreement with this rule: NTf_2^- anion increases the thermal stability of the polymers of more than $100\text{ }^\circ\text{C}$ compared to Br^- anions and the T_g of the corresponding polymers is much lower than that of those with small bromide anion, except for **poly3**. This specific PIL with hydrogen substituent has a remarkably high T_g despite its bulky NTf_2^- counter-anion, most likely due to the strong hydrogen bonding capacity of this proton, which could decrease the chain mobility by cross-linking. It is also observed that the hydroxyethyl substituent results in an increase in T_g compared to the ethyl substituent: the T_g of the corresponding polymers increase in the order $\text{poly}[\text{VEIM}]\text{NTf}_2 < \text{poly}[\text{VHEIM}]\text{NTf}_2 < \text{poly}[\text{VEIM}]\text{Br} < \text{poly}[\text{VHEIM}]\text{Br}$.

Table II.3. T_d (from TGA) and T_g (from DSC) for the polymerized products

Sample	Chemical name	$T_d / ^\circ\text{C}$	$T_g / ^\circ\text{C}$
Poly1	poly[VEIM]Br	309	94
Poly2	poly[VEIM]NTf ₂	430	29
Poly3	poly[VHIM]NTf ₂	416	131
Poly4	poly[VHEIM]NTf ₂	421	57
Poly5	poly[VHEIM]Br	308	157

II.2.3 Non-covalent functionalization of CNTs by PIL

As mentioned in Chapter I, CNTs can be non-covalently functionalized using two main methods (i) solution-mixing of the polymer with CNTs or (ii) *in situ* polymerization in the presence of CNTs. In this study, we used both methods to compare their efficiency for MWCNT functionalization. Pristine MWCNTs have been used as received. To break CNT bundles moderate sonication has been used. The mild sonication conditions (low power, short time) that we used for PIL functionalization is not expected to damage the tube walls. CNTs are somewhat resistant to mechanical damage from low power ultrasound since after short processing times no accumulation of damage is typically observable [64].

In both cases, the functionalized nanotubes were recovered by filtration and washed thoroughly with solvent to remove the non-interacting polymer. For both methods, MWCNTs (5 wt.% with respect to the monomer or polymer) were used as received. The composites resulting from solution-mixing are named CNT–**polyxa**, whereas those produced by *in situ* polymerization are named CNT–**polyxb**.

II.2.3.1 Functionalization by solution-mixing

The experiments were carried out either in ethanol (for **poly1** and **poly3**) or in a 1:1 mixture acetone/ethanol (for **poly2**), depending on the polymer solubility. Solution-mixing method could not be used to prepare functionalized CNTs with **poly4** and **poly5** as CNTs cannot be separated from the gel by washing. Instead, a composite can be prepared, which will be detailed at the end of this chapter. We noticed that 22 h of reaction and a vigorous stirring with moderate heating (65 °C) were necessary to obtain significant amounts of adsorbed polymer. The Raman spectra of the functionalized samples showed the typical features of the MWCNTs without any shift in the frequency of the signals (Figure II.22).

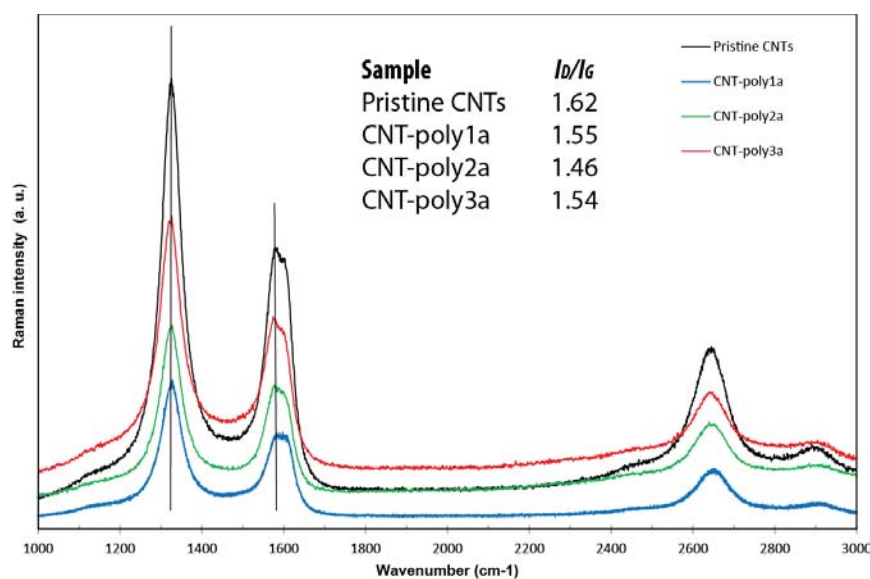


Figure II.22. Raman spectra of pristine CNTs and PIL functionalized CNTs *via* solution-mixing.

The intensity ratio between the D-band at 1322 cm^{-1} and the G-band at 1576 cm^{-1} (I_D/I_G) indicates the degree of disorder and defects in MWCNTs. An increase in this ratio is usually attributed to the sp^3 -hybridized carbons or other defects created in the wall structure of the

nanotubes. This ratio decreased from 1.62 for pristine CNTs to between 1.46–1.55 for the functionalized samples. This type of decrease has already been reported for PIL functionalized CNTs [52] but it could not be rationalized. The results from Raman analysis indicate that the solution-mixing process does not lead to any obvious structural damage of the CNTs.

To determine the amount of polymer present in the functionalized CNT samples, thermogravimetric analysis (TGA) was performed (Figure II.23). The pristine CNTs were stable up to 500 °C under air. According to the TGA analysis of the neat PILs, the thermal decomposition of the grafted polymer is mainly completed before 500 °C in the presence of air. For CNT samples functionalized by **poly1** and **poly2**, the weight losses before 500 °C were 24 and 9%, respectively. The much lower amount of adsorbed **poly2** compared to that of **poly1** should result from the steric hindrance caused by the bulky NTf_2^- anion. We will see below if *in situ* method helps to increase the quantity of the adsorbed polymer. The weight loss due to polymer is 70% for the CNTs functionalized by **poly3** (CNT-**poly3a**). The sample was washed again excessively to further remove any remaining free polymer but the high amount of polymer was not due to insufficient washing. This result will be also discussed later. As observed from the TGA curves, PIL adsorption has resulted in a decrease in the thermostability of the CNTs. The decomposition end-point temperature was decreased from 670 °C for pristine CNTs to 640 °C for CNT-**poly1a** and CNT-**poly2a** and to 620 °C for CNT-**poly3a**. This phenomenon has also been reported in a study on IL grafted CNTs. The residual weight content attributed to metal impurities varies in the samples. The ash content at 800 °C in the first sample is higher than expected (13.2 wt.%) while the second sample contains an appropriate amount (9.2 wt.%). Since the third sample is mainly composed of polymer, the relative amount of metal impurities coming from CNT is as low as expected (2.8

wt.%). Some variations in the amount of metal impurity content can be expected because of the heterogeneity of the starting CNT material.

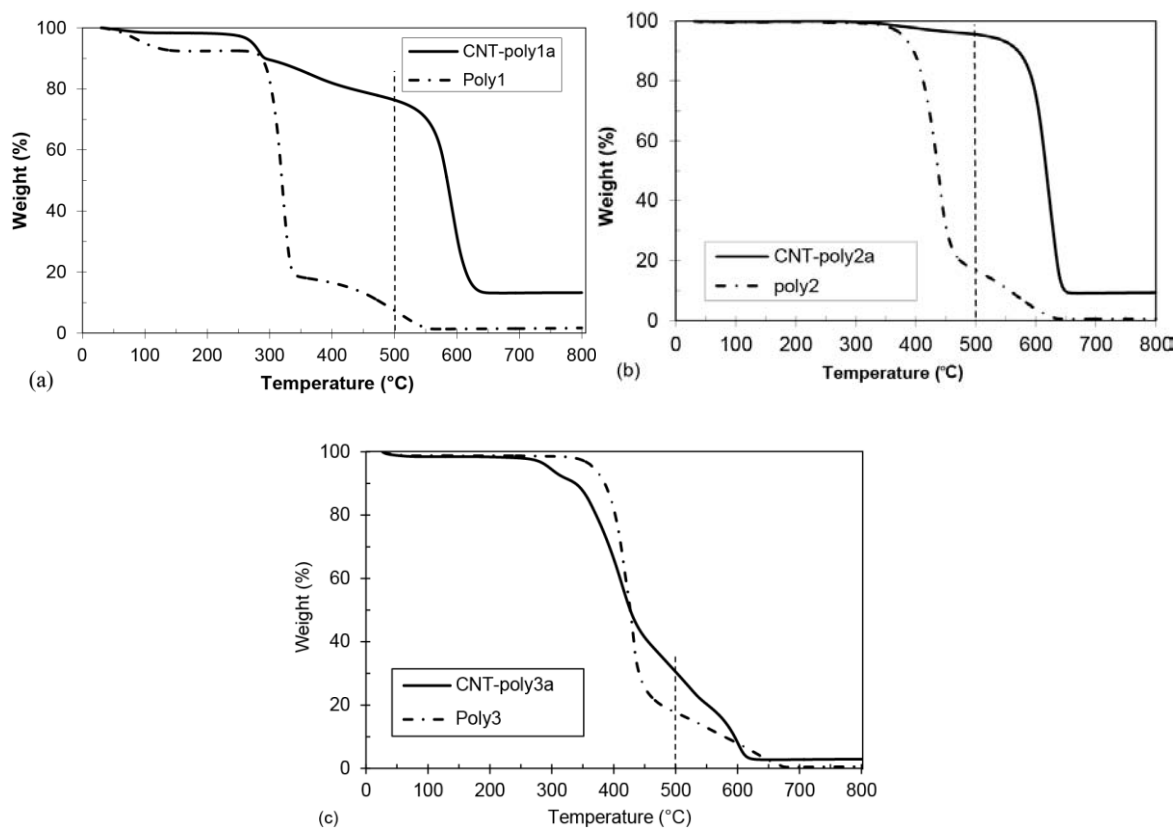
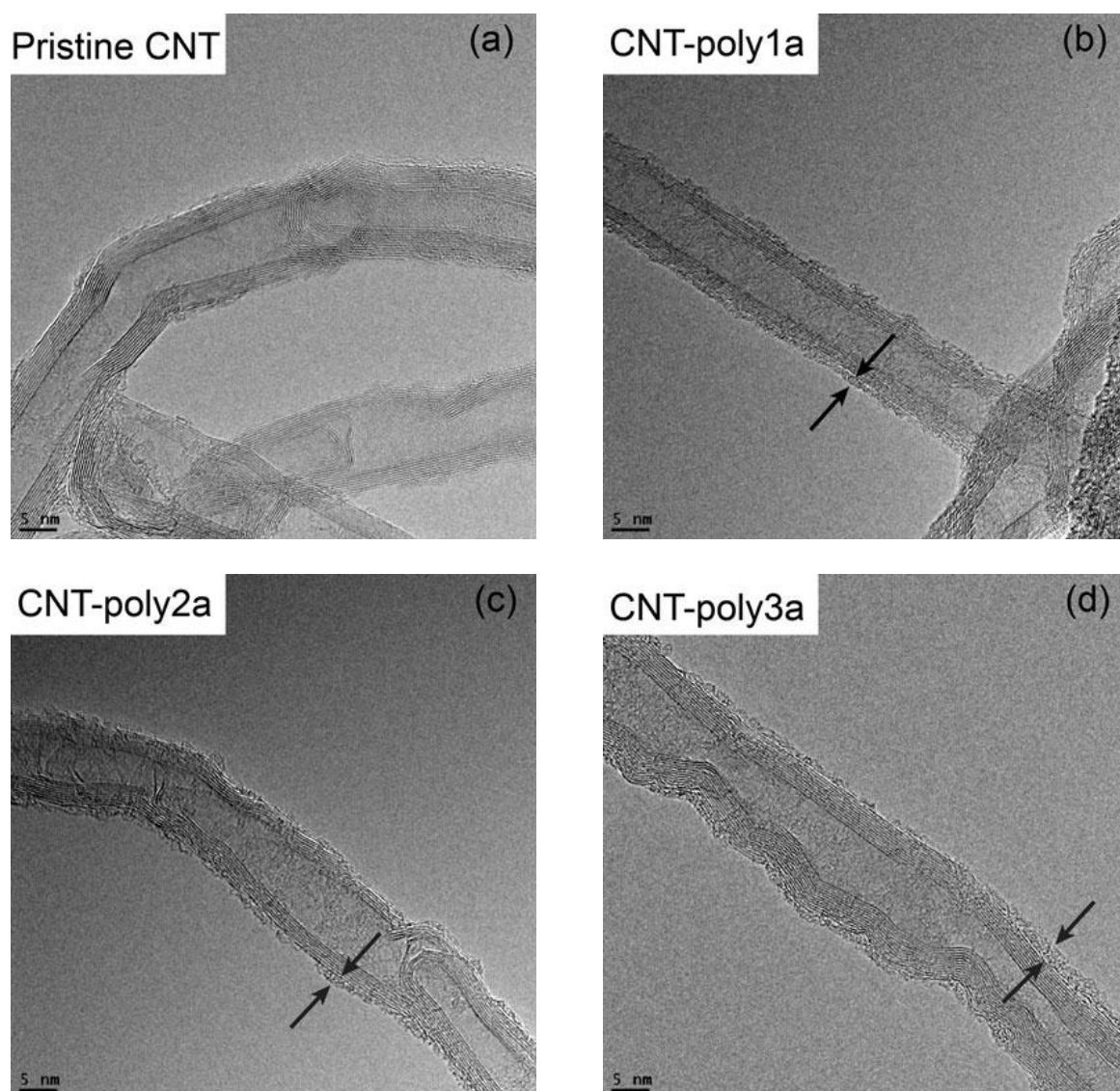


Figure II.23. TGA curves of (a) CNT–poly1a and neat poly1, (b) CNT–poly2a and neat poly2, (c) CNT–poly3a and neat poly3.

From TGA analysis, it is also found that the PIL adsorbed onto the CNT surface decomposes earlier than its neat form. PIL decomposes in two major steps. As calculated from the first derivative weight loss (DTG) curves, the decomposition temperature of the first step shifted from 318 °C to 279 °C for poly1, from 438 °C to 374 °C for poly2 and from 439 °C to 412°C for poly3. This decrease in stability can be attributed to the changes in the PIL structure as a result of the interactions with CNTs [65].

As shown in Figure II.24, the TEM analysis of the CNT–PIL hybrids showed the presence of a non-continuous polymer coating (up to 2.5 nm thickness) on the nanotube surface whatever the polymer. On the low magnified TEM image of CNT–**poly3a**, which shows a high PIL loading by TGA, an agglomeration of polymer is observed (Figure II.24 (h)). These agglomerates also encapsulate or bridge several nanotubes. This result is most likely due to the protic nature of the PIL which has a high tendency to form strong intramolecular H-bonding.



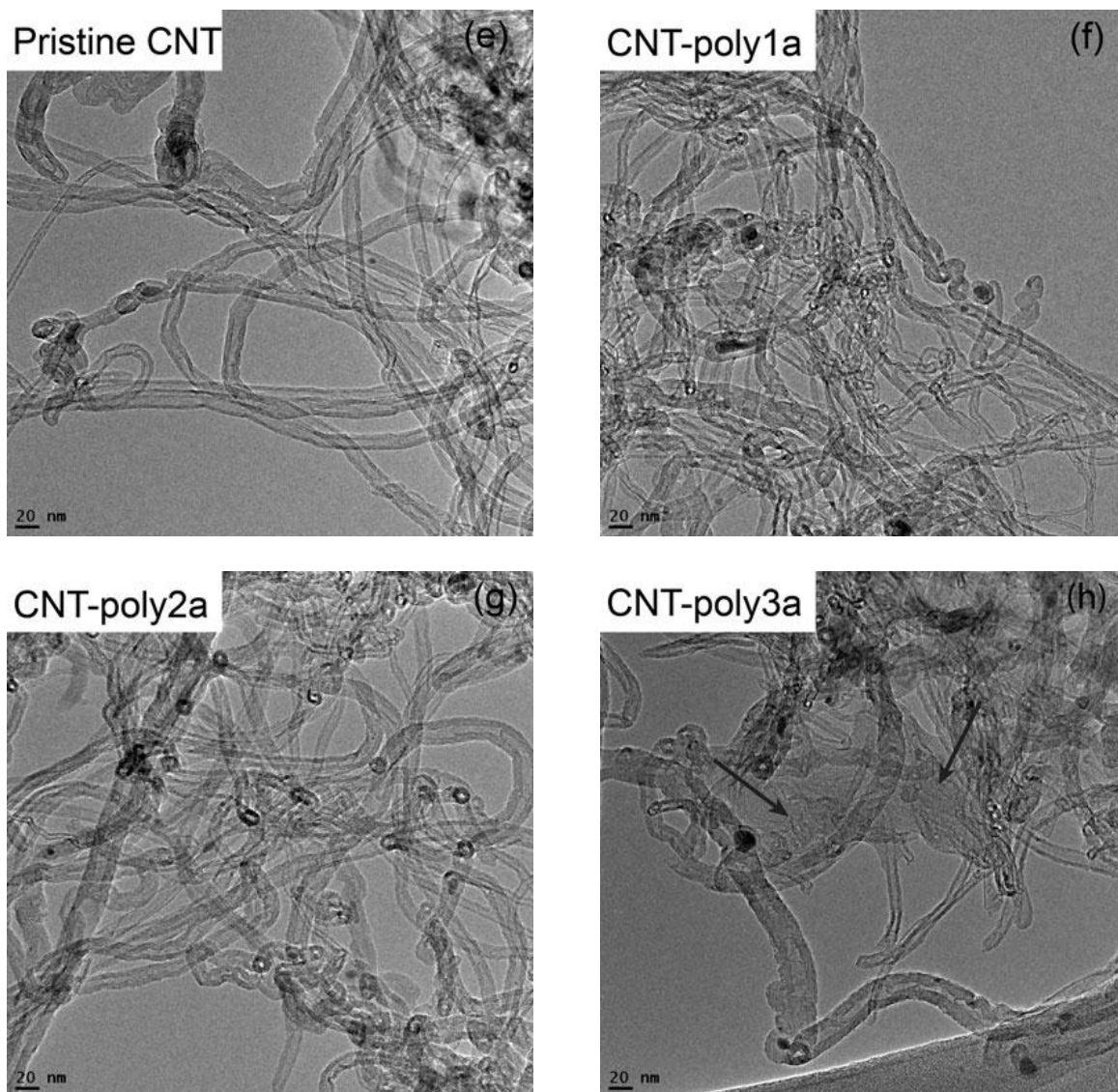


Figure II.24. TEM images of pristine CNT, CNT–**poly1a**, CNT–**poly2a** and CNT–**poly3a** at (a-d) high magnification (scale bar = 5 nm) and (e-h) low magnification (scale bar = 20 nm).

II.2.3.2 Functionalization by *in situ* polymerization

In situ polymerizations of IL monomers were carried out in an adequate solvent (ethanol for **poly1**, **poly2** and **poly3**; acetone for **poly4**) in the presence of pristine CNTs (5 wt.% with respect to the polymer) at 65 °C or 85 °C. At the end of the reactions, it was observed that the viscosity of the medium increased as a result of polymerization. **Poly5** was prepared by exchanging the counter-anion of **poly4** with Br⁻. As in the case of the CNTs functionalized *via* solution-mixing method, the Raman spectra of CNT–**polyxb** do not differ significantly

from the spectrum of pristine CNTs (Figure II.25). A decrease in I_D/I_G compared to pristine was also observed.

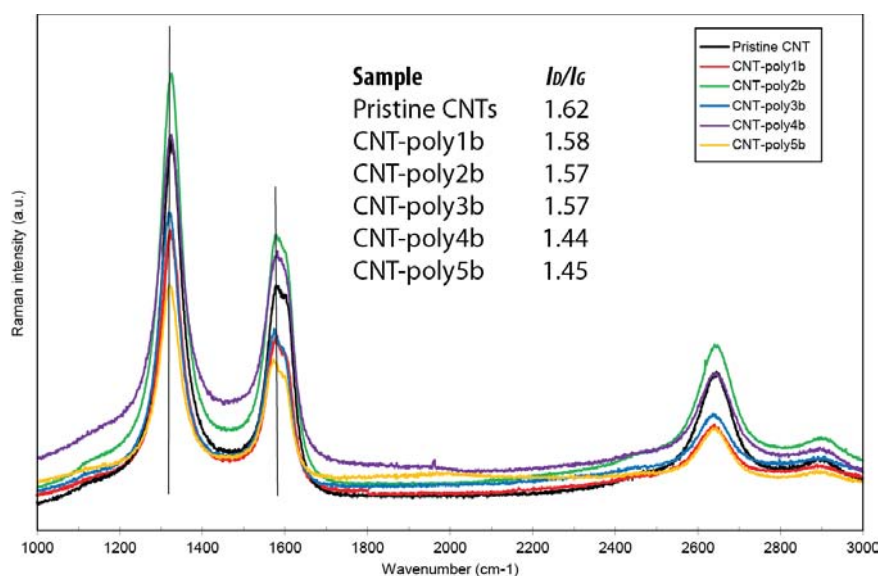


Figure II.25. Raman spectra of pristine CNTs and PIL functionalized CNTs *via in situ* method.

The TGA analysis of the recovered samples (Figure II.26) showed that the CNTs functionalized with **poly1** and **poly2** contained more or less the same amount of polymer compared to the ones functionalized *via* solution-mixing. The weight losses found for CNT-**poly1b** and CNT-**poly2b** below 500 °C are 22% (24% for CNT-**poly1a**) and 13% (9% for CNT-**poly2a**), respectively. The weight loss of CNT-**poly4b** is 32% whereas it decreases to 14% for the anion-exchanged homologue, CNT-**poly5b**. This shows that the NTf_2^- anions were completely exchanged with Br^- anion. For CNT-**poly3b** we measured a significantly lower amount of polymer, 36 wt.%, compared to the amount obtained with the solution-mixing method (70 wt.%).

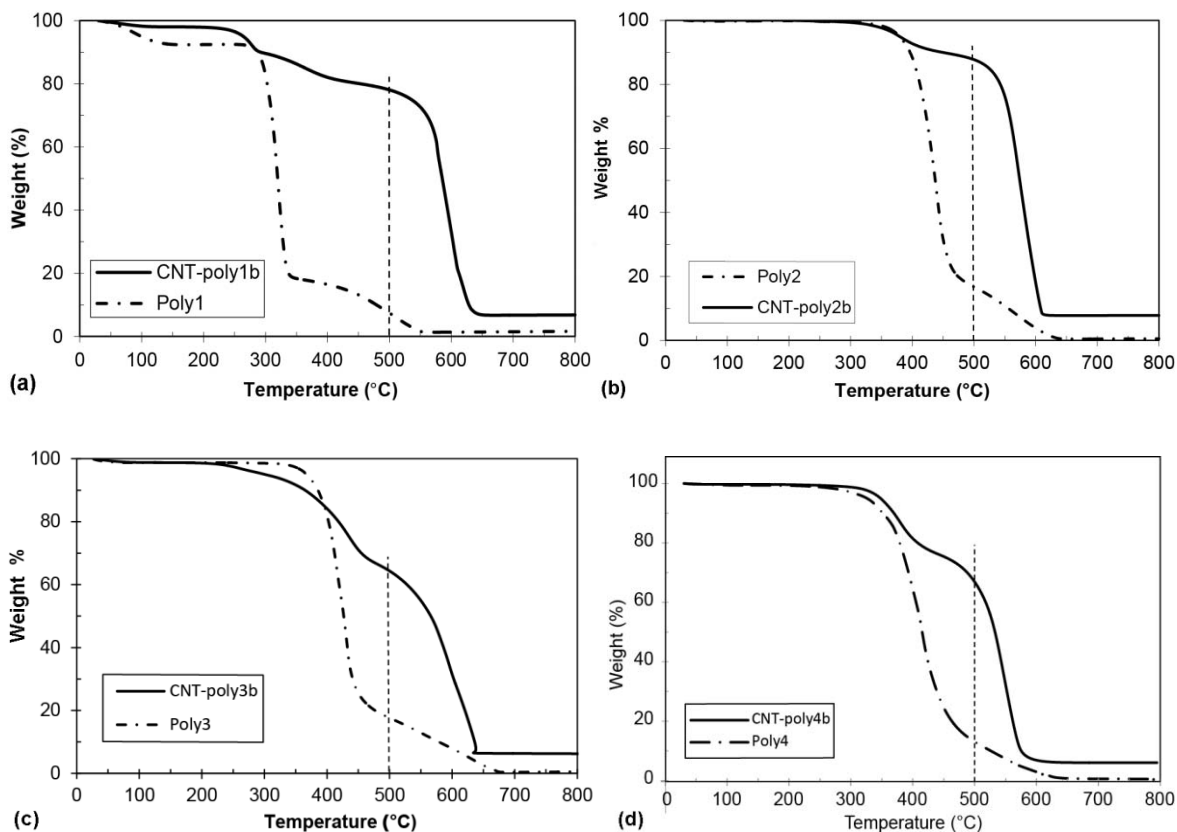
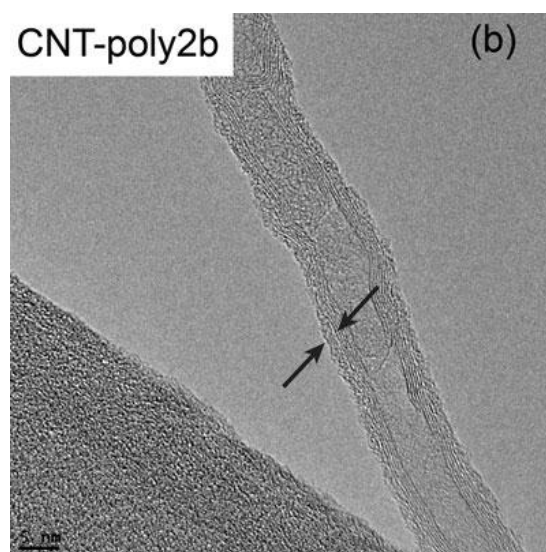
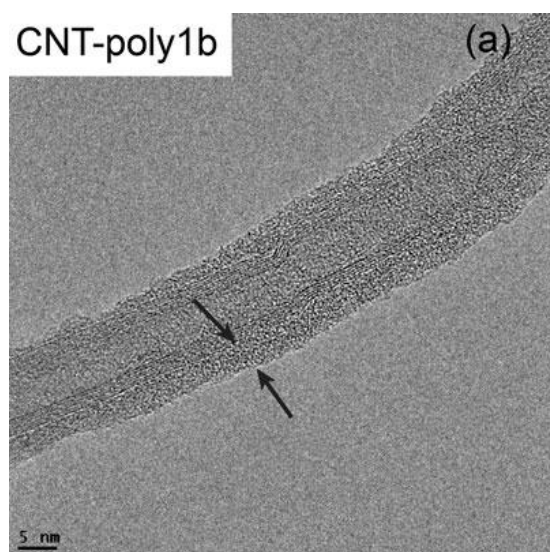


Figure II.26. TGA curves of (a) CNT–**poly1b** and neat **poly1**, (b) CNT–**poly2b** and neat **poly2**, (c) CNT–**poly3b** and neat **poly3** and (d) CNT–**poly4b** and neat **poly4**.

Similarly to what was observed for the CNTs functionalized *via* solution-mixing, the polymers decomposed at a lower temperature when adsorbed on the CNT surface. We also calculated the first derivative of the weight loss attributed to the CNT fraction in the samples. We noticed an anion effect on the thermostability of the CNTs, similarly to a previous study on MWCNTs covalently modified with ILs (Chapter I, Figure I.12). However, in our case the Br anion increased the thermal stability of the CNTs, whereas in the other study, both Br and NTf₂ anions were found to decrease the stability. For the poly[VEIM]⁺ backbone, the CNT thermostability was in the order Br (593 °C) > pristine CNTs (582 °C) > NTf₂ (569 °C). For the poly[VHEIM]⁺ backbone, a similar order was found: Br (591 °C) > pristine CNTs (582 °C) > NTf₂ (550 °C). For the **poly3b**, the thermostability of the CNTs did not differ much

(587 °C) compared to the pristine CNTs, which could be due to a lower amount of PIL in interaction with the CNT surface.

TEM analysis of CNT–**poly3b** at low magnification reveals the absence of the excessive polymer aggregation (Figure II.27 (d)). This result shows that the PIL synthesized by the *in situ* method can form a better coating on the surface of CNTs, which could be attributed to the fact that the IL monomers at the beginning of the reaction break the CNT bundles. For the other samples, the thin layer of PIL can also be observed on the surface of the CNTs in the high-magnification images. The thickness of the PIL layers varies between 1 and 5 nm. The samples contain well covered CNTs while there are also nanotubes coated with a discontinuous polymer layer.



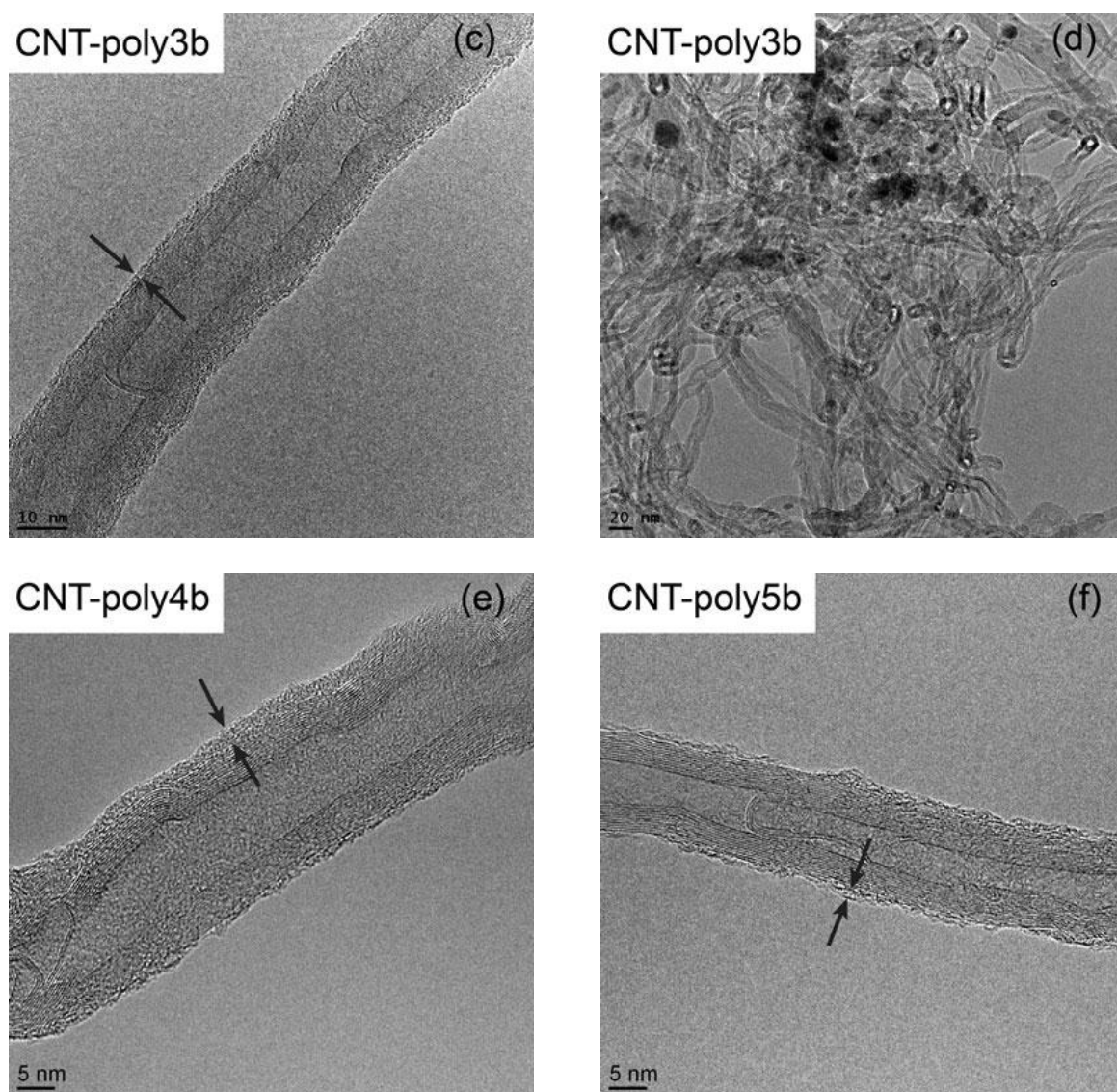


Figure II.27. TEM images of CNT-poly1b, CNT-poly2b, CNT-poly3b, CNT-poly4b, CNT-poly5b (a-c and e-f) at high magnification (scale bar = 5 nm) and CNT-poly3b (d) at low magnification (scale bar = 20 nm).

From TGA analysis, a slight increase (from 9 wt.% to 13 wt.%) in the amount of the adsorbed PIL was observed for CNT-poly2b sample compared to CNT-poly2a. The difference is small but expected as in free radical polymerization the chain formation step is very fast after the initiation of the monomers. Thus, the steric hindrance caused by the bulky anions of the polymer chain should be as much as in the case of the solution-mixing method.

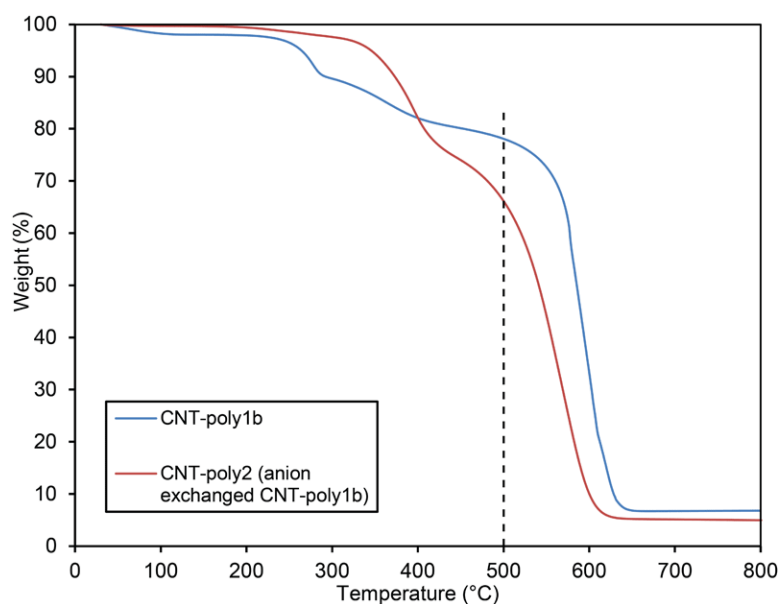


Figure II.28. TGA curves of CNT–**poly1b** and its anion-exchanged homologue.

We exchanged the Br^- anion of the CNT–**poly1b** with NTf_2^- anion to see if the CNTs could be functionalized with a higher amount of **poly2**. Normally the anion exchange reaction of PIL is completed quantitatively in a short time (< 30 min) [66]; even so, we stirred the CNTs in a solution of LiNTf_2 for 24 h to ensure the complete anion exchange. Based on the weight loss at 500 °C in the TGA curve, the amount of **poly2** on the CNT surface is determined to be approximately 34 wt.%. The completion would result in 42 wt.% PIL. This means that either the anion exchange was not complete or a part of the adsorbed polymer has been removed from the CNT surface. Nevertheless, this experiment shows that functionalization of CNTs with a small anion bearing PIL and subsequent anion-exchange is a useful strategy to obtain CNT–PILs based on bulky anions with a considerable amount of polymer loading (> 10 wt %). In the TGA curves in Figure II.28, the counter-anion influence on the CNT thermostability is very obvious. According to the differential weight loss curves, the CNTs degrade at 563 °C with NTf_2^- anion, whereas their decomposition point increases to 593 °C with Br^- anion.

It is worth noting that during the *in situ* radical polymerization method, polymer chains can be covalently grafted onto the CNT surface. Jia et al [67] suggested that π bonds of the CNT graphitic network can be opened by the radical initiator during the *in situ* radical polymerization of methyl methacrylate and in this way CNTs can take part in the polymerization process. We have also used this method to covalently graft vinyl polymers to the surface of pristine CNTs, which will be detailed in Chapter IV. On the other hand, up to now, covalent grafting of polymerized ionic liquids onto CNT surface by this method has never been reported. In this study, we have not observed any proof of covalent grafting either; therefore, we assume that PILs have been physically adsorbed onto the CNT surface. It is likely possible that the physical adsorption of PILs onto CNT surface is favored over the radical grafting during the *in situ* radical polymerization as in the case of some polymers. For example, Tang et al [68] observed that the CNTs were physically wrapped with poly(phenylacetylene) chains during the *in situ* radical polymerization of phenylacetylene. The authors suggested that the monomer has been adsorbed on the CNT surface due to the $\equiv\text{C}-\text{H}\cdots\pi$ hydrogen-bonding and the polymerization of such adsorbed monomers produced polymer chains non-covalently wrapping up the nanotubes. Similarly, we can propose that the strongly adsorbed IL monomers by possible $\pi-\pi$, cation- π or van der Waals interactions on the CNT surface can prevent the covalent grafting of the polymer chains.

II.2.4 Solvent dispersions of CNTs

Dispersions of pristine and functionalized CNTs in water and organic solvents (ethanol or acetone) were prepared with the aid of ultrasonication (Figure II.28 and 29). Pristine CNTs quickly precipitated in the solvents used as soon as the sonication stopped. On the other hand, depending on the nature of the anion, the CNT-PIL hybrids form dispersions that are stable in water (Br^-) or organic solvents like ethanol, THF, acetone or N-methyl-2-pyrrolidone for

several weeks. While *in situ* method allowed us to prepare solvent-dispersible CNTs functionalized with all types of PIL studied, we could obtain dispersible CNTs functionalized with only **poly1** and **poly2** using solution-mixing method. Although CNT-**poly3a** contains 70 wt.% of polymer, the sample does not disperse at all even after prolonged sonication. An explanation of this could be that the polymer agglomerates observed by TEM act as bridges between CNTs, thus hindering their dispersion.

On the other hand, all of the PIL-functionalized CNTs obtained by *in situ* method were dispersible in appropriate solvents depending on the solubility of the adsorbed polymer (Figure II.29). CNT-**poly3b** could be dispersed in ethanol but starts to settle down soon after the sonication is stopped and settle down completely within one hour. The intramolecular H-bonding interactions of **poly3** should be much stronger than the **poly3**-CNT interactions, which leads to the agglomeration of the CNTs. The dispersions of other *in situ* functionalized CNTs stay black upon standing for several weeks although some sedimentation occurs.

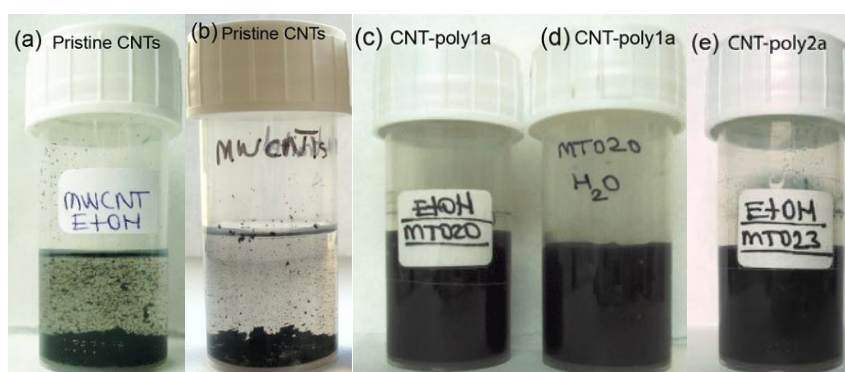


Figure II.28. Dispersions of pristine CNTs (1 g L^{-1}) in ethanol (a), water (b); and PIL functionalized CNTs *via* solution-mixing: CNT-**poly1a** in ethanol (c), water (d); and CNT-**poly2a** in ethanol (e) after standing for a half hour.

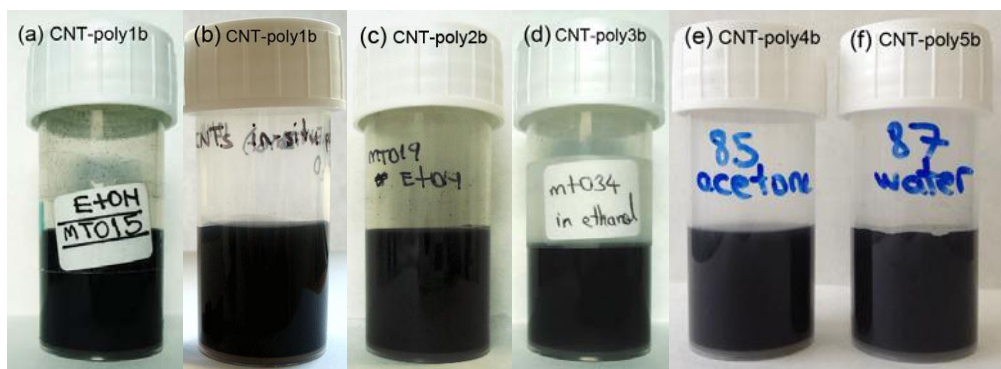


Figure II.29. Dispersions of PIL functionalized CNTs (1 g L⁻¹) *via in situ*: CNT–poly1b in ethanol (a), water (b); CNT–poly2b in ethanol (c); CNT–poly3b in ethanol (d); CNT–poly4b in acetone (e); and CNT–poly5b in water.

Particle size analysis by laser diffraction technique is a useful method to evaluate the quality of CNT dispersions [69]. However, it should be noted that this technique measures the volume weighted mean diameter ($D_{[4,3]}$) of the equivalent sphere for particles between 0.020 μm and 2000 μm . The diameter of the sphere of the equivalent volume corresponding to an individual nanotube used in this study is between 0.025 and 0.15 μm . The improved stability of the dispersions that we obtained by functionalization with PIL allowed us to perform this analysis. Although nitric acid oxidation improves the dispersibility of the nanotubes by the introduction of oxygen containing groups to the CNT surface, the corresponding dispersions in water or in the investigated organic solvents (ethanol and acetone) are instable. The mean diameter results found between 0.10 μm and 61 μm were not reproducible.

Table II.4. Particle size analysis of the CNT dispersions.

Sample	Method	Vol weighted mean diameter (μm)		
		in water	in ethanol	in acetone
CNT–poly1	a Sol. mix.	45	19	–

	b <i>In situ</i>	48	12	–
CNT– poly2	a Sol. mix.	–	25	Not stable
	b <i>In situ</i>	–	13	Not stable
CNT– poly3	a Sol. mix.	–	Not stable	–
	b <i>In situ</i>	–	15	–
CNT– poly4	b <i>In situ</i>	–	–	17
CNT– poly5	b <i>In situ</i>	23	–	–
CNT– COOH	Acid reflux	Not stable	Not stable	Not stable

(–) The polymer is not soluble in the corresponding solvent.

From the particle size analysis of the stable dispersions of PIL-functionalized CNTs (Table II.4), it is found that the mean size of the CNT agglomerates after functionalization by *in situ* method is generally smaller compared to that of those obtained using the *solution-mixing* method. It could be due to a more homogeneous coating of the polymer onto the nanotubes by the *in situ* method as evidenced by the TEM images. Among water dispersible CNTs, CNT–**poly5b** disperse relatively better than CNT–**poly1**, most likely due to the hydroxyl groups present in the polymer chain of the former. However, it should be noted that although dispersions appear homogeneous to the naked eye, they consist of many different sized CNT bundles and the above table gives only the average values. Thus, we should look at the particle size distributions of the CNTs (Figure II.30). From these, it is clearly observed that the ethanol dispersion of CNTs functionalized with **poly1** via *in situ* method contains significantly larger amount of small agglomerates and individual CNTs: the D[4,3] of the 23 vol.% of total particles is between 0.036 and 2 μm . This exfoliated fraction can be separated by centrifugation.

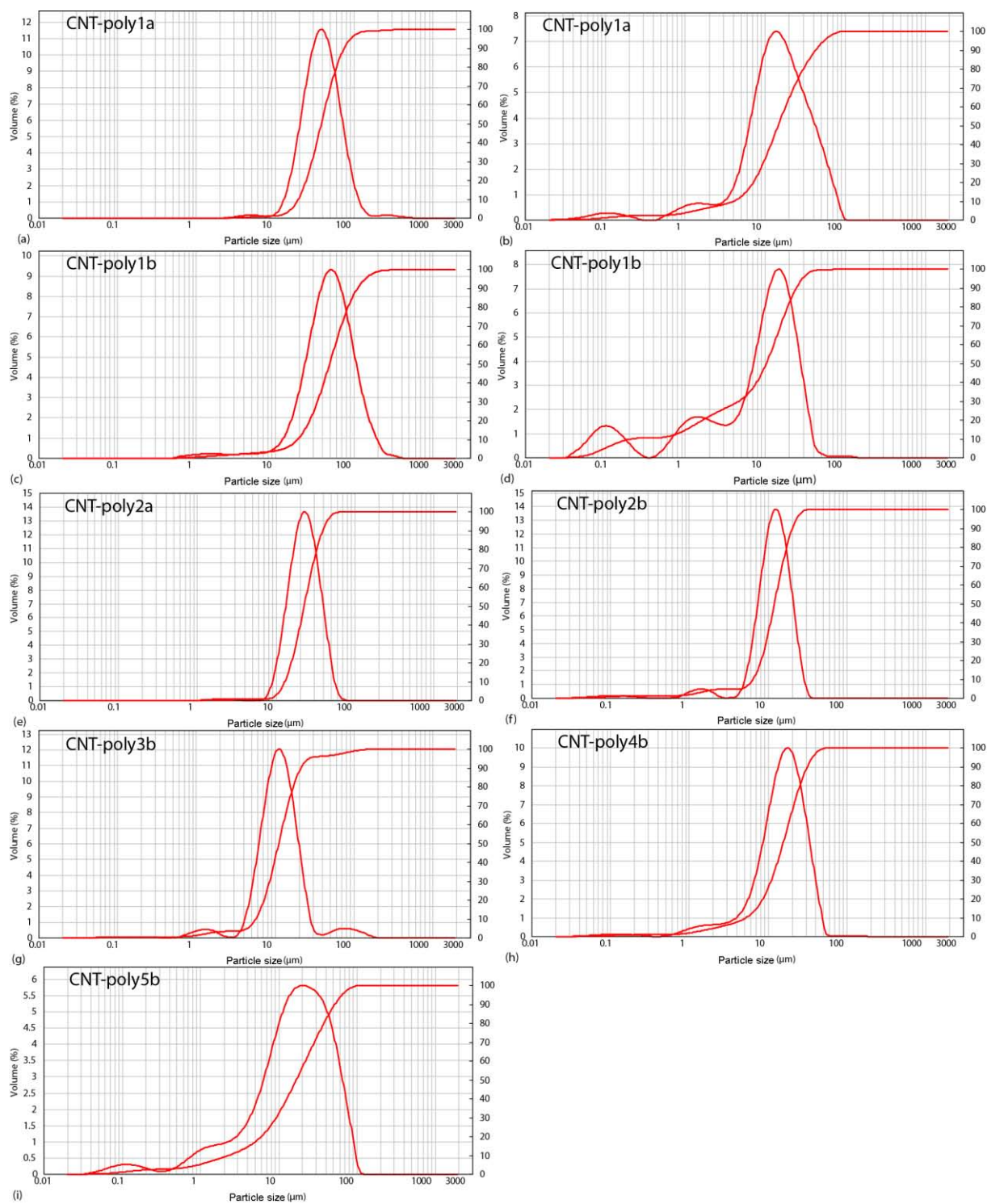


Figure II.30. Particle size distributions of CNT–poly1 prepared by solution-mixing (a) in water, (b) in ethanol; CNT–poly1 prepared by *in situ* method (c) in water, (d) in ethanol; CNT–poly2 prepared (e) by solution-mixing in ethanol, (f) by *in situ* method in ethanol; (g) CNT–poly3 prepared by *in situ* in ethanol; (h) CNT–poly4 prepared by *in situ* method in acetone and (i) CNT–poly5 prepared by *in situ* method in water.

II.2.5 Incorporation of CNTs into gels

Preparation of gels from CNTs and imidazolium ILs has already been reported [70]. In such soft materials, also called bucky gels, CNTs act as physical cross-linkers. The CNT/PIL gels described in this study are different from the bucky gels. The polymer network formed by the intramolecular H-bonding ($-O\cdots H-O$) of **poly3**, leads to a gel formation with certain solvents. CNTs can be dispersed in the PIL gel due to the specific interactions. We used pristine and acid-oxidized MWCNTs to prepare composites with PIL organo- and hydrogels, respectively. To prepare CNT/PIL organogel composites, pristine CNTs (1, 3 or 5 wt.% with respect to the polymer) were shortly sonicated in acetone (34 times of the polymer weight) and **poly4** was added into the dispersion formed. The dispersion was sonicated for 1 h to obtain a good homogeneity. Upon acetone evaporation at 60 °C, a solid polymer composite was obtained.

For the preparation of the CNT/hydrogel composites, we used oxidized CNTs which are dispersible in water. Following a short sonication, **poly5** was added into the dispersion. In a few seconds, the gelation took place. Extrudable CNT/-hydrogels at concentrations of 1, 3 and 5 wt.% with respect to the polymer were thus prepared (Figure II.31). The morphology of the CNTs was analyzed by SEM. From the images, it is clearly observed that the CNTs in the polymer matrices appear larger in diameter than they are (Figure II.32). The average outer diameter of the CNTs was estimated to be increased from 12 to 20 nm and to 26 nm, after incorporation into the organo- and hydro-gel matrix, respectively. This increase in diameter is attributed to the adsorbed polymer on the surface of the CNTs.

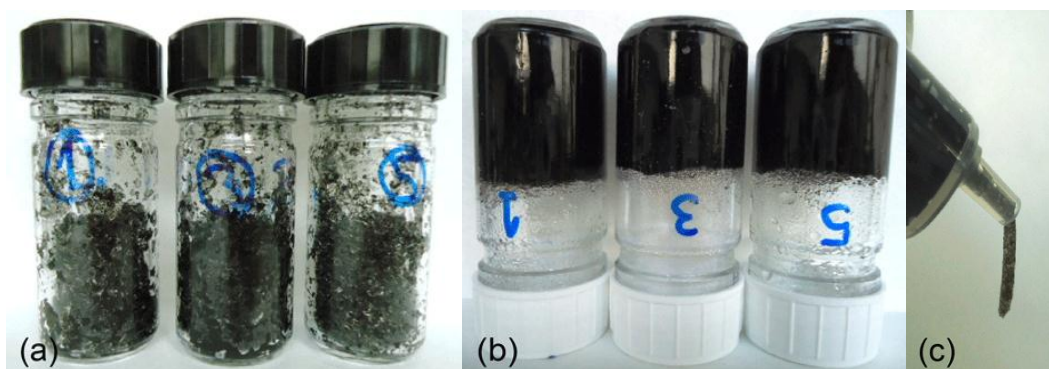


Figure II.31. Photographs of (a) vials containing CNT/organogel at concentrations of 1, 3 and 5 wt %, (b) vials containing CNT/hydrogel at concentrations of 1, 3 and 5 wt %; (c) Extrusion of the CNT/hydrogel (1 wt % of CNT).

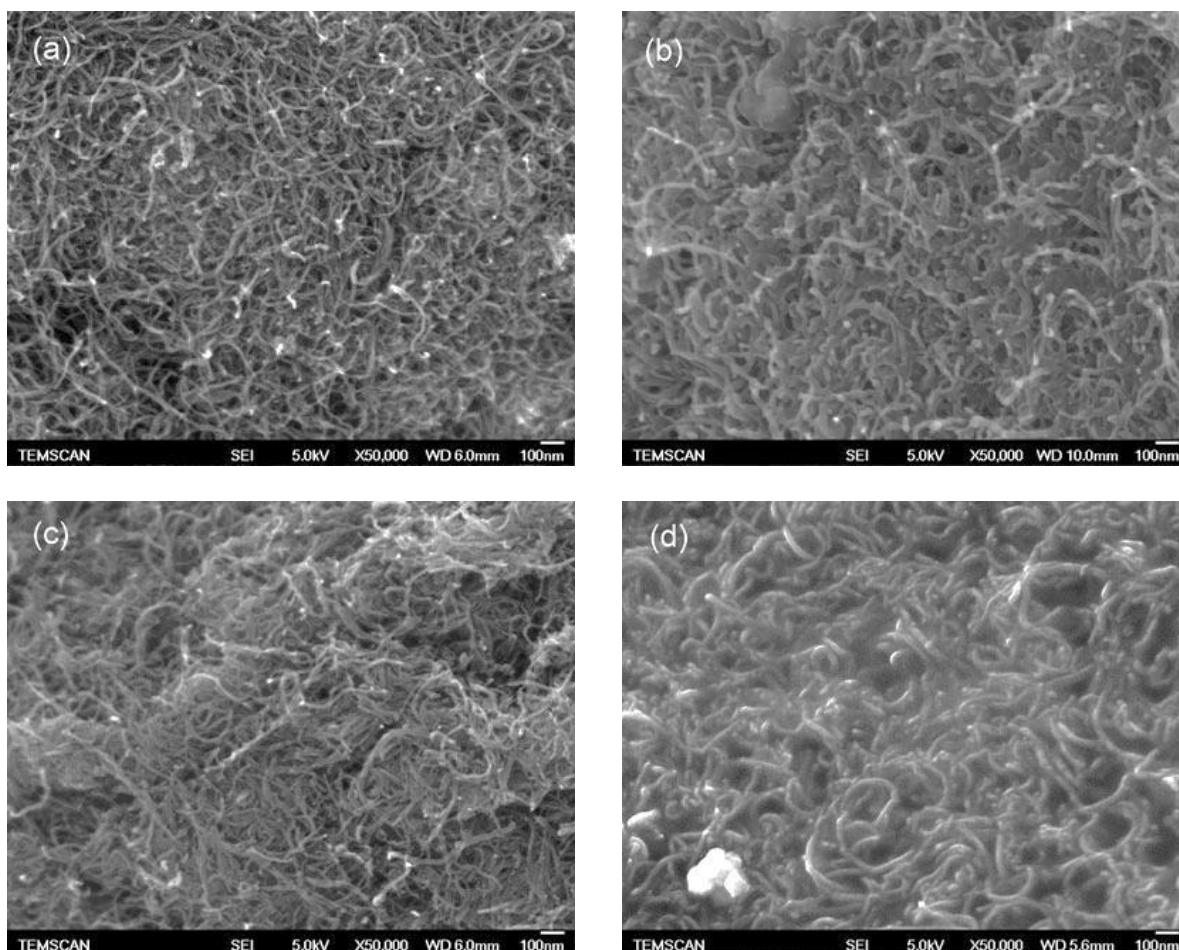


Figure II.32. SEM images (magnification: 50 000) of (a) pristine CNTs, (b) CNT/organogel (5 wt.%), (c) oxidized CNTs, (d) oxidized CNT/hydrogel (5 wt.%). (scale bar = 100 nm).

The Raman spectroscopy was used to further probe the structure of the CNT–polymer composites. While the Raman signals of the PILs (**poly4** and **poly5**) are masked by overwhelming luminescence interference (spectra are not shown here), CNT signals can be observed without any interference coming from the polymer matrix in the CNT–PIL composites (Figure II.33). Both the G and D bands of the CNTs in the composites (particularly in **CNT/poly5** composite) are significantly broader and weaker in intensity compared to the neat or oxidized CNTs. Furthermore, the D to G intensity ratio (I_D/I_G) is much more reduced in the composites compared to the functionalized ones (CNT–**poly4b** and CNT–**poly5b**). If a high content of polymer has affected the Raman signals, it is not because the CNT content is too low to be detected but because the tubes are wrapped by the polymer chains that may result in energy transfer between tubes and polymers [71]. Therefore, because of the higher coverage of the CNTs by the PIL matrix in the composites compared to the discontinuous polymer wrapping around the CNT surface in the functionalized ones, the CNT–polymer interactions are enhanced. As a result, the Raman signals of the CNTs in the composite are further affected.

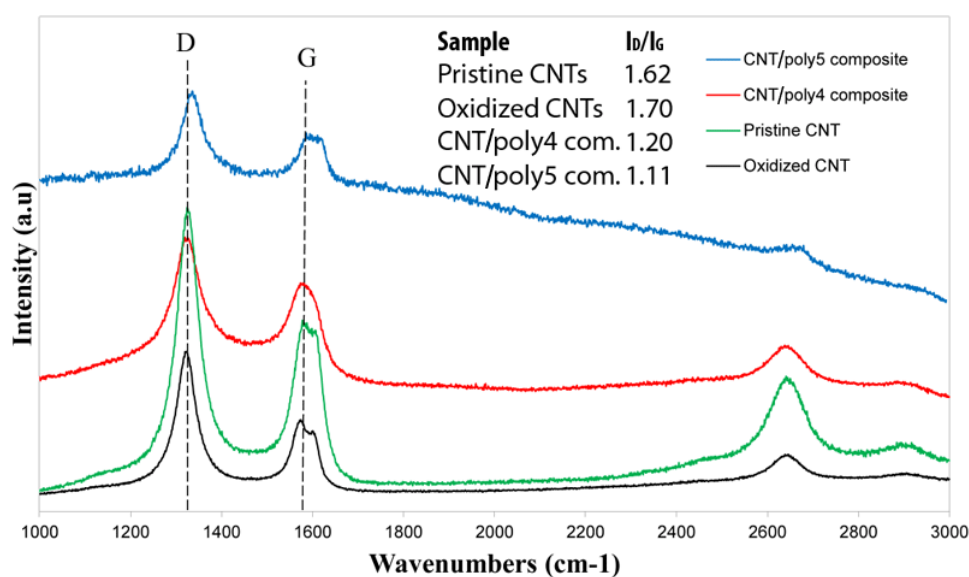


Figure II.33. Raman spectra of pristine CNTs, oxidized CNTs and CNT/PIL composites.

II.3. Conclusions

Non-covalent functionalization of MWCNTs with several polymerized ionic liquids based on two methods, namely, *in situ* and solution-mixing, has been studied. It was shown that the type of PIL, as well as the method, influences the functionalization of CNTs.

The following conclusions can be drawn from this study:

- Among all polymers studied, poly[VEIM]Br (poly1) has given the best results concerning the amount of the adsorbed polymer on the surface of the CNTs and the exfoliated CNTs in organic solvent.
- The effect of the counter-anion on the adsorption of PIL on the CNT surface has been shown with various experiments carried out on the poly[VEIM]⁺ chain. The results suggest that due to the larger steric effect of the bulky NTf₂⁻ anion, the wrapping of the corresponding polymer chain around the CNTs and/or its penetration into the spaces between the CNT bundles are highly hindered. This suggests that the counter-anion of the polymer is associated with the polycation chain in organic solvents.
- Therefore, functionalizing CNTs firstly with small counter-anion (e.g. Br⁻) bearing PILs and subsequently carrying-out an anion-exchange reaction will allow to maximize the amount of polymer adsorbed onto the CNT surface.
- Generally, compared to the solution-mixing method, the *in situ* method promotes coating on the CNT surface in such a way that excessive polymer aggregation, particularly for polymers which have high inter-chain interactions, is reduced and the adsorption of the polymers with bulky anions are slightly facilitated

- Protic ionic liquid polymers are not suitable for non-covalent functionalization of CNTs, due to the formation of possible intramolecular hydrogen bonding, which results in poorly dispersible CNTs.
- A new PIL, poly(1-hydroxyethyl-3-vinylimidazolium), which forms organic- or hydro-gels in appropriate solvents, has been synthesized. CNTs can be incorporated into these gels to prepare new PIL/CNT materials.

References

- [1] in het Panhuis M, Maiti A, Dalton AB, van den Noort A, Coleman JN, McCarthy B, et al. Selective Interaction in a Polymer–Single-Wall Carbon Nanotube Composite. *J Phys Chem B* 2002;107(2):478-82.
- [2] Srebnik S. Physical association of polymers with nanotubes. *J. Polym Sci, Part B: Polym Phys* 2008;46(24):2711-8.
- [3] Qin S, Qin D, Ford WT, Herrera JE, Resasco DE, Bachilo SM, et al. Solubilization and Purification of Single-Wall Carbon Nanotubes in Water by in Situ Radical Polymerization of Sodium 4-Styrenesulfonate. *Macromolecules* 2004;37(11):3965-7.
- [4] Kim SW, Kim T, Kim YS, Choi HS, Lim HJ, Yang SJ, et al. Surface modifications for the effective dispersion of carbon nanotubes in solvents and polymers. *Carbon* 2012;50(1):3-33.
- [5] O'Connell MJ, Boul P, Ericson LM, Huffman C, Wang Y, Haroz E, et al. Reversible water-solubilization of single-walled carbon nanotubes by polymer wrapping. *Chem Phys Lett* 2001;342(3–4):265-71.
- [6] Star A, Stoddart JF, Steuerman D, Diehl M, Boukai A, Wong EW, et al. Preparation and Properties of Polymer-Wrapped Single-Walled Carbon Nanotubes. *Angew Chem Int Ed* 2001;40(9):1721-5.
- [7] Baskaran D, Mays JW, Bratcher MS. Noncovalent and Nonspecific Molecular Interactions of Polymers with Multiwalled Carbon Nanotubes. *Chem Mater* 2005;17(13):3389-97.
- [8] Gurevitch I, Srebnik S. Conformational behavior of polymers adsorbed on nanotubes. *J Chem Phys* 2008;128(14):144901.

- [9] Gurevitch I, Srebnik S. Monte Carlo simulation of polymer wrapping of nanotubes. *Chem Phys Lett* 2007;444(1–3):96-100.
- [10] Tallury SS, Pasquinelli MA. Molecular Dynamics Simulations of Flexible Polymer Chains Wrapping Single-Walled Carbon Nanotubes. *J Phys Chem B* 2010;114(12):4122-9.
- [11] Tallury SS, Pasquinelli MA. Molecular Dynamics Simulations of Polymers with Stiff Backbones Interacting with Single-Walled Carbon Nanotubes. *J Phys Chem B* 2010;114(29):9349-55.
- [12] Zhao W, Liu Y-T, Feng Q-P, Xie X-M, Wang X-H, Ye X-Y. Dispersion and noncovalent modification of multiwalled carbon nanotubes by various polystyrene-based polymers. *J Appl Polym Sci* 2008;109(6):3525-32.
- [13] Zhou T-n, Hou Z-c, Wang K, Zhang Q, Fu Q. Polystyrene-wrapping multi-walled carbon nanotubes obtained via simple physical modification of melt mixing. *Polym Adv Technol* 2011;22(9):1359-65.
- [14] Zheng Q, Xue Q, Yan K, Hao L, Li Q, Gao X. Investigation of Molecular Interactions between SWNT and Polyethylene/Polypropylene/Polystyrene/Polyaniline Molecules. *J Phys Chem C* 2007;111(12):4628-35.
- [15] Narizzano R, Nicolini C. Mechanism of Conjugated Polymer Organization on SWNT Surfaces. *Macromol Rapid Commun* 2005;26(5):381-5.
- [16] Yang M, Koutsos V, Zaiser M. Interactions between Polymers and Carbon Nanotubes: A Molecular Dynamics Study. *Phys Chem B* 2005;10 (20) :1000 -14.
- [17] Foroutan M, Nasrabadi AT. Investigation of the Interfacial Binding between Single-Walled Carbon Nanotubes and Heterocyclic Conjugated Polymers. *J Phys Chem B* 2010;114(16):5320-6.

- [18] Giulianini M, Waclawik ER, Bell JM, Crescenzi MD, Castrucci P, Scarselli M, et al. Regioregular poly(3-hexyl-thiophene) helical self-organization on carbon nanotubes. *Appl Phys Lett* 2009;95(1):013304.
- [19] Zou J, Liu L, Chen H, Khondaker SI, McCullough RD, Huo Q, et al. Dispersion of Pristine Carbon Nanotubes Using Conjugated Block Copolymers. *Adv Mater* 2008;20(11):2055-60.
- [20] Bahun GJ, Wang C, Adronov A. Solubilizing single-walled carbon nanotubes with pyrene-functionalized block copolymers. *J Polym Sci, Part A: Polym Chem* 2006;44(6):1941-51.
- [21] Shvartzman-Cohen R, Florent M, Goldfarb D, Szleifer I, Yerushalmi-Rozen R. Aggregation and Self-Assembly of Amphiphilic Block Copolymers in Aqueous Dispersions of Carbon Nanotubes. *Langmuir* 2008;24(9):4625-32.
- [22] Mountrichas G, Pispas S, Tagmatarchis N. Aqueous Carbon-Nanotube–Amphiphilic-Block-Copolymer Nanoensembles: Towards Realization of Charge-Transfer Processes with Semiconductor Quantum Dots. *Small* 2007;3(3):404-7.
- [23] Yan Y, Yang S, Cui J, Jakisch L, Pötschke P, Voit B. Synthesis of pyrene-capped polystyrene for dispersion of pristine single-walled carbon nanotubes. *Polym Int* 2011;60(10):1425-33.
- [24] Itzhak R, Raichman D, Shahar Z, Frey GL, Frey J, Yerushalmi-Rozen R. Tailoring Triblock Copolymers for Dispersion of Individual, Pristine, Single-Walled Carbon Nanotubes in Organic Solvents. *J Phys Chem C* 2010;114(9):3748-53.
- [25] Ji Y, Huang YY, Tajbakhsh AR, Terentjev EM. Polysiloxane Surfactants for the Dispersion of Carbon Nanotubes in Nonpolar Organic Solvents. *Langmuir* 2009;25(20):12325-31.

- [26] Zou J, Khondaker SI, Huo Q, Zhai L. A General Strategy to Disperse and Functionalize Carbon Nanotubes Using Conjugated Block Copolymers. *Adv Funct Mater* 2009;19(3):479-83.
- [27] Kim KT, Jo WH. Noncovalent functionalization of multiwalled carbon nanotubes using graft copolymer with naphthalene and its application as a reinforcing filler for poly(styrene-co-acrylonitrile). *J Polym Sci, Part A: Polym Chem* 2010;48(19):4184-91.
- [28] Sun J-T, Hong C-Y, Pan C-Y. Surface modification of carbon nanotubes with dendrimers or hyperbranched polymers. *Polym Chem* 2011;2(5):998-1007.
- [29] Yang L-P, Pan C-Y. A Non-Covalent Method to Functionalize Multi-Walled Carbon Nanotubes Using Six-Armed Star Poly(L-lactic acid) with a Triphenylene Core. *Macromol Chem Phys* 2008;209(8):783-93.
- [30] Durmaz H, Dag A, Tunca U, Hizal G. Synthesis and characterization of pyrene bearing amphiphilic miktoarm star polymer and its noncovalent interactions with multiwalled carbon nanotubes. *J Polym Sci, Part A: Polym Chem* 2012;50(12):2406-14.
- [31] Petrie K, Docoslis A, Vasic S, Kontopoulou M, Morgan S, Ye Z. Non-covalent/non-specific functionalization of multi-walled carbon nanotubes with a hyperbranched polyethylene and characterization of their dispersion in a polyolefin matrix. *Carbon* 2011;49(10):3378-82.
- [32] Ogoshi T, Saito T, Yamagishi T-a, Nakamoto Y. Solubilization of single-walled carbon nanotubes by entanglements between them and hyperbranched phenolic polymer. *Carbon* 2009;47(1):117-23.
- [33] Woo S, Lee Y, Sunkara V, Cheedarala RK, Shin HS, Choi HC, et al. "Fingertip"-Guided Noncovalent Functionalization of Carbon Nanotubes by Dendrons. *Langmuir* 2007;23(23):11373-6.

- [34] Bahun GJ, Adronov A. Interactions of carbon nanotubes with pyrene-functionalized linear-dendritic hybrid polymers. *J Polym Sci, Part A: Polym Chem* 2010;48(5):1016-28.
- [35] Star A, Stoddart JF. Dispersion and Solubilization of Single-Walled Carbon Nanotubes with a Hyperbranched Polymer. *Macromolecules*. 2002;35(19):7516-20.
- [36] Kang YK, Lee O-S, Deria P, Kim SH, Park T-H, Bonnell DA, et al. Helical Wrapping of Single-Walled Carbon Nanotubes by Water Soluble Poly(p-phenyleneethynylene). *Nano Lett* 2009;9(4):1414-8.
- [37] Huang S-CJ, Artyukhin AB, Wang Y, Ju J-W, Stroeve P, Noy A. Persistence Length Control of the Polyelectrolyte Layer-by-Layer Self-Assembly on Carbon Nanotubes. *J Am Chem Soc* 2005;127(41):14176-7.
- [38] Mammeri F, Teyssandier J, Connan C, Le Bourhis E, Chehimi MM. Mechanical properties of carbon nanotube-PMMA based hybrid coatings: the importance of surface chemistry. *RSC Advances*. 2012;2(6):2462-8.
- [39] Manohar S, Tang T, agota A. Structure of Homopolymer DNA–CNT Hybrids†. *J Phys Chem C* 2007;111(48):17835-45.
- [40] Iamsamai C, Soottitantawat A, Ruktanonchai U, Hannongbua S, Dubas ST. Simple method for the layer-by-layer surface modification of multiwall carbon nanotubes. *Carbon* 2011;49(6):2039-45.
- [41] Wang D, Ji W-X, Li Z-C, Chen L. A Biomimetic “Polysoap” for Single-Walled Carbon Nanotube Dispersion. *J Am Chem Soc* 2006;128(20):6556-7.
- [42] Jo TS, Han H, Ma L, Bhowmik PK. Dispersion of single-walled carbon nanotubes with poly(pyridinium salt)s. *Polym Chem* 2011;2(9):1953-5.
- [43] Dobrynin AV, Rubinstein M. Theory of polyelectrolytes in solutions and at surfaces. *Prog Polym Sci* 2005;30(11):1049-118.

- [44] Liu G, Zhao J, Sun Q, Zhang G. Role of Chain Interpenetration in Layer-by-Layer Deposition of Polyelectrolytes. *J Phys Chem B* 2008;112(11):3333-8.
- [45] Etika KC, Cox MA, Grunlan JC. Tailored dispersion of carbon nanotubes in water with pH-responsive polymers. *Polymer* 2010;51(8):1761-70.
- [46] Mecerreyes D. Polymeric ionic liquids: Broadening the properties and applications of polyelectrolytes. *Prog Polym Sci* 2011;36(12):1629-48.
- [47] Chen H, Elabd YA. Polymerized Ionic Liquids: Solution Properties and Electrospinning. *Macromolecules* 2009;42(9):3368-73.
- [48] Li W, Zhang Z, Han B, Hu S, Xie Y, Yang G. Effect of Water and Organic Solvents on the Ionic Dissociation of Ionic Liquids. *J Phys Chem B* 2007;111(23):6452-6.
- [49] Wang H, Wang J, Zhang S, Pei Y, Zhuo K. Ionic Association of the Ionic Liquids [C4mim][BF4], [C4mim][PF6], and [Cnmim]Br in Molecular Solvents. *ChemPhysChem* 2009;10(14):2516-23.
- [50] Fukushima T, Kosaka A, Ishimura Y, Yamamoto T, Takigawa T, Ishii N, et al. Molecular Ordering of Organic Molten Salts Triggered by Single-Walled Carbon Nanotubes. *Science* 2003;300(5628):2072-4.
- [51] Wu B, Hu D, Kuang Y, Liu B, Zhang X, Chen J. Functionalization of Carbon Nanotubes by an Ionic-Liquid Polymer: Dispersion of Pt and PtRu Nanoparticles on Carbon Nanotubes and Their Electrocatalytic Oxidation of Methanol. *Angew Chem Int Ed* 2009;48(26):4751-4.
- [52] Kim T, Tung TT, Lee T, Kim J, Suh KS. Poly(ionic liquid)-Mediated Hybridization of Single-Walled Carbon Nanotubes and Conducting Polymers. *Chem Asian J* 2010;5(2):256-60.

- [53] Xiao C, Chu X, Wu B, Pang H, Zhang X, Chen J. Polymerized ionic liquid-wrapped carbon nanotubes: The promising composites for direct electrochemistry and biosensing of redox protein. *Talanta* 2010;80(5):1719-24.
- [54] Fukushima T, Kosaka A, Yamamoto Y, Aimiya T, Notazawa S, Takigawa T, et al. Dramatic Effect of Dispersed Carbon Nanotubes on the Mechanical and Electroconductive Properties of Polymers Derived from Ionic Liquids. *Small* 2006;2(4):554-60.
- [55] Collins PG. Defects and disorder in carbon nanotubes. In: A.V. Narlikar YYF, ed. *The Oxford Handbook of Nanoscience and Technology: Frontiers and Advances*. Oxford: Oxford Press 2010.
- [56] Charlier JC. Defects in Carbon Nanotubes. *Acc Chem Res* 2002;35(12):1063-9.
- [57] Geng J, Kong B-S, Yang SB, Youn SC, Park S, Joo T, et al. Effect of SWNT Defects on the Electron Transfer Properties in P3HT/SWNT Hybrid Materials. *Adv Funct Mater* 2008;18(18):2659-65.
- [58] McCarthy B, Coleman JN, Czerw R, Dalton AB, in het Panhuis M, Maiti A, et al. A Microscopic and Spectroscopic Study of Interactions between Carbon Nanotubes and a Conjugated Polymer. *J Phys Chem B* 2002;106(9):2210-6.
- [59] Dalton AB, Stephan C, Coleman JN, McCarthy B, Ajayan PM, Lefrant S, et al. Selective Interaction of a Semiconjugated Organic Polymer with Single-Wall Nanotubes. *J Phys Chem B* 2000;104(43):10012-6.
- [60] Coleman JN, Dalton AB, Curran S, Rubio A, Davey AP, Drury A, et al. Phase Separation of Carbon Nanotubes and Turbostratic Graphite Using a Functional Organic Polymer. *Adv Mater* 2000;12(3):213-6.
- [61] Solhy A, Machado BF, Beausoleil J, Kihn Y, Gonçalves F, Pereira MFR, et al. MWCNT activation and its influence on the catalytic performance of Pt/MWCNT catalysts for selective hydrogenation. *Carbon* 2008;46(9):1194-207.

- [62] Green MD, Salas-de la Cruz D, Ye Y, Layman JM, Elabd YA, Winey KI, et al. Alkyl-Substituted N-Vinylimidazolium Polymerized Ionic Liquids: Thermal Properties and Ionic Conductivities. *Macromol Chem Phys* 2011;212(23):2522-8.
- [63] Grady BP. Effects of carbon nanotubes on polymer physics. *J Polym Sci, Part B: Polym Phys* 2012;50(9):591-623.
- [64] Furtado CA, Kim UJ, Gutierrez HR, Pan L, Dickey EC, Eklund PC. Debundling and Dissolution of Single-Walled Carbon Nanotubes in Amide Solvents. *J Am Chem Soc* 2004;126(19):6095-105.
- [65] Hong S, Tung T, Huyen Trang L, Kim T, Suh K. Preparation of single-walled carbon nanotube (SWNT) gel composites using poly(ionic liquids). *Colloid Polym Sci* 2010;288(9):1013-8.
- [66] Marcilla R, Alberto Blazquez J, Rodriguez J, Pomposo JA, Mecerreyes D. Tuning the solubility of polymerized ionic liquids by simple anion-exchange reactions. *J Polym Sci, Part A: Polym Chem* 2004;42(1):208-12.
- [67] Jia Z, Wang Z, Xu C, Liang J, Wei B, Wu D, et al. Study on poly(methyl methacrylate)/carbon nanotube composites. *Mater Sci Eng, A* 1999;271(1-2):395-400.
- [68] Tang BZ, Xu H. Preparation, Alignment, and Optical Properties of Soluble Poly(phenylacetylene)-Wrapped Carbon Nanotubes†. *Macromolecules* 2001;32(8):256-76.
- [69] Wang Y, Wu J, Wei F. A treatment method to give separated multi-walled carbon nanotubes with high purity, high crystallization and a large aspect ratio. *Carbon* 2003;41(15):2939-48.
- [70] Fukushima T, Aida T. Ionic Liquids for Soft Functional Materials with Carbon Nanotubes. *Chem Asian J* 2007;13(18):5048-58.

[71] Gao C, Jin YZ, Kong H, Whitby RLD, Acquah SFA, Chen GY, et al. Polyurea-Functionalized Multiwalled Carbon Nanotubes: Synthesis, Morphology, and Raman Spectroscopy. *J Phys Chem B* 2005;109(24):11925-32.

Chapter III:

Polymerized ionic liquid functionalized carbon nanotube/polyetherimide composites

Chapter III: Polymerized ionic liquid functionalized carbon nanotube/polyetherimide composites

III.1 Introduction

The thin PIL layer adsorbed on the surface of CNTs can provide stable binding sites for polymer matrices to attach. The number of studies reported on polymer composites filled with PIL-functionalized CNTs is very limited [1, 2]. They have been shortly described in the section I.2.2.4 in Chapter I. It would be appropriate to say that the potential of PIL functionalized CNTs has not yet been fully explored in polymer composites.

Polyetherimide (PEI) is a high-performance thermoplastic, which has extensive uses in many fields such as medical, electronic, microwave, automotive and aerospace [3]. By adding CNTs into the PEI matrix, it is expected to obtain unique properties in the newly formed composite. From an industrial point of view, melt-processing is the most suitable method for high-volume production of polymer composites. However, the extremely high viscosity and high processing temperature of this polymer makes the nanocomposite preparation by melt-processing challenging. Ultrasound assisted twin screw extrusion has been studied to help the dispersion of CNTs [4]; yet, the improvement obtained by ultrasonication is not significant compared to the unsonicated samples prepared at the same loading. Solution-based processing methods offer advantages of lower viscosities, which facilitate dispersion, provided that highly stable dispersions of CNTs are used. Combining solution casting and melt-mixing in two steps can also enhance the dispersion of CNTs in the matrix. The number of studies carried-out on the preparation of PEI composites filled with CNTs is limited [3–8]. Table III.1 summarizes the relevant studies that have been reported up to now.

Table III.1 Mechanical and thermal properties of CNT-based polyetherimide composites.

CNT type	Additive	CNT loading (wt %)	Processing method	Composite tensile strength (% increase)	Composite Young modulus (% increase)	Composite storage modulus (% increase)	T_g (°C increase)	Thermal degradation (°C increase)	Ref.
Oxidized MWCNTs	–	0.5	Solution mixing in DCM-melt mixing	–	–	10	2	24	[3]
Oxidized MWCNTs	–	0.5	Solution mixing in DMF-melt mixing	–	–	13	6	33	[3]
Oxidized MWCNTs	–	7	Solution mixing	–	–	54	10	106	[5]
Pristine MWCNTs	–	1	Ball milling-ultrasound assisted twin screw extrusion	–2	7	–	–	–	[4]
Pristine MWCNTs	–	10	Ball milling-ultrasound assisted twin screw extrusion	13	62	–	–	–	[4]
Pristine MWCNTs	Triton X100	1	Solution mixing	13	–	–	–	9	[6]
Pristine MWCNTs	CTAB	1	Solution mixing	7	–	–	–	9	[6]
Pristine MWCNTs	SDS	1	Solution mixing	–10	–	–	–	7	[6]
Oxidized MWCNTs	–	1	Solution mixing-Thermal curing (imidization)	2	39	146	9	–	[8]
Oxidized MWCNTs (6 h)	–	1	Solution mixing	6	–	–	4	–	[7]
Oxidized MWCNTs (3 h)	–	1	Solution mixing	–12	–	–	–	–	[7]

DCM: Dichloromethane, DMF: Dimethylformamide, Triton X100: polyoxyethylene octyl phenyl ether, CTAB: cetyl trimethyl ammonium chloride, SDS: sodium dodecyl chloride

Different surface modification approaches, including acid-oxidation and use of ionic or nonionic surfactants, have been applied to CNTs in order to obtain stable dispersions in suitable solvents for PEI processing. It has been also found that the type of solvent used in the solution casting step has influence on the final properties of the composite due to the dispersion state of the CNTs [3]. From the data given in Table 1, the most remarkable mechanical improvement has been observed in the storage modulus of the polyetherimide composite *in situ* cured in the presence of oxidized MWCNTs. However, the tensile strength did not change and the polymer film became very brittle at 1 wt.% CNT loading compared to neat PEI. It is seen from these studies that thermal stabilities of the PEI composites improved generally significantly, whereas improvements in mechanical properties are not usually remarkable and require high CNT loading. In some cases [6, 7], negative effects of CNT addition on mechanical properties have been observed.

This chapter deals with the preparation of PEI composites loaded with PIL-functionalized CNTs; to be more precise, MWCNTs non-covalently functionalized with poly(1-vinyl-3-ethyl imidazolium) dodecylbenzene sulfonate (poly[VEIM]DBS). PEI composite films with pristine and oxidized MWCNTs have also been studied for comparison. The effect of the introduction of the above mentioned types of CNTs on the morphological, mechanical, thermal and electrical properties of PEI matrix will be presented.

III.2 Results and discussion

III.2.1. Functionalization of MWCNTs with PIL

We anticipated that coating a thin film of PIL on the nanotube surface could result in a better adhesion between CNT and PEI matrix. PEI, which is a highly solvent resistant polymer, is soluble in halogenated solvents such as chloroform, DCM, and in *N*-Methyl-2-pyrrolidone

(NMP). DCM was chosen as the processing solvent due to its low boiling point and relatively lower toxicity compared to NMP. This requires that the PIL used to modify the CNT surface is also soluble in DCM. As we already mentioned, the nature of the counter-anion greatly influences the final properties of PILs, such as solubility, viscosity and thermal stability. Table III.2 lists the solubility of poly[VEIM]⁺X⁻ with various counter-anions in DCM determined by a literature research [9]. Dodecylbenzene sulfonate (DBS⁻, C₁₂H₂₅C₆H₄S₃⁻), was chosen as the counter-anion of the PIL because of its much higher thermal stability compared to bis(2-ethylhexyl)phosphate (C₁₆H₃₄P₄⁻). Furthermore, due to the aromatic ring in the structure of the DBS⁻ anion, the corresponding PIL may have enhanced interactions with the PEI matrix as illustrated in Figure III.1.

Table III.2 Solubility of poly[VEIM]⁺X⁻ in DCM.

Counter anion (X ⁻)	Solubility
Br ⁻ /Cl ⁻	-
PF ₆ ⁻	-
CF ₃ S ₃ ⁻	-
(CF ₃ S ₂) ₂ N ⁻	-
(CF ₃ CF ₂ S ₂) ₂ N ⁻	-
C ₁₂ H ₂₅ C ₆ H ₄ S ₃ ⁻	+
CH ₃ C ₆ H ₄ S ₃ ⁻	-
C ₁₆ H ₃₄ P ₄ ⁻	+

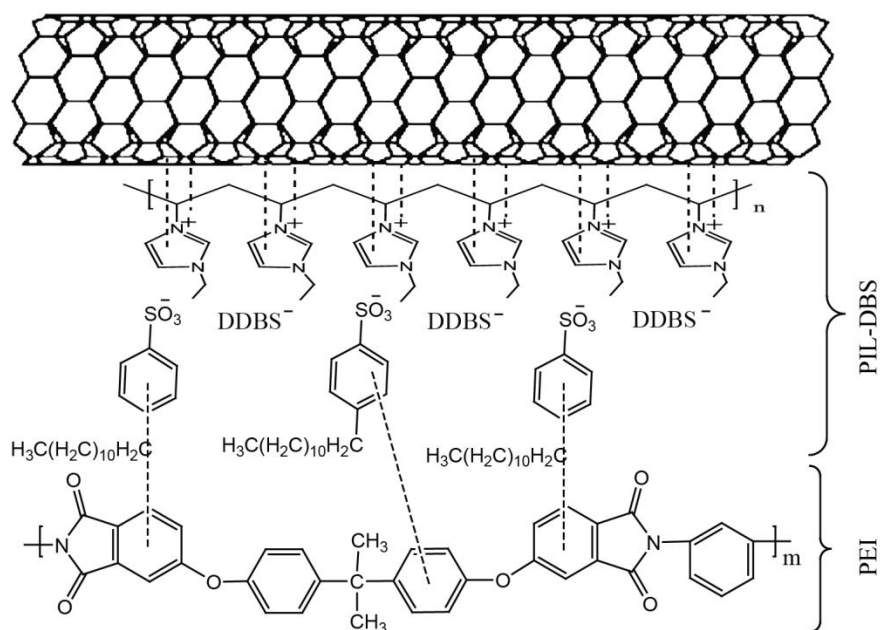


Figure III.1. Illustration of poly[VEIM]DBS linking CNT and PEI by possible non-covalent interactions.

We showed in Chapter II that carrying out the anion-exchange reaction into the CNTs functionalized with polycations containing halide anions is the best way to obtain PIL functionalized CNTs bearing bulky anions. Furthermore, *in situ* polymerization should ensure a better coating of PIL on the CNT surface. Therefore, we followed this procedure and first prepared CNT–poly[VEIM]Br using the *in situ* method. Neat poly[VEIM]DBS was synthesized carrying-out the anion-exchange reaction directly into the neat poly[VEIM]Br precursor, which was polymerized in the presence of CNTs for 24 hours. The glass transition temperatures (T_g) of poly[VEIM]Br and poly[VEIM]DBS were found to be 229 °C and 114 °C, respectively, as determined by DSC (20 °C min⁻¹). This result is in agreement with the general rule, larger anions gives lower T_g values compared to small anions due to weaker ionic interactions. In the ¹H NMR spectrum corresponding to the poly[VEIM]DBS, in addition to the polycation protons, further signals of the organic anion are observed (Figure III.2). Aromatic protons of the anion show two signals at 7.7 and 7.1 ppm, while the signals at 0.7 and 1.5 ppm are assigned to the aliphatic protons.

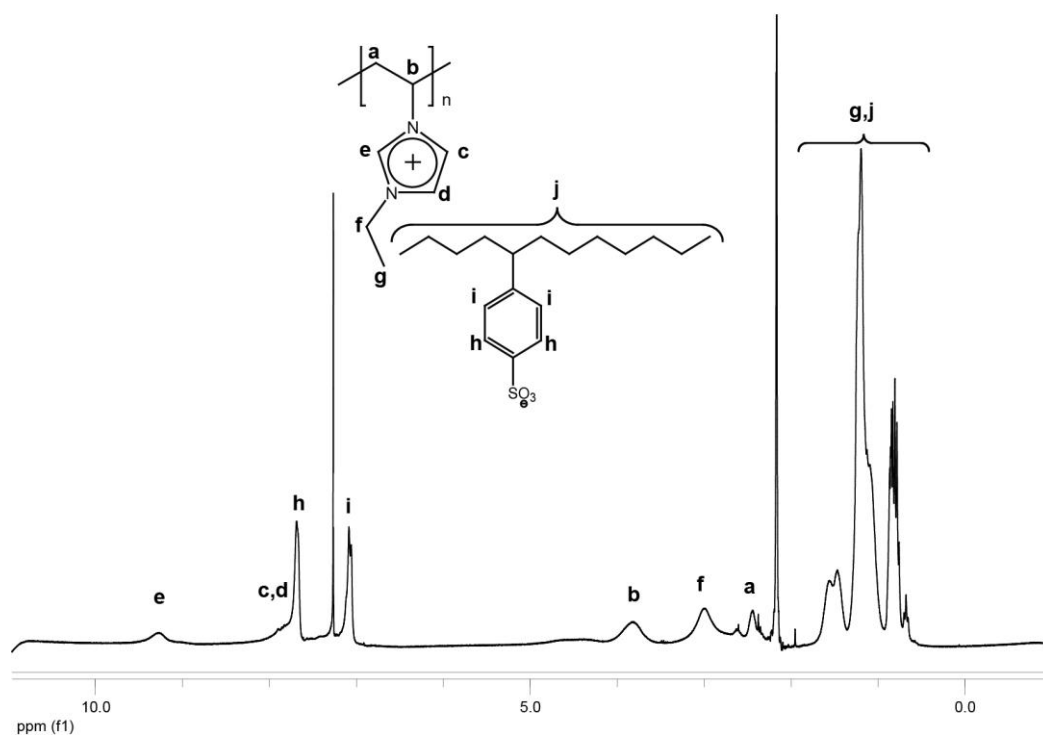


Figure III.2. 300-MHz ^1H NMR spectra of (a) poly[VEIM]DBS in CDCl_3 .

In the next step, the similar anion-exchange process was applied to the CNT–poly[VEIM]Br (Figure III.3).

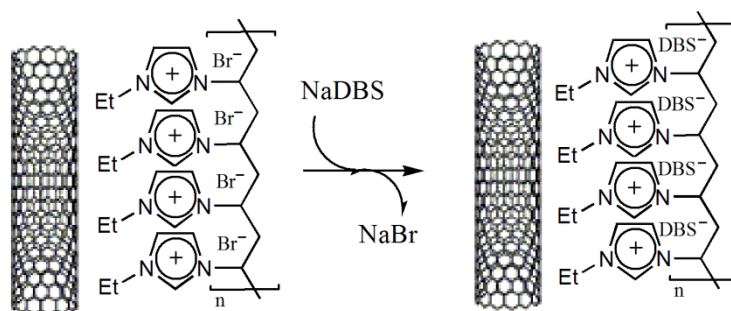


Figure III.3. Counter-anion exchange reaction of CNT–poly[VEIM]Br.

To verify the anion-exchange reaction, TGA measurements were performed for the initial and final CNT–PIL hybrids. CNT–poly[VEIM]Br contains 11.5 wt.% of PIL while after anion-exchange, the amount becomes 19 wt.% due to the higher molecular weight of the DBS^- anion (Figure III.4). This amount slightly less than the theoretical one (24 wt.%) in the

case of complete anion-exchange. All samples decomposed in two major steps under inert atmosphere. Table III.3 shows the decomposition temperatures of the neat PILs and functionalized CNTs. In agreement with the study presented in Chapter II, the adsorbed PILs start to degrade at a lower temperature compared to the neat PILs.

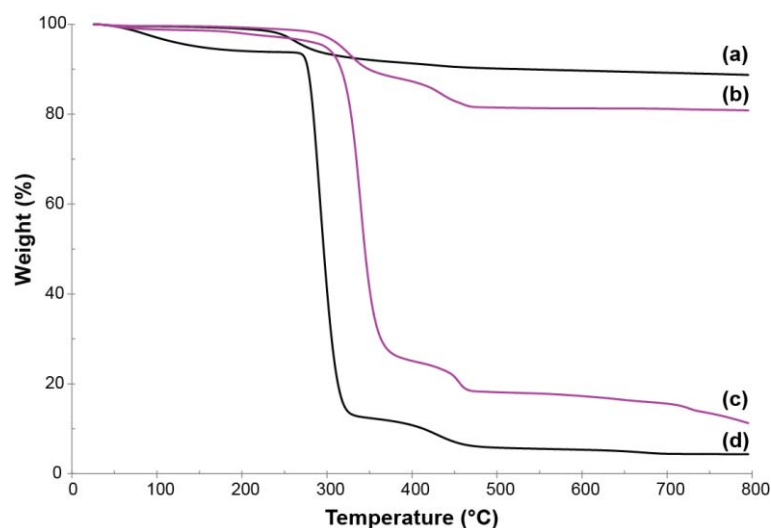


Figure III.4. TGA curves of (a) CNT–poly[VEIM]Br, (b) CNT–poly[VEIM]DBS, (c) poly[VEIM]DBS and (d) poly[VEIM]Br under nitrogen flow.

Table III.3. Decomposition temperatures of PILs and PIL functionalized CNTs.

Sample	T_d (°C)	
Poly[VEIM]Br	289	431
CNT–poly[VEIM]Br	262	431
Poly[VEIM]DBS	337	451
CNT–poly[VEIM]DBS	325	434

The successful anion-exchange can also be confirmed by IR spectroscopy. The IR spectra of both PIL functionalized CNTs show the bands attributed to the poly[VEIM]⁺ cation in the region 2800–3200 cm⁻¹ and at 1550 cm⁻¹. In the spectrum of CNT–poly[VEIM]DBS, the

characteristic bands of the $C_{12}H_{25}C_6H_4SO_3^-$ anion [10], S=O asymmetrical stretching band at 1193 cm^{-1} , CH aromatic bending bands at 830 cm^{-1} , 1010 cm^{-1} and 1026 cm^{-1} are clearly observed (Figure III.5).

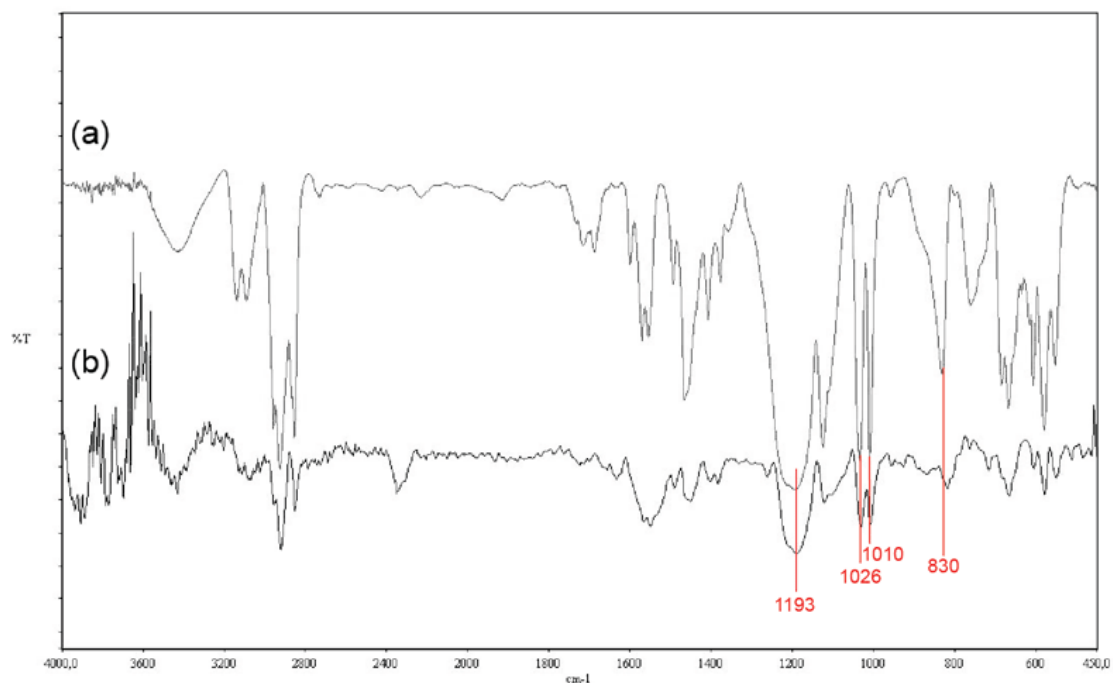


Figure III.5. FTIR spectra of (a) poly[VEIM]DBS (b) CNT– poly[VEIM]DBS.

The thin PIL layer non-covalently attached to the surface of the CNTs can be observed by TEM analysis (Figure III.6). The TEM image in Figure III.6 shows the presence of a continuous thin polymer layer up to 1.7 nm around the CNT.

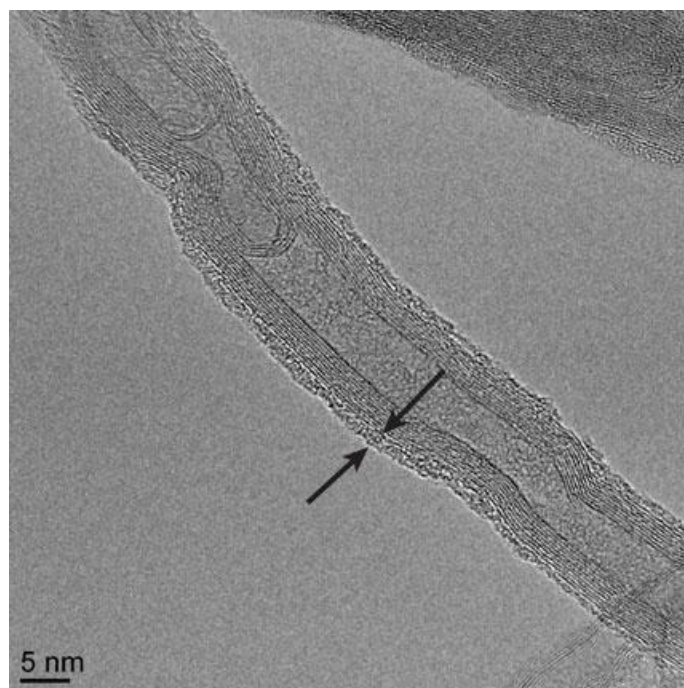


Figure III.6. TEM micrograph of CNT-poly([VEIM]DBS).

After sonication in DCM for half-an-hour, a black suspension was observed for the three types of CNTs (pristine, oxidized and PIL functionalized) (Figure III.7). However, we observed with the naked eye that the dispersions of pristine and oxidized CNTs contained large agglomerates while the suspension of PIL functionalized CNTs dispersed better. After standing for one week, the dispersion state of the CNTs were in the order CNT-PIL > pristine CNTs > oxidized CNTs. The laser granulometry measurements confirmed that the dispersions of both pristine and oxidized CNTs in DCM were unstable. The volume weighted mean diameter (D [4,3]) values of three measurements ranged from 27.9 to 53.2 μm and from 13.3 to 34.8 μm for pristine CNTs and oxidized CNTs, respectively. On the contrary, CNT-PIL gave very stable dispersions in DCM with an average particle diameter of 13.0 μm (± 0.2), and as seen from the particle size distribution graphs in Figure III.8, the number of small particles below 0.5 μm was higher in this sample.

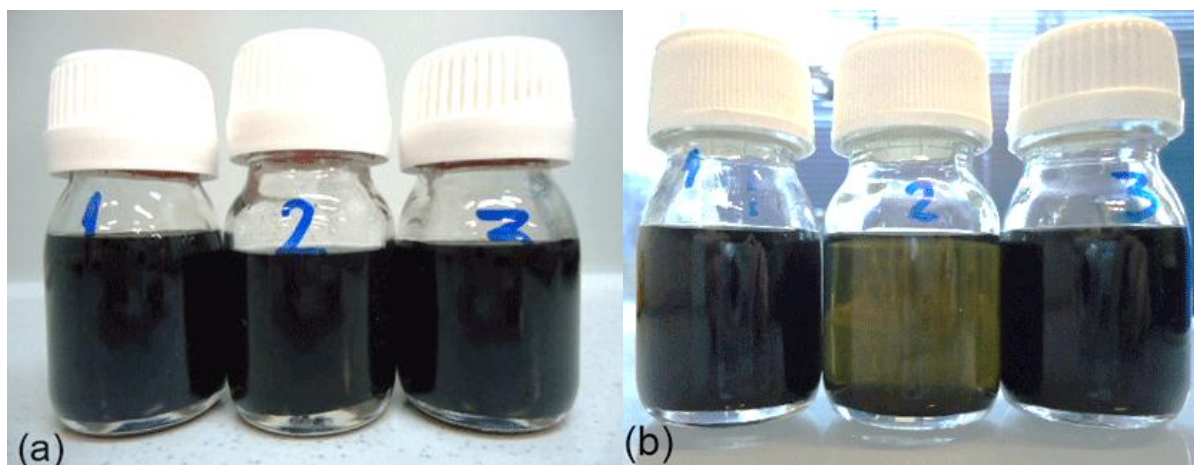


Figure III.7. Dispersions of CNTs (1 g L^{-1}) (from left to right: pristine CNTs, oxidized CNTs and CNT-PIL) in DCM: (a) just after sonication and (b) upon standing for one week.

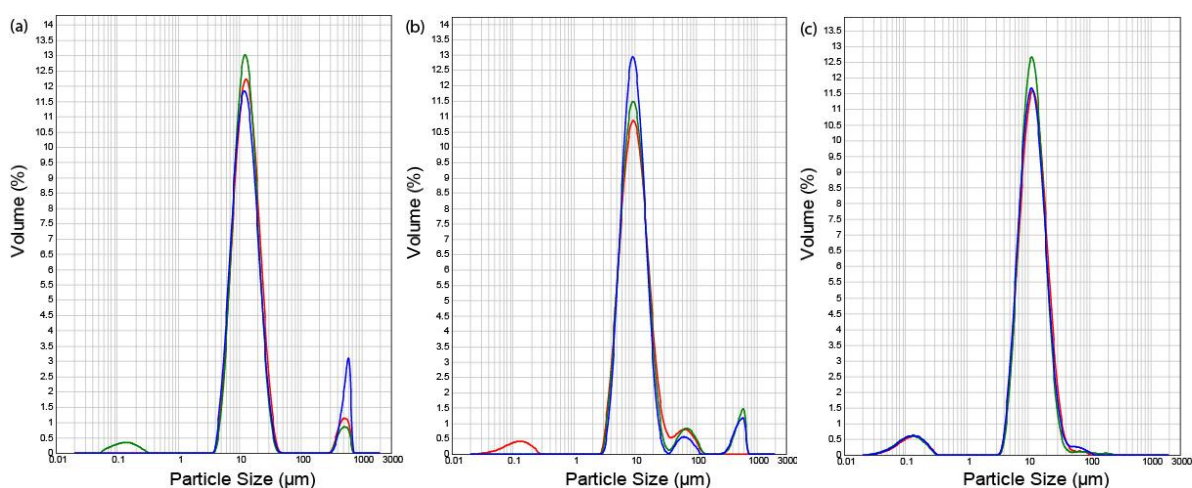


Figure III.8. Particle size distribution graphs of CNT dispersions in DCM (superposition of 3 measurements), (a) pristine CNTs, (b) oxidized CNTs and (c) CNT-PIL.

III.2.2. Incorporation of CNTs into the polymer matrix

We prepared a series of PEI/CNT films by using the procedure summarized in Figure III.9.

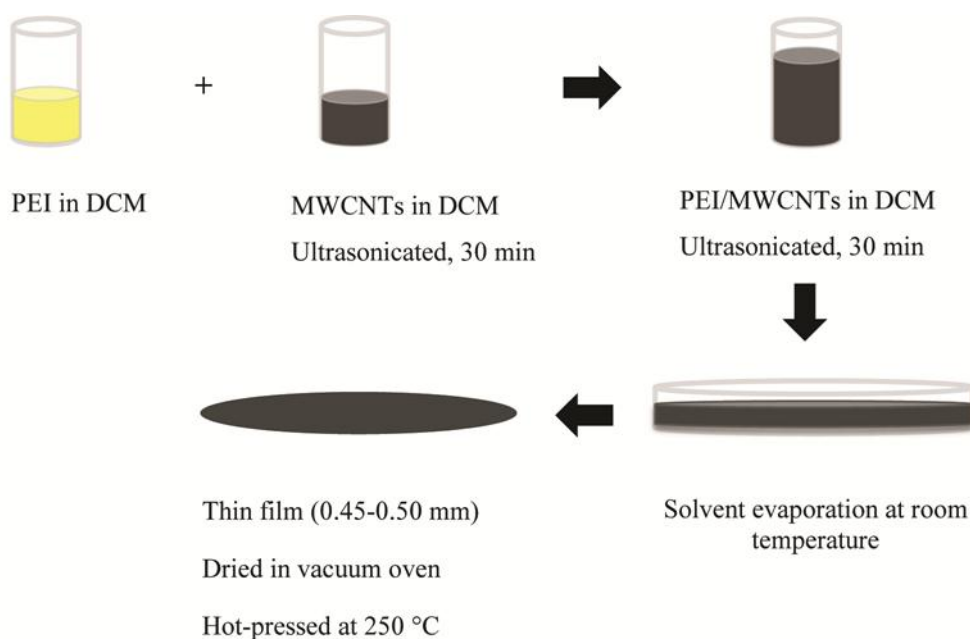


Figure III.9. Procedure for processing PEI/CNT composite films.

Briefly, the given amount of PEI dissolved in DCM and the CNTs were separately dispersed in DCM under horn-type ultrasonication at a low amplitude (20%) for 30 min. Then, both the PEI solution and the CNT dispersion were mixed by horn-type ultrasonication for another 30 min. Thin films were obtained by casting the mixture into molds and evaporating the solvent slowly at room temperature. All the composite films were further dried in a vacuum oven. The drying process is particularly important, as any residual solvent remained trapped within the polymer film decreases the glass transition temperature of PEI and furthermore, causes the film to lose its transparency and to deform seriously at temperatures higher than 150 °C. It was found that the residual solvent can be completely removed by drying the films first at 100 °C for two days, and then at 150 °C for one day under vacuum. The obtained composites were compression molded under a pressure of 240 bars at 250 °C for 4 min. The CNT content in the final composites varied from 0.1 wt.% to 3 wt.%. For comparison, a neat PEI film and composite films with pristine and oxidized MWCNTs without PIL functionalization were prepared following the same procedure described above.

The ATR–FTIR spectra of the composites prepared with the three types of CNTs at 0.1 wt.% loading are the same as the spectrum of the neat PEI (Figure III.10). We observed the characteristic carbonyl bands of imide at 1777 cm^{-1} and 1716 cm^{-1} and the C-N stretching band at 1350 cm^{-1} . This shows that addition of CNTs at 0.1 wt.% loading does not have any influence on the IR absorption of the polymeric matrix.

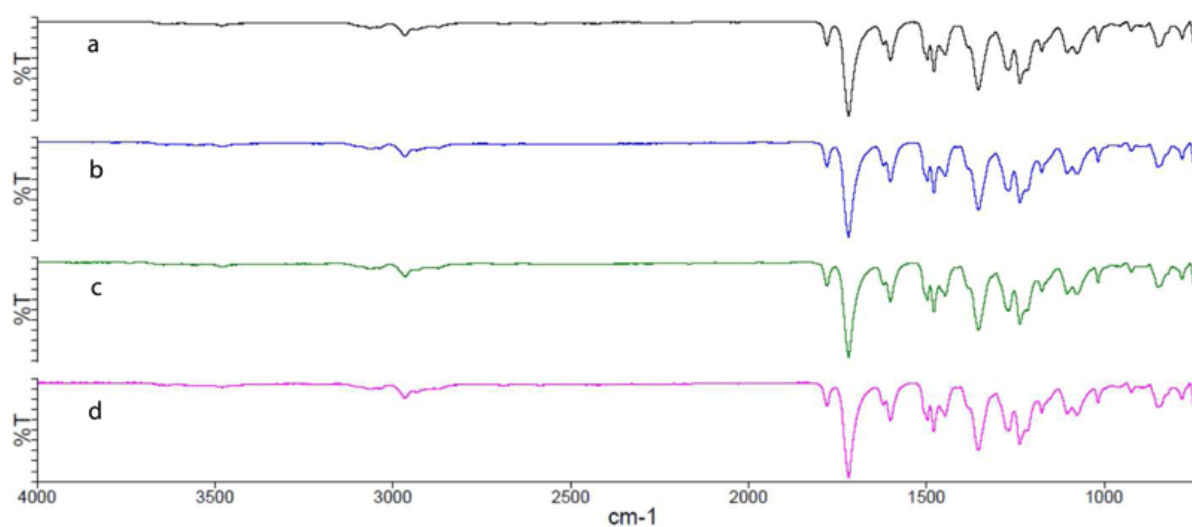


Figure III.10. ATR-FTIR spectra of (a) neat PEI, (b) PEI/pristine CNTs (0.1 wt.%), (c) PEI/CNT–COOH (0.1 wt.%), (d) PEI/CNT–PIL (0.1 wt.%).

The dispersion state and the morphology of the resulting PEI/CNT composite films were characterized by TEM. The TEM micrographs in Figure III.11 show the CNT distribution in the polymer matrix at 1 wt.% CNT loading. While all the samples contain agglomerated CNTs, more individual CNTs are present in the samples containing modified CNTs.

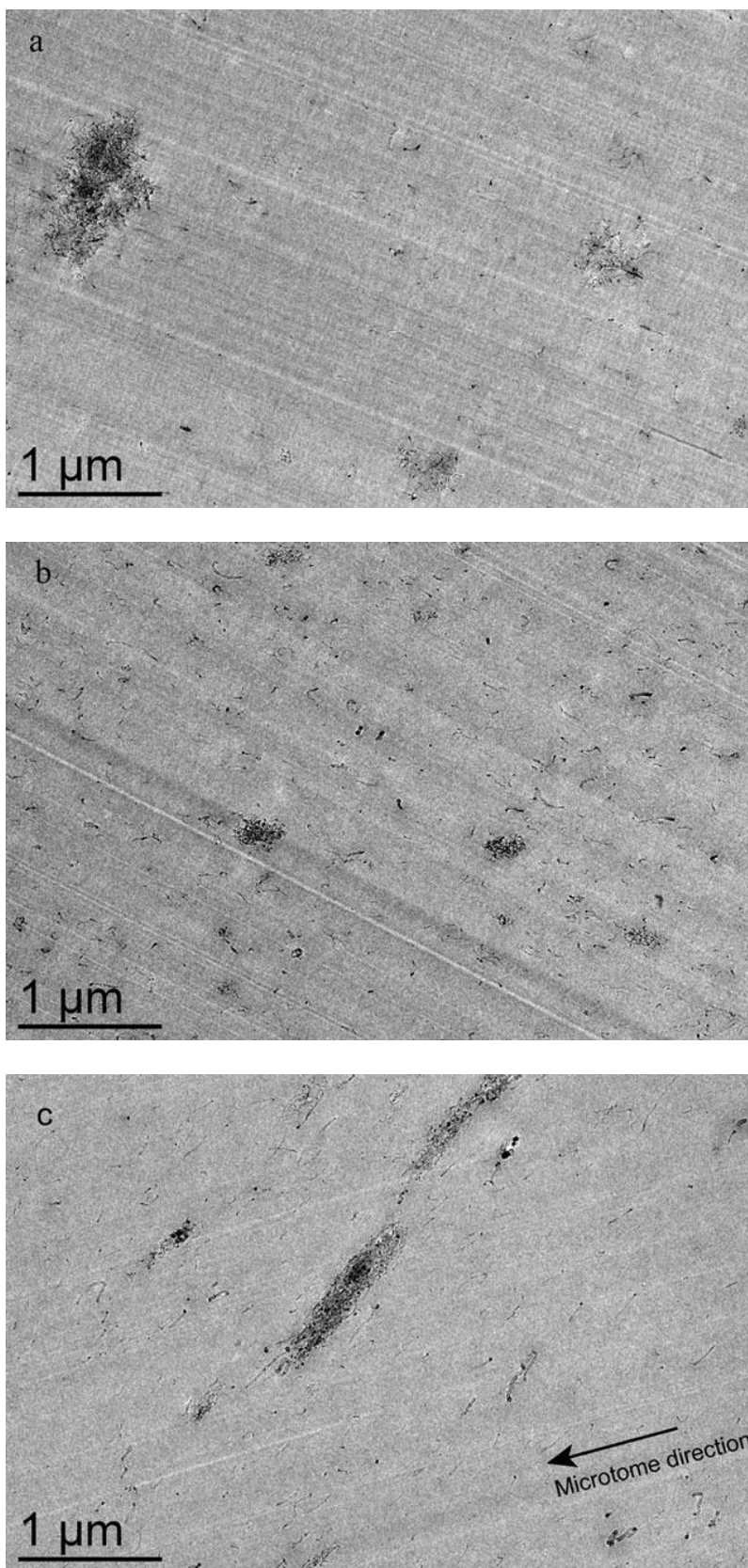


Figure III.11. TEM micrographs of PEI/CNT composite films at 1 wt.% loading of (a) pristine CNTs, (b) oxidized CNTs and (c) CNT-PIL.

Moreover, TEM analysis reveals an interesting feature on the morphology of the PEI/CNT–PIL composite. In Figure III.11 (c), it is observed that the CNTs are aligned. The direction of the cutting traces of the diamond knife is indicated with an arrow. Clearly, the diamond knife did not align the CNTs during the TEM specimen preparation. The alignment of CNTs in polymer matrix is usually induced by an applied field such as force-, electric- or magnetic-field, but self-organizing alignment of CNTs in a thermoplastic polymer arising from solvent-polymer interactions has also been reported [11].

III.2.3. Mechanical, thermal and electrical properties of the composites

As for most materials, a simple tensile stress–strain curve provides a good start towards understanding the mechanical behaviour of a particular polymer. This curve is usually established by continuously measuring the force developed as the sample is elongated at a constant rate of extension until it breaks. The data obtained from the tensile tests describes many mechanical features of the polymer. The stress–strain behaviour of a thermoplastic polymer is characterized by a linear elastic region, a yielding followed by a drop in stress, a formation of a neck, an increase in stress due to straightening of polymer chain, and finally fracture. Figure III.12 below shows a typical stress–strain curve for a thermoplastic polymer, and Table III.4 describes the features of a stress–strain curve.

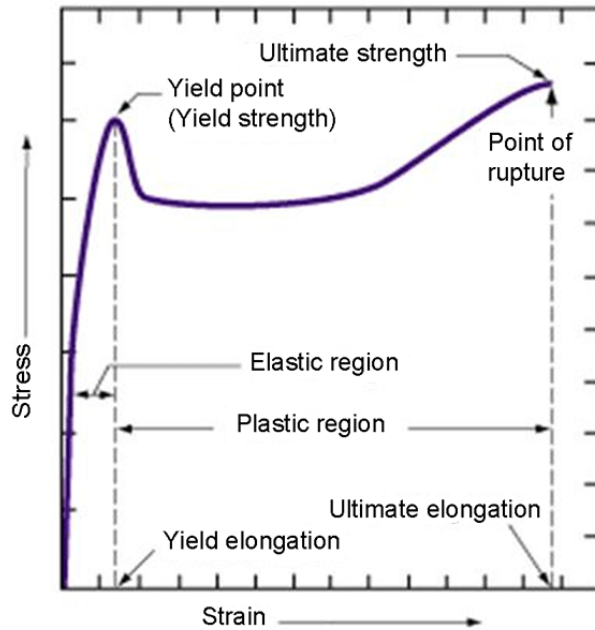


Figure III.12. Typical stress–strain curve of a thermoplastic polymer.

Table III.4. Definition of terms on a stress–strain curve.

Term	Definition
Yield Point (strength)	Yield point is a measure of the strength of the material and of its resistance to permanent deformation. It is the first point at which the specimen yields. This is when the specimen's cross-sectional area begins to decrease. This is called necking.
Modulus of Elasticity (Young's modulus)	The ratio of stress to strain within the elastic region of the stress-strain curve. It is a measure of stiffness.
Yield Elongation	The strain at the yield point
Elastic Region	The portion of the curve before the yield point
Plastic Region	The portion of the curve after the yield point
Ultimate (tensile) strength	Ultimate tensile strength is the maximum stress a material can withstand before failing.

Tensile tests were carried out on neat PEI and CNT loaded PEI composite films using dog-bone specimens (Figure III.13 (a) and (b)). The results in terms of Young's modulus, yield stress and strain of the films, corresponding to an average of at least five samples tested for each type of film, are reported in Table III.5. Each result is averaged from at least five experimental results. Figure III.13 (c) shows typical tensile stress–strain curves obtained for the films. By introduction of CNTs, no major reinforcement was obtained in the tensile properties of the composites. When loaded in excess of 1 wt.% CNT, the films became very brittle. The high brittleness of the composites at a loading of 3 wt.% of oxidized CNTs or CNT–PIL did not allow any sampling.

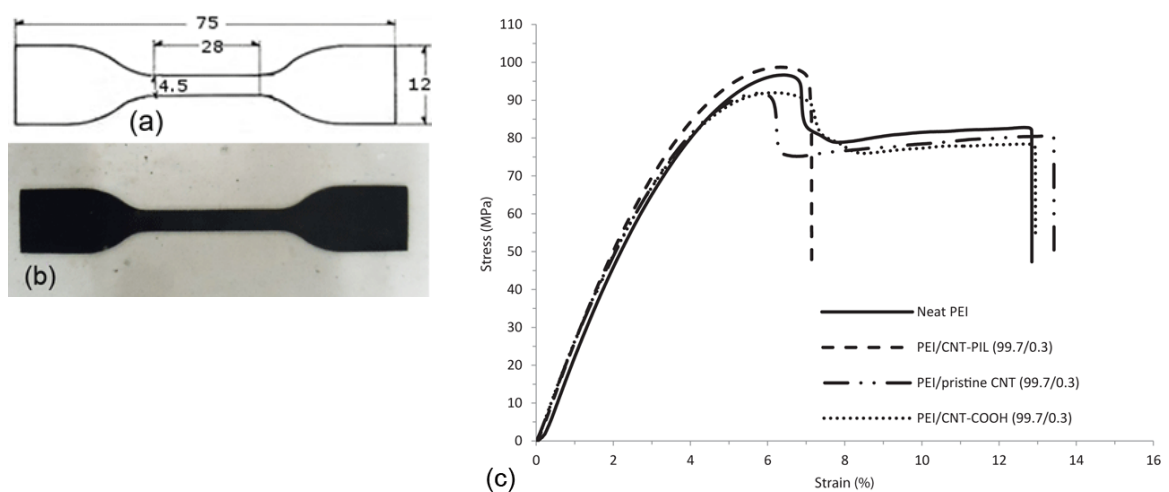


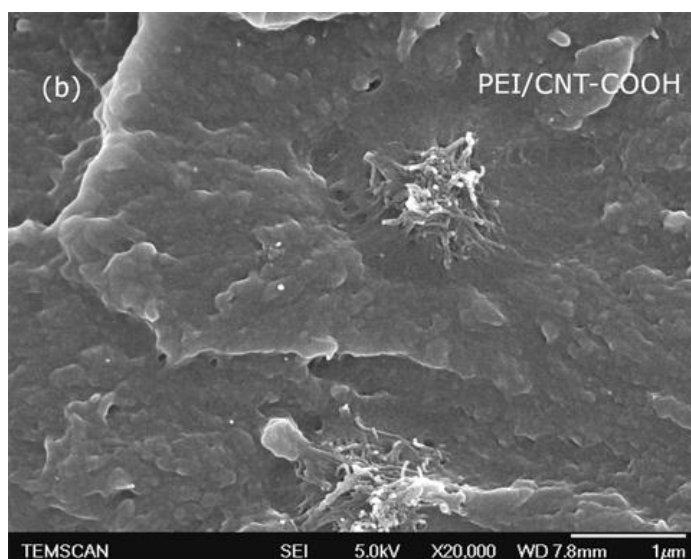
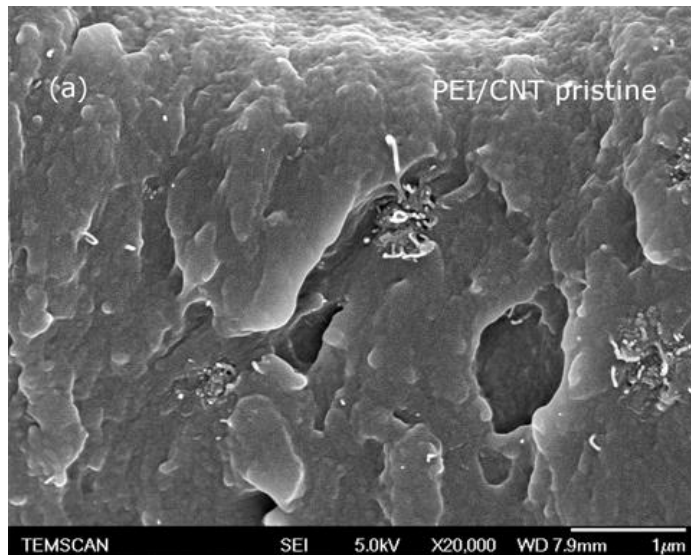
Figure III.13. (a) The dimensions of the dog-bone specimen used (in mm), (b) A typical dog-bone PEI/CNT composite prepared (at 1 wt.% loading), (c) Typical tensile stress–strain curves of neat PEI and PEI/CNT composites at 0.3 wt.% of CNT.

Table III.5. Tensile properties of neat PEI and PEI/CNT composites.

Material	CNT loading (wt.%)	Young's modulus (GPa)	Yield stress (MPa)	Yield strain (%)	Stress at break (MPa)	Strain at break (%)
Neat PEI	0	2.69 ± 0.05	95.0 ± 2.7	6.2 ± 0.5	79.5 ± 2.8	10.0 ± 3.9
	0.1	2.69 ± 0.12	94.6 ± 3.1	6.1 ± 0.4	79.5 ± 3.8	13.6 ± 5.0
PEI/pristine CNTs	0.3	2.69 ± 0.02	93.2 ± 1.2	6.1 ± 0.3	79.1 ± 3.0	12.9 ± 6.3
	0.6	2.62 ± 0.12	93.9 ± 1.7	6.4 ± 0.3	79.5 ± 5.9	13.7 ± 7.4
	1	2.71 ± 0.05	92.1 ± 1.4	6.1 ± 0.2	77.9 ± 3.5	9.7 ± 2.2
	3	2.76 ± 0.05	92.5 ± 6.2	5.5 ± 0.9	84.2 ± 5.4	6.2 ± 1.7
	0.1	2.63 ± 0.04	93.4 ± 2.4	6.1 ± 0.5	86.8 ± 6.0	8.4 ± 4.6
PEI/oxidized CNTs	0.3	2.67 ± 0.08	92.3 ± 1.2	5.9 ± 0.3	79.1 ± 2.4	10.3 ± 5.0
	0.6	2.64 ± 0.05	93.2 ± 1.7	6.3 ± 0.1	77.1 ± 1.0	15.7 ± 6.7
	1	2.64 ± 0.08	92.3 ± 2.5	6.0 ± 0.4	79.7 ± 7.3	7.8 ± 1.9
PEI/CNT–PIL	0.1	2.65 ± 0.06	92.5 ± 1.9	6.1 ± 0.1	78.7 ± 2.5	14.4 ± 6.3
	0.2	2.63 ± 0.07	94.9 ± 2.6	6.3 ± 0.1	83.8 ± 6.0	13.6 ± 9.2
	0.3	2.75 ± 0.08	96.1 ± 3.3	6.2 ± 0.1	83.5 ± 9.5	7.8 ± 1.6
	0.4	2.72 ± 0.06	95.1 ± 1.8	6.0 ± 0.4	84.5 ± 7.4	7.8 ± 2.7
	0.6	2.62 ± 0.09	94.7 ± 3.2	6.2 ± 0.4	82.9 ± 6.1	11.6 ± 5.0
	1	2.56 ± 0.04	90.0 ± 2.9	5.5 ± 0.7	84.8 ± 7.0	6.1 ± 1.4

SEM was used to observe the morphology of the failure surfaces of the composites after tensile testing. Micrographs obtained from the fractured surfaces of all three composite films show agglomerates of CNTs being pulled half way out from the matrix (Figure III.14). These

agglomerates act as stress concentration sites and prevent a homogeneous stress distribution in the matrix.



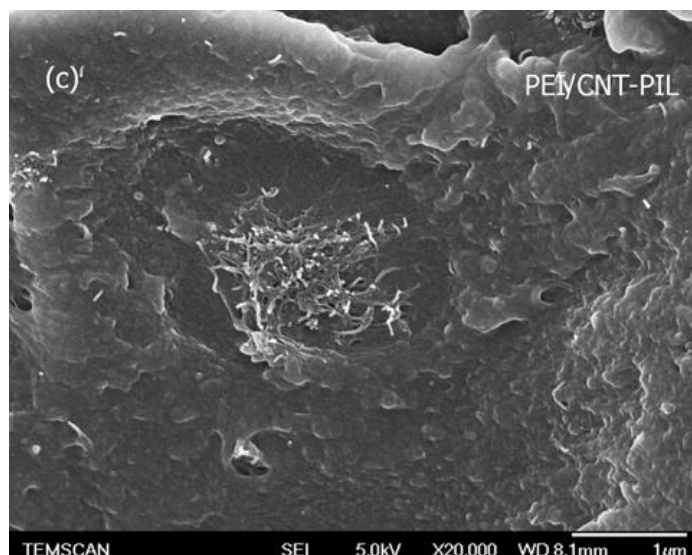
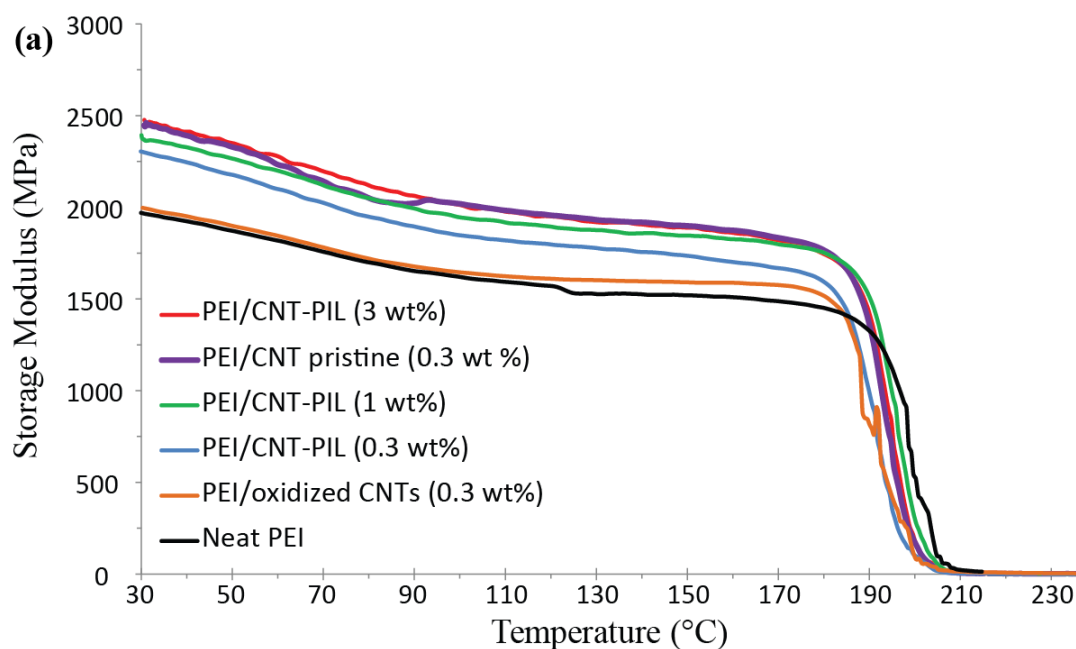


Figure III.14. SEM micrographs of the failure surfaces of PEI and PEI/CNTs composites at 1 wt % loading of: (a) pristine CNT, (b) oxidized CNT (CNT–COOH) and (c) CNT–PIL.

Dynamic mechanical analysis (DMA) is a thermal analysis technique that measures the properties of materials as they are deformed under periodic stress. The dynamic properties provide information at the molecular level to understanding the polymer mechanical behavior. The storage modulus describes the ability of the material to store potential energy and release it upon deformation. It is often associated with the stiffness of a material and is related to the Young's modulus. The loss modulus is indicative of the energy loss due to the friction of polymer chain movement. The ratio of loss modulus to storage modulus is called $\tan \delta$ (tan delta), whose peak is an indication of a glass transition. Figure III.14 displays the dynamic mechanical spectra (storage modulus and $\tan \delta$) as a function of temperature for PEI and PEI/CNT composites. The storage modulus (E') of the composites containing CNT–PIL is higher than that of neat PEI in the temperature range of 30–190 °C. There is no significant difference in storage modulus between different loadings (0.3 and 3 wt.%). At a loading of 3 wt.%, an improvement of around 25% in storage modulus was obtained. However, a similar increase was also obtained in the case of pristine CNTs. $\tan \delta$ (damping) is also a measure of

how well the material can disperse energy. The damping peaks of all the PEI/CNT composites showed a decrease in maximum peak height, from 2.02 for pure PEI to 1.29 for PEI/CNT–PIL composite at 0.3 wt.% loading. The height of the damping peaks reveals the efficiency of the stress transfer to the CNTs, which depends on the CNT/matrix adhesion. CNTs carry a greater proportion of the stress and allow only a small part of it to strain the interface. Therefore, a stronger interface is characterized with lower energy dissipation [3, 12]. According to this, dispersion and interfacial stress transfer is the highest for PEI/CNT–PIL composite at 0.3 wt.% loading.

DMA is known to be a sensitive tool for the determination of glass transition temperature (T_g). The temperature corresponding to the maxima of a $\tan \delta$ peak is associated with T_g . As observed from the $\tan \delta$ versus temperature graphs in Figure III.15 (b), the T_g of the neat PEI appeared at approximately 209 °C, while the T_g of the PEI/CNT composites shifted to a lower temperature by around 5 °C. This decrease is likely due to the increased mobility of the polymer chains because of the free space around CNT agglomerates in the polymer matrix.



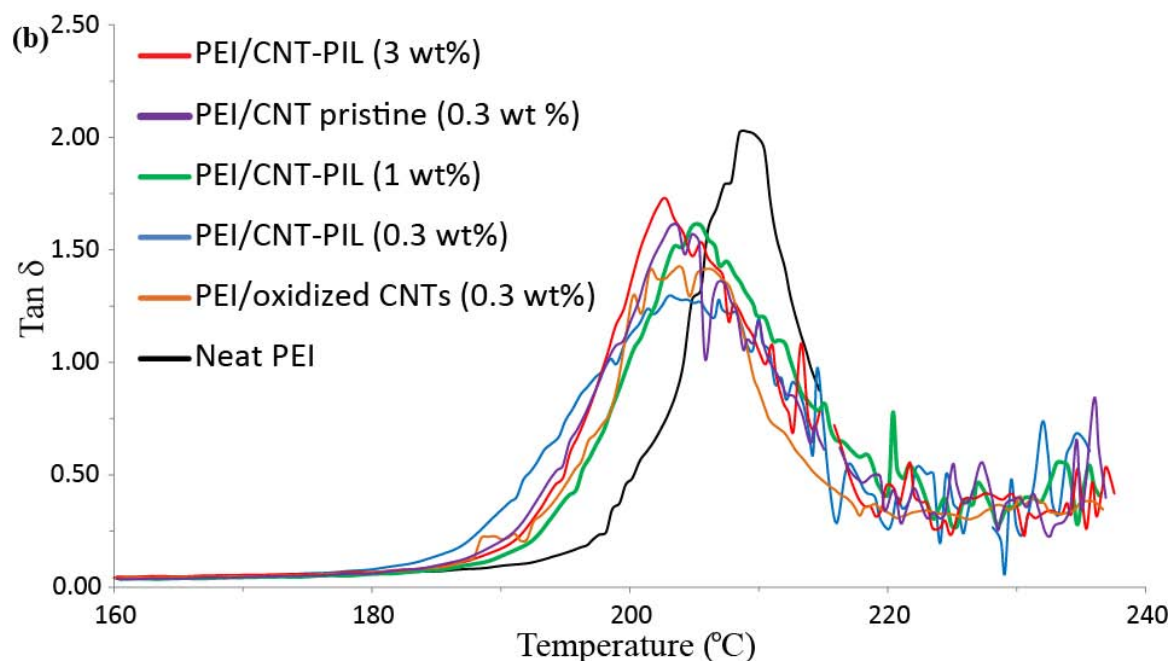


Figure III.15. DMA curves of (a) storage modulus and (b) $\tan \delta$ versus temperature for PEI and PEI/CNT composites.

To investigate the thermal behavior of the neat PEI films and the PEI/CNTs films, TGA and DSC analysis were carried out. Degradation temperatures (T_d) were measured at 5% weight loss. All the PEI/CNT composites show an overall higher thermal stability compared to the neat PEI (Table III.5). Incorporation of CNTs increased the degradation temperature of the composites by up to 11 °C.

Table III.7 shows the room temperature volume resistivity of the neat PEI and PEI/CNT composites. The introduction of 3 wt.% of pristine CNTs dramatically decreased the volume resistivity of the composite film by nine orders of magnitude, indicating that the percolation threshold lies between 1 and 3 wt.% CNT loading for the composites containing pristine CNTs. However, no improvement in conductivity was observed for the composites loaded with oxidized and PIL functionalized CNTs at concentrations up to 3 wt.%.

Table III.6. Thermal properties of PEI and PEI/CNT composites.

Sample	CNT loading (wt.%)	T_g (by DSC) (°C)	T_d (by TGA) (°C)
Neat PEI	0	213	494
	0.1	214	505
	0.3	210	503
PEI/pristine CNTs	0.6	212	504
	1	206	505
	3	211	505
	0.1	212	504
PEI/oxidized CNTs	0.3	206	504
	0.6	213	502
	1	213	502
	3	207	502
PEI/ CNT–PIL	0.1	210	500
	0.2	214	504
	0.3	209	503
	0.4	211	505
	0.6	215	502
	1	213	499
	3	211	502

Table III.7. Room temperature volume resistivity of PEI and PEI/CNT composites.

Sample	CNT ratio (wt %)	Volume resistivity (Ω cm)
Neat PEI	0	3.1×10^{12}
PEI/pristine CNTs	1	1.0×10^{12}
PEI/oxidized CNTs	1	3.5×10^{12}
PEI/CNT–PIL	1	0.8×10^{12}
PEI/pristine CNTs	3	1.3×10^3
PEI/oxidized CNTs	3	1.8×10^{12}
PEI/CNT–PIL	3	1.1×10^{12}

The electrical conductivity of the oxidized CNTs is expected to be reduced due to the partial loss of the conjugated conduction path and the possible shortening of the tubes by acid treatment. In this study, as the PIL functionalized CNTs have been prepared by a mild non-destructive method, the π -conjugated system and the aspect ratio of the CNTs have been preserved. Therefore, the low conductivity could be attributed to the insulating PIL layer around the CNTs, which could increase the nanotube/nanotube contact resistance and inhibit the efficient charge transfer between CNTs as already reported for several polymer wrapped CNTs [13]. Yet, electrically conductive films of an imidazolium-based PIL has been obtained by the incorporation of SWCNTs [14], and the conductivity of a polymer composite, poly(3,4-ethylenedioxythiophene), has been highly improved with the use of imidazolium-based PIL functionalized SWCNTs [1]. Another possible explanation could be based on the alignment of CNTs. Indeed, it has been shown that the lowest percolation threshold and the maximum conductivity occur when CNTs are randomly oriented and reaggregated in the matrix [15, 16]. When the number of contacts between CNTs is reduced, the conductive path

is formed at a relatively higher CNT concentration. In our study, the interconnecting conducting channels are formed with pristine CNTs at a loading below 3 wt.%, whereas the alignment and improved dispersion of PIL functionalized CNTs in the composite can lead to a percolation threshold at a CNT loading greater than 3 wt.%.

III.3 Conclusion

Polyetherimide composite thin films have been prepared by a solution-based processing method using three types of MWCNT samples: pristine CNTs, HNO₃ oxidized pristine CNTs and lastly, pristine CNTs non-covalently functionalized with polymerized ionic liquid thin films of approximately 2 nm. This last sample shows a better dispersion in dichloromethane. Additionally, in the PEI composite thin films containing CNT-PIL, a preferential orientation of CNT bundles and individual CNTs has been observed.

The incorporation of CNTs does not have much influence on the tensile properties of the composites while it led to a moderate increase of up to 25% (CNT-PIL, 3 wt.%) in storage modulus. The lowered height of the damping ($\tan \delta$) peaks shows that there is indeed stress transfer to CNTs and it is most efficient at 0.3 wt.% CNT-PIL loading. The electrical resistivity of the composite decreased by nine orders of magnitude at 3 wt.% loading of pristine CNTs, whereas for the same loading of modified CNTs no improvement was noticed. These results can be rationalized as follows. In the case of oxidized CNT, damages of CNT structure can explain the low electrical conductivity. For CNT-PIL, both the presence of an electrically insulating thin film on the CNT surface and the fact that CNT-PIL are partially aligned in the composite could explain the low electrical conductivity. According to DMA analysis, addition of CNTs reduces T_g by about 5 °C. Furthermore, the thermal stability of the polymer composite increased by *ca* 10 °C whatever the type of CNT used.

Although a very effective dispersion of PIL functionalized CNTs in the PEI matrix was not achieved in this study, we still believe that this functionalization method could be an easy and effective way to improve the dispersion of CNTs in polymer matrices. PEI, being a high performance thermoplastic, exhibits a high modulus and tensile strength. Therefore, increasing its mechanical properties by CNT incorporation should require a very effective dispersion of the particles in the matrix and very intimate mixing with the polymer. In this regard, the processing method is particularly important. It is evident from our study that a simple sonication of PEI solution in the presence of CNTs is not sufficient for the effective dispersion of the CNTs. A further increase of the mechanical properties of CNT/PEI composite can be expected by the improvement of the processing method, such as a combined process of solution mixing and melt blending.

References

- [1] Tung TT, Kim TY, Suh KS. Nanocomposites of single-walled carbon nanotubes and poly(3,4-ethylenedioxythiophene) for transparent and conductive film. *Org Electron* 2011;12(1):22-8.
- [2] Kim T, Tung TT, Lee T, Kim J, Suh KS. Poly(ionic liquid)-Mediated Hybridization of Single-Walled Carbon Nanotubes and Conducting Polymers. *Chem Asian J* 2010;5(2):256-60.
- [3] Kumar S, Sun LL, Lively B, Zhong WH. Thermal and Mechanical Enhancements of Polyetherimide/Multi-Walled Carbon Nanotube Composite Performance Using "Solid Nano-Nectar" Assisted Melt Dispersion. *J Nanosci Nanotechnol* 2011;11(3):1976-85.
- [4] Isayev AI, Kumar R, Lewis TM. Ultrasound assisted twin screw extrusion of polymer–nanocomposites containing carbon nanotubes. *Polymer* 2009;50(1):250-60.
- [5] Kumar S, Li B, Caceres S, Maguire RG, Zhong W-H. Dramatic property enhancement in polyetherimide using low-cost commercially functionalized multi-walled carbon nanotubes via a facile solution processing method. *Nanotechnology* 2009;20(46):465708.
- [6] Goh PS, Ng BC, Ismail AF, Aziz M, Sanip SM. Surfactant dispersed multi-walled carbon nanotube/polyetherimide nanocomposite membrane. *Solid State Sci* 2010;12(12):2155-62.
- [7] Shao L, Bai Y-P, Huang X, Meng L-H, Ma J. Fabrication and characterization of solution cast MWNTs/PEI nanocomposites. *J Appl Polym Sci* 2009;113(3):1879-86.
- [8] Liu T, Tong Y, Zhang W-D. Preparation and characterization of carbon nanotube/polyetherimide nanocomposite films. *Compos Sci Technol* 2007;67(3–4):406-12.

- [9] Marcilla R, Blazquez JA, Fernandez R, Grande H, Pomposo JA, Mecerreyes D. Synthesis of Novel Polycations Using the Chemistry of Ionic Liquids. *Macromol Chem Phys* 2005;206(2):299-304.
- [10] Xu ZP, Braterman PS. High affinity of dodecylbenzene sulfonate for layered double hydroxide and resulting morphological changes. *J Mater Chem* 2003;13(2).
- [11] Chen W, Tao X. Self-Organizing Alignment of Carbon Nanotubes in Thermoplastic Polyurethane. *Macromol Rapid Commun* 2005;26(22):1763-7.
- [12] Sarasua JR, Pouyet J. Dynamic Mechanical Behavior and Interphase Adhesion of Thermoplastic (PEEK, PES) Short Fiber Composites. *J Thermoplast Compos Mater* 1998;11(1):2-21.
- [13] Zeng Y, Liu P, Du J, Zhao L, Ajayan PM, Cheng H-M. Increasing the electrical conductivity of carbon nanotube/polymer composites by using weak nanotube-polymer interactions. *Carbon* 2010;48(12):3551-8.
- [14] Fukushima T, Kosaka A, Yamamoto Y, Aimiya T, Notazawa S, Takigawa T, et al. Dramatic Effect of Dispersed Carbon Nanotubes on the Mechanical and Electroconductive Properties of Polymers Derived from Ionic Liquids. *Small* 2006;2(4):554-60.
- [15] Du F, Fischer JE, Winey KI. Effect of nanotube alignment on percolation conductivity in carbon nanotube/polymer composites. *Phys Rev B* 2005;72(12):121404.
- [16] Bryning MB, Islam MF, Kikkawa JM, Yodh AG. Very Low Conductivity Threshold in Bulk Isotropic Single-Walled Carbon Nanotube-Epoxy Composites. *Adv Mater*.2005;17(9):1186-91.

Chapter IV:
**Polymer grafted carbon nanotubes using covalent
functionalization strategy**

Chapter IV: Polymer grafted carbon nanotubes using covalent functionalization strategy

Covalent grafting of polymers onto CNTs can be accomplished using two main approaches: “grafting to” and “grafting from”. This chapter has been similarly divided into two main parts: the covalent “grafting from” approach and the covalent “grafting to” approach.

IV.1 The covalent “grafting from” approach

IV.1.1 Introduction

Generally, the “grafting from” approach involves the *in-situ* polymerization of monomers from surface-derived initiators on CNTs (Figure IV.1).

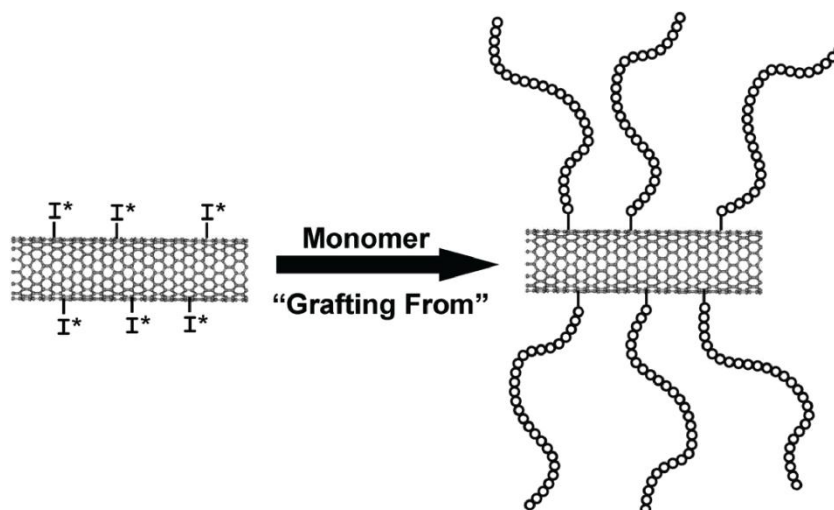


Figure IV.1. Schematic representation of the “grafting from” approach to CNT functionalization with polymers [1].

These initiators are covalently attached using the various functionalization reactions developed for small molecules, including side-wall addition and oxidized wall

functionalization of CNTs. This approach has been successfully used to attach many polymers to CNTs *via* radical, cationic, anionic, ring-opening, and condensation polymerizations [2]. The main advantage of this “grafting from” technique is that the polymer growth is not limited by steric hindrance, allowing a high grafting density. However, this method requires strict control of the amounts of initiator and substrate as well as accurate control of conditions required for the polymerization reaction [1].

Polyamide (PA), or nylon as commonly referred, is an important thermoplastic widely used in industry. In practice it is often reinforced with different nanofillers in practice due to its relatively low tensile strength. Different mechanical tests show that the incorporation of a small amount of CNTs into a PA matrix can improve the modulus, strength and hardness of the composites [3]. Unlike most other nylons, polyamide-6 (PA6) is not a condensation polymer, but instead is formed by the ring opening polymerization (ROP) of caprolactam. CNT/PA6 nanocomposites have been successfully prepared via melt compounding or in situ polymerization in the presence of oxidized CNTs using grafting to approaches [4-7]. However, there are only few reports for the CNT surface-initiated ROP of PA6 [8-10].

IV.1.2 Results and discussion

IV.1.2.1 PA6 functionalized CNTs

IV.1.2.1.1 Synthesis

First of all, PA6 polymer was synthesized by anionic ring opening polymerization of caprolactam in the absence of carbon nanotubes according to a procedure reported in the literature [11]. Caprolactam was carefully dried as any traces of water can prevent the polymerization. The monomer is liquid at 140 °C; therefore, bulk polymerization was carried out. The use of the activator, N-acetylcaprolactam, was necessary for the polymerization.

Caprolactam in the presence of sodium hydride can be maintained between 130 and 140°C for hours without polymer formation. The polymerization occurs rapidly after addition of the activator. This was also verified by our experiments. Indeed, the slowest step of the reaction is the first ring opening step. The caprolactam amide anion that is produced by the ring opening is not as stable as the imide anion, thus, the addition of a small amount of N-acetylcaprolactam to the reaction mixture accelerates the polymerization (Figure IV.2). The M_w of the synthesized PA6 was 36962 g mol⁻¹ with a polydispersity (M_w/M_n) index of 2.3 as determined by gel permeation chromatography.

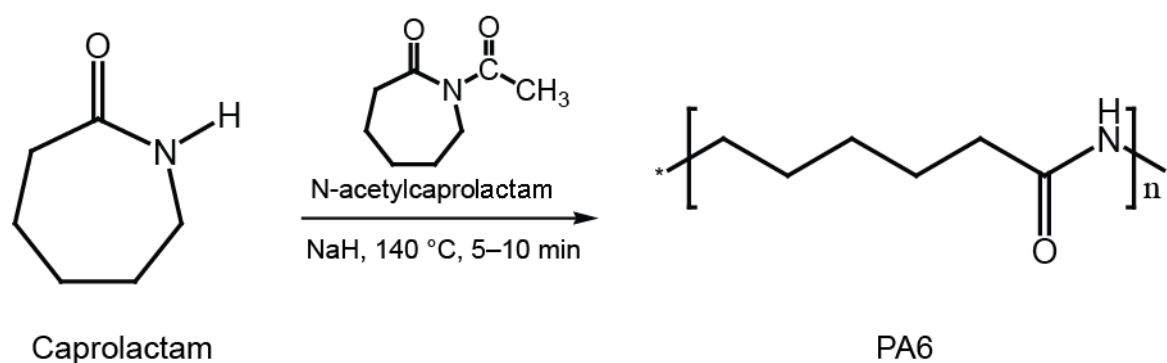


Figure IV.2. Anionic ring opening polymerization of PA6.

Covalent functionalization of CNTs with PA6 was accomplished by anionic ring-opening polymerization (AROP) of caprolactam in the presence of sodium hydride as a catalyst and caprolactam functionalized MWCNTs as initiator. A two-step grafting-process was used (Figure IV.3). The functionalization of CNTs with caprolactam was the first step. The purified carbon nanotubes were oxidized in concentrated HNO₃ at 120 °C for 6 h to introduce carboxylic acid groups onto the CNT surface. The presence of the surface carboxylic acid groups was confirmed from the characteristic carbonyl band at 1722 cm⁻¹ in the FTIR spectrum. By acid–base titration, the number of acidic groups was calculated to be 0.39 mmol/gr CNTs. This corresponds to approximately 2.3 carboxylic acid functions for 500 nanotube carbon atoms. The carboxylic acid groups attached to the CNTs were converted into

acyl chlorides by refluxing the oxidized nanotubes in thionyl chloride. The CNTs were further reacted with caprolactam to prepare CNT–caprolactam (CNT–CL).

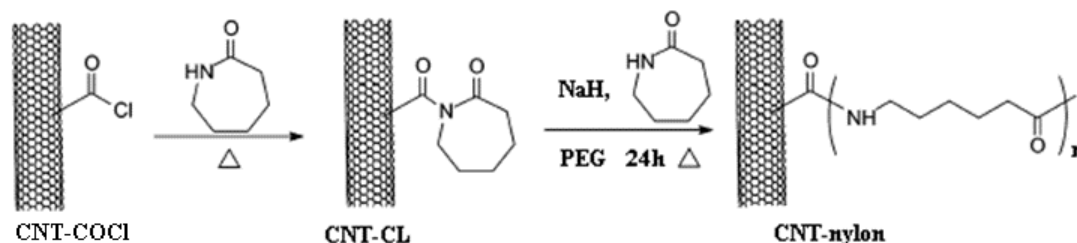


Figure IV.3. Functionalization route to CNT–PA.

The second step is the sodium-initiated anionic-ring opening polymerization to obtain the PA6 functionalized CNTs. CNT–CL was added to CL in a concentration of 5 wt.%. We did not use N-acetylcaprolactam to ensure that the polymer chains grow from the surface of the CNTs and not individually in the reaction mixture. However, in that case, the polymerization rate would be very low. To compensate this, we used polyethyleneglycol (PEG), which will make the caprolactam anion more reactive, by complexing to the sodium cation as shown in Figure IV.4. We also let the polymerization continue for 24 h. Furthermore, as an imide is formed when a caprolactam ring attaches to the nanotube wall, the CNTs can play the role of activator for the surface-initiated ROP.

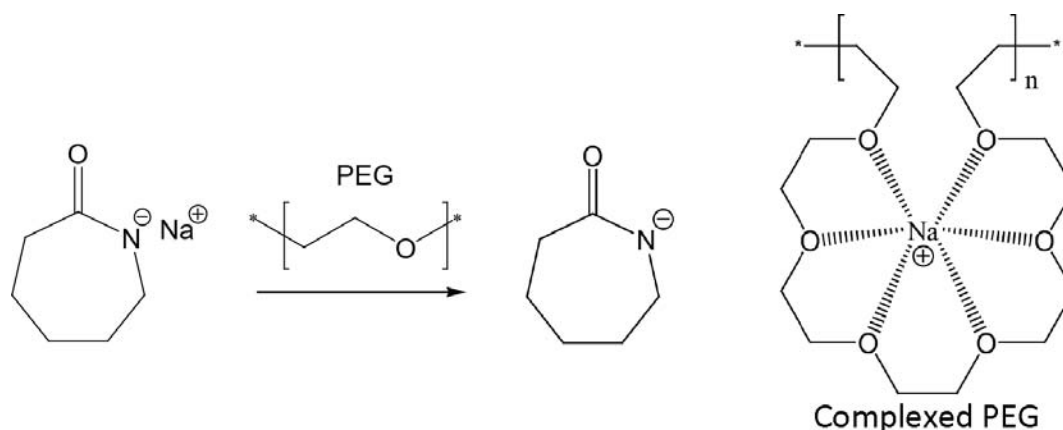


Figure IV.4. Activation of the caprolactam anion by the PEG complexing agent.

At the end of the reaction, it was observed that the viscosity of the reaction mixture did not increase. CNTs were filtered and washed thoroughly with water and methanol to remove sodium salts and monomers, and with formic acid to remove the unattached polymer. No free polymer could be recovered by precipitation in water. The water became blurry, which suggests that the reaction could have afforded short oligomer chains.

TGA measurements were performed to determine the quantity of polymer grafted to the CNTs. The CL grafted CNTs showed a 14 wt.% loss before 500 °C, corresponding to the grafted fragments. As observed from the TGA curves in Figure IV.5, the weight loss of the CNT-PA6 has not considerably increased (18 wt.%) compared to the CNT-CL (14 wt.%). This means that the grafted polymer chains are rather short and in low amounts.

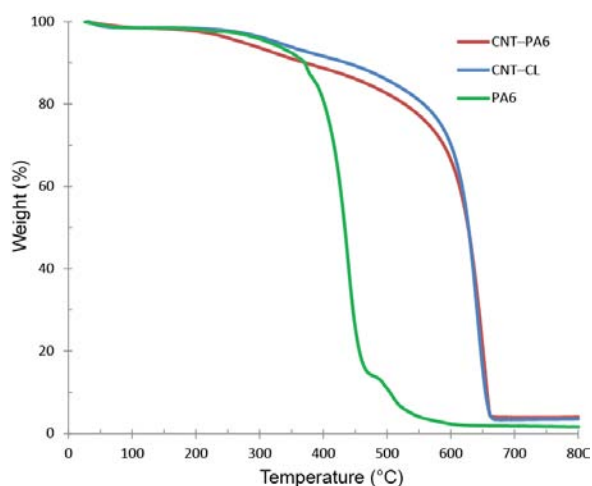


Figure IV.5. TGA curves of PA6, CNT-CL and CNT-PA6.

FTIR spectroscopic analysis provided evidence that the CNT surface was successfully modified with the monomer and polymer (Figure IV.6). All the samples showed the typical bands corresponding to the C-H stretching vibrations at around 2855 and 2925 cm^{-1} . These bands observed with a weak intensity on the spectrum of the oxidized CNTs are associated with the defects [12]. In addition, neat caprolactam (CL) shows a characteristic amide carbonyl stretching absorbance at 1659 cm^{-1} . The polymerized sample exhibits two amide

peaks at 1638 cm^{-1} and 1540 cm^{-1} corresponding to the C=O stretching (« amide I ») and N–H bending (« amide II ») absorptions, respectively. Prior to functionalization with CL, the carboxylic acid groups of oxidized CNTs give rise to a strong absorption band at 1720 cm^{-1} . The IR spectrum of CNT–CL suggests that not all the carboxylic acid groups have been consumed during grafting and looking at the peak intensity, we can say that there is still significant amount of unreacted carboxylic acid group. However, a new peak, overlapping with the one at 1720 cm^{-1} , appears at around 1680 cm^{-1} , which is attributed to the imide carbonyl stretching. This confirms that CL has been successfully grafted to the surface carbonyl groups of the CNTs. The band intensities of the CNT–PA6 spectrum are not very strong, though, the spectrum clearly indicates that the signal at around 1680 cm^{-1} that was present prior to polymerization has disappeared. This is probably due to the opening of the CL rings that are grafted onto the CNT surface.

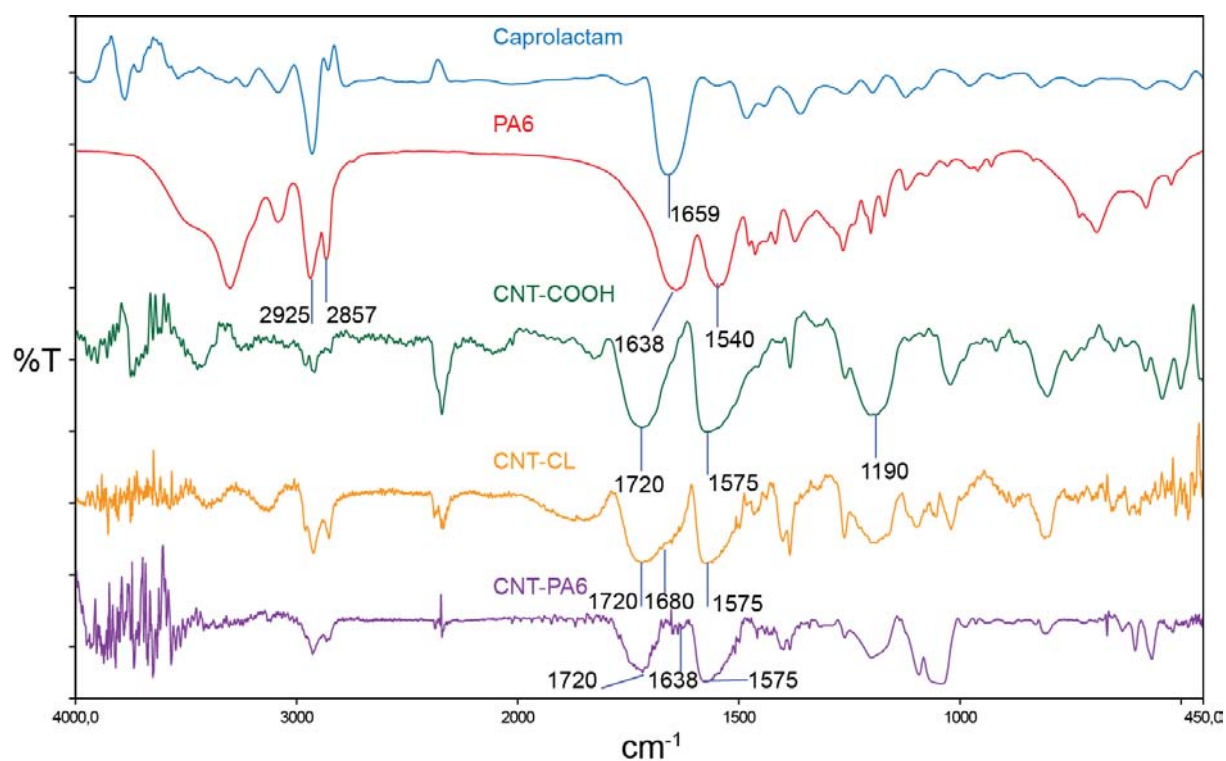


Figure IV.6. FTIR spectra of CL, PA6, CNT–COOH, CNT–CL and CNT–PA6.

The surface modification also influences the Raman spectra of the CNTs. The purified CNTs exhibit the tangential mode band, G-band, at 1591 cm^{-1} and the D-band at 1328 cm^{-1} (Figure IV.7). The oxidation procedure of the CNTs does not change the band positions, whereas the D- to G-band intensity ratio (I_D/I_G) increases slightly from 1.64 to 1.76, due to the defect introduction onto the CNT surface. For CNT-CL, the I_D/I_G ratio does not differ from that of the oxidized CNTs, whereas the G-band shifts to 1580 cm^{-1} . The CNT-PA6 shows a red shift to 1322 cm^{-1} in the D-band and also a shift to 1573 cm^{-1} in the G-band with an enhanced I_D/I_G ratio.

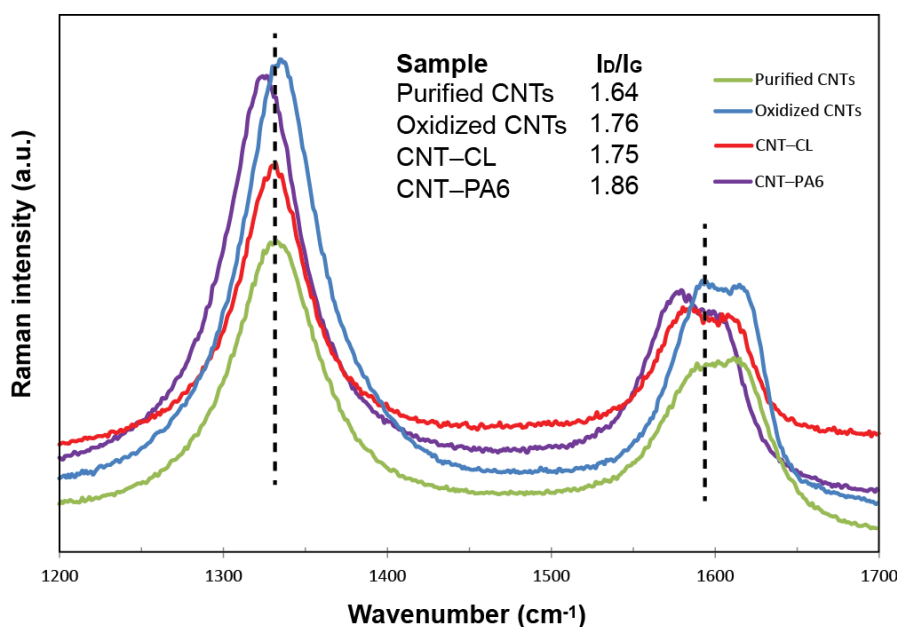
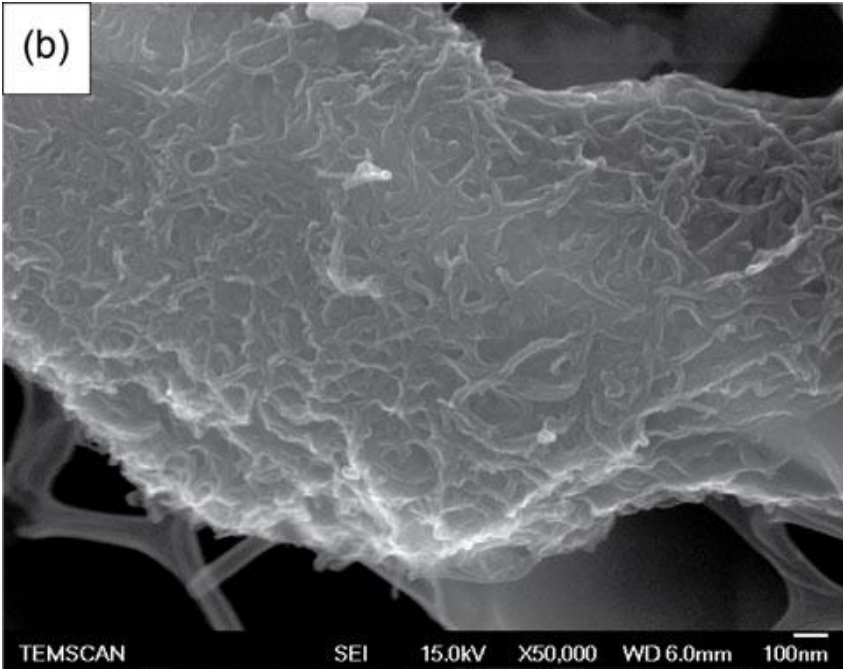
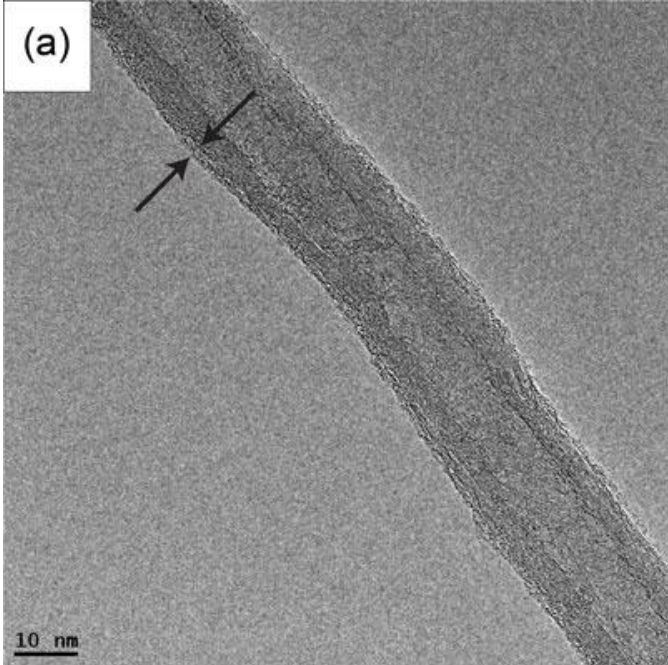


Figure IV.7. Raman spectra of purified CNTs, CNT-CL and CNT-PA6. (Raman excitation = 632.82 nm).

TEM and SEM analysis was performed on the PA6 functionalized CNTs. The TEM image in Figure IV.8 (a) reveals that the CNTs are coated with a thin layer with an approximate thickness of 1 nm . The surface modification of the nanotubes is more evident in the SEM images of the CNTs (Figure IV.8 (b) and (c)). The polymer-modified material is coated with

an amorphous polymer layer, whereas the purified CNTs show the classical nanotube morphology.



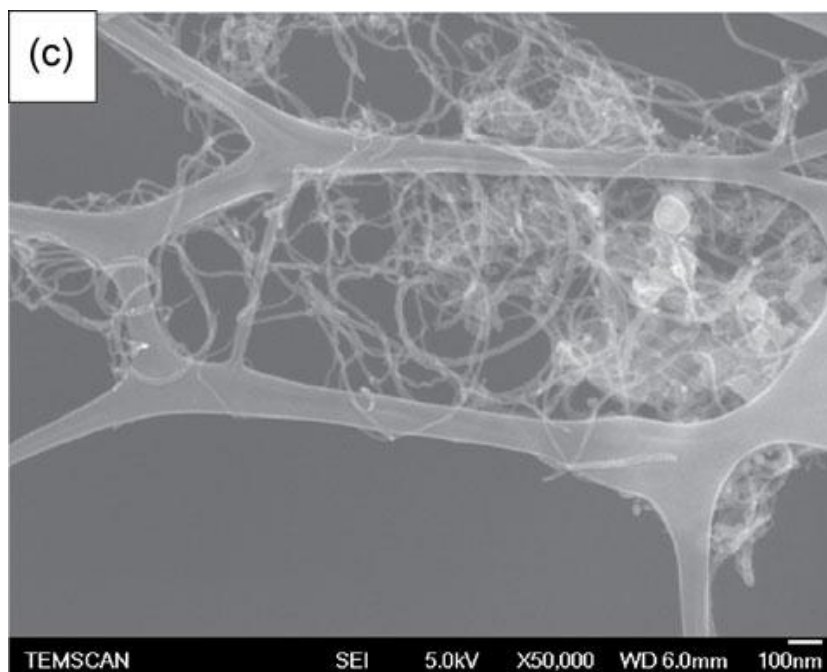


Figure IV.8. (a) TEM image of CNT–PA6, (b) SEM images of CNT–PA6 and (c) purified CNTs.

We tested the dispersibility of the CNTs in formic acid, a good solvent for PA6. Figure IV.9 shows two vials containing equal volumes of solvent and equal masses of CNT–CL and CNT–PA6. It was found that the PA6 functionalized CNTs can be easily dispersed in formic acid, whereas caprolactam functionalized CNTs completely precipitates shortly after sonication. The dispersion containing CNT–PA6 stays as dark black for a period of at least 6 months. The good dispersibility of CNT–PA6 in formic acid indicates that despite the low density of the grafted PA6 and the short chain length, the surface properties of the CNTs have been modified.

The reasons for the short polymer chains formed in the presence of CNTs might be several. In the absence of an added activator, the activating effect of the grafted CL might be insufficient. Moreover, the presence of CNTs might play an inhibitor role for the polymerization. Penu et al [13] showed that even in the presence of an activator, MWCNTs slowed down the anionic polymerization kinetics of caprolactam. Its inhibiting effect became more important as the

amount of MWCNTs increased. Moreover, the better the state of dispersion of the MWCNT in the polymerizing system, the more severe was the inhibiting effect.

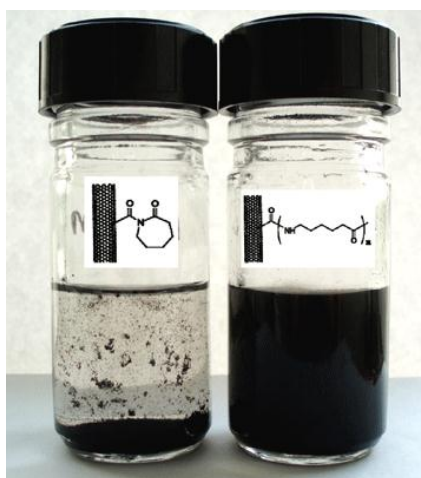


Figure IV.9. Dispersions of (a) CNT–caprolactam and (b) CNT–PA6 in concentrated formic acid at a concentration of 0.5 g L^{-1} upon standing for one hour after sonication.

IV.1.2.1.2 Polyamide/CNT composites

The effect of CNT functionalization on the mechanical properties of the PA/CNT composites was investigated. In addition to CNT–PA6, amine functionalized CNTs (CNT–NH₂) were prepared by the gas phase chemical derivatization of oxidized CNTs with 1,8-diaminooctane [14]. Typically, the 3 h nitric acid treated CNTs with a carboxyl concentration of 2.54 mmol/gr CNT and the amine were placed together in a steel vial. The vial was heated at 160 °C under vacuum for 4 h. This easy procedure resulted in CNT–NH₂ with a 2.48 % N content as determined by elemental analysis. The PA/CNT composites were prepared by melt-blending using a co-rotating twin screw mini extruder. The main problem encountered in the processing of PA matrix is the thermal degradation; in fact this kind of thermoplastic matrix show a thermal degradation at the processing temperature (at around 280 °C). Thus, different matrices were tested. Despite the good mechanical performance, the DURETAN A30S matrix system shows a significant thermal degradation at the processing temperature just after 1

minute. This short processing time does not allow the good dispersion of the CNTs, also as evidenced by a very brittle behavior of the materials in the tensile tests. The second matrix, Rhodia 27EA1, shows a thermal stability of 10 min at the same temperature, which allows to process the composites with the CNTs for a longer time. A rotation speed of 150 rpm, which is the maximum speed of the extruder, and a temperature profile of 280/290/295 °C were used. The most suitable processing time was investigated by analyzing the mechanical properties of the neat composite. Table IV.1 lists the tensile properties of neat Rhodia 27EA1 as a function of processing time.

Table IV.1. The tensile properties of neat Rhodia 27EA1 as a function of processing time.

Processing time (min)	Young's Modulus (MPa)	Yield Strength (MPa)	Yield Strain (%)	Tensile Strength (MPa)	Tensile Strain (%)
Directly extruded	2480 ± 28	58.4 ± 0.2	19.5 ± 0.6	82.0 ± 8.9	250.2 ± 32.5
1	2477 ± 24	58.2 ± 0.1	19.2 ± 0.4	81.0 ± 8.3	248.0 ± 29.7
5	2478 ± 33	59.3 ± 0.4	19.1 ± 0.2	80.0 ± 2.9	247.3 ± 19.9
10	2674 ± 53	57.9 ± 0.2	7.3 ± 0.3	52.8 ± 6.2	23.4 ± 4.2

As it is observed from the results, 5 min is the ideal processing time. Therefore, the Rhodia 27EA1 matrix was melt blended with 1 wt.% pristine, amine functionalized or polyamide functionalized CNTs for 5 minutes using the determined temperature profile. Table IV.2 summarizes the experimental results obtained from the tensile tests and the histograms in Figure IV.10 compare the properties of each material.

Table IV.2. Tensile properties of neat PA and PA/CNT (1 wt.%) composites.

Material	Young's Modulus (MPa)	Yield Strength (MPa)	Yield Strain (%)	Tensile Strength (MPa)	Tensile Strain (%)
PA	2478 ± 33	59.3 ± 0.4	19.1 ± 0.2	80.0 ± 2.9	247.3 ± 20.0
PA/CNTs	2429 ± 62	65.1 ± 0.1	20.6 ± 0.8	57.4 ± 0.4	33.0 ± 2.7
PA/CNT-PA6	3156 ± 47	69.0 ± 0.5	12.4 ± 0.4	59.7 ± 7.4	21.4 ± 5.7
PA/CNT-NH ₂	2723 ± 105	64.2 ± 0.7	16.9 ± 1.5	63.2 ± 0.4	19.6 ± 2.9

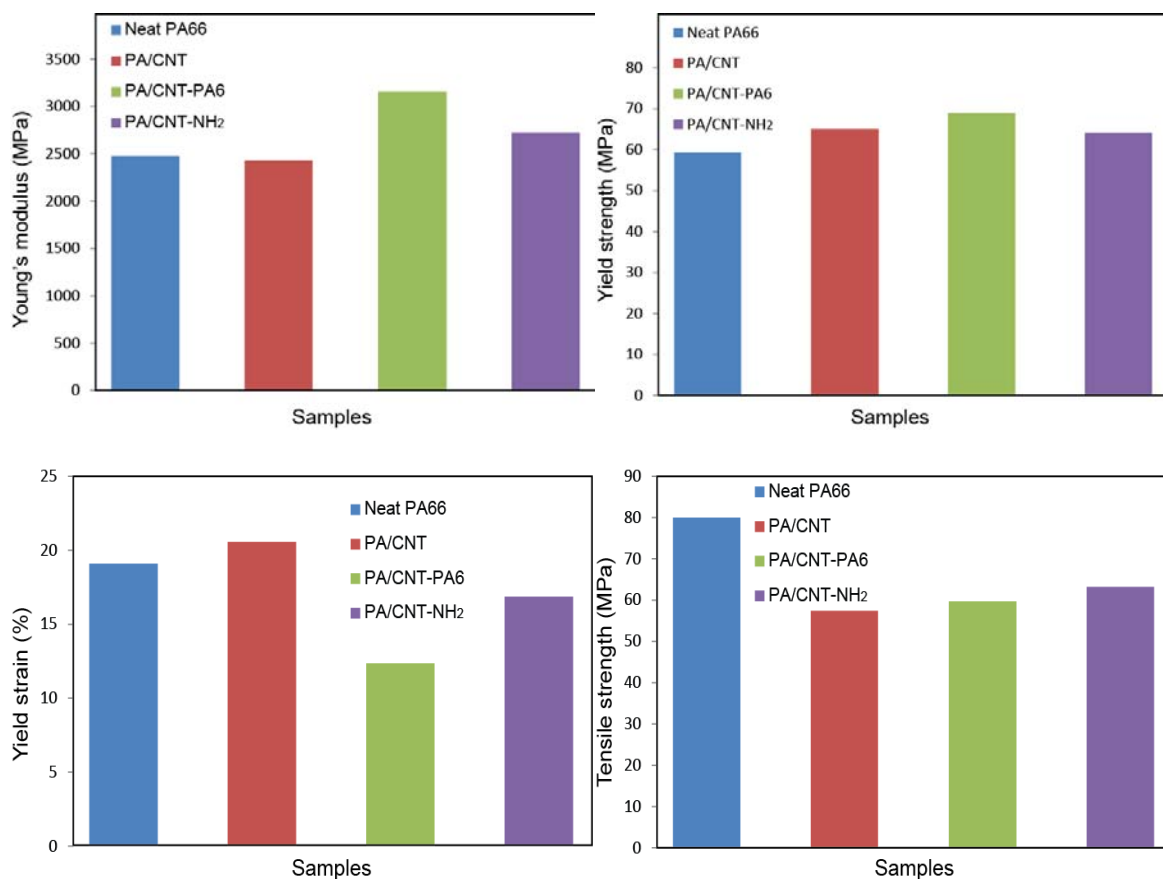


Figure IV.10. Comparison of the tensile properties of the PA66/CNT composites.

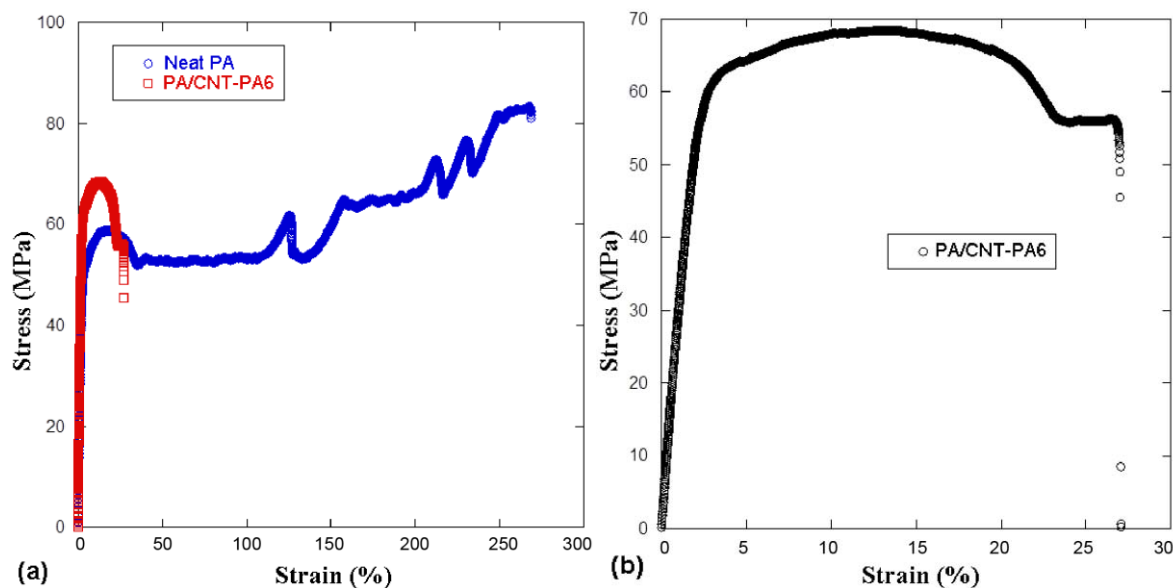


Figure IV.11. Stress-strain curves of (a) neat PA and PA/CNT–PA6, and (b) PA/CNT–PA6.

The best improvement in terms of Young’s modulus and yield strength was achieved with CNTs functionalized with PA6, probably due to the improved CNT–matrix interfacial interaction. By incorporation of 1 wt.% CNT–PA6, the Young’s modulus increased by 27% while the improvement in yield strength was 16%. Figure IV.11 shows the typical stress-strain curves of neat PA and PA/CNT–PA6. It is observed that after the plastic deformation point, the yield strength, the material starts to strain and an increase in stress is observed till the point of rupture due to the straightening of polymer chains, which gives rise to high tensile strength. On the other hand, by the addition of CNTs the material becomes stiffer and more resistant to plastic deformation, which causes a high decrease in tensile strain. A similar behaviour was observed for all the CNT incorporated composites. These results evidence that, despite the low molecular weight of the grafted PA6 units, the material loaded with CNT–PA6 showed the best mechanical improvement.

IV.1.2.2 Covalent polymerized ionic liquid functionalization of CNTs

Covalent approach has also been studied for the functionalization of CNTs with polymerized ionic liquid (PIL). The synthesis steps are shown in Figure IV.12. The MWCNTs were

purified and oxidized with nitric acid. Then, the hydroxyl-terminated IL monomers were grafted to the acyl chloride groups of the MWCNTs.

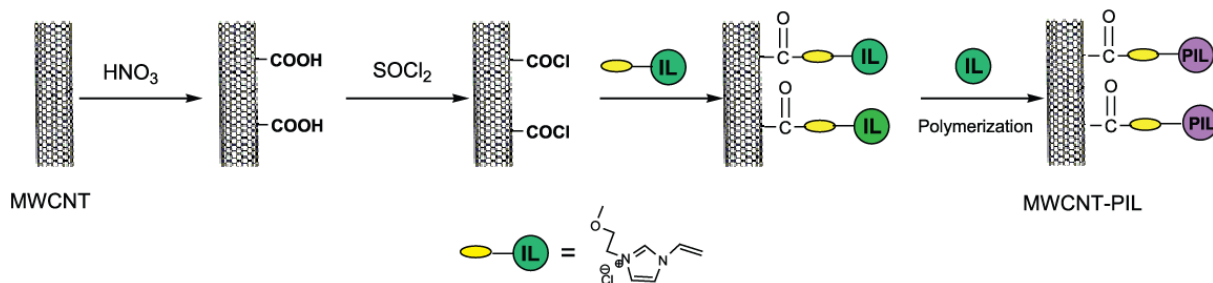


Figure IV.12. Illustration of the process of PIL grafting from the surface of CNTs.

The presence of grafted IL was confirmed by elemental analysis, the sample contained 3.7 wt.% N. The TGA weight loss due to the grafted IL was 13 wt.% as determined by TGA. Theoretically it should be 4 wt.%. This suggests that IL has been also noncovalently adsorbed on the CNTs. *In situ* free radical polymerization of [VEIM] based IL monomers was conducted using AIBN as initiator in the presence of the IL grafted CNTs. Apart from Cl^- anion, both Br^- and NTf_2^- counter anions were used for the reactions. After 24 h, the CNTs were separated from the reaction mixture by filtration. The filtrate was poured into a suitable solvent to precipitate the PIL formed in the presence of CNTs. The IR analysis of the IL grafted CNTs, also shows that the vinyl bands at 1660 cm^{-1} disappears (Figure IV.13). This shows that polymerization took place. However, the resulted CNTs do not show any dispersibility in any solvent, which shows that the polymer chains did not grow enough from the surface grafted ILs. The IL functionalized CNTs are probably attracted to each other preventing the growth of the polymer chains.

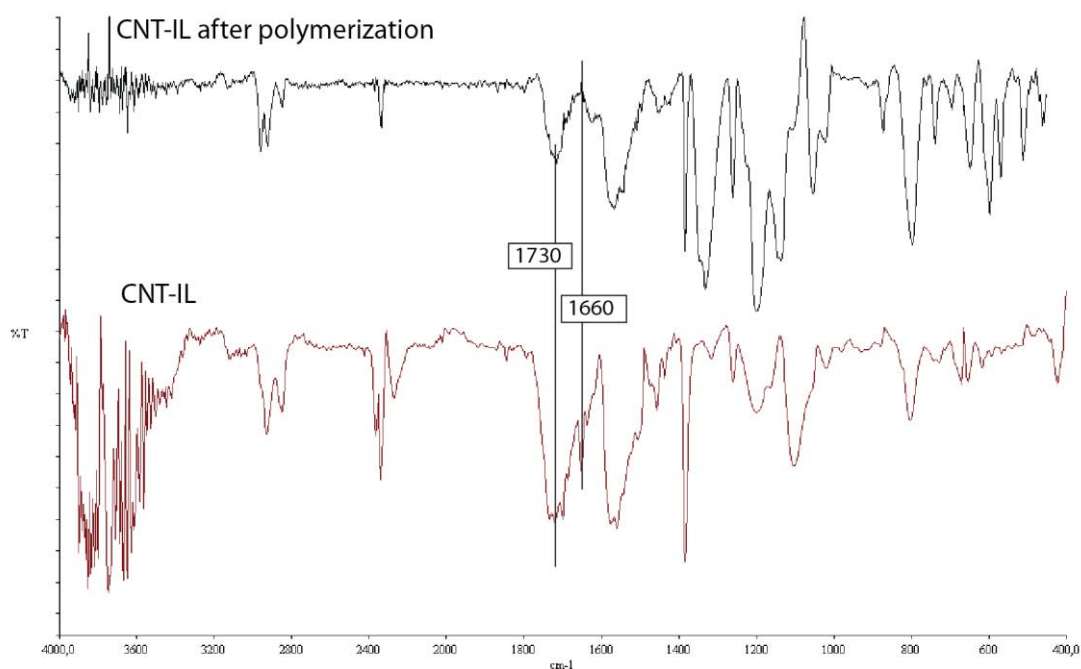


Figure IV.13. FTIR spectra of CNT-[VEIM]NTf₂ prior to and after polymerization.

We also tried adding the monomer-grafted CNTs with the radical initiator prior to the addition of the monomer to promote the polymer growth from the CNT surface. However, as observed by SEM (Figure IV.14), the CNTs formed macroscopic assemblies probably by cross-linking with each other through chemical reactions between the vinyl groups attached to the CNT walls. Similar cross-linking has also been observed with other type of functional groups attached to CNTs and these robust assemblies have been reported to have potential applications for sensors, transistors, electrodes, actuators and fibers [15-17]. The Raman spectrum of the CNT-[VEIM]Cl and cross-linked CNTs are shown in Figure IV.15. It was observed that the I_D/I_G ratio decreased from 1.71 to 1.57 as a result of cross-linking.

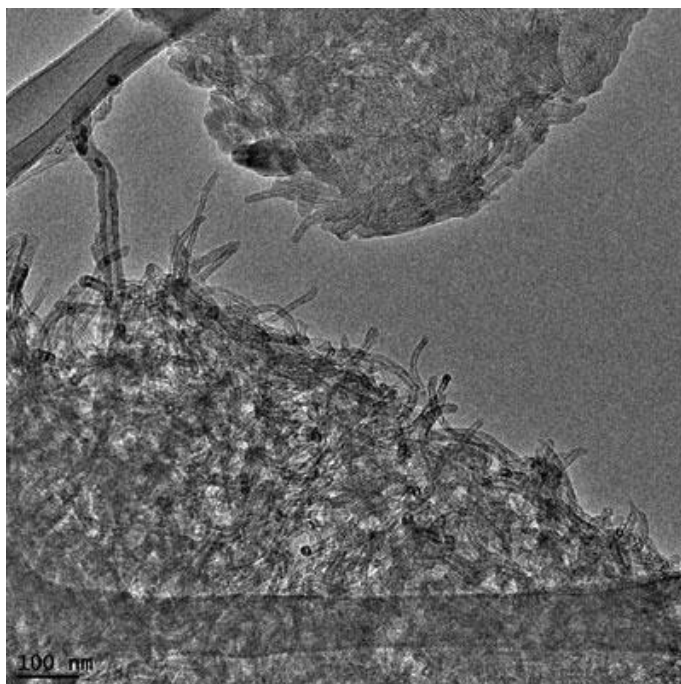


Figure IV.14. Cross-linked macroscopic assemblies of IL monomer-grafted MWCNTs.

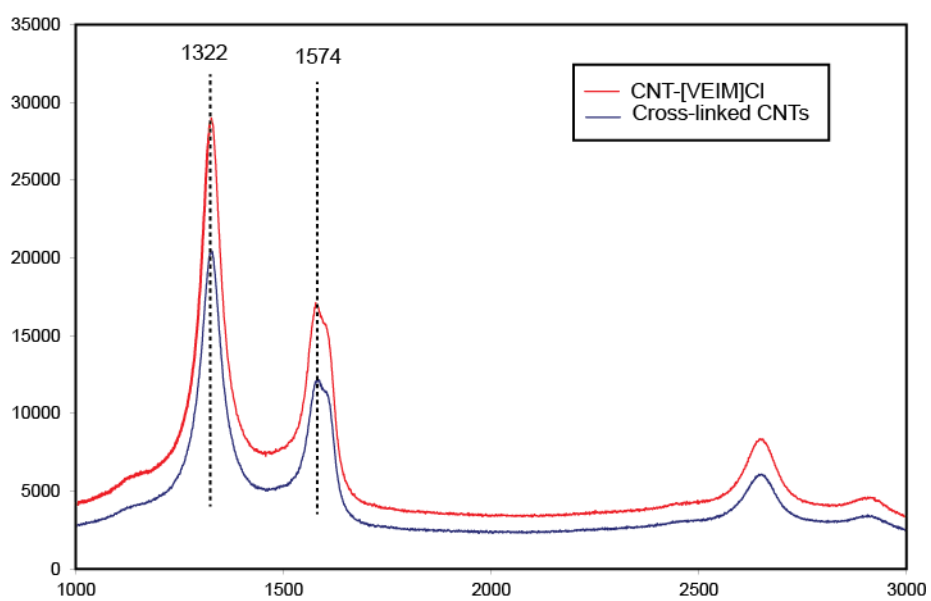


Figure IV.15. Raman spectra of CNT-[VEIM]Cl and the cross-linked CNTs.

IV.2 The covalent “grafting to” approach

IV.2.1 Introduction

In general, the “grafting to” approach involves pre-formed polymer chains either reacting with the pristine CNT sidewall or reacting through carboxylic groups present on the sidewall (Figure IV.16).

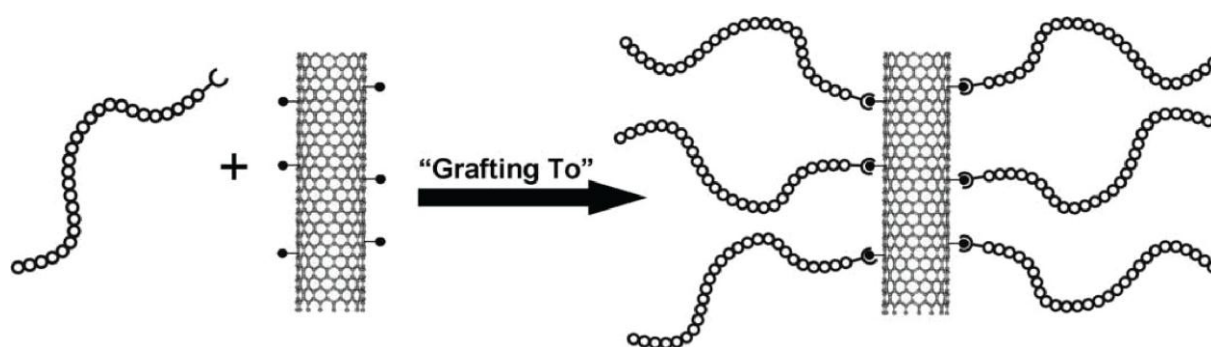


Figure IV.16. Schematic representation of the “grafting to” approach to CNT

functionalization with polymers [1].

For the latter, CNTs are simply submitted to an oxidation process using HNO_3 for example. This kind of functionalization is also known as defect site functionalization since it has been shown that the defect sites, including the tube ends, are more prone to oxidation [12, 18, 19]. The main limitation of the “grafting to” technique is that the initial binding of polymer chains sterically hinders the diffusion of additional macromolecules to the CNT surface, which could lead to a low grafting density, particularly with high molecular weight polymers.

Apart from the defect site functionalization, a number of addition reactions are also possible on the nanotube sidewalls. Since the curvature of the nanotubes imparts a significant strain upon the sp^2 hybridized carbon atoms that make up their framework, the energy barrier required to convert these atoms to sp^3 hybridization is lower than that of the flat graphene

sheets, making them susceptible to various addition reactions. One of the reactions exploited in this functionalization strategy has been the radical coupling to the nanotube surface as illustrated in Figure IV.17, a process found to be efficient with both nanotubes and C₆₀ [1]. Using the density functional theory, a quantum mechanical modeling method, it has been shown that the radical coupling to the nanotube surface is energetically favorable [20]. The free radical that is generated by the coupling of an initiator to the CNT surface is delocalized over several nanotube carbon atoms. The polymer macroradicals, which react with the C=C bonds of the CNTs can be produced using two main approaches: (i) the dissociation of specific polymer chain end groups such as nitroxyl [21] or bromide [22], and (ii) the *in situ* radical polymerization of the monomers in the presence of pristine CNTs. For the first method the preparation of the end-capped polymer is needed; however, it is advantageous because it allows for complete characterization of the polymer structure prior to immobilization on the nanotube surface. In *in situ* grafting polymerization, the polymerization is carried out in the presence of CNTs; however, the termination of the free radicals due to coupling with each other competes with the grafting of the polymer chains to the CNT surface. This in turn makes the control of the grafting degree relatively difficult.

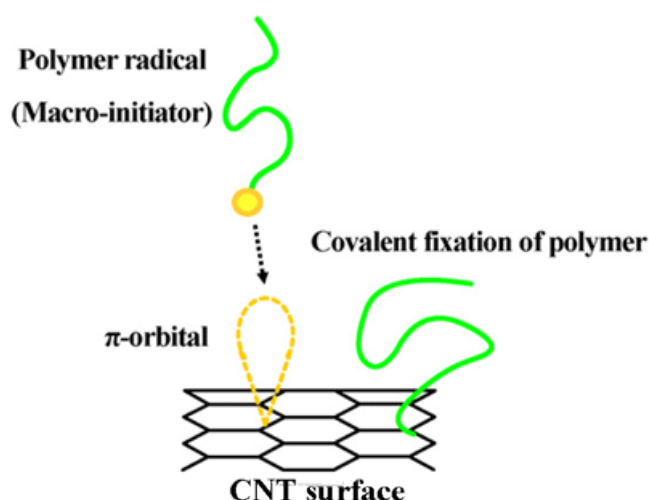


Figure IV.17. Illustration of the covalent fixation of a polymer radical onto the CNT surface.

Functionalized CNTs for epoxy matrices

Epoxy or polyepoxide is a thermosetting epoxide polymer that cures (polymerizes and cross-links) when mixed with a curing agent or "hardener". Most common epoxy resins are produced from the ring-opening reaction between epichlorohydrin and bisphenol A and common hardeners are based on diamine-substituted monomers. Figure IV.18 shows the molecular structure of bisphenol A based epoxy resins and the cross-linking of the polymer chains by a hardener. Epoxy resin is most commonly used as a matrix for advanced composites due to their superior thermal, mechanical and electrical properties; dimensional stability and chemical resistance.

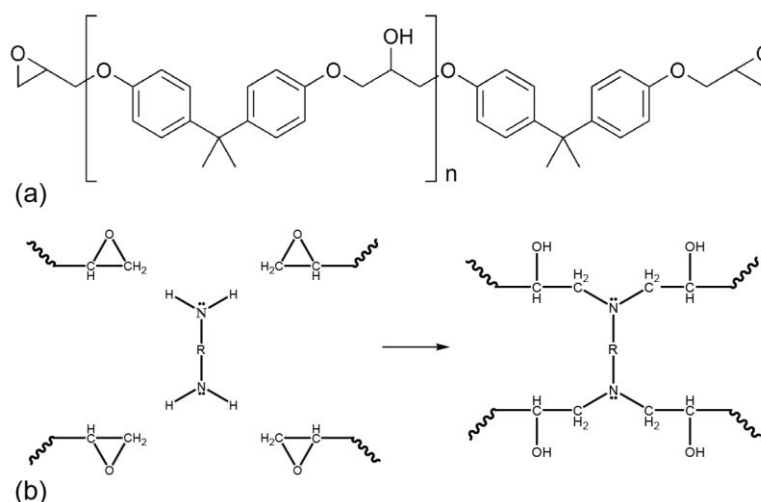


Figure IV.18. (a) The molecular structure of epoxy resin and (b) crosslinking of epoxy resin.

In recent years, different types of polymer composites have been synthesized by incorporating CNTs into various polymer matrices. Among these, epoxy matrices have been one of the most widely studied due to the extensive uses of epoxy resins in the areas of electronics, automotive, aeronautics and marine industry and others [23]. Following the first report on the preparation of aligned MWCNT arrays formed by cutting an epoxy/CNT composite [24], there have been continuous efforts to incorporate CNTs into various types of epoxy resins to

obtain functional composite materials [25, 26]. The modification of epoxy resins with CNTs could endow the composites with some superior mechanical, thermal and electrical properties. Most of the reports published so far on these materials advocate surface functionalization of CNTs and the use of a surfactant as possible routes to enhance the dispersion and interfacial adhesion between CNTs and the epoxy matrix. We will not go into detail about these studies here; Table 2 presents a summary of the experimental results of some selected publications, involving the covalent “grafting to” approach. Studies on various amine functionalized CNTs have been also included since the covalent attachment of the epoxy matrix to the CNTs can occur during the curing process as illustrated in Figure IV.19.

Table 2. A summary of the selected studies on CNT/epoxy composites prepared using “grafting to” approach.

Functionalization Strategy	Improvements	Challenges/remarks	Ref.
Functionalization of acid oxidized MWCNTs with triethylenetetramine (TETA)	Improvements in T_g (19% at 0.5 wt.%) and impact strength (97% at 0.5 wt.%)		[27]
Functionalization of acid oxidized MWCNTs with (1) Polyacryloyl chloride (PACl) and (2) epoxy	Improvements in T_g (18% at 1 wt.%), tensile strength (40% at 0.7 wt.%) and modulus (90% at 0.1 wt.%)	Decrease of modulus at CNT contents > 1 wt.%	[28]
Functionalization of MWCNTs with different amino groups	Improvements in flexural strength (120.41% at 1 wt.%) and T_d (36 °C at 0.25 wt.%)	Reduced T_g , the improvements depend on the molecular structure of the amine modifier	[29]
Functionalization of MWCNTs with amine	Improvements in curing kinetics, T_g (5% at 3 wt.%), flexural strength (~25% at 3wt.%) and storage modulus (53% at 3 wt.%)	Damping property decreased	[30]
Plasma assisted functionalization of MWCNTs with (1) Maleic anhydride (2) diamine (3) epoxy	Improvements in tensile strength (50% at 1 wt.%) and modulus (100% at 1 wt.%) in electrical conductivity (percolation threshold at between 0.1 and 0.2 wt %) and in thermal stability (21 °C at 1 wt.%)		[31]
Functionalization of acid oxidized MWCNTs with diglycidyl ether of bisphenol A (DGEBA)	Improvement in flexural strength (115% at 3 wt.%) and elastic modulus (15% at 3 wt.%)	No change in T_g	[32]

Side-wall functionalization of SWCNTs with an amino hardener	Improvement in storage modulus (25% at 0.5 wt.%)	Decrease in T_g (due to the reduced cross-linkage)	[33]
Functionalization of acid functionalized SWNTs with (1) dicarboxylic acid acyl peroxide treatment, (2) diamines	Improvements in storage modulus (47% at 4 wt.%), tensile strength (25% at 1 wt.%) and tensile modulus (68% at 4 wt.%)	Decrease in tensile strength and T_g at loadings ≥ 4 wt.%.	[34]
Functionalization of acid oxidized MWCNTs with TETA	Improvements in tensile strength (30% at 0.5 wt.%) and modulus (38% at 0.5 wt.%)	Mechanical properties starts to decrease at a loading > 0.75 wt.%.	[35]
Functionalization of acid oxidized MWCNTs with TETA	Improvement in flexural strength (29% at 0.6 wt%), flexural modulus (22% at 0.6 wt.%) and impact strength (84% at 0.6 wt.%)	Decrease of mechanical properties at CNT contents > 0.6 wt.%.	[36]
Functionalization of MWCNTs with polyethylenimine	Improvement in storage modulus (8% at 1 wt.%)	No change in T_g , reduced electrical conductivity	[37]
Functionalized of DWCNTs with amine	Improvements in tensile modulus (6% at 0.1 wt.%), very slight increase in tensile strength at 1 wt.%		[38]
Functionalized of DWCNTs and MWCNTs with amine	Improvements in tensile strength (14% at 0.5 wt.% of DWCNTs and 8% at 0.5 wt.% of MWCNTs) and in ultimate tensile strength (8% at 0.5 wt.% of DWCNTs)	No significant improvement in tensile strength with MWCNTs. Due to their concentric structure, MWCNTs have an effective surface area of only 9% of their total weight.	[39]

Functionalization of SWCNTs with poly(glycidyl methacrylate)	Improvements in storage modulus (42% at 1 wt.%), tensile strength (40% at 1 wt.%) and tensile modulus (60% at 1 wt.%)	High decrease in T_g due to reduced cross-linking of the epoxy matrix	[40]
--	---	---	------

Functionalization of MWCNTs with poly(glycidyl methacrylate)	Improvements in storage modulus (518% at 3 wt.%), T_g (11 °C at 3 wt.%) and thermal conductivity (183% at 3 wt.%)		[41]
--	---	--	------

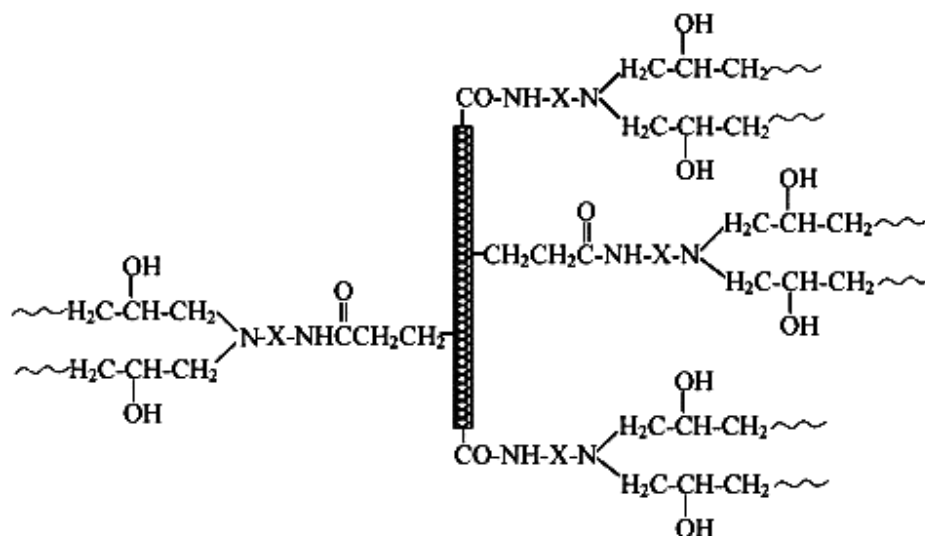


Figure IV.19. Integration of the functionalized CNTs into the epoxy matrix [34].

These reported results indicate that the covalent bond formation between the functionalized CNTs and the epoxy matrix would lead to a more effective stress transfer and form a denser cross-linked structure; thus, mechanical and thermal properties of epoxy composites could be improved. Likewise, covalent surface modifications with polymers compatible with the epoxy matrix play an active role in the enhancement of mechanical properties of CNT-reinforced epoxy composites. The decrease in T_g of the composites reported in some studies can be due to two things. The CNTs can interfere with the curing reaction of the epoxy, leading to reduced T_g . In addition, when CNTs do not disperse well, they form holes in the matrix where polymer chains can move easily, resulting also in low T_g .

We studied several functionalization strategies for the preparation of functionalized CNTs for epoxy matrices. These involve covalent grafting of polymers bearing amino groups and epoxy terminal groups (Figure IV.20 (a) and (b)), which can react with the epoxy matrix and the amine curing agents, respectively. This will lead to covalently bonded CNT/epoxy composites. Furthermore, another strategy consists in grafting a polyacrylate, structurally similar to the epoxy matrix (Figure IV.20 (c)). The idea here is to prepare polymer grafted CNTs, which can non-covalently interact with the epoxy matrix.

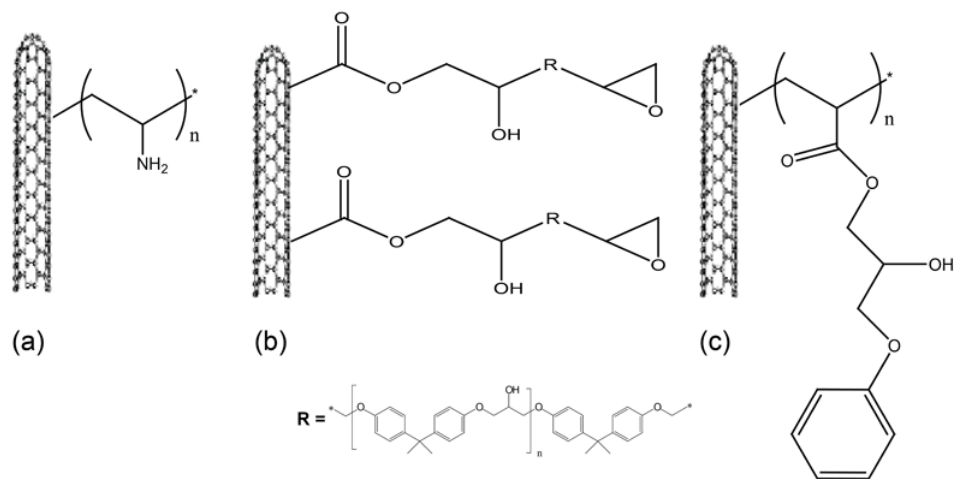


Figure IV.20. Polymer functionalized CNTs prepared in this study: (a) polyvinylamine functionalized CNTs, (b) glycidyl end-capped poly(bisphenolA-co-epichlorohydrin) functionalized CNTs and (c) poly(2-hydroxy-3-phenoxypropyl acrylate) (PHPPA) functionalized CNTs.

The two synthesis approaches used for grafting the above polymers to the CNT surface are based on the *in situ* free radical polymerization and the reaction between the carboxylic acid groups of the oxidized CNTs and the polymer.

IV.2.2 Results and discussion

IV.2.2.1 Functionalization of CNTs by radical addition

IV.2.2.1.1 Polymer synthesis

The first step was the polymer preparation to determine the suitable synthesis conditions. Polyvinylamine (PVA) cannot be directly synthesized from its corresponding monomer due to the instability of vinylamine. Therefore, we used commercially available *N*-vinylformamide (NVF), a precursor developed for simple and economical production of PVA. PNVF can be easily converted into PVA by hydrolysis, in either acidic or basic aqueous solution. The synthesis route that we adopted is described in Figure IV.21. We preferred the base hydrolysis route as it leads to complete hydrolysis, whereas the acid hydrolysis is completed with a 80%

conversion because of the electrostatic repulsion between the cationic amine groups generated during hydrolysis and the proton hydrates [42]. The drawback of the base hydrolysis is that the removal of the hydrolysis by-product, sodium formate, is problematic. Therefore, the hydrolyzed sample was acidified with a concentrated HCl solution and precipitated as PVA.HCl in methanol.

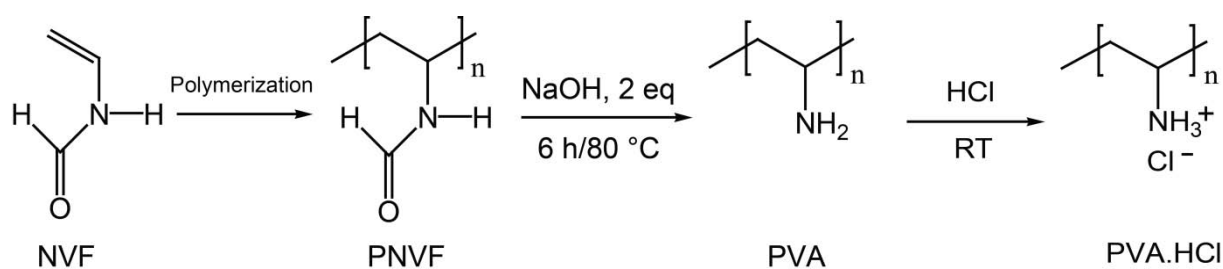


Figure IV.21. Synthesis route of PVA *via* base hydrolysis of PNVF and its isolation as PVA.HCl.

As evidenced from the ^1H NMR spectra of PVF and PVA.HCl (Figure IV.22), the peaks of PNVF attributed to the formamide groups in the 7.5–8.2 ppm region were completely disappeared after hydrolysis. This indicated that the amide groups in PNVF were totally converted to amine groups by hydrolysis, affording PVA. The FTIR spectra of the polymers are shown in Figure IV.23. The PNVF sample exhibit a characteristic C=O stretching band at 1672 cm^{-1} , a C-N stretching band at 1385 cm^{-1} and a N-H bending band at 1597 cm^{-1} . The broad band in the 3000 cm^{-1} region was attributed to the N-H stretching of the amide, whereas PVA.HCl shows a very broad peak at around 2961 cm^{-1} due to the N-H stretching of the NH_3^+ salt. It showed other strong bands at 1597 cm^{-1} assigned to the N-H bending, 1508 cm^{-1} and 1402 cm^{-1} .

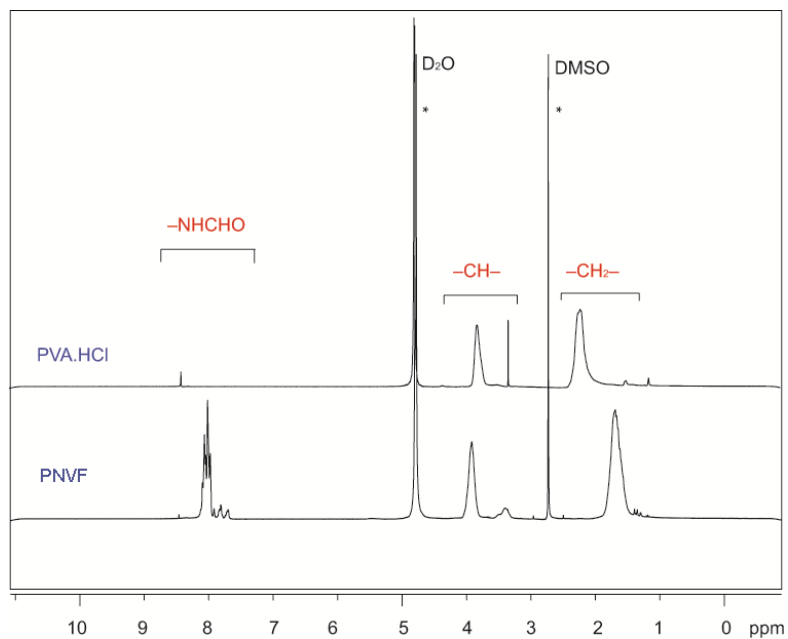


Figure IV.22. 300-MHz ¹H NMR spectra of PVF (bottom) and PVA.HCl (top) in D₂O.

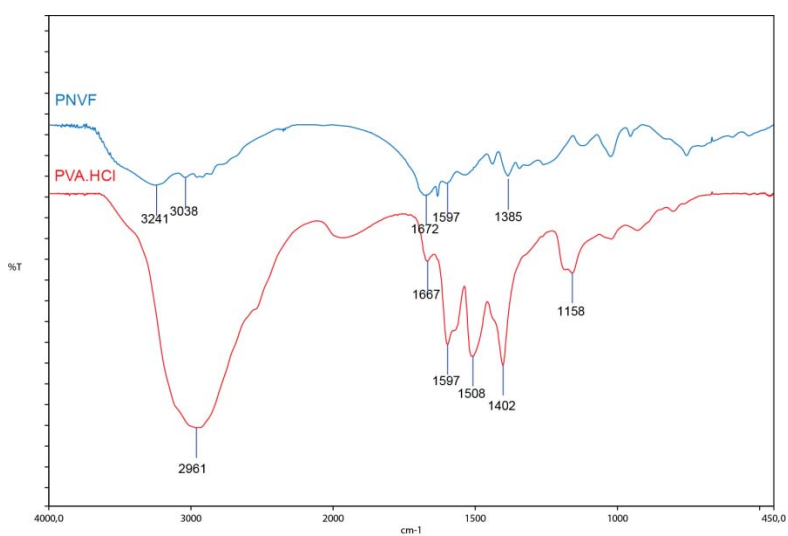


Figure IV.23. FTIR spectra of PNVF (top) and PVA.HCl (bottom).

Poly(2-hydroxy-3-phenoxypropyl acrylate) (PHPPA) was also successfully polymerized using the similar radical polymerization with AIBN as initiator. The polymer structure was characterized by ¹H NMR spectroscopy (Figure IV.24).

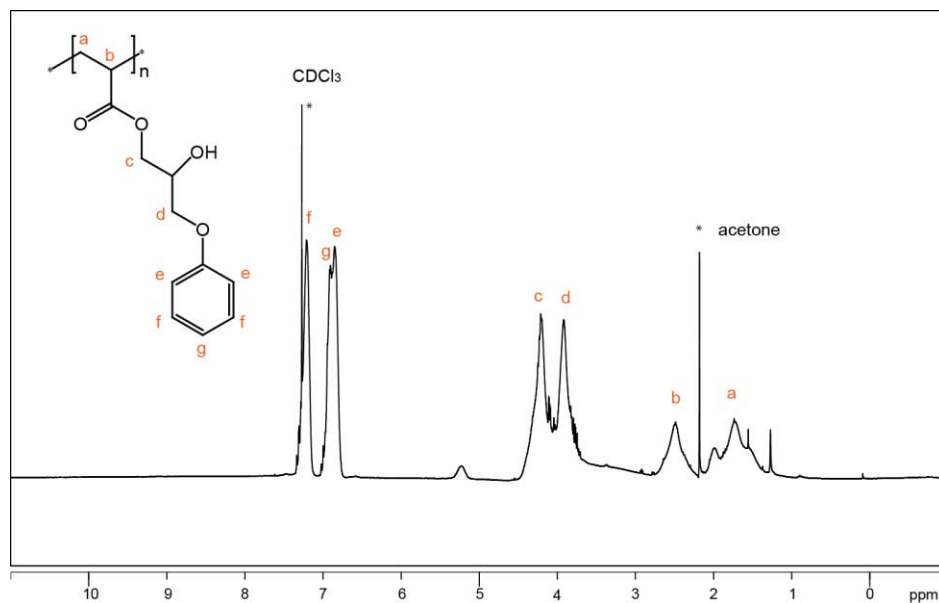


Figure IV.24. 300-MHz ^1H NMR spectra of PHPPA in CDCl_3 .

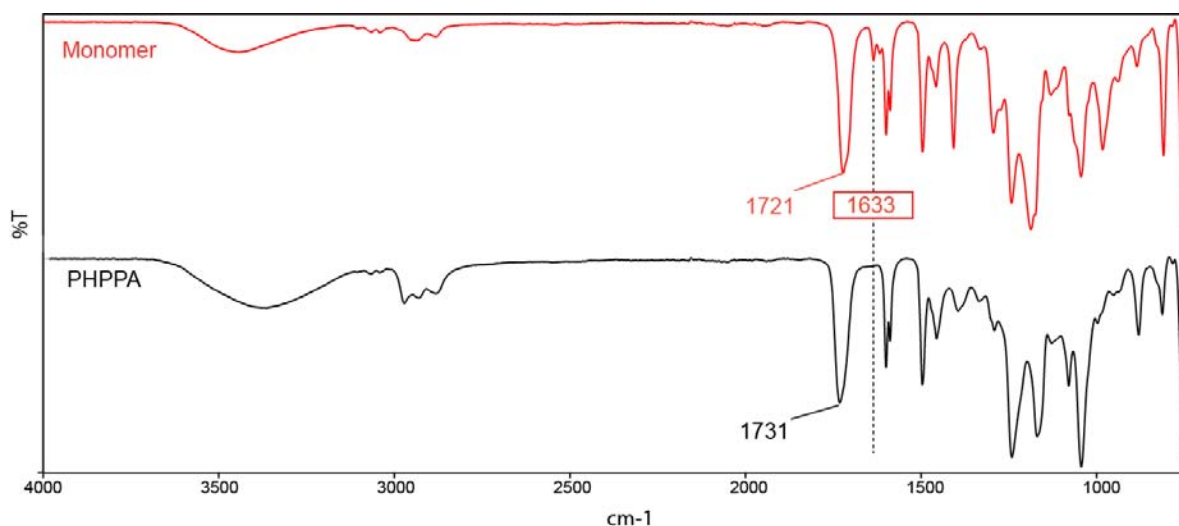


Figure IV.25. ATR-IR spectra of (a) the monomer, HPPA and (b) the polymer, PHPPA.

Figure IV.25 presents the ATR-IR spectra of the HPPA monomer and the corresponding polymer. After polymerization, the carbonyl stretching band of the monomer at 1721 cm^{-1} shifted to 1731 cm^{-1} and the relative intensity of the C-H stretching bands between 2850 and 3000 cm^{-1} increased. Furthermore, the disappearance of the C=C stretching band at 1633 cm^{-1} in the spectra of the polymerized sample clearly indicates that the polymerization was successful.

IV.2.2.1.2 Functionalization of CNTs

As any impurities or the various oxygen containing groups were suspected to hinder the grafting of the polymer onto the CNT sidewall, the CNTs were purified using H_2SO_4 that does not introduce such groups. The grafting of PNVF and PHPPA to MWCNTs was carried out by dispersing the CNTs with the aid of ultrasonication in a solution of the corresponding monomer and polymerizing with AIBN as radical initiator using the determined conditions. As produced PNVF grafted CNTs were further treated with base to hydrolyze the amide groups to amine. The separation of the hydrolysis by-product could be carried out by simply washing the PVA-grafted CNTs several times with distilled water and ethanol. FTIR spectroscopic analysis provided additional evidence that the hydrolysis was successful (Figure IV.26). The strong amide $\text{C}=\text{O}$ stretching band at 1674 cm^{-1} on the spectrum of CNT–PNVF decreased sharply after hydrolysis and N–H stretching band appeared at 3458 cm^{-1} . The elemental analysis of the CNT–PVA sample gave about 4.5 wt.% N atom.

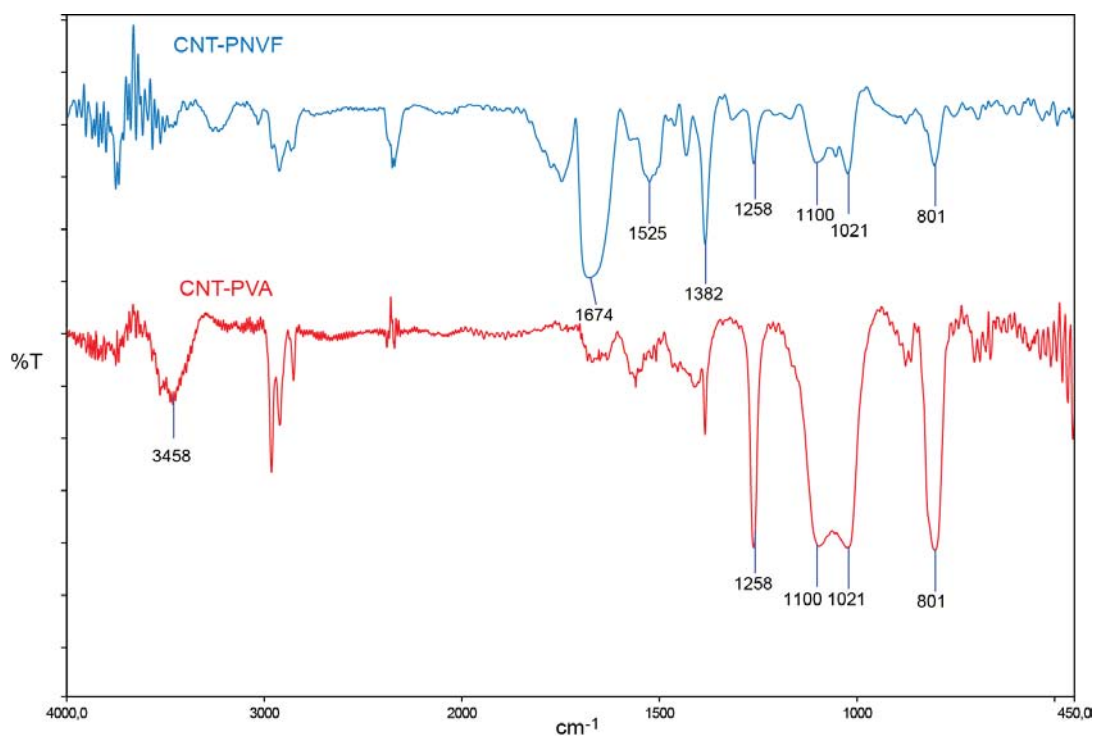


Figure IV.26. FTIR spectra of CNT–PNVF (top) and CNT–PVA (bottom).

TGA measurements were performed to determine the amount of polymer grafted to the CNTs. As determined by the weight losses of the TGA curves in Figure IV.27), the polymer content was 14 wt.% and 10 wt.% for CNT–PVA and CNT–PHPPA, respectively.

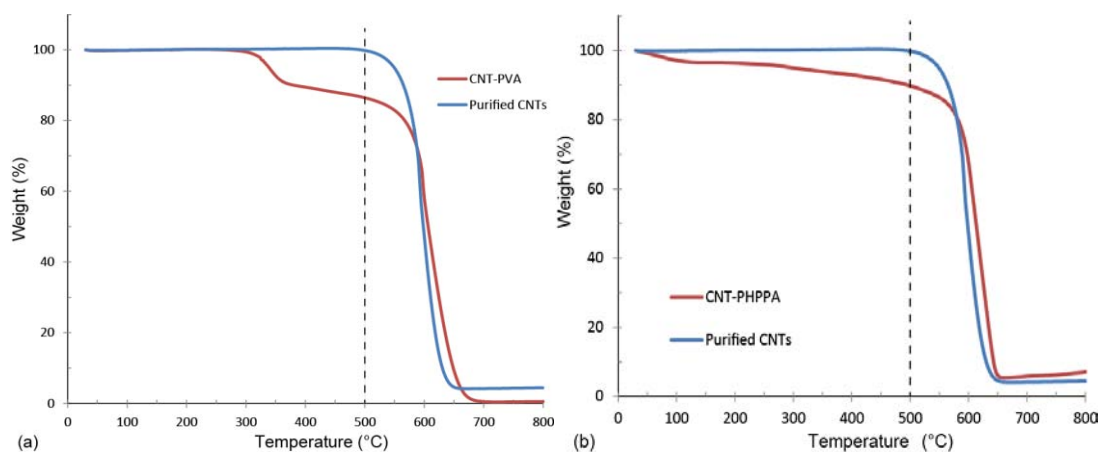
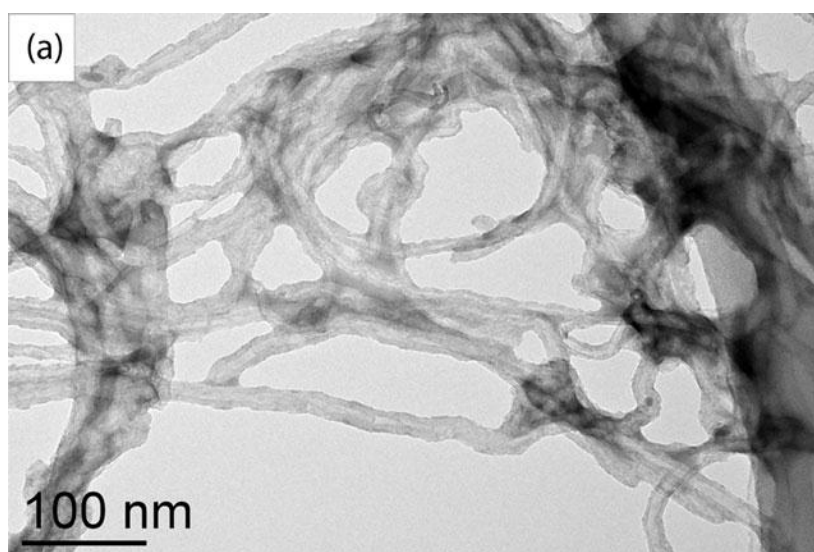
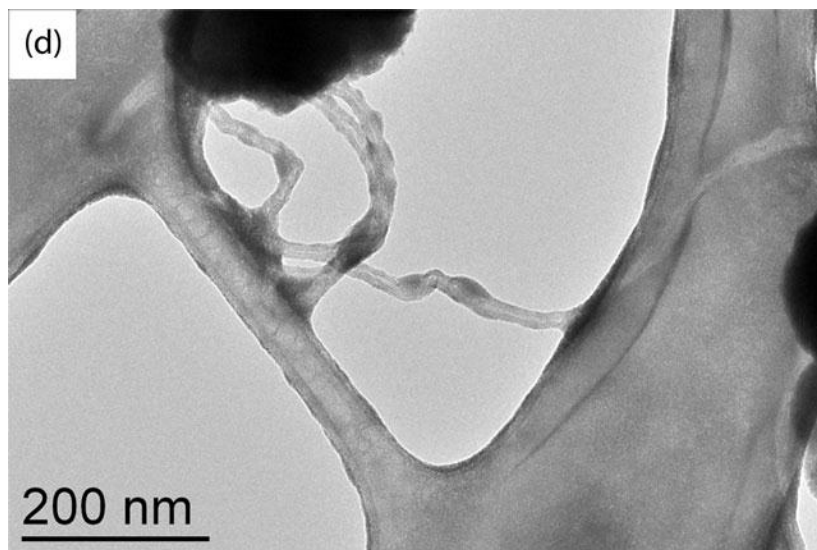
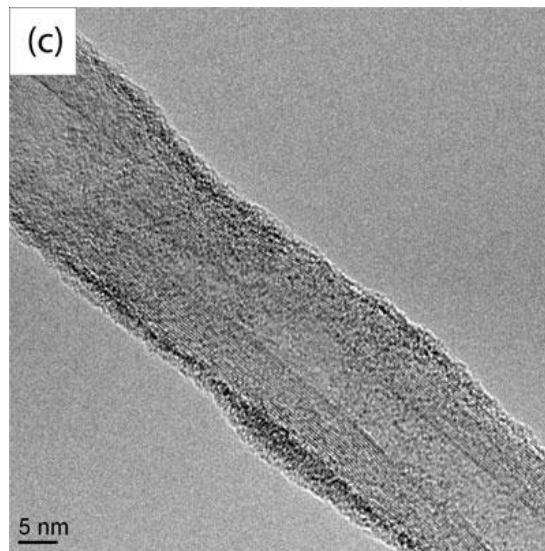
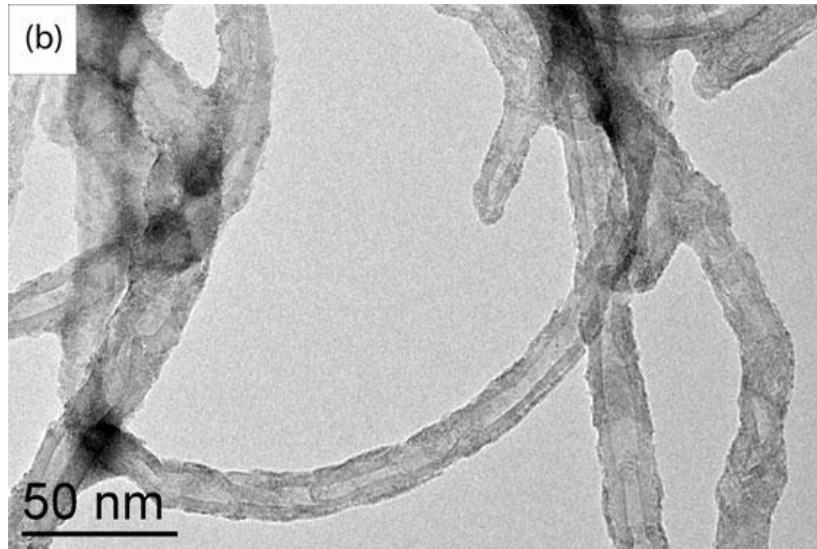


Figure IV.27. TGA curves of purified CNTs and (a) CNT–PVA, (b) CNT–PHPPA.

Figure IV.28 shows the TEM images of PVA and PHPPA grafted CNTs. We enhanced the image contrast for polymers by using a staining agent. The polymer layers with darker contrast are clearly observed in the TEM images with a varying thickness of up to 10 nm.





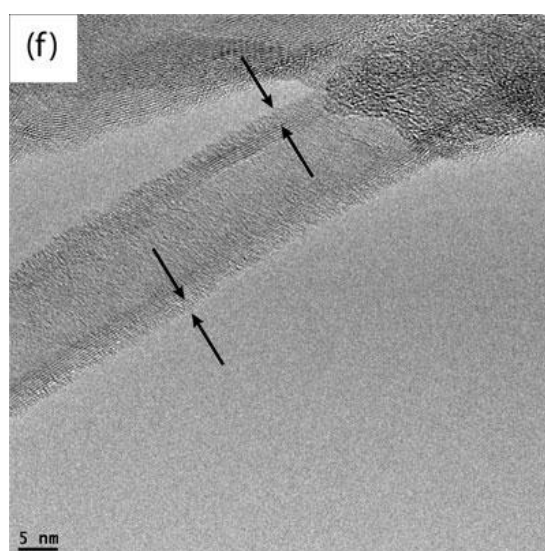
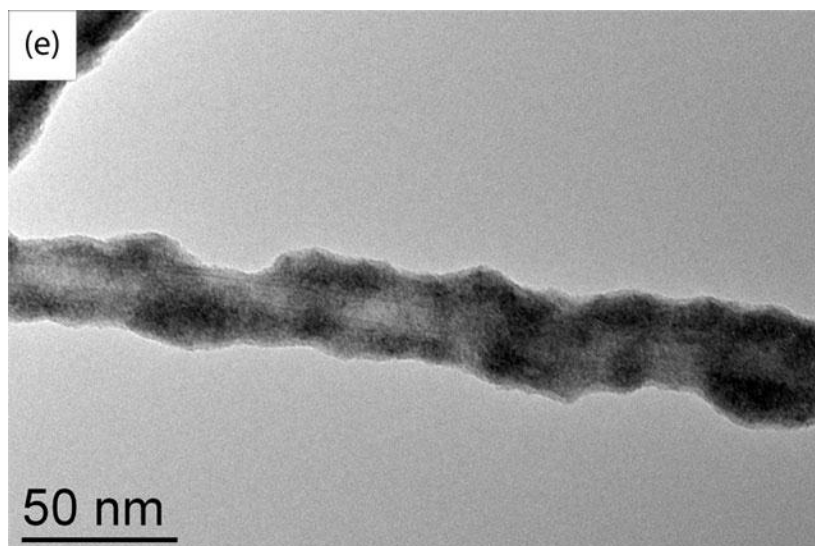


Figure IV.28. TEM images of (a-c) CNT–PVA with phosphotungstic acid staining, and CNT–PHPPA with (d-e) RuO₄ and (f) phosphotungstic acid staining.

We also studied the effect of the grafted polymers on the Raman spectrum of the CNTs. Figure IV.29 shows the Raman spectra of the purified CNTs and CNTs grafted with PVA and PHPPA. Purified CNTs exhibit the so-called G-band at 1587 cm^{-1} and D-band at 1328 cm^{-1} . The D-band is due to defect and disorder sites in the hexagonal framework of CNT walls. The I_D/I_G ratio is 1.64 for the purified CNTs and increases to 1.75 and 1.73 for the CNTs grafted with PVA and PHPPA, respectively. Such kind of surface functionalization enhanced D-band intensity has been reported in many studies and has been directly associated with covalent

grafting [43-46]. However, the sp^3 carbons of the polymer layer on the CNTs can also contribute to the D-band. Therefore, we carried out control experiments by mixing purified CNTs with the polymers at room temperature. We observed an increase (1.83) and a decrease (1.50) in the I_D/I_G ratio of the CNTs mixed with PHPPA and PVA, respectively. This shows that different types of polymers used for CNT functionalization can differently affect the Raman spectrum of the CNTs. Therefore, the I_D/I_G ratio cannot be used as a direct evidence of covalent grafting for polymers.

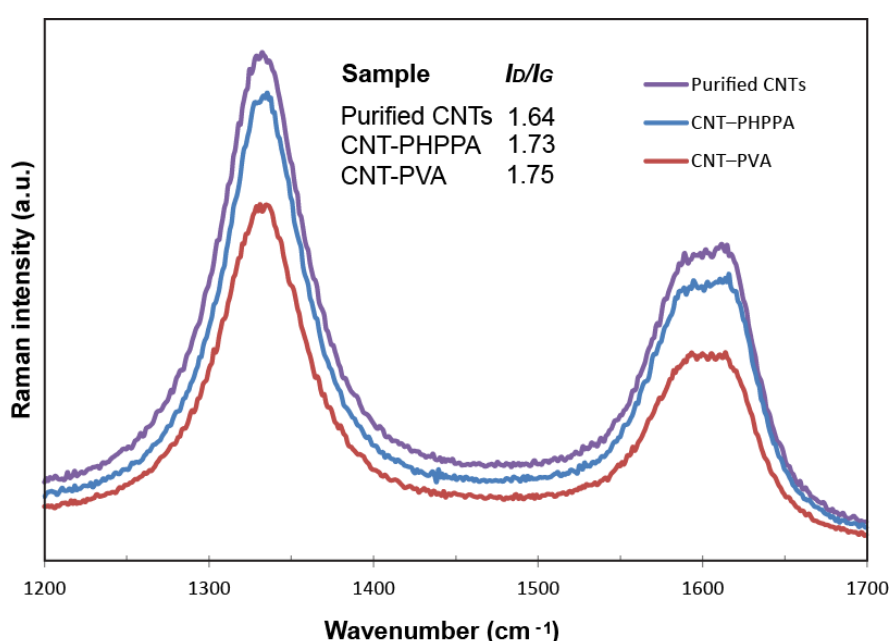


Figure IV.29. Raman spectra of the purified and polymer grafted CNTs.

The dispersibility of the resulted CNTs was tested in the suitable solvents (Figure IV.30). The CNT-PHPPA showed good dispersibility in THF, a good solvent for PHPPA, whereas the pristine CNTs quickly precipitated after sonication. Due to the abundant amino groups, the PVA functionalized CNTs dispersed easily in water with the aid of mild sonication. The particle size distribution curve of the CNT-PVA in water was obtained from the laser diffraction particle size analysis (Figure IV.31). The curve shows that the 28 vol.% of the

CNT bundles have a mean diameter of less than 10 μm . This fraction can be separated by a simple centrifugation for further processing.

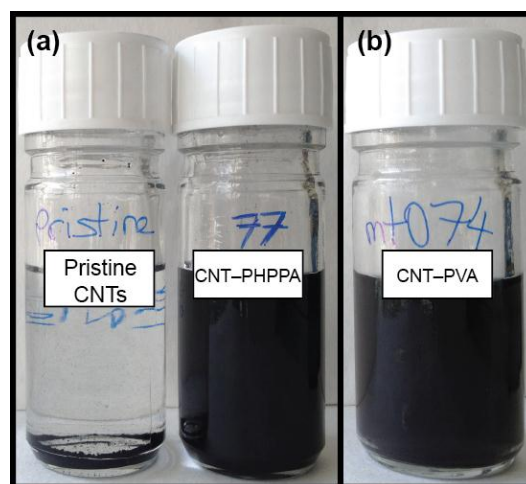


Figure IV.30. Dispersions of (a) pristine CNTs (left) and CNT-PHPPA (right) in DCM and (b) CNT-PVA in water (0.5 g L^{-1}) upon standing for one hour after sonication.

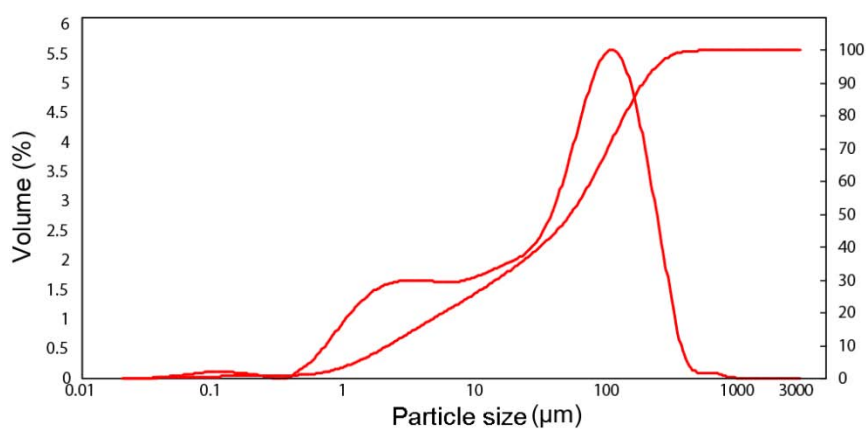


Figure IV.31. Size distribution curve of CNT-PVA in water.

The polymers formed in the presence of 5 wt.% CNTs were recovered and characterized. Their properties were compared with those of the polymers synthesized in the absence of CNTs using the same conditions. The glass transition temperatures (T_g) are given in Table 3.

Table 3. Glass transition temperatures of the polymers in the presence of, or without, CNTs.

Sample	T_g (°C) (from DSC)
PNVF	125.4
PNVF <i>in situ</i> polymerized	147.3
PHPPA	25.5
PHPPA <i>in situ</i> polymerized	18.1

We also measured the molecular weights of the polymers to examine the effect of CNT on the polymerization reaction by size-exclusion chromatography (SEC). The results of SEC analysis are summarized in Table 4. It is observed that the molecular weight of both polymers are decreased (by 37%, M_w) if polymerized in the presence of CNTs.

Table 4. Results of SEC analysis of the polymers prepared in the presence of, or without, CNTs.

Sample	M_w (g mol ⁻¹)	M_n (g mol ⁻¹)	Polydispersity index, M_w/M_n
PNVF	36940	21790	1.69
PNVF <i>in situ</i> polymerized	23270	14160	1.64
PHPPA	12350	6378	1.94
PHPPA <i>in situ</i> polymerized	7765	4362	1.78

As the AIBN quantity, monomer concentration, solvent, reaction time and temperature were the same for both polymers synthesized in the presence of, or without, CNTs, it is not the reaction parameters that lead to the difference in the polymer molecular weight. This result suggests that the CNTs obstruct the further polymerization of the PNVF and PHPPA

molecules as reported by some groups [47, 48] for poly(methyl methacrylate). Furthermore, it was observed that the molecular weight of the polymer decreases with the increase of the CNT content. The proposed processes of free radical polymerization in the presence of CNTs are illustrated in Figure IV.32.

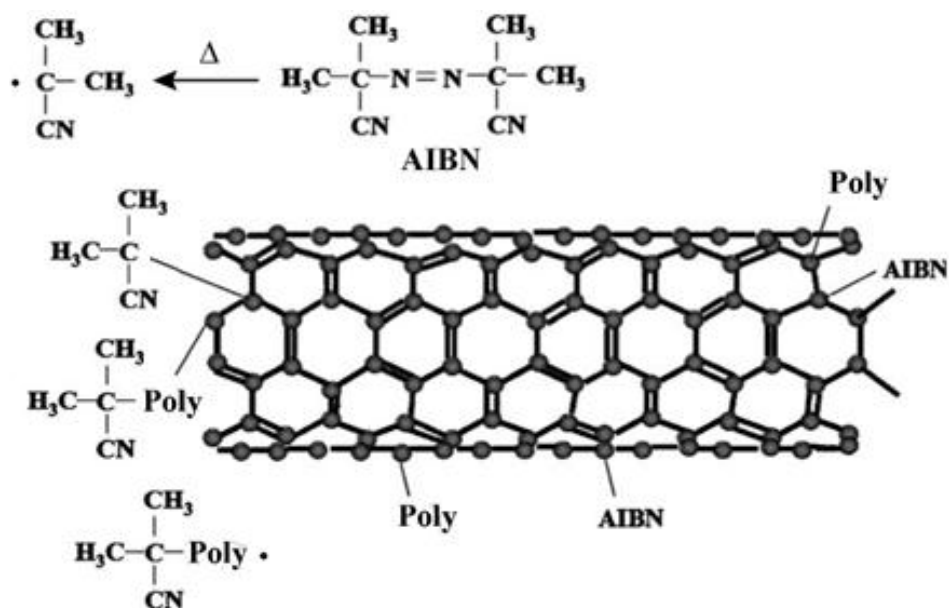


Figure IV.32. Susceptible processes of radical polymerization in the presence of CNTs.

The primary radicals formed by thermal initiation could react either with the vinyl monomers, thus initiating the polymerization, or with the π bonds of the CNTs. Subsequently, there are four possible scenarios [47, 48]: (i) the polymerization will be terminated by the disproportionation of two growing polymer chains, (ii) a growing polymer chain will covalently bind to the surface of the CNTs by the attack of an active polymer chain end to the carbon skeleton, (iii) polymerization inhibition by chain termination and (iv) polymerization of the monomers by radicals present on the CNT surface. The above scenarios can take place simultaneously and/or competitively, leading to a mixture of free polymer chains and polymer grafted CNTs. The third scenario occurs if the free radical of a growing polymer chain is transferred to the nanotubes. This ends the polymer growth, resulting in relatively low

molecular weight polymer. According to Liu [49], the fourth scenario is not favorable. The author claims that it requires more activation energy to break the π -bonds on the CNT surface with the initiator. Therefore, it is assumed that most of the grafted polymer chains results from the breaking of the π -bonds on the CNT surface with the polymer free radicals. Another scenario is also possible if CNTs contain hydroxyl groups. These groups introduced to the CNT skeleton or to the carbonaceous impurities during oxidation can act as a scavenger of radicals as shown by Gonçalves et al. [48]. Partial loss of the initiation activity results also in polymerization retardation. However, in this study we used a purification procedure, which does not oxidize the CNT surface.

Then, in our case, it is likely that the macromolecule radicals attack and activate the CNT surface. In addition, the grafted chains generate active radicals on the CNT surface which can also initiate other monomers. On the other hand, polymer chains can also be terminated by the scavenging effect of the CNT structure, leading to relatively short, ungrafted polymer chains.

IV.2.2.2 Functionalization of CNTs by “defect site” chemistry

Commercial glycidyl terminated epoxy resin with a M_n value of 355 was used for the modification of CNT surface. Low molecular weight was preferred to favor high grafting density. Furthermore, as chain ends are terminated by epoxy groups, CNTs can be interconnected if both ends interact. To minimize the formation of the interconnected CNTs, an excess amount of resin had to be used. The low viscosity of the resin ($T_g = -17.6$ °C) enabled to use the resin as reaction solvent. The grafting of the phenoxy onto the CNTs was achieved through blending the nitric acid oxidized CNTs and the resin at 80 °C (Figure IV.33). As mild heating was used, tributylamine (NBu₃) was added to the reaction mixture as activator.

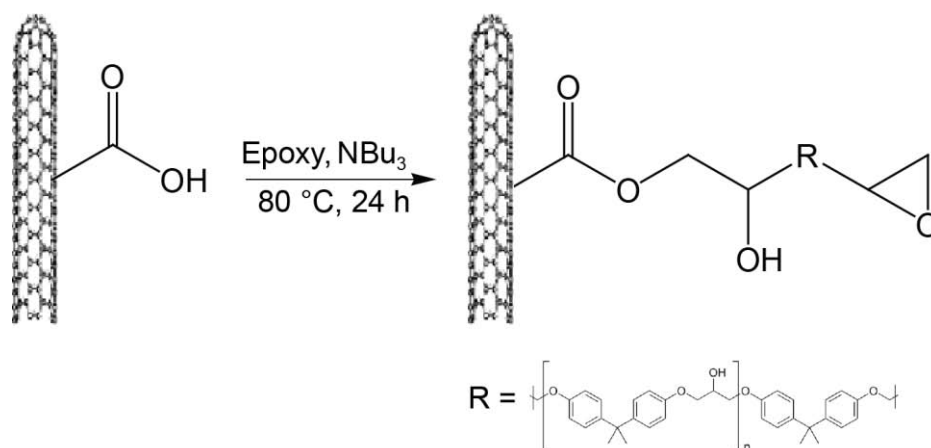


Figure IV.33. Illustration of the epoxy grafting to the CNT surface.

FTIR analysis was used to verify the successful grafting. The spectrum of the epoxy grafted CNTs resembles that of the neat epoxy, but with the presence of a carbonyl band at around 1717 cm^{-1} (Figure IV.33). Peaks located at 2920 cm^{-1} , 2850 cm^{-1} , 1457 cm^{-1} , are attributed to the C–H stretching, while the band at around 1235 cm^{-1} is due to the C–O vibration of aryl ethers [32]. The grafting involves the transformation of carboxylic acid groups to ester groups. As shown in Figure IV.34, the carbonyl bands of the CNT samples are quite broad with a peak at around 1717 cm^{-1} . No indication of the acid to ester conversion could be obtained from this peak. It is also possible that not all the carbonyl groups reacted with the epoxy resin. However, the appearance of a band at 1100 cm^{-1} , corresponding to the C–O bond formation between the carboxylic acid and the epoxide ring suggests the presence of a covalent grafting. The opening of the terminal epoxy rings during the grafting reaction should reduce the intensity of the C–O stretching band at 910 cm^{-1} [50]. The decrease in the relative intensity of this band that is observed in the spectrum of the CNT–epoxy provides further evidence for the covalent grafting.

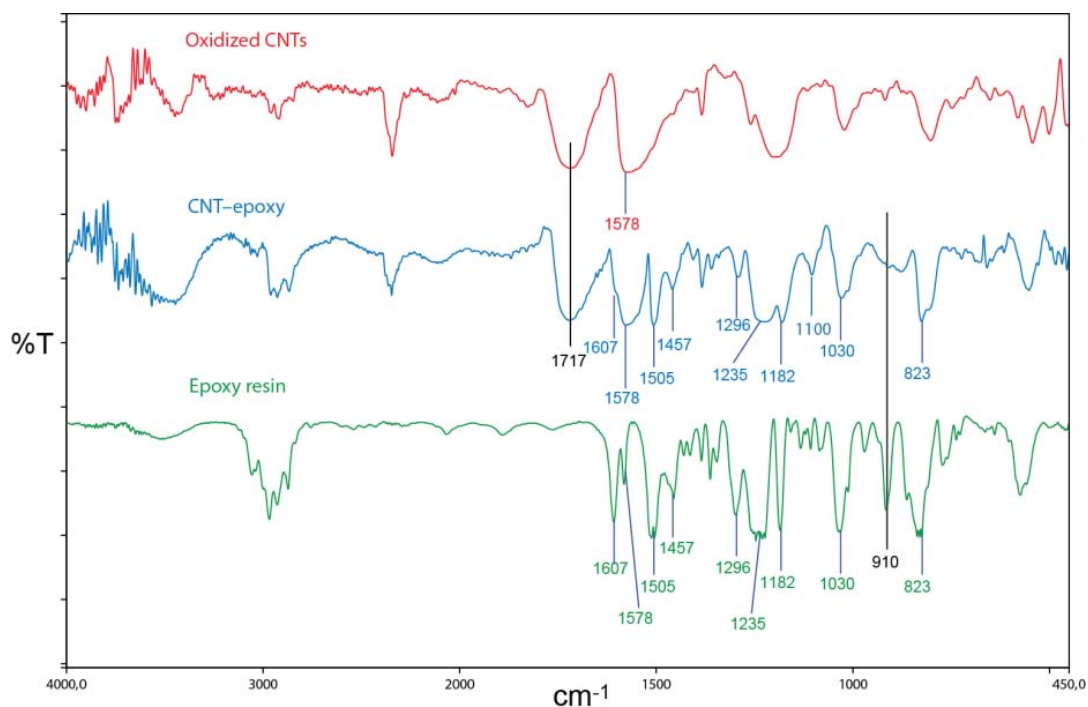


Figure IV.34. FTIR spectra of the oxidized CNTs, CNT–epoxy and neat epoxy resin.

TGA curves in Figure IV.35 shows the weight losses of the oxidized CNTs and the CNT–epoxy heated to 800 °C under air. If the mass loss of the CNTs at 500 °C is used as reference, the mass loss of the CNTs due to the grafted fragments is about 12 wt.% and 30 wt.% for the oxidized CNTs and the epoxy grafted CNTs, respectively. Knowing the M_n of the commercial epoxy and the weight loss due to the grafted epoxy fraction (18 wt.%), the grafting density is calculated to be roughly 0.51 mmol/g CNT.

The grafting degree was also determined using acid–base titrations. Titration with NaOH gives the amount of the total acidic sites of CNTs, including carboxylic acids, lactones and phenols. The difference between the initial and final concentration of the acidic sites determined by titration will give the number of grafted epoxy chains. The titration results are given in Table IV.5.

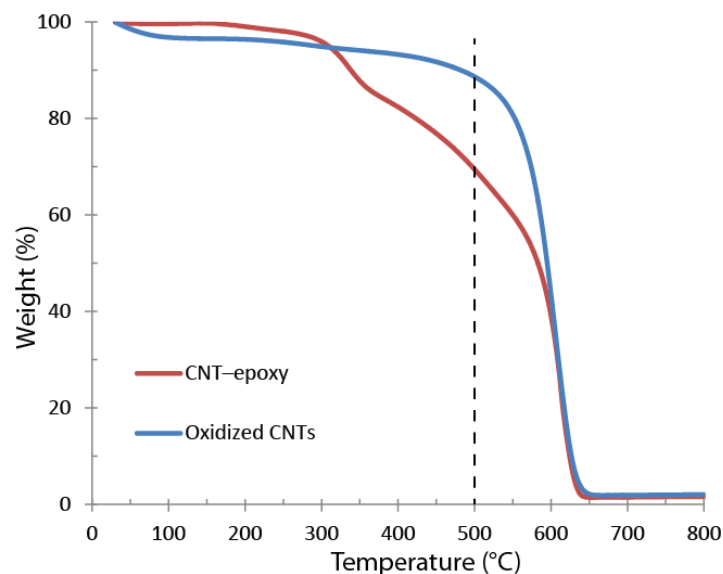


Figure IV.35. TGA curves of oxidized CNTs and CNT-epoxy.

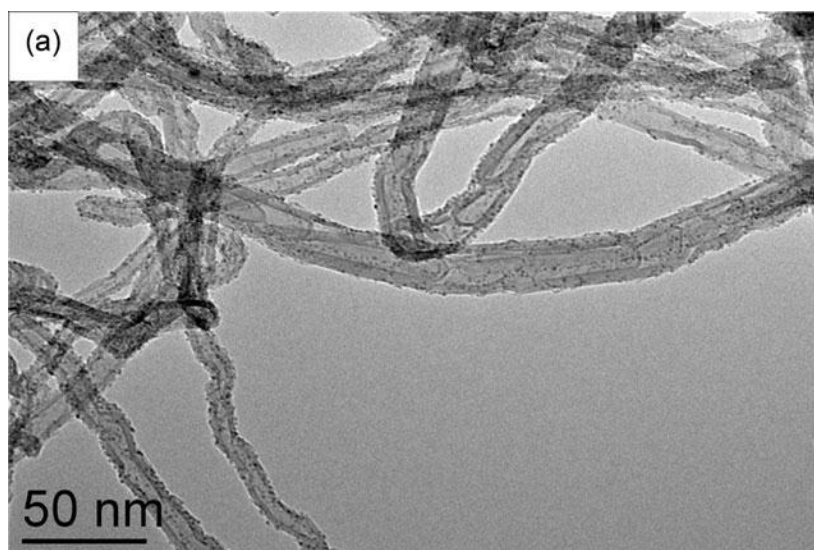
Table IV.5. Acidic site concentration of the CNT samples determined by chemical titration.

Sample	Acidic site concentration (mmol/g CNT)
Oxidized CNTs	1.37
CNT-epoxy	0.38
Oxidized CNTs + epoxy	1.12

Titration of the CNTs showed that 1 g oxidized CNTs used in this study contains 1.37 mmol acidic sites. Upon reaction with the epoxy resin, the acid concentration of the sample reduces to 0.38 mmol per 1 g functionalized CNTs. For a reliable comparison, based on the weight loss from the TGA, a mechanical mixture of oxidized CNTs and epoxy resin with an overall epoxy content of about 18 wt.% was prepared by stirring the CNTs and the resin in THF at room temperature and evaporating the solvent. The titration of the control sample showed an

acid concentration of 1.12 mmol/g CNT. This means that around 66% of the acid functions in the oxidized CNTs were consumed for the epoxy grafting. Similarly, the grafting density is calculated to be roughly 1 epoxy chain for 100 C atoms of the nanotube.

Figure IV.36 shows the TEM micrographs of the epoxy grafted CNTs. In order to increase the contrast of the grafted polymer, the sample was treated with a TEM staining agent. The TEM analysis revealed that the morphology of the functionalized CNTs is different from the previously studied polymer coated CNTs. The surface of the epoxy grafted CNTs is coated with many nanosized particles. Indeed, it should be noted that the chain length of the epoxy used in this study is quite small for a polymer; it has an average repeating unit, n , of around 1.4. Therefore, it would be more appropriate to refer to it as oligomer. These images show that the grafted oligomers have been homogeneously distributed on the surface of the CNTs. The epoxy grafted sample does not show good dispersibility in solvents such as THF that solubilizes the epoxy resin, most likely due to the short chains.



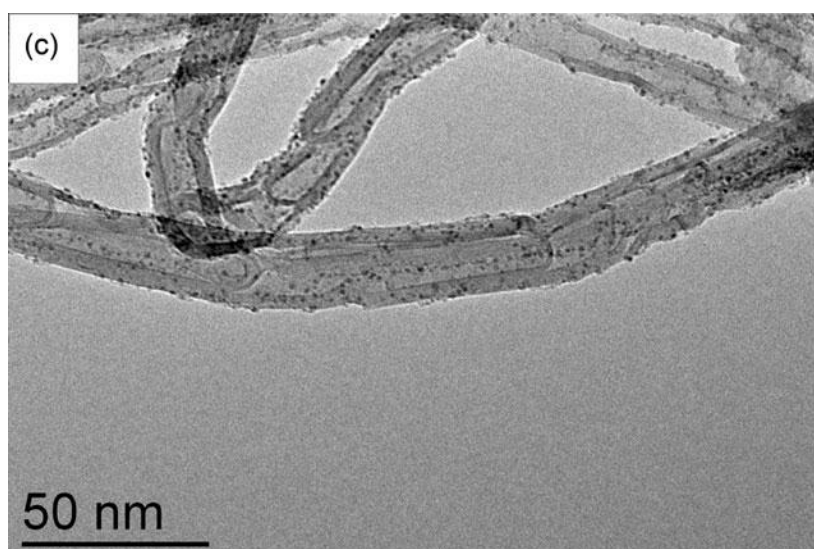
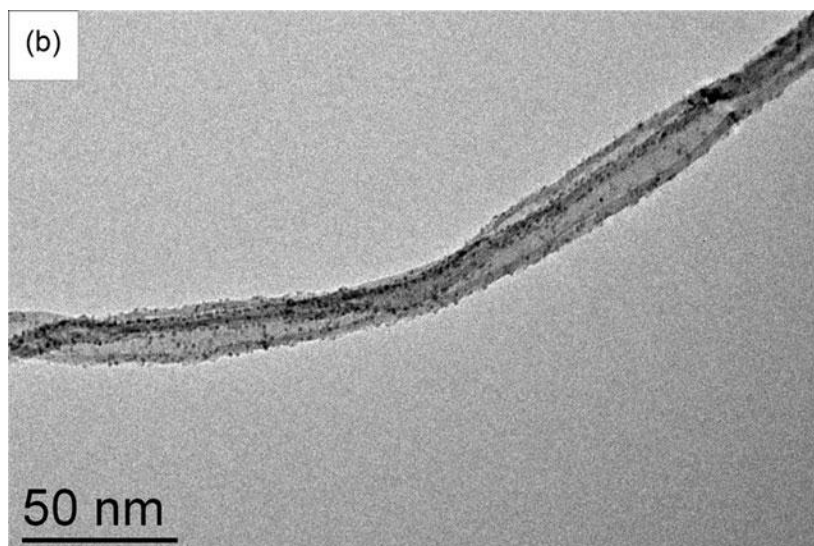


Figure IV.36. (a-c) TEM images of epoxy grafted CNTs.

As shown in the Raman spectra of Figure IV.37, the oxidized CNTs show a D-band at 1334 cm^{-1} and a G-band at 1588 cm^{-1} . After epoxy grafting, the G-band shifts slightly to 1585 cm^{-1} . Furthermore, the D- to G-band intensity ratio (I_D/I_G) decreases from 1.76 to 1.59. While a similar red shift was observed for the mechanical CNT/epoxy mixture, the I_D/I_G ratio remained similar compared to the oxidized CNTs. This indicates that covalent grafting of the epoxy alters the Raman features of the CNTs. A Raman study [51] carried out on polyurea functionalized MWCNTs revealed that the Raman signals of functionalized CNTs are

strongly dependent on the given polymers and their structures. However, the authors concluded that detailed studies are needed to fully understand the effect of polymer functionalization of CNTs in terms of Raman spectra and the possible CNT–polymer energy transferring mechanism.

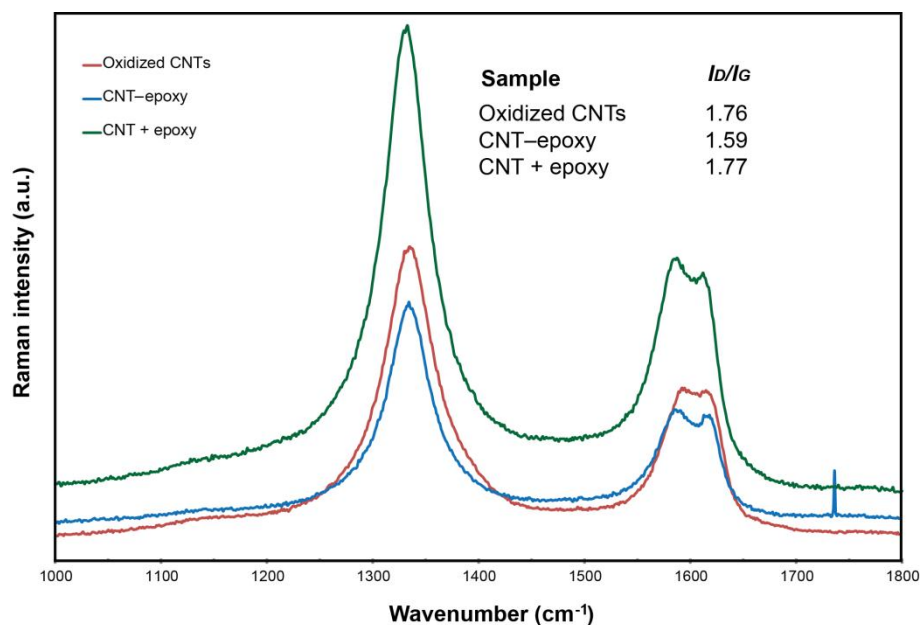


Figure IV.37. Raman spectra of oxidized CNTs, epoxy grafted CNTs and CNT/epoxy mixture.

IV.3 Conclusions

Two covalent grafting approaches were used to functionalize CNTs with polymers. It has been shown that PA functionalization of the CNTs results in low amounts of polymer which is probably due to both the retarding effect of the nanotubes on the polymerization rate and the low activation of the polymerization in the absence of *N*-acetylcaprolactam. Despite this, at only 1 wt.% CNT loading, PA grafted CNTs increased the mechanical properties of the PA composites more than the pristine or amine functionalized CNTs. The free radical polymerization of the polymerized ionic liquids did not sufficiently proceed from the surface

of the IL grafted CNTs. The solvent dispersibility of the CNTs did not improve. In the absence of monomer, the radically initiated IL grafted CNTs were cross-linked to each other.

On the other hand, "grafting to" approach offered a simple and direct method to obtain three kinds of polymer functionalized CNTs. Particularly, radical addition reaction did not require any CNT modification prior to polymerization and proceeded well with both vinyl imidazolium monomers used (N-vinylformamide and 2-hydroxy-3-phenoxypropyl acrylate) studied. Subsequent base hydrolysis of the CNT-PNVF allowed us to prepare CNTs bearing a large amount of amine groups. We also showed that the molecular weight of the polymers was reduced in the presence of CNTs during the *in situ* polymerization. This effect could be due to the active participation of the CNTs in the radical polymerization process and/or to simply the steric hindrance arising from the CNTs. Lastly, we showed that epoxy chains can be grafted onto the CNT surface in a controllable manner using the "defect site" chemistry. Using a low molecular weight polymer, we obtained epoxy functionalized CNTs with a high grafting density: ~74% of the acid sites on the CNTs were reacted.

References

- [1] Homenick CM, Lawson G, Adronov A. Polymer Grafting of Carbon Nanotubes Using Living Free-Radical Polymerization. *Polym Rev* 2007;47(2):265-90.
- [2] Sahoo NG, Rana S, Cho JW, Li L, Chan SH. Polymer nanocomposites based on functionalized carbon nanotubes. *Prog Polym Sci* 2010;35(7):837-67.
- [3] Chen P, Kim H-S, Jin H-J. Preparation, properties and application of polyamide/carbon nanotube nanocomposites. *Macromol Res* 2009;17(4):207-17.
- [4] Gao J, Itkis ME, Yu A, Bekyarova E, Zhao B, Haddon RC. Continuous Spinning of a Single-Walled Carbon Nanotube–Nylon Composite Fiber. *Am Chem Soc* 2005;127(11):3847-54.
- [5] Liu, Phang IY, Shen L, Chow SY, Zhang W-D. Morphology and Mechanical Properties of Multiwalled Carbon Nanotubes Reinforced Nylon-6 Composites. *Macromolecules* 2004;37(19):7214-22.
- [6] Gao J, Zhao B, Itkis ME, Bekyarova E, Hu H, Kranak V, et al. Chemical Engineering of the Single-Walled Carbon Nanotube–Nylon 6 Interface. *J Am Chem Soc* 2006;128(23):7492-6.
- [7] Yan D, Xie T, Yang G. In situ synthesis of polyamide 6/MWNTs nanocomposites by anionic ring opening polymerization. *J Appl Polym Sci* 2009;111(3):1278-85.
- [8] Yan D, Yang G. A novel approach of in situ grafting polyamide 6 to the surface of multi-walled carbon nanotubes. *Mater Lett* 2009;63(2):298-300.
- [9] Yang M, Gao Y, Li H, Adronov A. Functionalization of multiwalled carbon nanotubes with polyamide 6 by anionic ring-opening polymerization. *Carbon* 2007;45(12):2327-33.

- [10] Qu L, Veca LM, Lin Y, Kitaygorodskiy A, Chen B, McCall AM, et al. Soluble Nylon-Functionalized Carbon Nanotubes from Anionic Ring-Opening Polymerization from Nanotube Surface. *Macromolecules* 2005;38(24):10328-31.
- [11] Carraher CE. Synthesis of caprolactam and Nylon 6. *J Chem Educ* 1978;55(1):51.
- [12] Solhy A, Machado BF, Beausoleil J, Kihn Y, Gonçalves F, Pereira MFR, et al. MWCNT activation and its influence on the catalytic performance of Pt/MWCNT catalysts for selective hydrogenation. *Carbon* 2008;46(9):1194-207.
- [13] Penu C, Hu G-H, Fonteix C, Marchal P, Choplin L. Effects of carbon nanotubes and their state of dispersion on the anionic polymerization of ϵ -caprolactam: 1. Calorimetry. *Polym Eng Sci* 2010;50(12):2287-97.
- [14] Basiuk VA, Salvador-Morales C, Basiuk EV, Jacobs RMJ, Ward M, Chu BT, et al. 'Green' derivatization of carbon nanotubes with Nylon 6 and l-alanine. *J Mater Chem* 2006;16(45):4420-6.
- [15] Ventura DN, Stone RA, Chen K-S, Hariri HH, Riddle KA, Fellers TJ, et al. Assembly of cross-linked multi-walled carbon nanotube mats. *Carbon* 2010;48(4):987-94.
- [16] Zhang J, Jiang D. Interconnected multi-walled carbon nanotubes reinforced polymer-matrix composites. *Compos Sci Technol* 2011;71(4):466-70.
- [17] Cha SI, Kim KT, Lee KH, Mo CB, Jeong YJ, Hong SH. Mechanical and electrical properties of cross-linked carbon nanotubes. *Carbon* 2008;46(3):482-8.
- [18] Wang C, Zhou G, Liu H, Wu J, Qiu Y, Gu B-L, et al. Chemical Functionalization of Carbon Nanotubes by Carboxyl Groups on Stone-Wales Defects: A Density Functional Theory Study. *J Phys Chem B* 2006;110(21):10266-71.
- [19] Gerber I, Oubenali M, Bacsá R, Durand J, Gonçalves A, Pereira MFR, et al. Theoretical and Experimental Studies on the Carbon-Nanotube Surface Oxidation by Nitric

Acid: Interplay between Functionalization and Vacancy Enlargement. *Chem Eur J* 2011;17(41):11467-77.

[20] Mylvaganam K, Zhang LC. Nanotube Functionalization and Polymer Grafting: An ab Initio Study. *J Phys Chem B* 2004;108(39):15009-12.

[21] Lou X, Detrembleur C, Sciannamea V, Pagnouille C, Jérôme R. Grafting of alkoxyamine end-capped (co)polymers onto multi-walled carbon nanotubes. *Polymer* 2004;45(18):6097-102.

[22] Wu H-X, Tong R, Qiu X-Q, Yang H-F, Lin Y-H, Cai R-F, et al. Functionalization of multiwalled carbon nanotubes with polystyrene under atom transfer radical polymerization conditions. *Carbon* 2007;45(1):152-9.

[23] Guadagno L, De Vivo B, Di Bartolomeo A, Lamberti P, Sorrentino A, Tucci V, et al. Effect of functionalization on the thermo-mechanical and electrical behavior of multi-wall carbon nanotube/epoxy composites. *Carbon* 2011;49(6):1919-30.

[24] Ajayan PM, Stephan O, Colliex C, Trauth D. Aligned Carbon Nanotube Arrays Formed by Cutting a Polymer Resin—Nanotube Composite. *Science* 1994;265(5176):1212-4.

[25] Bose S, Khare RA, Moldenaers P. Assessing the strengths and weaknesses of various types of pre-treatments of carbon nanotubes on the properties of polymer/carbon nanotubes composites: A critical review. *Polymer* 2010;51(5):975-93.

[26] Spitalsky Z, Tasis D, Papagelis K, Galiotis C. Carbon nanotube–polymer composites: Chemistry, processing, mechanical and electrical properties. *Prog Polym Sci* 2010;35(3):357-401.

[27] Wang J, Fang Z, Gu A, Xu L, Liu F. Effect of amino-functionalization of multi-walled carbon nanotubes on the dispersion with epoxy resin matrix. *J Appl Polym Sci* 2006;100(1):97-104.

- [28] Zou W, Du Z-j, Liu Y-x, Yang X, Li H-q, Zhang C. Functionalization of MWNTs using polyacryloyl chloride and the properties of CNT–epoxy matrix nanocomposites. *Compos Sci Technol* 2008;68(15–16):3259-64.
- [29] Shen J, Huang W, Wu L, Hu Y, Ye M. The reinforcement role of different amino-functionalized multi-walled carbon nanotubes in epoxy nanocomposites. *Compos Sci Technol* 2007;67(15–16):3041-50.
- [30] Choi WJ, Powell RL, Kim DS. Curing behavior and properties of epoxy nanocomposites with amine functionalized multiwall carbon nanotubes. *Polym Compos* 2009;30(4):415-21.
- [31] Tseng C-H, Wang C-C, Chen C-Y. Functionalizing Carbon Nanotubes by Plasma Modification for the Preparation of Covalent-Integrated Epoxy Composites. *Chem Mater* 2006;19(2):308-15.
- [32] Chen W, Auad ML, Williams RJJ, Nutt SR. Improving the dispersion and flexural strength of multiwalled carbon nanotubes–stiff epoxy composites through β -hydroxyester surface functionalization coupled with the anionic homopolymerization of the epoxy matrix. *Eur Polym J* 2006;42(10):2765-72.
- [33] Wang S, Liang Z, Liu T, Wang B, Zhang C. Effective amino-functionalization of carbon nanotubes for reinforcing epoxy polymer composites. *Nanotechnology* 2006;17(6):1551.
- [34] Zhu J, Peng H, Rodriguez-Macias F, Margrave JL, Khabashesku VN, Imam AM, et al. Reinforcing Epoxy Polymer Composites Through Covalent Integration of Functionalized Nanotubes. *Adv Funct Mater* 2004;14(7):643-8.
- [35] Li S, Wang F, Wang Y, Wang J, Ma J, Xiao J. Effect of acid and TETA modification on mechanical properties of MWCNTs/epoxy composites. *J Mater Sci* 2008;43(8):2653-8.

- [36] Yang K, Gu M, Guo Y, Pan X, Mu G. Effects of carbon nanotube functionalization on the mechanical and thermal properties of epoxy composites. *Carbon* 2009;47(7):1723-37.
- [37] Liu L, Etika KC, Liao K-S, Hess LA, Bergbreiter DE, Grunlan JC. Comparison of Covalently and Noncovalently Functionalized Carbon Nanotubes in Epoxy. *Macromol Rapid Commun* 2009;30(8):627-32.
- [38] Gojny FH, Wichmann MHG, Köpke U, Fiedler B, Schulte K. Carbon nanotube-reinforced epoxy-composites: enhanced stiffness and fracture toughness at low nanotube content. *Compos Sci Technol* 2004;64(15):2363-71.
- [39] Gojny FH, Wichmann MHG, Fiedler B, Schulte K. Influence of different carbon nanotubes on the mechanical properties of epoxy matrix composites – A comparative study. *Compos Sci Technol* 2005;65(15–16):2300-13.
- [40] Wang S, Liang R, Wang B, Zhang C. Reinforcing polymer composites with epoxide-grafted carbon nanotubes. *Nanotechnology* 2008;19(8):085710.
- [41] Teng C-C, Ma C-CM, Yang S-Y, Chiou K-C, Lee T-M, Chiang C-L. Thermal conductivity and dynamic mechanical property of glycidyl methacrylate-grafted multiwalled carbon nanotube/epoxy composites. *J Appl Polym Sci* 2012;123(2):888-96.
- [42] Gu L, Zhu S, Hrymak AN. Acidic and basic hydrolysis of poly(N-vinylformamide). *J Appl Polym Sci* 2002;86(13):3412-9.
- [43] Qin S, Qin D, Ford WT, Herrera JE, Resasco DE, Bachilo SM, et al. Solubilization and Purification of Single-Wall Carbon Nanotubes in Water by in Situ Radical Polymerization of Sodium 4-Styrenesulfonate. *Macromolecules* 2004;37(11):3965-7.
- [44] Hsin Y-L, Lai J-Y, Hwang KC, Lo S-C, Chen F-R, Kai JJ. Rapid surface functionalization of iron-filled multi-walled carbon nanotubes. *Carbon* 2006;44(15):3328-35.

- [45] Wu H-X, Qiu X-Q, Cai R-F, Qian S-X. Poly(N-vinyl carbazole)-grafted multiwalled carbon nanotubes: Synthesis via direct free radical reaction and optical limiting properties. *Appl Surf Sci* 2007;253(11):5122-8.
- [46] Hu H, Hui KN, Hui KS, Lee SK, Zhou W. Facile and green method for polystyrene grafted multi-walled carbon nanotubes and their electroresponse. *Colloids Surf A* 2012;396(0):177-81.
- [47] Jia Z, Wang Z, Xu C, Liang J, Wei B, Wu D, et al. Study on poly(methyl methacrylate)/carbon nanotube composites. *Mater Sci Eng A* 1999;271(1-2):395-400.
- [48] Goncalves G, Cruz SMA, Ramalho A, Gracio J, Marques PAAP. Graphene oxide versus functionalized carbon nanotubes as a reinforcing agent in a PMMA/HA bone cement. *Nanoscale* 2012;4(9):2937-45.
- [49] Liu P. Facile graft polystyrene onto multi-walled carbon nanotubes via in situ thermo-induced radical polymerization. *J Nanopart Res* 2009;11(4):1011-6.
- [50] Yang B-X, Shi J-H, Pramoda KP, Goh SH. Enhancement of stiffness, strength, ductility and toughness of poly(ethylene oxide) using phenoxy-grafted multiwalled carbon nanotubes. *Nanotechnology* 2007;18(12):125606.
- [51] Gao C, Jin YZ, Kong H, Whitby RLD, Acquah SFA, Chen GY, et al. Polyurea-Functionalized Multiwalled Carbon Nanotubes: Synthesis, Morphology, and Raman Spectroscopy. *J Phys Chem B* 2005;109(24):11925-32.

General conclusions and perspectives

General conclusions and perspectives

In this thesis, different functionalization methods have been investigated in order to improve the dispersibility of CNTs in solvents and polymer matrices. The grafting strategies are based on covalent and noncovalent interactions. For the noncovalent functionalization, we used « *in situ* polymerization » and « solution mixing », whereas « grafting to » and « grafting from » methods were used for the covalent approach.

The noncovalent functionalization has been studied with imidazolium based polymerized ionic liquids which adsorb onto the CNT surface *via* possible π - π and/or cation- π interactions. The results obtained during the solution dispersion tests as well as the particle size analysis indicate that the *in situ* method leads to a better CNT debundling, thus to a higher stability of the dispersions. We investigated the effect of both PIL cation and anion on the resulting hybrid material. Using the poly[VEIM]⁺ backbone, we observed a higher amount of adsorbed PIL in the case of Br⁻ compared to the bulky NTf₂⁻ anion, suggesting a steric effect. The nature of the cation has a more pronounced effect on the hybrid material. The use of protic polymerized ionic liquids (presence of the proton on the quaternized nitrogen atom), which show a strong H-bonding tendency, results in the agglomeration of the CNTs and a poor dispersion. The use of hydroxyl terminated PILs, which show a weaker intramolecular H-bonding, allows to obtain good dispersions, provided the *in situ* method is used. When the solution-mixing method is employed, we obtained a gel material loaded with CNT. Finally, we noticed a more pronounced influence of the nature of the PIL anion compared to the cation on the thermostability of the carbon nanotubes.

The effect of noncovalent PIL functionalization on the dispersion of the CNTs in a polymeric matrix has been evaluated in the case of polyetherimide (PEI). For the preparation of the

composites, dichloromethane has been used as casting solvent. The solubility issue has prompted us to perform an anion metathesis on the PIL (poly([VEIM]Br)) functionalized CNTs with sodium dodecylbenzene sulfonate. Pristine CNTs, nitric acid oxidized CNTs and CNT–PIL have been compared. The effect of CNT addition on the tensile, dynamic mechanical, thermal and electrical properties has been evaluated. Except the tensile properties, the other properties of the PEI composite were improved by CNT addition (0.1-3 wt.%). For thermal and dynamic mechanical properties, we did not observe any benefits of CNT functionalization compared to the pristine CNTs; whereas a negative effect was noticed for the electrical conductivity. The partial alignment of the CNT–PIL in the PEI matrix as well as the insulating properties of the PIL thin film could be at the origin of this phenomenon.

The covalent CNT functionalization has been studied for both “grafting from” and “grafting to” approaches. Using the former approach we functionalized CNTs with polyamide-6 (PA6) for the preparation of PA66/CNT–PA6 composites. In addition, PIL functionalization was performed with the [VHEIM]Cl grafted CNTs. The latter approach was employed to functionalize CNTs with polyvinylamine (PVA), poly(2-hydroxy-3-phenoxypropyl acrylate) (PHPPA) and poly(bisphenolA-*co*-epichlorohydrin) to be used as nanofillers in epoxy matrices. Despite a low level of polymerization on the CNT surface, the PA composites containing CNT–PA6 gave the best results in terms of Young’s modulus and yield strength compared to pristine and amine functionalized CNTs. For the PIL functionalization, we noticed a lack of reactivity of the grafted monomer compared to the free one; therefore, no measurable quantity of PIL was observed. However, in the absence of the monomer, the grafted monomers react with the initiator to produce cross-linked CNTs. Functionalization of CNTs with PHPPA and PVA produced thin films of polymer on the CNT surface, which improved the dispersion of the CNTs in the appropriate solvents. For the poly(bisphenolA-*co*-

epichlorohydrin) which is composed of short chains, well-dispersed nanoparticles of polymer were deposited on the CNT walls. Such functionalization does not allow good dispersion in solvents. In the frame of the P C project, the CNTs functionalized by the “grafting to” approach will be incorporated into epoxy matrices to evaluate the mechanical and electrical properties.

The results obtained during this exploratory work opened several perspectives. First of all, many new materials have been prepared among them we believe that: (i) the PIL gel, as well as, the PIL-CNT gel could find interesting application in electrochemistry (lithium batteries, sensors...), (ii) the cross-linked CNTs could be of interest for actuators and "bucky papers", (iii) due to their potential biocompatibility, CNT-PVA could be interesting as vectors for drug delivery or for other medical applications and (iv) the well dispersed polymer nanoparticles could be used for anchoring of metallic nanoparticles for sensors and catalysis. Finally, the preliminary results obtained with CNT polymer composites clearly show the importance of the processing method on the final properties of the material. Thus, the future work should include more efficient processing methods to take full advantage of CNT functionalization.

Chapter V:
Experimental details

Chapter V: Experimental details

V.1 Materials

Multi-walled carbon nanotubes produced via chemical vapor deposition (CVD) method (average number of walls 5-15, length 0.1-10 μm , diameter 10-15 nm, purity > 90%) were supplied from the same batch by Arkema, France under the trademark Graphistrength®. Samples of 3-ethyl-1-vinylimidazolium bromide ([VEIM]Br), 3-ethyl-1-vinylimidazolium bis(trifluoromethanesulfonyl)imide ([VEIM]NTf₂) and 1-Vinyl-3H-imidazolium bis(trifluoromethanesulfonyl)imide ([VHIM]NTf₂) were supplied by Solvionic, France. Larger quantities of [VEIM]Br and [VEIM]NTf₂ were synthesized using the procedures described below. Nitric acid (69%) was purchased from Panreac. 1-vinylimidazole (99%) was purchased from Alfa Aesar and distilled before use. 2-chloroethanol, lithium bis(trifluoromethanesulfonyl)imide (99%), tetrabutylammonium bromide (99+%), 2,2'-azobis(2-methyl-propionitrile) (98%), phosphotungstic acid hydrate and ruthenium tetroxide (0.5% solution in water) were purchased from Acros Organics. Sulfuric acid (95-97%), dry sodium hydride (95%), N-acetylcaprolactam (99%), polyethylene glycol (average M.W.= 6000), 2-bromoethane (98%), sodium dodecylbenzene sulfonate, caprolactam (99%), 1,8-diaminooctane (98%), N-Vinylformamide (98%), 2-hydroxy-3-phenoxypropyl acrylate and poly(bisphenolA-co-epichlorohydrin) (M_n ~355) were purchased from Aldrich. N-vinylformamide and 2-hydroxy-3-phenoxypropyl acrylate contain 25-55 ppm 4-hydroxy-TEMPO and 250 ppm monomethyl ether hydroquinone as polymerization inhibitor, respectively. These monomers were used as-received. Polyetherimide in pellet form (grade ULTEM 1000) was supplied by SABIC Innovative Plastics TM. All other solvents were used as received from Aldrich or Acros Chemicals.

V.2 Experimental procedures

V.2.1 Purification of CNTs

CNTs were suspended in a solution of concentrated sulfuric acid and water (1:1) and refluxed at 140 °C for 3 hours. Subsequently, the reaction mixture was filtered without cooling and the CNTs were washed with hot and cold distilled water until neutralization of the filtrate and dried in air at 130 °C for 48 days.

V.2.2 Preparation of oxidized CNTs

The purified CNTs were suspended in concentrated nitric acid (69%) and refluxed at 120 °C for 3 or 6 hours. After cooling, the CNTs were filtered, washed with distilled water until neutralization of the filtrate and dried in air at 130 °C for 48 days.

V.2.3 Acid–base titration of CNTs

100 mg of CNTs were stirred in a sodium hydroxide (NaOH) solution (40 mL, 0.01 M) in a plastic vial overnight. The NaOH concentration of the resulted mixture was determined by titration with a solution of hydrochloric acid (0.01 M). The acid concentration of the CNTs was calculated from the change between the initial and final concentrations of NaOH.

V.2.4 Preparation of ionic liquid monomers

V.2.4.1 Preparation of 1-vinyl-3-ethylimidazolium bromide, [VEIM]Br

2-bromoethane (120 g, 1.1 mol) was added dropwise to a solution of freshly distilled 1-vinylimidazole (89.90 g, 0.955 mol) in ethyl acetate (150 mL) under nitrogen atmosphere. The reaction mixture was stirred under N₂ at 60 °C for 4 h. The reaction mixture was diluted

with distilled water and separated from the solvents and unreacted vinylimidazole by distillation under reduced pressure, to give a viscous yellow oil in 77% yield.

V.2.4.2 Preparation of 1-vinyl-3-ethylimidazolium bis(trifluoromethanesulfonyl)imide, [VEIM]NTf₂

A solution of LiNTf₂ (22.10 g, 0.077 mol) in distilled water (50 mL) was added dropwise to 1-vinyl-3-ethylimidazolium bromide, [VEIM]Br (15.63 g, 0.077 mol) with vigorous stirring. The mixture was further stirred at room temperature for 30 min. The reaction mixture was extracted with DCM. The organic phase was washed five times with distilled water and dried under vacuum at 80 °C overnight to give a yellow oil in 80% yield. Activated carbon (5 wt.%) was added to the ionic liquid and the mixture was stirred at 70 °C for 4 days for decoloration.

V.2.4.3 Preparation of 1-(2-hydroxyethyl)-3-vinylimidazolium chloride, [VEHIM]Cl

Freshly distilled 1-vinylimidazole (10.00 g, 0.106 mol) was added dropwise to chloroethanol (16.00 g, 0.198 mol) at 65 °C under nitrogen atmosphere. The temperature is increased to 80 °C and the mixture was stirred under N₂ for 22 h. The reaction mixture was diluted with distilled ethanol and separated from the solvents and unreacted vinylimidazole by distillation under reduced pressure. The resulted brown viscous oil was stirred with activated carbon (5 wt.%) at 70 °C for 5 days to give a viscous yellow oil in 77% yield. ¹H NMR (300 MHz, D₂O): δ 3.91 (t, 2H), 4.33 (t, 2H), 5.39 (dd, J= 8.7, 2.8, 1H), 5.78 (dd, J= 15.6, 2.8, 1H), 7.12 (dd, J= 15.6, 8.7, 1H), 7.59 (t, J= 1.7, 1H), 7.77 (t, J= 1.8, 1H), 9.05 (s, 1H).

V.2.4.4 Preparation of 1-(2-hydroxyethyl)-3-vinylimidazolium bis(trifluoromethanesulfonyl)imide, [VEHIM]NTf₂

1-(2-hydroxyethyl)-3-vinylimidazolium chloride, [VEHIM]Cl, was dissolved in water and mixed with an aqueous solution of LiNTf₂ (2 mol. equivalent) at room temperature.

Immediately after mixing, the new monomer precipitated. It was soluble only in acetone among the solvents tested (DCM, methanol, ethanol, toluene, ethyl acetate, acetonitrile). ^1H NMR (300 MHz, acetone- d_6): δ 4.01 (q, 2H), 4.50 (t, 2H), 5.49 (dd, $J=7.4, 2.7$, 1H), 6.00 (dd, $J=14.3, 2.7$, 1H), 7.39 (dd, $J=11.63, 8.7$, 1H), 7.86 (t, $J=1.8$, 1H), 8.09 (t, $J=1.9$, 1H), 9.29 (s, 1H).

V.2.5 General procedure for the polymerization of ionic liquid monomers

Polymerized ionic liquids were synthesized by conventional free-radical polymerization. In a typical polymerization experiment, imidazolium monomer (5 g), and ethanol (acetone for [VEHIM]NTf₂, **4**) (5mL) were purged with N₂ for 30 min and AIBN (2 wt%) was added to the solution, purged with N₂ for another 10 min and stirred in an oil bath at 65 °C (85 °C for [VEHIM]NTf₂, **2**) for 3 hours. After polymerization, the mixture was diluted with the reaction solvent and was poured into water to precipitate the poly[VEIM]NTf₂ (**Poly2** 60%), poly[VIM]NTf₂ (**Poly3** 45%) and poly[VEHIM]NTf₂ (**Poly4** 57%). Acetonitrile was used similarly to precipitate the poly[VEIM]Br (**Poly1** 70%). The polymers were washed three times before drying under vacuum at 60 °C.

V.2.5.1 Preparation of poly[3-(2-hydroxyethyl)-1-vinylimidazole] bromide, poly[VEHIM]Br, Poly5

A solution of 1.5 g of tetrabutylammonium bromide in acetone was added dropwise to a solution of 1.8 g of poly[VEHIM]NTf₂ (**Poly 4**) in acetone in a round-bottom flask. After stirring for 30 min at room temperature, the resulting white-yellow solid (95%) was washed with acetone and dried at 80 °C.

V.2.6 Non-covalent functionalization of CNTs with polymerized ionic liquids

V.2.6.1 General procedure for solution-mixing

Polymer solutions (approximately 1:1 by volume) were prepared by dissolving the polymerized ionic liquids in ethanol (ethanol/acetone mixture for **poly2**). Carbon nanotubes at 5 wt.% loading of the polymer were added to the polymer solution. The mixture was sonicated for 1 h and then refluxed for 22 h at 65 °C (85 °C for **poly2**) under vigorous stirring. The mixture was subsequently filtered and washed with a solvent in which the polymer was soluble several times to thoroughly remove physically adsorbed polymer from the surface of the CNT. The final products, referred to as CNT–polyxa, were then dried in an oven at 120°C to remove the residual solvent.

V.2.6.2 General procedure for in situ polymerization

The non-covalent *in situ* functionalization of CNT was done by the following procedure. CNTs at 5 wt.% loading of the monomer were added to ethanol containing IL monomers (1:1 by volume) and 2 wt.% 2,2'-azobis(isobutyronitrile) (AIBN). After sonication for 1 h, the mixture was refluxed for 22 h at 65 °C (85 °C for **poly2**) under vigorous stirring and N₂ atmosphere. The reaction mixture was diluted, filtered and washed several times (water for CNT–**poly1b**; acetone otherwise) to thoroughly remove physically adsorbed polymer and unreacted monomer from the surface of the CNT and dried at 120°C. The final products thus obtained are referred to as CNT–polyxb.

V.2.6.3 Anion exchange of CNT–poly[VEIM]Br, CNT–poly1b

CNT–**poly1b** (1 g), CNT–poly[VEIM]Br prepared by *in situ* polymerization method, was added to distilled water (75 mL), and the solution was ultrasonicated for 30 min. Then, a solution of lithium bis(trifluoromethanesulfonyl)imide (1 g,) in distilled water (25 mL) was added dropwise to the CNT suspension with stirring. The dispersion was sonicated for another 10 min and stirred vigorously overnight in order to ensure the complete anion exchange. The resulted CNTs were thoroughly washed with distilled water and dried at 120 °C for 3 days.

V.2.6.4 General procedure for CNT–polymer gel preparation

CNT–polymer organogels containing 1, 3 and 5 wt% CNT with respect to the polymer were prepared as follows: The pristine CNTs were briefly (15 min) sonicated in acetone (34 times by weight relative to the polymer) to obtain a CNT dispersion. **Poly 4** was then added to the dispersion. The resulting gel mixture was sonicated for 1 h. The corresponding hydrogels were prepared by repeating the same procedure in pure water (70 times by weight relative to the polymer) followed by the addition of **Poly 5**.

V.2.6.5 Functionalization of CNTs with poly(3-vinyl-1-ethylimidazolium dodecylbenzene sulfonate), poly[VEIM]DBS

First CNT–poly[VEIM] was prepared using the general procedure for the *in situ* polymerization with the following quantities. CNTs = 4.0 g, [VEIM]Br = 73.0 g in ethanol = 100 mL, AIBN, 1.5 g. Then, 500 mg of CNT–poly[VEIM]Br were added to 75 mL of distilled water, and the solution was ultrasonicated with an ultrasonic probe at 25% amplitude for 10 min. Then, a solution of sodium dodecylbenzene sulfonate (500 mg) in distilled water (25 mL) was added dropwise to the CNT suspension with stirring. The dispersion was sonicated for another 10 min and stirred vigorously overnight in order to ensure the complete anion exchange. The resulted CNTs were thoroughly washed with distilled water and dried at 115 °C for 3 days.

V.2.7 Preparation of polyetherimide/carbon nanotube composite films

Polyetherimide (2.750 g) was dissolved in 12 mL of DCM by stirring continuously until the matrix polymer was completely dissolved. The oxidized CNTs were prepared by a 3 h nitric acid treatment at 120 °C and the acidic group concentration was 0.23 mmol/g CNT as determined by acid–base titration. Various amounts of pristine, acid-oxidized and CNT–poly[VEIM]DBS were then added to the polymer solutions, and the resulted dispersions were

ultrasonicated for 30 min. Then, they were casted into Teflon coated aluminum foil molds and the solvent was allowed to evaporate slowly at room temperature. All the composite films were further dried in a vacuum oven first at 100 °C for two days, then at 150 °C for one day to remove completely the residual solvent. Then, the obtained composites were compression molded under a pressure of 240 bars at 250 °C for 4 min. The thickness of the final films was between 0.45 and 0.50 mm. The CNT content in the final composite films varied from 0.1 wt % to 3 wt %. For comparison, a neat PEI film was prepared following the same procedure, skipping the steps of CNT addition and sonication.

V.2.8 Polymerization of caprolactam

Caprolactam (5.0 g, 0.044 mol) was dried under vacuum at 110 °C overnight. Sodium hydride (0.1 g, 0.004) was added to the molten caprolactam under nitrogen atmosphere. Throughout the reaction the nitrogen flow was maintained. A few minutes later N-acetylcaprolactam (0.07 g, 0.0004 mol) was added to the reaction mixture at 140 °C. The polymerization was completed in 5-10 min. The yellow-brown reaction mixture was dissolved in formic acid and precipitated in water. Then, the precipitates were filtered and washed with distilled water. Polyamide was dried under vacuum at 70 °C and obtained quantitatively as a white powder.

V.2.9 Polymerization of N-vinylformamide

N-vinylformamide was polymerized by free radical polymerization in DMSO using 1.0 mol % AIBN as the initiator. A solution of NVF (7.11 g, 0.10 mol) in DMSO (50 mL) was purged with N₂ for 30 min and AIBN (164 mg, 0.001 mol) was added to the solution, purged with N₂ for another 10 min and stirred in an oil bath at 75 °C for 24 h. After polymerization, the mixture was poured into methanol to precipitate the polymer. Drying under vacuum at 60 °C for 48 h gives the poly(N-vinylformamide) as a white solid in 75 % yield. ¹H NMR (300 MHz, D₂O): δ 1.69 (–CH₂–CH–N–), 3.40 (–CH₂–CH–N–, isotactic), 3.92 (–CH₂–CH–N–,

syndiotactic), 7.70–7.83 (m, $H-C=O-$, isotactic), 7.92–8.12 (m, $H-C=O-$, syndiotactic).

V.2.10 Preparation of polyvinylamine hydrochloride

Polyvinylamine was prepared by the base hydrolysis of poly(N-vinylformamide) (PNVF). A sodium hydroxide solution with a concentration 1.5 mol L^{-1} was prepared by dissolving NaOH pellets (2.48 g, 0.062 mol) in distilled water (42 mL). The PNVF (2.20 g) was added to the base solution and the mixture was stirred at $80 \text{ }^{\circ}\text{C}$ for 6 h. After cooling, the reaction media was first neutralized and then acidified by slow addition of concentrated HCl (37 %). The hydrolyzed polymer was precipitated as PVA.HCl into methanol. The product was dried under vacuum at $60 \text{ }^{\circ}\text{C}$ for 48 h to give a white solid in a quantitative yield. $^1\text{H NMR}$ (300 MHz, D_2O): δ 2.21 ($-\text{CH}_2-\text{CH}-\text{N}-$), 3.82 ($-\text{CH}_2-\text{CH}-\text{N}$).

V.2.11 Polymerization of 2-hydroxy-3-phenoxypropyl acrylate

2-hydroxy-3-phenoxypropyl acrylate (HPPA) was polymerized by free radical polymerization in THF using 0.36 mol.% AIBN as initiator. A solution of HPPA (11.13 g, 0.050 mol) in THF (50 mL) was purged with N_2 for 30 min and AIBN (30 mg, 0.182 mmol) was added to the solution, purged with N_2 for another 10 min and stirred in an oil bath at $75 \text{ }^{\circ}\text{C}$ for 24 h. After polymerization, the mixture was poured into distilled water to precipitate the polymer. Drying under vacuum at $60 \text{ }^{\circ}\text{C}$ for 48 h gives the poly(2-hydroxy-3-phenoxypropyl acrylate) as a transparent solid in 93% yield. $^1\text{H NMR}$ (300 MHz, CDCl_3): δ 1.74 ($-\text{CH}-\text{CH}_2-\text{COO}-$), 2.50 ($-\text{CH}_2-\text{COO}-$), 3.92 ($-\text{O}-\text{CH}_2-\text{C}-\text{OH}$), (4.23 ($-\text{COO}-\text{CH}_2-\text{C}-\text{OH}$), 6.85 (1H^2 , $-\text{C}_6\text{H}_5$), 6.90 (1H^4 , $-\text{C}_6\text{H}_5$), 7.21 (2H^3 , $-\text{C}_6\text{H}_5$).

V.2.12 Covalent functionalization of CNTs

V.2.12.1 Functionalization of CNTs with caprolactam

Oxidized CNTs were first prepared by treating the purified CNTs with nitric acid at 120 °C for 6 hours. The carboxylic acid content was found to be 0.39 mmol/g CNT as determined by acid-base titration. Oxidized CNTs (5.0 g) were suspended in thionyl chloride (80 mL), and stirred under nitrogen at 70 °C for 24 h. Upon removal of excess thionyl chloride under vacuum, caprolactam (50 g) was added. The mixture was stirred at 110 °C for 24 h and then cooled to room temperature. The mixture was diluted with chloroform and filtered. CNTs were thoroughly washed with distilled water and methanol to remove the unreacted caprolactam. The CNTs were dried at 120 °C for 2 days.

V.2.12.2 Polyamide functionalized CNTs

Caprolactam (~ 100 g) was dried in vacuum at 100 °C overnight. 200 mg PEG was added to the reaction mixture and the temperature was increased to 140 °C and was left in vacuum for two hours more. Caprolactam functionalized carbon nanotubes (5.0 g) were added to the molten caprolactams. Flushed with N₂ and sodium hydride, NaH, (140 mg, 0.0058 mol) was added to the mixture as initiator. The mixture was flushed with N₂ for 40 more minutes. 24 h later, the heating was turned off and the reaction mixture was filtered and the CNTs were thoroughly washed successively with water (500 mL x 3), methanol (250 mL x 2) and formic acid (250 mL x 2) to remove the sodium salts, monomer and the unattached polymer. The CNTs were dried in oven at 120 °C for 48 h.

V.2.12.3 Functionalization of CNTs with 1,8-diaminooctane

140 mg of oxidized CNTs with a carboxyl concentration of 2.54 mmol/gr CNT and 70 mg (0.48 mmol) of 1,8-diaminooctane were placed together in a steel vial. The vial was heated at 160 °C under vacuum for 4 h. Then, the excess amine was evaporated at the same temperature under vacuum for 2 h. The functionalized CNTs contain 2.48 % N as determined by elemental analysis.

V.2.12.4 Functionalization of CNTs with 1-(2-hydroxyethyl)-3-vinylimidazolium chloride, bromide or bis(trifluoromethanesulfonyl)imide

Oxidized CNTs (200 mg) with a carboxylic acid content of 0.23 mmol/g CNT were suspended in thionyl chloride (40 mL), and stirred under nitrogen at 70 °C for 24 h. Upon removal of excess thionyl chloride under vacuum, 1-(2-hydroxyethyl)-3-vinylimidazolium chloride (3.0 g) was added. The mixture was continuously sonicated under nitrogen at 70 °C overnight and then cooled to room temperature. The mixture was diluted with distilled water and filtered. Recovered CNTs were thoroughly washed with distilled water to remove the unreacted ionic liquid. The CNT-[VEHIM]Cl was dried at 120 °C for 2 days. CNT-[VEHIM]NTf₂ was prepared by stirring the CNT-[VEHIM]Cl (115 mg) with a solution of lithium bis(trifluoromethanesulfonyl)imide (1 g) in distilled water (35 mL) at room temperature overnight. CNT-[VEHIM]Br was prepared by stirring the CNT-[VEHIM]NTf₂ (62 mg) with a solution of tetrabutylammonium bromide (200 mg) in acetone (30 mL) at room temperature overnight.

V.2.12.5 Preparation of cross-linked CNTs

CNT-[VEHIM]Cl (15 mg) were dispersed in dimethylformamide (5 mL) with the aid of sonication in a ultrasonic cleaner for 2 h. AIBN (6 mg) was added to the dispersion purged with N₂ and the mixture was stirred under nitrogen at 65 °C for 24 h. The CNTs were filtered and washed with ethanol.

V.2.12.6 In situ polymerization of 1-vinyl-3-ethylimidazolium

bis(trifluoromethanesulfonyl)imide in the presence of CNT-[VEHIM]NTf₂

CNT-[VEHIM]NTf₂ (86 mg) was added to a solution of 1-vinyl-3-ethylimidazolium bis(trifluoromethanesulfonyl)imide (3.0 g) in ethanol (5 mL). 2,2'-azobis(isobutyronitrile) (2 wt.%, 60 mg), AIBN, was added to the flask flushed with nitrogen. The mixture was stirred

vigorously under nitrogen at 85 °C for 22 h. The filtered and washed CNTs were dried at 110 °C for 48 h. The filtrate was precipitated into water to recover the polymer synthesized in the presence of CNTs.

V.2.12.7 In situ polymerization of 1-vinyl-3-ethylimidazolium bromide in the presence of CNT-[VEHIM]Br

CNT-[VEHIM]Br (28 mg) was added to a solution of 1-vinyl-3-ethylimidazolium bromide (1.5 g) in ethanol (3 mL). 2,2'-azobis(isobutyronitrile) (2 wt.%, 30 mg), AIBN, was added to the flask flushed with nitrogen. The mixture was stirred vigorously under nitrogen at 65 °C for 22 h. The filtered and washed CNTs were dried at 110 °C for 48 h. The filtrate was precipitated into acetonitrile to recover the polymer synthesized in the presence of CNTs.

V.2.12.8 Functionalization of CNTs with polyvinylformamide

Purified CNTs (3.5 g) were added to a solution of NVF (70 g, 1 mol) in DMSO (492 mL). A suspension of CNTs was obtained with the aid of sonication at room temperature for 30 min. The mixture was flushed with nitrogen for 20 min and AIBN (1.616 g, 0.01) was added. After refluxing under vigorous stirring and N₂ atmosphere at 75 °C for 24 h, the reaction mixture was vacuum filtered. The recovered CNTs were washed thoroughly with distilled water and dried under vacuum at 80 °C for 48 h. The filtrate was precipitated into methanol to recover the polymer synthesized in the presence of CNTs. The precipitated polymer was washed with methanol and dried under vacuum at 60 °C for 48 h.

V.2.12.9 Functionalization of CNTs with polyvinylamine

Poly(vinylamine) functionalized CNTs (CNT-PVA) were prepared by base hydrolysis of CNT-N-polyvinylformamide (CNT-PNVF). CNT-PNVF (3.30 g) was added to a solution of NaOH (30 g) in distilled water (500 mL). After sonication for 30 min, the mixture was

refluxed under vigorous stirring at 80 °C for 6 h. The hydrolyzed CNTs were then separated from the mixture by filtration and washing thoroughly with distilled water until neutralization of the filtrate. The recovered CNTs were dried under vacuum at 60 °C for 48 h, yielding CNT–PVA.

V.2.12.10 Functionalization of CNTs with poly(2-hydroxy-3-phenoxypropyl acrylate)

Purified CNTs (4.35 g) were added to a solution of 2-hydroxy-3-phenoxypropyl acrylate (HPPA) (87 g, 0.39 mol) in THF (355 mL). A suspension of CNTs was obtained with the aid of sonication at room temperature for 30 min. The mixture was flushed with nitrogen for 20 min and AIBN (0.231 g, 0.0014 mol) was added. After refluxing under vigorous stirring and N₂ atmosphere at 75 °C for 24 h, the reaction mixture was vacuum filtered. The recovered CNTs were washed thoroughly with THF and dried under vacuum at 80 °C for 48 h. The filtrate was precipitated into distilled water to recover the polymer synthesized in the presence of CNTs. The precipitated polymer was dried under vacuum at 60 °C for 48 h, yielding CNT–PHPPA.

V.2.12.11 Functionalization of CNTs with epoxy

Oxidized CNTs were first prepared by treating the purified CNTs with nitric acid at 120 °C for 3 hours. The carboxylic acid content was 1.37 mmol/g CNT as determined by acid-base titration. Commercial glycidyl end-capped poly(bisphenolA-co-epichlorohydrin) (300 mL) with a Mn = 355 was diluted with THF (100 mL) containing tributylamine (10 mL). The CNT–COOH (4.20 g) was added and the mixture was sonicated at room temperature for 30 min. The reaction mixture was flushed with nitrogen for 30 min and stirred vigorously at 80 °C for 24 h. The filtered solid was washed thoroughly with THF until the supernatant liquid was clear. The recovered CNTs were dried under vacuum at 60 °C for 48 h, yielding CNT–epoxy.

V.2.13 Preparation of polyamide/CNT composites

The polyamide/CNT composites were prepared in collaboration with ECNP, Florence, Italy. Rhodia 27EA1 matrix was melt blended with 1 wt.% pristine, amine functionalized or polyamide functionalized CNTs in a DSM co-rotating twin-screw mini extruder. The rotation speed and temperature profile were 150 rpm and 280/290/295 °C, respectively.

V.3 Instruments and measurements

V.3.1 Transmission electron microscope

Transmission electron microscope (TEM) images were obtained using a JEOL JEM 2100F FEG at 200 kV or JEOL JEM-1400 at 120 kV. Samples were prepared by suspending the nanotubes in solution (ethanol, acetone, THF or distilled water) under ultrasonic vibration. Some drops of the thus produced suspensions were deposited onto carbon-coated copper grids.

V.3.1.1 Microtoming

The PEI/CNT composite specimens were microtomed into thin (70 nm) films using a Reichert Ultracut microtome. The slices were placed on copper grids and examined by TEM 1400.

V.3.1.2 Staining

A commercial 0.5 wt.% aqueous solution of ruthenium tetroxide (RuO_4) or 5 wt.% aqueous solution of phosphotungstic acid hydrate was used for staining. 1 g phosphotungstic acid hydrate was dissolved in 20 mL distilled water and the pH of the solution was adjusted to around 7.0 by NaOH solution. One drop of this solution was put on the TEM grid bearing the sample; it was let for some minutes and dried with a filter paper. The RuO_4 staining was

carried out by exposing the grid with the sample to the vapors of RuO₄ solution for 15 minutes in a glass covered dish.

V.3.2 Field emission gun scanning electron microscopy

A JEOL JSM 6700F Field Emission Gun scanning electron microscope (FEG-SEM) was used to obtain SEM images. The tensile fractured surfaces were coated with a thin layer of platinum.

V.3.3 Thermogravimetric analysis

Thermogravimetric analysis (TGA) in air was conducted on a Setaram apparatus using a temperature program of 30–800 °C, with a heating rate of 10 °C/min. TGA measurements in nitrogen atmosphere were performed using a TA Instruments Q50. Samples were put on an open platinum pan and heated at 10 °C.min⁻¹ under 60 mL.min⁻¹ N₂ flow.

V.3.4 Differential scanning calorimetry

Differential scanning calorimetry (DSC) measurements were conducted using a TA Instruments Q200 differential scanning calorimeter in a nitrogen atmosphere (flow rate = 50 ml min⁻¹). Samples were sealed in an aluminum pan. Unless stated otherwise, the heating/cooling curves of PILs were obtained at a scanning rate of 10 °C min⁻¹. To erase the thermal history of the samples, each sample was stabilized at –60 °C and heated to 250 °C and kept at that temperature for 2 min. Then, the sample was allowed to cool again to –60 °C. After 2 minutes, it was heated to 300 °C. The heating/cooling curves of PEI and PEI/CNT composites were obtained at a scanning rate of 10 °C.min⁻¹. To erase the thermal history of the samples, each sample was stabilized at –60 °C and heated to 230 °C and kept at that temperature for 2 min, and the sample was allowed to cool again to –60 °C. After the sample was kept at that temperature for 2 min, it was heated to 300 °C.

V.3.5 Particle size analysis

The particle size analysis was performed with a Mastersizer 2000 laser diffraction particle size analyzer from Malvern Instruments.

V.3.6 Elemental analyses

The elemental analyses for C, H, O and N were performed on a Perkin Elmer 2400 series II microanalyser. The analyses of Al and Fe, were carried out by the “Service central d’analyse du CNRS” in Solaize, France.

V.3.7 XPS analysis

XPS analyses were performed on a VG Escalab model MK2 spectrophotometer with pass energy of 20 eV and with Al K α (1486.6 eV, 300 W) photons as an excitation source.

V.3.8 Specific surface area and porosity measurements

The specific surface area, pore volume, and pore sizes were measured by nitrogen physisorption at $P/P_0 = 0.99$, of nitrogen and liquid nitrogen temperature using a Belsorp-mini (BEL Japan Inc. apparatus). Prior to the measurement, the CNTs were degassed for 16 h at 150 °C. The specific surface area was calculated according to the Brunauer–Emmet–Teller (BET) theory, while the pore size and the pore volume were calculated by the BJH method based on the desorption branch of the isotherm.

V.3.9 Molecular weight analysis

The molecular weight analysis of poly(2-hydroxy-3-phenoxypropyl acrylate) was performed on a size-exclusion chromatography (SEC) system equipped with a refractive index detector (RI 2000), a triple angle light scattering detector (Mini Dawn Wyatt) and a Varian PLgel 5 μ m Mixed-D column. THF was used as the eluent at a flow rate of 1 mL min⁻¹. The molecular

weights of polyvinylamine and poly(N-vinylformamide) were determined on a SEC equipped with a refractive index detector (RID Shimadzu), a triple angle light scattering detector (Mini Dawn Wyatt) and two columns (Shodex OH Pack SB 804 HQ and SB 802 HQ). An aqueous tampon (NaNO_3 à 0.1M/ NaN_3 at 200 ppm, pH7) was used as the eluent at a flow rate of 0.5 mL min⁻¹. The specific refractive index increments (dn/dc) of the polymers were measured at 620 nm on a detector from Polymer Standards Service. The molecular of polyamide 6,6 was analyzed using a gas chromatograph equipped with a KNAUER differential refractometer and a PLgel 5 μm , MiniMIX-C column. Pentafluorophenol/chloroform was used as the eluent at a flow rate of 0.3 mL min⁻¹.

V.3.10 Raman analysis

Raman spectrum was recorded with a Labram HR800 of Jobin Yvon Raman spectrometer (excitation wavelength = 632.82 nm).

V.3.11 Infrared spectroscopy

FTIR spectroscopy was performed with a Perkin-Elmer 1710 Fourier Transform spectrophotometer using KBr salt for solid pellet analysis. The ATR-FTIR measurements were performed using a PerkinElmer Spectrum 100 Universal ATR-FTIR (Attenuated Total Reflectance-Fourier Transform InfraRed analysis) instrument equipped with a diamond/ZnSe crystal single reflection.

V.3.12 Nuclear magnetic resonance spectrometer

Solution ¹H NMR (300 MHz) spectra were recorded on a Bruker DPX-300 spectrometer. Solid NMR analysis was performed on a Bruker Avance 400WB spectrometer.

V.3.13 Ultrasonication

The carbon nanotubes were dispersed using a Fisher Scientific FB15051 ultrasonic bath cleaner unless otherwise stated. The carbon nanotube solutions for casting were sonicated using an ultrasonic probe (Vibra Cell 75115, 500 W, Bioblock Scientific) at amplitude of 20% in an ice bath.

V.3.14 Compression molding

The polyetherimide/CNT composite films were compressed into flat films using compression molding by a Collin, P 200 E.

V.3.15 Tensile testing

The compression molded thin films of PEI/CNT were punched into dog-bone specimens using a manual hollow die punch (Instruments J. Bot S.A., model 690). The stress–strain curves of the PEI/CNT composites were obtained using an Instron model 5565 mechanical tester at 20-21 °C. The strain speed was 5 mm min⁻¹ under a load of 1 kN. The values reported represent an average of the results for tests run on at least five specimens. The tensile tests of polyamide composites were carried out by a LLOYD Instruments, model 30K electronic dynamometer.

V.3.16 Dynamic mechanical analysis

Dynamic mechanical analysis (DMA) was conducted on the Mettler Toledo DMA/SDTA861e in tension mode.

V.3.17 Electrical measurements

An Agilent 4156C precision semiconductor parameter analyzer equipped with a 16442A test fixture was used to measure the electrical resistivity of the samples. The 0.5 mm thick CNT/PEI composite films were cut into rectangular specimens of 20 mm x 10 mm, and upper

and lower surfaces of the specimens were coated with conducting silver paint to ensure an intimate contact between the specimen surfaces and electrodes.